Heat driven adsorption cooling utilising enhanced effective thermal conductivity monolithic adsorbent generators for refrigeration and ice production in developing countries

Gareth N L Davies

This thesis is submitted in fulfilment of the degree Doctor of Philosophy

University of Warwick - School of Engineering

August 2000

Contents

List of Figures

List of Tables

Nomenclature

a	Constant	[-]
b	Adsorption Coefficient	[-]
c	Constant	[-]
c'	Constant	[-]
h	Specific Enthalpy	[kJ kg^{-1}]
h	Heat Transfer Coefficient	[W $m^{-2}K^{-1}$]
ho	External Heat Transfer Coefficient	[W $m^{-2}K^{-1}$]
k	Constant	[-]
k	Thermal Conductivity	[W $m^{-1}K^{-1}$]
m	Mass	[kg]
$\dot{m}$	Mass Flow Rate	[kg s^{-1}]
n	Dubinin-Astakhov Constant	[-]
n	Number of Molecular Layers	[-]
$\dot{q}$	Specific Power	[W kg^{-1}]
r	Radius	[m]
t	Time	[s]
u	Nodal Heat Transfer Coefficient	[W $m^{-2}K^{-1}$]
v	Gas Velocity	[m s^{-1}]
x	Concentration	[kg kg^{-1}]

A	Gradient	[-]
A	Area	[m^2]
B	Micropore Structure Coefficient	[-]
B	Material Shape Factor	[m^{-1}]
Cp	Specific Heat at Constant Pressure	[J $kg^{-1}K^{-1}$]
$\dot{H}$	Internal Heat Generation Rate Per Unit Volume	[W m^{-3}]
K	Dubinin-Astakhov Constant	[-]
K	Permeability	[m^2]
M	Mass	[kg]
P	Pressure	[N m^{-2}]
P	Power	[W]
Q	Energy	[J]
$\dot{Q}$	Energy Flux	[W]
R	Specific Gas Constant	[J $kg^{-1}K^{-1}$]
T	Temperature	[°C] or [K]
To	External Temperature	[°C] or [K]
V	Volume	[m^3]
α	Thermal Diffusivity	[m^2s^{-1}]
β	Affinity Coefficient	[-]
θ	Fraction of Internal Porous Surface Area	[-]
μ	Dynamic Viscosity	[N $m^{-2}s$]
ρ	Density	[kg m^{-3}]
ψ	Void Fraction	[m^3m^{-3}]
Δl	Length from Node Centre to Control Volume Interface	[m]

Δr	Radial Space-Step	[m]
Δt	Half-Cycle Duration	[s]
Δx	Change in Concentration	[kg kg^{-1}]
Δz	Axial Space-Step	[m]
ΔP	Pressure Drop	[N m^{-2}]
ΔT	Temperature Difference or Temperature Gradient	[°C] or [K]
$\Delta \zeta$	Total Generator Length	[m]

Subscripts:

a	Ammonia
ads	Adsorption
alum	Aluminium
c	Carbon
car	Carbon
cond	Condenser
cool	Start of Cooling Half-Cycle
cooling	Cooling (Half-Cycle)
cycle	Complete Thermodynamic Cycle
evap	Evaporator
fc	Liquid Leaving Condenser
g	Gas
ge	Vapour Leaving Evaporator
gen	Generator
heat	Start of Heating Half-Cycle
heating	Heating (Half-Cycle)
i	Internal/Inside

i,j	Nodal Position
interface	Material Junction/Interface
lam	Laminate
m	Mean Value
material	Material Type
material 1	Material Node 1 to Interface
material 2	Material Node 2 to Interface
max	Maximum
min	Minimum
o	External/Outer
r	Radial
sat	Saturation Conditions
sp	Specific
steel	Steel
v	Vaporisation
x	X-Direction
y	Y-Direction
z	Z-Direction
N	North
S	South
E	East
W	West
0	Limiting or Maximum Value
1	Point 1
2	Point 2

Superscripts:

n	Time Level
p	P Solution Sweep/Variable
q	Q Solution Sweep/Variable
A	Effective Specific Heat Coefficient A
B	Effective Specific Heat Coefficient B
C	Effective Specific Heat Coefficient C
D	Effective Specific Heat Coefficient D
E	Effective Specific Heat Coefficient E

Acknowledgements

I would like to thank my supervisor Dr. R. E. Critoph for his help, guidance and assistance throughout the duration of this research. Dr. R. Thorpe and Dr. Z. Tamainot-Telto also provided invaluable advice, inspiration and encouragement. I would like to thank Mr J. Matteri for his technical assistance and candour during the experimental phases of this work as well as all of the technical staff who contributed to the completion of the experimental rig. With regard to the experimental rig, I would particularly like to thank Mr. P. Meesum and Mr. C. Major in the engineering workshops for their machining skill and patience. Finally, I would like to thank my wife Liz - without her love and support this thesis would never have been completed.

Abstract

An experimental and numerical study is presented on the design, construction and evaluation of a prototype heat driven adsorption cooling system utilising the carbon-ammonia adsorption pair. The primary objective of the research was to enhance the effective thermal conductivity of the monolithic carbon material so as to enable more rapid thermal cycling and provide increased specific cooling power. The overall design was guided towards the goal of a system appropriate for refrigeration and ice production in developing countries.

A novel carbon-aluminium laminate structure was selected to enhance the effective thermal conductivity of the monolithic carbon. A two dimensional finite difference model was applied in order to determine the optimal internal geometry for this laminate. The laminate consists of a stainless steel shell containing alternate activated carbon and aluminium disc layers formed *in situ*. Sample sections of the laminate viewed under the microscope indicate good thermal contact between the constituent laminate materials.

A prototype cooling rig was constructed based on two generators operating 180° out of phase, each containing one metre lengths of the carbon-aluminium laminate. Experimental results indicate that for a twenty minute thermodynamic cycle duration the specific cooling power achieved is 144 W kg^{-1} which is an improvement in performance over the previous results of 30-60 W kg^{-1}. The total semi-continuous cooling power for both generators is 458 W with a cooling coefficient of performance (COP) of 0.35 and a Carnot COP of 3.12.

The numerical model was validated against the temperature, pressure and concentration data obtained from the experimental rig. A good correlation was seen between the numerical and experimental data for an external heat transfer coefficient during heating of 1000 W $m^{-2}K^{-1}$ and an external heat transfer coefficient during cooling of 500 W $m^{-2}K^{-1}$.

Performance predictions utilising the validated numerical model suggest that significant further improvement in the specific cooling power should be obtained by reducing the cycling time and increasing the generating temperature. Future design modifications will focus on reducing thermal mass, utilising heat pipes for generator cooling and adapting the system for use in developing countries.

Chapter 1

Introduction

1.1 Refrigeration Requirements In Developing Countries

In a number of developing countries around the world there is a requirement for refrigeration systems driven by heat which are simple, robust and capable of producing large quantities of ice. Refrigeration and ice supply are required for uses such as vaccine storage and food preservation. In particular, ice is needed for preservation of food such as fish catches [1] and agricultural produce in order to prevent the food spoilage which would otherwise result in the hot climates encountered. In order to meet this need the purpose of the following research is to design and construct a refrigeration system based on a thermally driven adsorption cycle. Although conventional vapour compression cycles may be applied to this end they require an electricity supply which is often not available in developing countries. The advantage of thermally driven adsorption cycles is that they have the flexibility to be driven from a number of different heat sources such as solar heat or bio-fuels.

Bearing the above in mind it is important to optimise the system as far as possible without adversely affecting its suitability for applications in developing countries. A number of guiding criteria were applied, as far as possible, in order to serve as a specification for directing the course of the research.

The research guiding criteria were as follows:

- Design for Ice Production - Aim for 1 tonne of ice per day (produced locally).
- Heat Driven Cycle - Avoids requirement for local electricity supply. Utilise local energy source such as solar or biomass (effectively free energy sources).
- Low Environmental Impact - Avoid use of ozone depleting refrigerants such as CFCs.
- Low Capital Cost - Minimise material costs and hence aim to maximise specific cooling power, rather than maximise COP as a primary design aim.
- Simplicity & Reliability - Aim to keep maintenance requirements to a minimum.
- Manufacture - Possibility of local manufacture/assembly in country of use.
- Robustness - Ability to withstand rough handling and adverse environmental conditions.
- Safety - Low refrigerant toxicity and isolation from dangerous high/low temperatures.
- Portability - Minimise overall weight and size to ease installation and relocation.
- Climate - Consideration of climatic conditions affecting system such as ambient temperature at which waste heat will be rejected.

1.2 Heat Driven Refrigeration Cycles

Heat driven cycles are preferable to conventional electrically driven vapour compression cycles as they avoid the need for any electricity supply whether it be grid supplied or via a generator or photovoltaic panels. Poor infrastructure and lack of grid supply in rural areas of developing countries leads to the need for a refrigeration system which is not reliant on an electricity supply. Although photovoltaic systems can be used to drive conventional refrigeration systems they tend to be rather expensive to manufacture and maintain while the photovoltaic panels themselves are susceptible to damage. Although work is being carried out to reduce the overall cost of using photovoltaic panels by utilising devices such as solar concentrators and tracking solar arrays these systems further complicate the overall design of a refrigeration system. It is intended that the final refrigeration system should have the flexibility to be driven from a readily available indigenous heat source such as solar heat or that provided by low grade organic fuels and biomass. There are a number of

options as far as choosing a heat driven cycle are concerned with some systems being inherently more suited to the final desired application than others. Heat driven refrigeration systems have the distinct advantage of being capable of supplying cold/ice without the need for any form of electricity supply unless some form of pumping system is incorporated (as may be the case for certain forced convection systems). Heat driven refrigeration systems may be broadly classified as either absorption or adsorption systems.

1.3 Choice of Adsorption or Absorption Cooling

Absorption systems generally utilise liquid absorption pairs such as lithium bromide-water or ammonia-water. An intermittent absorption cycle ice maker would need to be excessively large in order to manufacture one tonne of ice per day. Although it is possible to design rapid cycling absorption systems in order to increase specific cooling powers, less than perfect rectification of the refrigerant in the evaporator tends to have an adverse effect on overall performance. If a continuous absorption system was selected instead then an electrically driven solution pump would be required. This goes against the idea of having a purely heat driven system independent of electricity supply.

In the case of the Platen-Munters diffusion absorption system a combination of water, ammonia and hydrogen are utilised [2, 3]. As the system is continuous, has no moving parts and has good heat transfer by virtue of operating as a liquid system it would appear to offer the desired solution. However the Platen-Munters system needs to be carefully optimised otherwise the system performance may be drastically compromised. This can be achieved by incorporating thermostats, pumps and control systems but again this adds to the overall system complexity and cost. Additionally, the Platen-Munters system may not be sufficiently robust to operate reliably in rural locations where maintenance might pose problems. Hence, although the Platen-Munters system was considered as a possible option, because the system relies on vapour diffusion a relatively large system would need to be built rather than the smaller type of system offered by rapid cycling adsorption designs. The choice was between an absorption or an adsorption system. Given the need for a simple system with fewer moving parts and the inherent difficulties associated with the Platen-

Munters system, an adsorption system offered the more desirable properties. Additionally the departmental expertise makes the adsorption system the more desirable option. However, adsorption systems also pose a number of fundamental problems, particularly if the requirement is for a rapid cycling system as is the present case.

Adsorption systems use an adsorbent-adsorbate pair as the basis of the refrigeration system. Common adsorbents include zeolites, activated carbon, silica gels and chemical adsorbents such as calcium chloride. Adsorbates also commonly encountered include ammonia, water and methanol. Essentially polar molecules are required which are readily adsorbed but which also possess high latent heats of adsorption and desorption so as to maximise the refrigeration effect per cycle of operation and minimise the overall inventory of adsorbate required. This leads to a reduction in the sensible heating required thus improving thermodynamic performance. Of the adsorbents available activated carbon appears to be the most promising as it provides one of the largest changes in adsorbate concentration. Overall, zeolites do not tend to be as desirable for adsorption purposes as activated carbons although researchers are divided as to which one is the best to use. Silica gels have been used previously in conjunction with sulphur dioxide or water. A modern silica gel-water adsorption refrigerator, produced by the Japanese company Mycom [4], is presented in Figure 1.1.

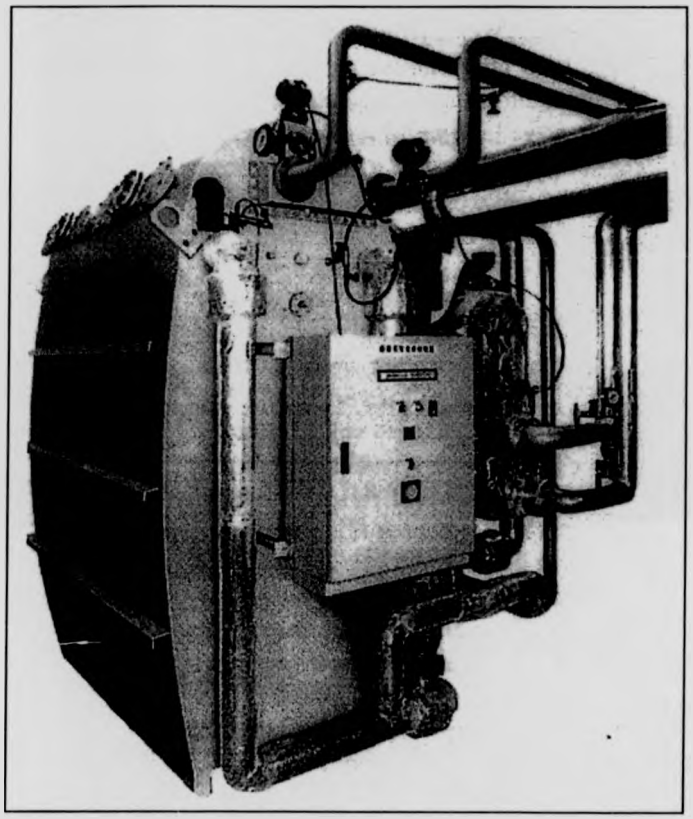

Figure 1.1: Mycom Silica Gel-Water Adsorption Refrigerator

Chemical adsorbents provide large changes in adsorbate concentration. However, they do tend to suffer from degradation due to swelling during adsorption particularly over many cycles as would be encountered in a rapid cycling system. Considering adsorbates, although water by virtue of its high latent heat would appear to be the ideal adsorbate, its very low vapour pressure would mean a refrigeration machine operating below atmospheric pressure. A methanol system would also operate at sub-atmospheric pressures. This then means that any leaks in the system would result in an air flow into the system and hence prevent system operation. However, as ammonia has a high vapour pressure and operates well above atmospheric pressure any small system leaks would result in losses in refrigerant

and degradation of cycle performance but would probably still allow the system to operate up to a certain point.

The main difficulty involved in designing adsorption systems to produce significant amounts of cooling is that of heat transfer. In order to achieve a given degree of cooling it is possible to scale up previous devices in terms of the amount of adsorbent and adsorbate required. However, for a one tonne a day ice maker operating on a diurnal cycle this would require an extremely large and heavy design. Alternatively rapid cycling of the adsorbate can be used to increase the number of cooling cycles over a given time period. When this is the case the problem encountered is that of heat and mass transfer.

1.4 Adsorbent Properties

By their very nature, microporous adsorbents are also good insulators. Hence, in order to achieve a rapid cycling design the heat transfer characteristics of the adsorbent bed need to be improved. The adsorbents themselves are normally available in the form of powders or granules where the point contact between the adsorbent particles tends to lead to a poor heat conduction path.

Many ideas have been put forward in order to improve the heat transfer characteristics. Some of them involve adding high conductivity materials in the form of particles or powders to the adsorbent. However, in general these have little effect on the overall conductivity due to the nature of the point contact between the adsorbent and conduction particles. Some work has also been carried out on using metallic foams in conjunction with adsorbents to provide an anisotropic matrix. However, although the methods have proved to be effective they tend to be overly expensive. Incorporating fins and heat transfer structures into the adsorbent bed has also been carried out to improve heat transfer. It is particularly important to ensure a good bond between the heat transfer surface and adsorbent in order to minimise the thermal contact resistance. To gain further improvement in the bed conductivity monolithic carbons have been produced which increase the heat transfer through the adsorbent bed. Including graphite or sintering in metallic powders into these monolithic carbons has the effect of improving heat transfer

still further. However, with these monolithic carbons mass diffusion can be a problem. Hence, these adsorbents are best used in thin sections or with channels cut in situ to increase the adsorbate mass transfer.

1.5 History of Adsorption Machines

The history of solid adsorption refrigeration dates back to the middle of the 19th Century when Michael Faraday first demonstrated the system in 1848 by adsorbing ammonia onto silver chloride. Little further development occurred until the early part of the 20th century when the cycle was utilised for applications such as domestic heating and refrigeration. Plank and Kuprianoff [5] documented the use of adsorption cycles for heat pumping and refrigeration during the early 1900s. In the 1920s a silica gel-sulphur dioxide adsorption pair was utilised in the United States for the air conditioning system of railway carriages [6, 7]. The heat input was obtained directly from an open gas flame while heat rejection was via natural convection. The system did not require any form of electrical input which was an important consideration before the days of a national electricity network [8].

Following the advent of the hermetically sealed compressor and electrically driven vapour compression cycles adsorption systems went out of favour. Half a century followed where very little development was carried out on adsorption cycles. However, in the 1970s research was initiated into their application for low temperature solar air conditioning [8]. Since then, and up to the present day, with the concern over the use of ozone depleting CFCs and the production of greenhouse gases, interest in adsorption cycles has again increased both for providing heating and cooling. Adsorption systems do not need to use ozone depleting refrigerants thus making them more environmentally friendly.

At present the adsorption systems seem most promising for use in developing countries where there is a need for cooling, because overall system efficiency is not of paramount importance when a plentiful source of energy such as solar or biomass is available. However, in developed countries work is on going to improve system efficiency so that systems are competitive with the more commonplace electrically driven vapour compression and liquid absorption systems.

1.6 Conclusions

A research specification has been developed with a number of criteria stated to direct the course of the research. A requirement has been identified for ice in developing countries. Thermally driven cooling cycles enable ice to be produced without the need for a local electricity supply. Absorption and adsorption cycles have both been considered as possible candidates for a thermally driven cooling cycle. In general, absorption systems tend to be more complex with more moving parts while adsorption systems tend to be simpler with fewer moving parts and are thus more consistent with the research specification. Many different adsorbent-adsorbate pairs are available, each with their own pros and cons, with their application dictated to a great extent by the system requirements, such as operating temperature range or temperature lift. The primary difficulty identified is that of heat and mass transfer. For a smaller system, employing rapid cycling to maximise specific cooling power, the overall heat and mass transfer appears to be fundamental in determining system performance.

References

[1] **Harvey, A.B.**, Study of an Intermittent Regenerative Cycle for Solar Cooling, PhD Thesis, Department of Engineering, University of Warwick, **1990**.

[2] **Backstrom, M.**, The Theory of the Evaporator Working by Diffusion, Kylteknisk Tidskrift, pp. 22–26, **1954**.

[3] **Critoph, R.E., Tarbaghia, T.M.**, Solar Powered Platen-Munters (Electrolux) Refrigeration Cycle for Large Scale Refrigeration, Proc. Int. Conf. on Applications of Solar and Renewable Energy, Cairo, pub. ISES, p. 6, April **1992**.

[4] **Van Bogaert, G.**, Adsorption Refrigerator Uses Low-Temperature Waste Heat, Caddet Newsletter, No. 1, pp. 7–9, March **2000**.

[5] **Plank, R., Kuprianoff, J.**, Die kleinkältemaschine, Springer-Verlag, **1960**.

[6] **Hulse, G.E.**, Freight Car Refrigeration by an Adsorption System Employing Silica Gel, Refrigerating Engineer, Vol. 17, No. 2, **1929**.

[7] **Miller, E.B.**, The Development of Silica Gel Refrigeration, The American Society of Refrigerating Engineers, Vol. 17, No. 4, **1929**.

[8] **Shelton, S.V., Wepfer, W.J., Miles, D.J.**, Ramp Wave Analysis of the Solid/Vapor Heat Pump, Journal of Energy Resources Technology, Vol. 112, pp. 69–78, **1990**.

Chapter 2

Literature Review

2.1 Introduction

In the previous chapter, heat and mass transfer were identified as the critical factors affecting the performance of adsorption systems. In the literature review that follows several areas including heat and mass transfer are investigated in order to highlight the variety of options and approaches that are possible. The work of other researchers in the adsorption field is considered so as to provide an indication of present developments and techniques. On this foundation, the aim of the following literature review is to ensure that the subsequent research is able to provide a positive and original contribution to the overall body of research knowledge.

2.2 Thermodynamic Cycles

Many researchers have investigated the thermodynamics of solid adsorption cycles with a view to improving cycle efficiency, cycling time and overall cycle performance. Many different cycles have been proposed varying in complexity from simple intermittent cycles to more complex systems utilising internal heat regeneration and thermal wave systems. One of the main areas in which improvements are sought is in the cycle Coefficient of Performance (COP) or Coefficient of Amplification (COA) in order to make adsorption cycles more competitive with more conventional technologies such as electrically driven vapour compression systems.

Douss and Meunier [1, 2], identify the performance of the simple adsorption cycle as depending on the level of the four key operating temperatures. Bougard and Boussemaere [3] also consider that the thermodynamic cycle may be described completely by these four cycle temperatures at which the heat is supplied and rejected for a given adsorbent-adsorbate pair. Alternatively, Ülkü [4] mentions that if the system operates according to the Carnot cycle then a system operating at four temperature levels may also be described by two systems operating between two temperature levels. The significant cycle temperatures are the evaporator temperature, condenser temperature and the temperature of the adsorber at the beginning and end of the heating phase. Critoph [5] discusses the effect that the cycle temperatures have on the cycle performance.

Generally the evaporating temperature will vary between +5°C and -20°C depending on the applications which may range from air conditioning to ice production and deep freezing. The condensing temperature at which heat rejection occurs should be as near as possible to ambient conditions for improved efficiency while also satisfying heat transfer and economic requirements. The temperature of the adsorbent bed at the end of the adsorption period should be as low as possible so as to maximise the concentration change during the desorption period. By improving the change in concentration less adsorbent is required thus reducing the amount of sensible heating and cooling required and hence improving cycle efficiency. However, the temperature of the bed at the end of the adsorption period is also affected by factors such as the ambient temperature of heat rejection and the temperature gradient required for heat transfer.

For a zeolite-water adsorption pair Ülkü [4] indicates that as the amount adsorbed increases the corresponding heat of adsorption decreases. Hence the greater the amount of adsorbate re-adsorbed the lower the amount of heat to be rejected from the adsorber. The higher the maximum generation temperature of the adsorbent bed at the end of desorption the larger the amount of adsorbate that is driven off, the larger the change in adsorbate concentration and the greater the cooling effect achieved per mass of adsorbent. However, as the temperature is increased above a certain point progressively less adsorbate is driven off, since the additional heat supplied is used for sensible heating of the adsorbent and

adsorbate rather than for further desorption. The temperature difference of the adsorber between the beginning and end of the heating phase has a direct effect on the concentration change of adsorbate and hence, depending on the application, the cooling or heating effect achieved per mass of adsorbent. Therefore by varying the above cycle temperatures the overall cycle efficiency may be improved and optimised as required.

For an activated carbon-methanol adsorption pair Douss and Meunier [1] found that the COP decreased rapidly with both decreasing evaporating temperature and increasing adsorption temperature. This implies that for a cycle designed for ice production or deep freezing a certain degradation in COP must be accepted at the lower evaporating temperatures encountered. However, under most operating conditions Douss and Meunier [1] found the adsorption cycles they investigated to give higher COPs than the continuous ammonia-water liquid absorption cycle within the same temperature limits. As shown by Suzuki [6], faster cycle times and improved heat transfer coefficients yield greater cooling powers per mass of adsorbent which reduces the overall mass of adsorbent required and thus system size and cost.

There are a number of different adsorption cycles which can be utilised to achieve a cooling or heating effect, depending on whether the objective is for refrigeration or heat pumping. The simple adsorption cycle consists of one adsorbent bed which is alternately heated and cooled in order to produce an intermittent cooling or heating effect, depending on the application. During the heating phase of the cycle, the thermal energy supplied as heat is converted into both sensible heat to increase the temperature of the adsorbent bed to the desorption temperature and latent heat for the desorption of the adsorbate [7]. Examples of the simple cycle can be seen in solar refrigeration applications where an intermittent cooling effect is achieved while the adsorbent is alternately heated and cooled in a diurnal cycle. Although the simple adsorption cycle has been shown to be reliable in operation it has a relatively low COP. As Jones [8] points out, in the absence of any heat regeneration process, rejecting all the waste heat from the cycle to the environment results in a relatively poor thermal efficiency performance. The COP is defined for the simple intermittent refrigeration cycle as the ratio of the cooling power achieved to the heating

power supplied. Bougard and Boussemaere [3] state that the COP is a very sensitive function of the cycle source temperatures and the temperature and pressure gradients required for the heat and mass transfers during cycle operation. Irreversibilities throughout the standard intermittent adsorption cycle are the main factor in contributing towards low cycle efficiencies. Hence Bougard and Boussemaere [3] suggest that improvements in cycle performance will result due to the application of advanced cycles such as multistage cycles, multi-component cycles and cycles utilising internal heat regeneration.

For the simple intermittent adsorption cycle Cacciola and Restuccia [9] describe the main thermodynamic problems being related to the intermittent nature of heat transfer during heat pumping or refrigeration and the variation in the temperature of the heat during adsorption. However, the variation in the temperature of the heat during adsorption is only of concern for heat pumping applications.

For an intermittent adsorption cycle Passos et al [10] found that for active carbon-methanol pairs the COP of an adsorption system may also be improved, as mentioned previously, by increasing the maximum desorption temperature and minimising the final adsorption temperature thus increasing the change in adsorbate concentration. Pons and Guilleminot [7] also confirm that in order to maximise the change in concentration and the mass desorbed, the maximum temperature should be as high as possible and the final adsorption temperature as low as possible. However, no further gain in COP was achieved by Passos et al [10] above a given maximum generating temperature, indicating limits to the maximum generating temperature. This may have been as a result of the majority of adsorbate having been desorbed below this temperature and further sensible heating yielding a decrease in COP as a result of little further adsorbate being driven off as found by Shelton et al [11]. This would suggest that it is desirable to achieve the optimum maximum desorption temperature while also striving for the lowest final adsorption temperature practically possible. Additionally, Zhu et al [12] confirm that higher generation temperatures lead to reduced cycling times and thus reduced system size, weight and cost for a given cooling power.

Although for the basic intermittent cycle the cooling COP could be as high as 1, in reality losses within the system generally limit the cooling COP to less than 0.5 [11]. Meunier [13] found that the maximum COP value was always less than 0.5 for the basic intermittent cycle because of the sensible heat required during the temperature swings. Worsøe-Schmidt [14] also calculated for an intermittent chemisorption refrigeration system that the COP would never exceed 0.5.

In relation to the basic intermittent cycle Shelton et al [11] found that a large proportion of the heat rejected from the bed being cooled is at a temperature greater than or equal to that required by the bed being heated thus allowing the heat to be regenerated while also improving the COP by reducing the thermal energy input required. However, for a bivariant system utilising an adsorbent-adsorbate pair a large temperature swing is required on each adsorbent bed in order to achieve sufficient heat transfer throughout the regenerative cycle [13].

Two or more adsorbent beds out of phase with internal heat regeneration between beds may be utilised to achieve continuous rather than intermittent heating or cooling. Utilising such regenerative cycles it has been claimed by a number of researchers such as Härkönen and Aittomäki [15] and Shelton et al [11] that up to 80% of the heat required for desorption may be regenerated from the bed being cooled without violating the Second Law of Thermodynamics. However, for a zeolite system Härkönen and Aittomäki [15] found that during internal regeneration useful heat was obtained from the condenser only, thus degrading cycle performance somewhat. Although regenerative cycles also allow the output energy to be released within a small range of temperature variation [9] this is of less relevance for refrigeration cycles. By utilising internal heat regeneration improvements in cycle COP are also obtained, with COP generally increasing with increasing heat regeneration. If an isotropic temperature distribution is assumed for a multi-bed bed system then increasing the number of beds out of phase also increases the COP and reduces the time when there is no heating or cooling effect [16, 17], thus improving continuity of operation.

In order to achieve effective heat regeneration improvements are required in both the adsorbent bed thermal conductivity and the heat transfer between the heat transfer surfaces and the bed itself. By utilising internal heat regeneration the aim is to increase the cooling powers available per mass of adsorbent while also improving the cooling COP with the aim of achieving values of 1 or greater. Critoph [18] investigated the possible improvements in cycle COP by operating two adsorbent beds out of phase and regenerating the sensible heat rejected from the bed in the adsorption phase to preheat the bed entering the desorption phase. This method also allows a continuous/semi-continuous cooling effect to be achieved which is not possible when using one bed alone, as for continuous cooling at least two out of phase beds are required.

By using such a heat regeneration system the overall COP of the system could thus be considerably improved. However, for a rapid cycling machine, heat and mass transfer considerations would be far more important, necessitating improved bed heat transfer and thermal conductivity and increasing the overall complexity of the system. In support of regenerative cycles, researchers such as Douss et al [19], Meunier and Douss [2] and Karagiorgas and Meunier [20] found an increase in COP for a two adsorber cycle utilising internal heat regeneration as compared to the intermittent single adsorber cycle demonstrating the benefit of heat recovery. The two adsorber cycle is more than just the sum total of two single adsorber systems operating out of phase, since two heat recovery processes are involved whereby through each half of the cycle heat is regenerated from the bed being cooled to the bed being heated [2, 19]. However, as would be expected, a two adsorber cycle in the absence of a heat recovery process will have the same efficiency as the intermittent cycle [2]. Härkönen and Aittomäki [15] suggest that the main factors affecting the regeneration efficiency are the conductivity of the bed, thickness of bed and properties of the fluid chosen. They also calculate that for regeneration efficiencies below approximately 50% there is little gain in system performance and COP. Hajji and Khalloufi [21] also concluded following a parametric analysis that the cooling capacity could be increased considerably by reducing the bed thickness and increasing heat transfer between the bed and the heat exchange fluid.

Meunier [16] takes the idea of utilising a number of beds out of phase with internal heat regeneration a stage further; he considers an infinite number of beds each transferring heat ideally at the same temperature level. According to Meunier [16] the general objective of such cascade cycles is to reduce the entropy production of the system resulting from coupling irreversibilities between the external heat reservoirs and adsorbent beds, thus improving cycle performance. Using such an ideal system of cascades between given operating temperatures, Meunier [16] predicts a cooling COP of 1.85 equivalent to 68% of the ideal Carnot value, as opposed to a value of only 15% of the ideal Carnot value for the basic intermittent cycle. The ideal COP for an adsorption cycle is based on the Second Law of Thermodynamics. It takes into account the effective thermal capacitance of the heating cycle being greater than that for the cooling cycle, with the difference between the two being the non-recoverable work done in the cycle [8]. In practise, economics and complexity will limit the number of adsorbent beds utilised, with a diminishing return in COP improvement as the number of beds are increased above a certain level. Meunier [22] numerically predicted production of refrigeration at -10°C with a COP of 0.85 utilising double-effect cascading solid adsorption cycles, where beds running at a higher set of operating temperatures are used to transfer heat to beds running at a lower set of operating temperatures. He considered it difficult to obtain high COP values and low temperature refrigeration simultaneously.

An alternative approach to improving the COP is by using the so called thermal wave concept as investigated by Shelton et al [11] and discussed by Härkönen and Aittomäki [15]. For an anisotropic single bed system with a heat wave propagating along the adsorbent bed, Shelton et al [11] concluded that the closer the thermal wave front approximates to the ideal step wise behaviour, the smaller the reversal time during which no heating or cooling effect is achieved. For a thermal wave system the desired goal is to generate a steep temperature gradient, described as a thermal wave, in the same direction as the heat transfer fluid flow. This may be achieved by suitable design of heat transfer surfaces and choice of adsorbent bed material and construction, so that the rate of heat transfer between the heat transfer fluid and the adsorbent bed is greater than the rate of heat transfer along the path

of the fluid itself. In fact high axial thermal conductivity is actually detrimental to the performance of the thermal wave system [13]. This approach allows the majority of the adsorbent bed to be heated or cooled while maintaining a virtually constant heat transfer fluid exit temperature over a period of time.

Shelton et al [11] state that for cycle symmetry, the heat transfer fluid flow rate needs to be greater through the bed being heated than through the bed being cooled. The thermal wavefront propagates slowly from one end of the bed to the other. Due to its inherent regeneration of heat and ability to store high temperature heat from the cooled bed until required by the bed being heated, Shelton et al [11] predict large improvements in COP over previous system designs. They quote a cooling COP of approximately 0.8 and a heating COP of approximately 1.8 for the zeolite-ammonia pair used. Groll [23], states that at present thermal wave systems have achieved internal heat regeneration utilising isotropic reaction beds. However, anisotropic reaction beds should yield a considerable improvement in the rate of internal heat regeneration. IMPEX (Impregnated Blocks of Recompressed Expanded Natural Graphite) offers one possible form of anisotropic reaction bed where the heat conduction path along the graphite layers is considerably better than that across the graphite layers.

Critoph [24] mentions the use of a forced convection thermal wave system in order to improve heat transfer, predicting a heating COP of 1.3 with the possibility of achieving a heating COP as high as 1.9. In terms of improving COP by utilising internal heat regeneration Jones [8] predicted a cooling COP in excess of 1. For a carbon-ammonia pair operating on a 6 minute full cycle time Jones [8] measured a cooling power of 600 W kg^{-1}, which is a considerable improvement in terms of achieving cooling powers in the region of 1 kW kg^{-1}. The cycle time is also much improved on values achieved by other researchers as a result of major improvements in heat transfer and bed thermal conductivity. Following porosity testing Critoph and Turner [17] suggested that heating and cooling times in the region of 15 minutes could be achieved without too much difficulty, yielding times in the region required for a rapid cycling machine.

In terms of being competitive with conventional electrically driven vapour-compression CFC systems, as far as primary energy consumption is concerned, Meunier [13] suggests that cooling COPs in the vicinity of 1 and cooling powers in the range from 300 W kg^{-1}–1000 W kg^{-1} need to be achieved. In order to achieve higher cooling powers Meunier [13] indicates that the three main parameters to be considered are thermal conductivity, heat transfer coefficient and permeability. These factors may be improved to a certain extent by the use of composite materials, consolidated beds and design of heat transfer surfaces to optimise the bed properties as required. Additionally, internal heat regeneration between two or more adsorbent beds allows continuous cooling to be achieved with improvements in COP.

Even with the inclusion of heat conduction matrices to improve bed conductivity, Groll [25] still found the specific power outputs obtained to fall short of the desired goal of 1 kW kg^{-1}. Regardless of that fact, 1 kW kg^{-1} is by no means the upper limit of cooling power density. Suzuki [6] estimates that if a global heat transfer coefficient approaching 100 kW $m^{-2}K^{-1}$ is realised then a cooling capacity of 2.8 kW kg^{-1} could be achieved. Meunier [13] certainly considers this level of global heat transfer coefficient to be attainable, based on the research conducted by other investigators utilising chemical reactions and consolidated adsorbers. This is reinforced by the fact that utilising complex compound systems and enhanced reaction beds, power densities of 2.5 kW kg^{-1} have been obtained by some researchers [23].

However, as Critoph [5] points out, the COP of the system in many cases may not be the most important consideration particularly if the system is designed for the needs of the developing countries in which case simplicity, reliability, robustness, low cost and ease of maintenance may be the dominating factors. In general it will be possible to increase the COP but this will normally be at the expense of one or more of the factors named above. As a general comparison, the COP of intermittent sorption machines is generally in the range 0.2–0.5, for intermittent regenerative cycles it is up to approximately 0.7, while conventionally driven electrical vapour-compression cycles yield typical COP values from

1.0–1.5 [5]. However, if the COP is considered in terms of primary energy usage, although thermally driven refrigeration machines may have lower COP values, overall they may still be competitive with conventional vapour-compression systems.

Ideally the chosen refrigerant should have a high enthalpy of vaporisation, so as to maximise the cooling effect achieved, while also having a low specific heat capacity to reduce the sensible heating required. However, the properties of high latent heat and high specific heat capacity tend to be found together and thus to a certain extent the drawbacks of high specific heat have to be accepted [18]. As Critoph and Turner [17] also point out, one of the most desirable refrigerant properties is to have as high a volumetric latent heat as possible so as to maximise the heat input and outputs during evaporation and condensation processes. The sensible heat of the refrigerant does not contribute to the cooling or heat pumping effects and is thus thermodynamically wasted in the cycle. In terms of the adsorbent, again a low specific heat capacity is desirable in order to minimise the sensible heating required. However, the adsorbent chosen should give the largest change in adsorbate concentration possible between the upper and lower generating temperatures. In analysing the thermodynamics of adsorption cycles Critoph [18] concludes that further increases in refrigerant latent heat and concentration change, exceeding values of 1000 kJ kg^{-1} and 10% respectively, yields little further increase in cycle COP.

When designing an adsorption refrigeration system or heat pump the sizing of the various components may also influence the operation and performance of the system. In a parametric study carried out by Douss et al [19] it was concluded that for an undersized evaporator the evaporation temperature of the refrigerant will be considerably lower than that of the evaporating load. This temperature mismatch leads to a reduction in the overall cycle performance. Additionally Shelton et al [11] found the size of the adsorption bed heat exchanger to be of major importance as its thermal mass could have a considerable detrimental effect on cycle efficiency.

In conclusion, a number of researchers have investigated a range of thermodynamic cycles of varying complexity relating to adsorption systems. It is suggested that by operating

two or more adsorbent beds out of phase, continuous/semi-continuous cooling can be achieved. The cycle temperatures are seen to be fundamental in determining temperature swings, concentration changes and hence cooling powers and overall cycle efficiency.

2.3 Heat and Mass Transfer

For adsorption systems, whether they are applied to refrigeration or heat pumping applications, the heat and mass transfers within the system are critical to the level of performance achieved. Improvements in the heat transfer into and out of the adsorbent beds is of importance in order to reduce cycling times and thus reduce the adsorbent-adsorbate inventory required for a given cooling power. Reductions in adsorbent and adsorbate also leads to a reduced sensible heating requirement and therefore increased thermal efficiency. The thermal conductivity of the bed material itself is of vital importance if cycling times are to be reduced. Many methods have been proposed for improving bed conductivity but these need to be weighed against the porosity and permeability properties of the bed. Improved bed conductivity allows the system to be more responsive to heat fluxes. Hence if at all possible this should be maximised as increasing overall bed conductivity should prove to be the most worthwhile in terms of increasing specific power outputs [26]. Mass transfer through the bed material is also of importance in terms of the speed of adsorption and desorption as the adsorbate diffuses through the bed material.

A number of methods have been put forward by various researchers in order to improve bed heat and mass transfer, some of which are quite advanced high technology solutions. As the purpose of the present research is to design an ice maker for use in developing countries, it is important to maintain a balance between improving system performance and satisfying the requirement for a simple, robust system as required by developing countries.

Aittomäki and Härkönen [27] mention that the physical processes within the adsorbent bed are complex, involving simultaneous heat and mass transfers, with the material properties varying depending on the amount adsorbed. However, they assume that if the capacities of the evaporator and condenser are large enough the pressure can be considered

constant throughout the adsorption and desorption phases of the cycle. Aittomäki and Härkönen [27] also found that the thermal conductivity of the zeolite bed they used was low, limiting the level of heat transfers. In order to achieve shorter cycling times either the bed thermal conductivity needs to be increased or the bed thickness reduced [27].

Aittomäki and Härkönen [27] suggest increasing the heat transfer within the adsorbent bed by utilising a metal matrix or network. This would increase the bed thermal conductivity but it would have to optimised so as not to excessively increase the level of sensible bed heating required or adversely affect bed porosity and permeability. The use of a mixture of metal granules and zeolite granules is also suggested for improving bed heat transfer, however this approach has been shown to be relatively ineffective by researchers such as Turner [28] due to the discontinuous conduction path created by point contact between granules.

Cacciola et al [29] have also investigated heat and mass transfer in relation to adsorption systems, which they consider to be of vital importance to successful operation. Many physical conductivity enhancements have been proposed varying from the addition of conductive powders and granules, creating more consolidated beds, addition of expanded graphite or graphite fibres, addition of metallic foams, sintering in metallic powders to general metallic inserts. Cacciola et al [29] also indicate that the thermal contact between the heat exchange surfaces and the bed itself is vital for good system performance and therefore elected to use a solid block of adsorbent material.

It is also important when using consolidated adsorbent beds that mass diffusion is not adversely affected, and thus the adsorbate can be readily adsorbed and desorbed while passing to and from the condenser and evaporator. Some researchers suggest utilising porous gas tubes, channels or arteries within the solid adsorbent bed to improve mass transfer [23, 29]. Additionally slots and channels may be cut in the heat transfer surfaces to promote mass transfer [30]. Overall, in order to improve the heat transfer between the heat transfer fluid and the bed itself, the thermal conductivity of the bed needs to be increased as well as the rate of heat transfer between the heat transfer surfaces and the bed [9, 29].

Heat transfer fluids generally used include silicon based thermo-oils, water and steam. The advantage of utilising a heat transfer fluid is that the source of heat is then relatively independent of the system. Hence, a number of different heat sources, whether they be solar, bio-fuel, natural gas or alternative low grade heat sources can be used to provide a heat input for the system.

Critoph and Gong [31] state that steam has the advantage of providing very high heat transfer rates when condensing on the adsorber surface while also allowing the steam to be relatively easily switched between adsorbent beds for heating multi-bed systems. For cooling of the adsorbent bed and condenser, high external heat transfer rates can be achieved by utilising fluids such as water [23]. In terms of increasing the thermal conductivity of the bed itself the most promising approach would appear to be the use of solid monolithic blocks of adsorbent. A solid block of adsorbent also enables a better physical contact with the heat transfer surfaces than can be obtained with powders or granules. The better the fit at the adsorbent heat transfer surface interface the better the heat transfer. Hence, if at all possible the adsorbent blocks should have smooth regular surfaces and fit tightly within the heat exchanger.

The heat transfer to and from the adsorbent bed can be optimised by selection of a suitable heat exchanger. Cacciola et al [29] chose to use a plate type heat exchanger, building the bed from a stack of solid adsorbent bricks and heat exchanger plates. This provides good thermal contact between the adsorbent and the heat transfer surfaces. Increased resistance to mass transfer was overcome by cutting channels into the adsorbent blocks to promote mass diffusion [29]. Some researchers have employed copper heat exchangers [29]. However, this is not possible for ammonia systems as the two materials are incompatible. Cacciola and Restuccia [9] and Meunier [13] mention a number of different types of heat exchanger including finned tube, plate and shell and tube. Shell and tube heat exchangers have the advantage of being relatively cheap and easily available and have been used by a number of researchers. It is difficult to obtain a good thermal contact between the fins of the heat exchanger and the adsorbent bed material. However, if some method

for forming the fins and consolidated adsorbent together could be found thus binding them more tightly together this problem could be minimised.

As mentioned above, Cacciola et al [29] chose to use a plate type heat exchanger where the thermal contact was improved by the pressure differential between external atmospheric pressure of the heat transfer fluid and the sub-atmospheric pressure of the adsorbent bed. Mention is also made of a flat pipe heat exchanger where a flat pipe duct is folded back and forth over itself to form a serpentine structure. The adsorbent blocks can then placed between the folds of the duct. Although this type of heat exchanger solves the problem of heat transfer [9], as it is not produced on a commercial scale and would be relatively difficult to manufacture, its cost would in all likelihood be prohibitive for uses in developing countries. Additionally, with such a system some form of pump would be required to circulate the heat transfer fluid, increasing both the cost and complexity of the system.

It is desirable to minimise the thermal mass of the system so as to reduce the sensible heating required. Obviously, additional heat transfer structures will add to the sensible heating required thus reducing system performance. Hence the ratio of heat exchanger mass to that of adsorbent should be kept as low as possible while achieving the best improvements in heat transfer possible. A novel method for improving heat transfer through the adsorbent bed has been proposed by Critoph [24, 32]. This involves utilising forced convection to yield higher heat transfer rates by pumping the adsorbate in alternate directions through the adsorbent bed. However, this system is considerably more complex than more conventional systems and the requirement for a pump would reduce its suitability for use in developing countries.

The importance of bed thermal conductivity is stressed by Cacciola and Restuccia [9] as they indicate that for regenerative cycles it should be one of the main areas for further investigation. They summarise a number of conclusions reached by other researchers in the field. The conduction path can be improved by increasing the area of adjacent particles in contact with each other. This can be accomplished by using consolidated adsorbents

formed into bricks, blocks or other shapes as required where the particles are packed more closely together. If additives such as graphite or metallic foams are to be used they must satisfactorily bound in with the adsorbent itself. All researchers agree on the fact that heat and mass transfer considerations can have a dramatic effect on the overall performance of adsorption machines. Groll [23] considers the heat and mass transfer properties not solely as material properties but also being improved by suitable bed design and solid adsorbent treatment. Groll [23, 25] also discusses the use of a number of the thermal enhancement structures mentioned earlier such as metallic foams, internally finned tubes, metallic honeycombs and the use of encapsulated adsorbent material. These structures can be used to achieve a significant increase in bed thermal conductivity even for powder based or granular beds [23]. IMPEX is also seen to be effective at improving heat transfer. For the structures mentioned, porous gas distribution tubes were inserted through the structures to improve mass transfer.

In relation to metal hydrides, metal powder may also be mixed in with the hydride followed by compression and optional sintering to improve conductivity [23]. The thermal contact resistance between the adsorbent bed and bed wall can be reduced by using metallic foams or anisotropic graphite matrices which are well bonded to the bed walls [23]. The use of consolidated beds and metallic foams for improving bed conductivity are also mentioned by Guilleminot et al [33]. They suggest that performance can be improved to a certain extent with granular beds by utilising bimodal mixtures to reduce the voids and porosity between grains thus improving thermal conductivity. The grain size may also be reduced in order to improve the wall heat transfer coefficient. However, only small improvements in thermal conductivity tend to be obtained for bimodal mixtures of the low conductivity materials that are generally found as adsorbents [34]. Metallic foams can be combined with granules to improve conductivity but these tend to suffer from high thermal contact resistance between the foam and the granules.

However, technical and economical exploitation of adsorption heat pumps requires an improvement in the heat exchange from the external heat transfer fluid to the adsorbent bed itself [35]. Due to the inherent limitations of unconsolidated granular beds many

researchers believe that consolidated beds offer the best option. Guilleminot et al [33] describe the use of a compact composite material consisting of a consolidated mixture of a metallic foam combined with zeolite. With this combination the conductivity was enhanced by the presence of the metallic foam while the consolidation reduced the thermal contact resistance between the metallic foam and the adsorbent. The temperature gradient for the consolidated bed was found to be less than for a granular bed indicating a lower internal thermal resistance and thus improved thermal conductivity [33]. The heat transfer coefficient between the adsorbent and the bed wall was also found to be significantly improved. However, as would be expected the consolidation process was found to decrease mass transfer while increased bed packing was also found to reduce axial permeability.

According to Jones [8] relatively short cycle times and increased thermal conductivity were achieved by moulding the chosen carbon adsorbent to a finned aluminium tube using a specially formulated binder. Calculations showed the thermal resistance to be greater through the fins than from the fins to the carbon. Shell and tube heat exchangers may be used for other system components such as the condenser and evaporator. Mention is also made by researchers such as Hinotani et al [36] and Spinner [37] regarding the use of heat pipes to improve heat transfer within adsorbent beds.

The use of inert graphite binders to increase adsorbent bed thermal conductivity is discussed by Mauran et al [38]. Three different graphite binders and two different mixing techniques were investigated. The two mixing methods used were SOLDEX (mixing in the solid phase) and IMPEX (impregnation of adsorbent). The IMPEX technique was found to be the better of the two giving higher thermal conductivity and allowing the use of higher densities without encountering mass transfer problems. Spinner [37] also discusses the use of anisotropic porous blocks such as IMPEX in reducing cycling times. These anisotropic adsorbent blocks are manufactured by combining consolidated adsorbents with expanded graphite thus improving bed conductivity significantly.

Meunier [13] categorises the choice of adsorbent bed as either unconsolidated or consolidated. With unconsolidated beds consisting of powders or granules, the bed

conductivity and wall heat transfer coefficients tend to be low. Hence, the cooling powers achieved per mass of adsorbent also tend to be relatively low. Although the properties of the bed can be improved by the addition of devices to increase thermal conductivity, the gains achieved are not really sufficient. Hence, Meunier [13] considers that unconsolidated beds will only be useful in the future for applications such as storage and delayed cold production.

Consolidated beds on the other hand, such as monolithic activated carbons, offer the possibility of large increases in bed conductivity. The beds are consolidated by the use of a suitable binder. Mauran et al [38] report a value for bed thermal conductivity as high as 40 $W\ m^{-1}K^{-1}$ which is considerably larger than the best values obtained for unconsolidated beds. Consolidated beds also yield considerable improvements in the bed-wall heat transfer coefficient as a result of the improved thermal contact. Hence, consolidated beds should allow large increases in cooling powers per mass of adsorbent to be obtained. However, steps need to be taken to ensure that the mass transfer through the bed is not adversely affected. Reduction in mass transfer with increasing bed consolidation can be counteracted, as mentioned previously, by including channels within the adsorbent to promote mass diffusion.

Meunier [13] mentions the fact that consolidated materials which ordinarily would be thought of as insulators, such as activated carbon, have been improved in such a way as to give values for thermal conductivity usually associated with metals. Such improvements in conductivity should allow considerably higher specific cooling powers to be obtained.

In conclusion, the heat and mass transfer through the adsorbent material is critical to overall performance. Many methods of varying complexity have been suggested for improving the adsorbent thermal conductivity although there are generally trade-offs with bulk porosity, permeability and mass transfer. Some methods of improving mass transfer are also suggested. A range of heat sources, heat transfer methods and heat exchanger configurations are also discussed.

2.4 Adsorption Pairs

When designing an adsorption system, suitable adsorbent and adsorbate combinations need to be selected depending on the final application and any specified constraints. There are a wide range of possible adsorbates but the choice will also be governed by factors such as enthalpy of vaporisation, vapour pressure, polarity (small polar molecules desirable), molecular weight, viscosity, diffusivity, boiling point, toxicity, compatibility, availability, stability, flammability, corrosiveness, thermal conductivity, environmentally friendliness, legal restrictions and cost. Therefore in selecting a suitable adsorbent-adsorbate pair as many of the above factors as possible need to be taken into consideration. Additionally, some adsorbent-adsorbate pairs may not be suitable due to stability problems involving catalysis and chemical decomposition.

Ideally, the chosen adsorbate should have a vapour pressure slightly higher than atmospheric at the evaporation temperature. Also, the vapour pressure at the condensing temperature should not be excessively high so as to minimise the size and strength of system components required. The chosen adsorbate should also have a high specific latent heat so as to minimise the mass of adsorbate required and hence reduce the sensible heating requirement. An in depth review of several possible adsorbates has been carried out by Cacciola and Restuccia [9]. Ammonia, formaldehyde, sulphur dioxide, water, sulphur trioxide, methanol, ethanol, acetonitrile and methyl amine are characterised listing their attributes such as normal boiling point, density and heat of vaporisation. Sulphur trioxide is immediately rejected because of its chemical instability.

Based on their properties water, ammonia and methanol are selected as the most desirable adsorbates. All have high latent heats, 2258 kJ kg^{-1}, 1378 kJ kg^{-1} and 1102 kJ kg^{-1} respectively, but their working pressures are not considered to be in a favourable range. In comparing these three adsorbates Cacciola and Restuccia [9] see water as being the perfect option due to properties such as high specific latent heat, thermal stability and lack of toxicity. However, water systems are not ideal for cold production below 0°C effectively ruling them out for ice making applications.

Methanol offers the benefit of a decent specific latent heat, although lower than that of either water or ammonia. However, methanol has a number of negative aspects including toxicity, flammability, incompatibility with copper at higher temperatures, low vapour pressure and chemical instability and decomposition at higher temperatures.

Ammonia has a specific latent heat between that of methanol and water while being thermally stable, non-polluting and operating at pressures higher than atmospheric. The negative aspects of ammonia use include its toxicity, incompatibility with copper and the fact that it is flammable in certain concentrations with air. Additionally, the use of ammonia is forbidden or restricted in countries such as Japan and Germany while being widely used in countries such as the UK and USA [9].

Meunier [13] gives an overview of the pros and cons of a number of refrigerant adsorbates. Water would be ideal based on its high enthalpy of vaporisation, stability and non-toxicity. However, it has the drawbacks of generating very low system pressures below atmospheric thus necessitating a hermetically sealed unit and the need for anti freeze additives for low temperature refrigeration. Ammonia has the advantages of high enthalpy of vaporisation, stability, wide temperature range and low freezing temperature. Unfortunately, it has drawbacks in use such as odour, corrosion and safety risks due to high operating pressures and flammability in certain concentrations. Alcohols such as methanol and ethanol have been proposed as possible adsorbates based on their high enthalpies of vaporisation, although lower than those for ammonia or water. However, alcohols tend to become unstable at higher operating temperatures resulting in thermal decomposition as well as requiring the use of hermetically sealed units. Finally, hydrogen is considered as a possibility (in combination with metal hydrides) due to its easy availability, ease of mass transfer and heat of reaction. An obvious hazard of utilising such a system is the possibility of a hydrogen leak leading to an explosion, particularly as very low levels of static electricity can result in hydrogen ignition. Following a numerical simulation Sun et al [39] concluded that for low density adsorbates such as water or methanol, and large adsorbent beds, mass transfers are an important consideration whereas for an ammonia system, where the operating pressures are much higher, resistances to mass transfer may be considered

negligible. Therefore, ammonia is a more desirable adsorbate from the point of view of mass transfer and better suited than water or methanol to lower permeability densely packed consolidated beds.

Critoph [18] has also carried out a detailed study of possible adsorbates listing sixteen possible refrigerants by boiling point, latent heat and density. A figure of merit is also given based on the product of the liquid density and enthalpy of vaporisation. Based on this the best adsorbates would appear to be water, ammonia, sulphur trioxide and methanol in decreasing order of merit. One of the most important adsorbate criteria is high latent heat. Since the Dubinin-Radushkevich (D-R) equation, as given in equation (3.3), describes carbon pore filling as a volumetric process, latent heat per unit volume would appear to be a more important adsorbate parameter than latent heat per unit mass [18]. The physical mechanism of volume pore filling is described in more detail by Turner [28]. Water would appear to be the ideal adsorbate particularly with the highest latent heat of the adsorbates investigated by Critoph [18]. Unfortunately, for evaporating temperatures below about 10°C the very low vapour pressure and problems of freezing make it difficult to use for refrigerating applications. Although water has been evaporated out of ethylene glycol solution achieving temperatures as low as -15°C it is too difficult to achieve practically without unduly increasing the system complexity. After a process of elimination, Critoph [18] decided on ammonia, sulphur dioxide and formaldehyde as the best high pressure adsorbates and methanol, nitrogen dioxide, acetonitrile and methyl amine as the best low pressure adsorbates. Within these two groups of high and low pressure adsorbates, ammonia would appear to offer the best high pressure characteristics and methanol the best low pressure characteristics. However, methanol was found to give the highest values for COP of the adsorbates tested.

Critoph and Vogel [40] considered the use of a number of organic adsorbates such as hydrocarbons, halogenated hydrocarbons and CFCs in conjunction with adsorbents such as zeolite and charcoal. Certain advantages were found compared to an ammonia-water liquid absorption system, such as compatibility with copper. However, with greater understanding of ozone layer depletion, CFCs and HCFCs are no longer acceptable for use as refrigerants

although other organic refrigerants may still be used. In fact one of the main advantages of adsorption systems is that they can readily use safer alternatives to CFCs and HCFCs such as water, methanol or ammonia, which generally offer higher specific latent heats. For each of the adsorbent-adsorbate pairs tested [40], activated charcoal was found to be preferable to zeolite both in terms of efficiency and cost.

There are a number of different adsorbents available, the choice depending on factors such as porosity, permeability, conductivity, heat capacity, compatibility, availability and cost. There are three main types of solid-gas sorption systems depending on the type of solid adsorbent chosen. They may be classified as systems using physical adsorbents such as active carbon or zeolite, those using chemical compounds which undergo a chemical reaction such as calcium chloride and those based on the dissolution of hydrogen in metal hydrides [13]. Alternatively they may utilise a complex composite adsorbent consisting of a mixture of physical and chemical adsorbents with the inclusion of heat transfer enhancing structures.

According to Meunier [13], physical adsorption and chemical reaction systems are preferable for air conditioning or water chilling, chemical reaction systems for refrigeration down to -20°C and chemical reaction or metal hydrides for deep freezing between -30°C and -40°C. The adsorbent may also be in the form of a powder, granules or a consolidated block as mentioned in the previous section. The adsorbent should have a low specific heat capacity to reduce to sensible heating requirement. It should produce a large change in adsorbate concentration between the operating generating temperatures thus maximising the mass of adsorbate desorbed through each cycle while improving the cooling power.

Cacciola and Restuccia [9] briefly examine possible adsorbents. Essentially, suitable adsorbents should be highly porous and capable of adsorbing large quantities of adsorbate in the vapour phase. Additionally they should provide a large change in adsorbate concentration over a relatively small temperature range, be capable of operating over many cycles without degradation to performance, have a low cost while also having good thermal conductivity. In general, activated carbons, natural and synthetic zeolites and silica gels may

come in a different form depending on the characteristics such as porosity, permeability and consolidation required. For a given type of adsorbent material, smaller pore diameters results in increased adsorption energy and regeneration temperature [9]. Cacciola and Restuccia [9] consider zeolite-water, activated carbon-methanol and activated carbon-ammonia pairs to be the most suitable for heating and cooling applications. Suitable adsorbent-adsorbate combinations are given for applications such as freezing, refrigeration, air conditioning, space heating and industrial heat pumping.

According to Critoph [18], who also discusses possible adsorbents, although silica gel adsorbents have been used previously by other researchers [41] the vast majority of knowledge is based on the use of zeolites and activated carbons. Three main reasons are given for preferring to use activated carbons rather than zeolites. Activated carbons are actually cheaper than zeolites thus reducing the overall system cost. Activated carbons can be manufactured with the desired properties suitable to the final application by varying parameters such as activation time, activation method and temperature. However, as mentioned previously synthetic zeolites can also be manufactured to give the required pore diameter. Finally, the activated carbon can be manufactured from a number of different starting materials such as coconut shell and coal. This allows the activated carbon to be manufactured in the country of origin and use which is particularly advantageous for developing countries where overseas products may prove to be too expensive.

The most commonly chosen adsorbent-adsorbate pairs are active carbon-methanol [2, 7, 42], active carbon-ammonia [8, 24, 30], zeolite-water [4, 29, 43], zeolite-ammonia [11] or chemisorption with chemical pairs such as calcium chloride-ammonia [14] or manganese chloride-ammonia [37]. Some research has been carried out into the use of chemisorption although the bulk of adsorption research has concentrated on physical adsorbents. Physical adsorption systems are not prone to the same long term corrosion problems as chemical adsorption systems since the physical adsorbent itself, whether it be carbon or zeolite, is completely unreactive to metal containment vessels [8]. Additionally, physical adsorbents have the advantage of maintaining a constant volume during adsorption and desorption processes.

Aittomäki and Härkönen [27] chose to use a zeolite-methanol combination. Zeolites are highly microporous crystalline aluminosilicates which are available in both natural and synthetic forms. The size of the pores can be well controlled so that the pore size can be maintained constant. This inherent ordered pore microstructure gives zeolites sorptive properties which are unique [27]. Methanol was chosen as an adsorbate due to its vapour pressure range while allowing evaporation temperatures below 0°C to be obtained. Aittomäki and Härkönen [27] experienced problems with the synthetic zeolites 5A and 13X in pellet form. Using the 5A-methanol combination at higher temperatures a part of the methanol was decomposed catalytically into a number of hydrocarbons. Douss and Meunier [42] and Pons and Guilleminot [7] also state that the zeolite-methanol pair is unstable since as a result of a catalytic reaction dimethylether and water are produced. Although Aittomäki and Härkönen [27] found the 13X-methanol pair to be more stable, at maximum desorption temperatures above approximately 230°C a similar catalytic decomposition was found to occur. Methanol is a good choice of adsorbate for ice production as it evaporates below 0°C, it has a small molecule which is easily adsorbed, has a high enthalpy of vaporisation and is non-corrosive [7]. However, due to methanol instability the active carbon-methanol pair is limited to regeneration temperatures in the region of 150°C [42]. Nevertheless, for refrigeration purposes Douss and Meunier [1] concluded that an active carbon-methanol pair was the best option. For low temperature solar refrigeration Meunier and Mischler [44] also found the 13X-methanol pair to be quite satisfactory.

A number of adsorbent-adsorbate couples are compared by Bougard [45] such as silica gel-R12/R22, zeolite 13X-water, activated carbon with methanol, ethanol or ammonia and calcium chloride-ammonia. The three most promising couples are described as zeolite-water, active carbon-methanol and active carbon-ammonia. The zeolite-water pair is described as unsuitable for refrigeration purposes while requiring higher operating temperatures. Cacciola et al [29] utilised a zeolite-water pair for heat pumping using consolidated zeolite bricks to improve conductivity and heat transfer. Researchers such as

Meunier [43] have also used zeolite-water for solar refrigeration and ice production with some success.

Bougard [45] sees the active-carbon-methanol and active carbon-ammonia pairs as being comparable, the methanol system operating under vacuum and the ammonia system operating above atmospheric pressure. Since the adsorption, evaporation and condensation processes are more efficient when the adsorbate is the only vapour present, ideally the machine needs to be totally leak proof [7]. However, for an ammonia system any leaks would result in a loss of ammonia from the system but might still allow the system to continue operating at a lower level of performance. The operating pressure difference for an ammonia system is considerably higher than that for a methanol system necessitating a larger and more robust construction.

Alternative adsorbent-adsorbate pairs have been investigated by Critoph [46]. The two alternatives to ammonia investigated, R32 (difluoromethane) and R600 (butane), were found to give lower values for the COP. However, R32 is suggested as a possible refrigerant should low toxicity and the ability to use copper components be of more importance than COP. R600 was found to give poorer performance than R32. Critoph [46] has also tested a granular carbon, monolithic carbon and a PVDC based carbon block in order to compare performance. The COP was found to be higher for the monolithic and PVDC carbons while also enabling the pressure vessel volume to be reduced. Tamainot-Telto and Critoph [30] also predicted that for the same generator volume the cooling powers obtained with a monolithic carbon would be considerably higher than those obtained with a granular carbon. Jones [8] also compared ammonia and two alternatives, R22 and R134a, as possible refrigerants with a activated carbon adsorbent but found the ammonia to give by far the largest cooling capacity.

Bougard [45] mentions the possible advantages of using a chemical adsorption system based on a monovariant chemical reaction. In such as system utilising calcium chloride-ammonia the ammonia is desorbed at two well defined temperature levels. However, for such chemical adsorption systems the chemical reaction causes swelling which leads to very

large expansion of the adsorbent reactant by up to 400% [45]. This leads to problems in designing a system to contain the adsorbent, problems in compacting the adsorbent and the possibility of adsorbate degradation after many repeated cycles of swelling and shrinkage leading to voids and hardened regions of adsorbent where the adsorbate is unable to penetrate. Additionally, Spinner [37] found that for a manganese chloride chemical reactant, swelling of the salt resulted in a ten fold reduction in permeability. However, Worsøe-Schmidt [14] claims that for the calcium chloride-ammonia pair following treatment of the calcium chloride with a salt soluble in ammonia the resulting sorbent is mechanically stable and does not shrink. Although there are problems associated with applying chemical adsorbent systems Meunier [13] predicts that future chemical reactor designs will improve the results obtained.

For solar refrigeration, following a survey of possible sorption pairs Worsøe-Schmidt [14] found that in terms of both efficiency and simplicity a calcium chloride-ammonia pair offered the best solution.

According to Jüntgen [47], carbonaceous adsorbents are highly porous substances consisting mostly of carbon with a large internal surface area. Following further processing steps necessary for technical applications, such as activation to develop the required pore structure and surface properties, these materials with specific individual qualities are known as activated carbons. Jüntgen [47] states that carbonaceous adsorbents adsorb selectively non-polar rather than polar components. This would seem sensible based on the fact that activated carbons are used to remove organic impurities from water which is highly polar. However, a number of researchers have also implied that the more polar the adsorbate the better the adsorption. This would also seem to be logical as a more polar molecule would tend to form a stronger van-der-Waals bond and thus be adsorbed more easily and in higher concentrations.

Activated carbons may be manufactured from a number of different starting materials such as wood, peat, coals (lignites, bituminous coals and anthracites), coke as well as coconut shell, soft fruit stones (peaches, apricots, etc.) and agricultural or industrial organic

by-products [47, 48]. The raw starting materials may be activated either by chemical activation by mixing in a chemical additive such as zinc chloride with the organic precursor or more commonly by gas activation utilising oxidising gases such as carbon dioxide or steam to activate the pyrolysed starting material. The pore system within the subsequent activated carbon is subdivided into pores of varying sizes; macropores, mesopores and micropores. Micropores are defined as pores having a width less than 2 nm, mesopores as having a width between 2 nm and 50 nm with macropores having pore widths larger than 50 nm [49]. The larger pores, macropores and mesopores, are seen as diffusion pores which enable the adsorptive molecules to reach the internal surface of the carbon. The smaller micropores are adsorption pores where the molecular adsorptive is adsorbed onto the internal surface of the carbon. For an activated carbon the objective is to achieve the optimum ratio of diffusion pores to adsorption pores so as to achieve rapid transport of the adsorptives to the internal surfaces while also achieving a high micropore internal surface area to ensure a high adsorption capacity [47].

By careful selection of the starting material and subsequent control of the activation process it is possible to adapt the properties of the carbon, such as pore size distribution, to the desired end application. Active carbons in common with zeolites also tend to produce a molecular sieve action with carbons exhibiting preferential adsorption of smaller or flatter molecules which is consistent with the idea of slit shaped carbon micropores [48]. McEnaney and Masters [48, 50] describe the properties and structure of microporous carbons in more detail. Critoph and Turner [17] investigated a large number of different activated carbons ranging from powders, granules and extrusions to preformed carbons and carbon textiles. The porosity characteristics of the various carbons are seen as being crucial to performance. Ammonia is suggested as an adsorbate for use with activated carbons due to both its chemical stability and desirable thermophysical properties [17].

Jüntgen [47] mentions that for systems with a high adsorption energy the adsorption and desorption processes are not completely reversible where even at high temperatures a residual load of molecular clusters may remain on the adsorbent surface which act as catalysts. However, these strongly adherent molecular clusters can be removed by oxidation

at higher temperatures, the process of which is known as adsorbent reactivation. This would appear to be the principle behind the surface treatments performed by Critoph [51]. In order to improve the performance of active carbons and the change in adsorbate concentration they are able to achieve, researchers such as Critoph [51] and Turner [26] have suggested the addition or removal of surface oxygen sites on the carbon. Critoph [51] found that air and argon treatment of two active carbons yielded an increase in the concentration change achieved. As well as investigating air and argon treatments Turner [26] carried out a cold chemical treatment using hydrogen peroxide to add surface oxygen groups and found it to yield a considerable improvement in the figure of merit based on the change in adsorbate concentration between two temperature levels. Hence, this is one way in which the adsorbent properties of activated carbons might be developed further.

In conclusion, there are many different adsorbent-adsorbate combinations available, each with a different set of characteristics and operating temperature ranges. An adsorption pair consisting of a monolithic activated carbon and ammonia would seem to offer the most desirable properties. Activated carbons are readily available, in theory can be manufactured from local organic materials, have good adsorption properties and when formed into consolidated blocks also provide good thermal conductivity and heat transfer. Ammonia offers the benefits of high enthalpy of vaporisation, easy availability, stability and operating system pressures above atmospheric.

2.5 Solar Applications

Solar refrigerators combine a conventional refrigeration system with a method of collecting solar energy. Solar energy may either be converted into electricity and used to power a conventional cycle or harnessed directly within a heat driven cycle. Heat driven adsorption refrigeration cycles are ideally suited to solar applications since in the climates where the insolation is the greatest there is generally the greatest demand for cooling. Heat driven adsorption cycles can either be driven directly by solar heat where the heat is used directly for desorption or via a heat transfer fluid such as steam. Higher performance systems may also utilise parabolic solar collectors to increase the temperature of the solar source heat

[43]. In general, solar adsorption refrigerators are operate intermittently on a diurnal cycle where refrigerant is generated during the day and boiling of the refrigerant overnight produces the cooling effect. Hence heat losses from the solar collector need to be minimised during the day during the desorption period and maximised during the night during the adsorption period. Heat rejection at night may be improved by the addition of shutters or dampers to the solar collector which can be opened to reject heat by natural convection [43, 52]. In developed industrialised countries the main application of solar cooling is for air conditioning.

In remote areas of the developing world, where there is no electricity supply, vaccines still need to be maintained in the temperature range from 4°C to 8°C for use in immunisation programs [53]. The World Health Organisation (WHO) in its Expanded Programme of Immunisation identified several years ago the need for solar refrigerators in rural areas of developing countries without electrical infrastructure for maintaining the vaccine cold chain [54]. There is also the need for large scale ice production for preservation of agricultural foodstuffs and fish catches. Hence the cooling requirement in developing countries are polarised between small scale but high value cooling for medical supplies on the one hand and large scale but low capital cost cooling for food preservation on the other [5]. Generally, solar powered systems are advantageous in situations where higher energy density fuel sources such as biomass, oil, gas, kerosene or electricity are not available. If reliable fuel sources are not locally available then solar power refrigeration units offer a practical alternative.

Solar refrigerating machines are of interest both in the developed and developing world. Increasing environmental awareness has lead to a drive to improve renewable energy utilisation and reduce fossil fuel consumption and greenhouse gas emissions. Drastic reductions in carbon dioxide emissions are required to limit the effects of global warming such as polar ice cap depletion, glacial retreat and rise in mean sea level. In developing countries solar energy offers a freely available energy source while providing an alternative energy route to that followed by the industrialised nations.

Three groups of solar refrigerating machines may be considered consisting of photovoltaic powered vapour compression systems, heat driven liquid absorption systems and heat driven solid adsorption systems. However, as solar refrigerating machines are generally utilised in developing countries, the solid adsorption system tends to offer the most desirable attributes of simplicity, reliability and robustness. For commercial machines, the COP is often of prime importance as it is related to the overall capital cost of equipment. However, for solar machines utilised in developing countries the system specification tends to be of greater importance than overall efficiency. Solar adsorption cooling is suited to areas where cooling or refrigeration is required, where there is poor electrical infrastructure to drive conventional systems and where there is a good availability of solar energy. Ideally the system should be driven only by solar heat and should be simple, reliable, robust, autonomous and cost effective.

The majority of solar refrigeration systems built to date have been photovoltaic powered systems which tend to be expensive due to the cost of the solar panels, storage batteries and ancillary electronic control equipment [55, 56]. Adsorption systems offer the advantages of no moving parts, and hence negligible vibration, which results in increased system life and reliability. Additionally, adsorption systems do not require complex high tolerance manufacturing or complex system components. This allows the cost of adsorption systems to be kept at a relatively low level. Due to the technology involved the adsorption system could also be manufactured and maintained in the developing country of use without the need to rely on expensive replacement components from overseas.

In developing countries where there is no firm electricity supply, kerosene powered absorption refrigeration systems are used for cooling applications such as vaccine storage. However, the availability and quality of the kerosene supply tends to vary thus photovoltaic systems have been evaluated as an alternative. Unfortunately, the photovoltaic systems have been found to be considerable more expensive and less reliable. Hence, an alternative refrigeration system is required which is simpler, cheaper and requires less maintenance . Solar powered liquid absorption or solid adsorption machines may provide the desired

solution [40]. Adsorption machines are preferable to absorption machines as they do not require rectifiers, valves or liquid seals and are simpler in overall construction [18].

The Platen-Munters diffusion absorption cycle (Electrolux Cycle) has been considered as a possible choice for solar cooling. However, although it has been used in smaller kerosene and gas refrigerators and freezers it has 'proved difficult to scale up to larger sizes and to adapt to irregular heat sources such as solar energy [5]. A number of researchers have attempted to adapt the Platen-Munters cycle to solar refrigeration but have experienced difficulties at the lower generating temperatures involved. Additionally, due to the variable power and temperature input provided by solar heat, control systems would be required to regulate mass flow rates and rate of diffusion which would further increase the overall system complexity. However, Critoph and Tarbaghia [57] predict that the cost of any added complexity would be offset by improvements in system performance and the subsequent reduction in the area of solar collector required.

One of the challenges in applying adsorption cycles to solar refrigeration is in finding a suitable thermodynamic cycle for the temperature limits of the desired application [10]. For instance, utilising the zeolite-water pair it is generally not possible to achieve temperatures lower than 0°C while when using the zeolite-methanol pair difficulties associated with thermal decomposition may occur. Passos et al [10] have built a prototype ice making machine based on the activated carbon AC35-methanol pair from which the French company BLM has also manufactured an intermittent cycle adsorption refrigerator.

Following the work carried out by Bougard [45] on a solar adsorption refrigerating machine it was found that although the overall solar efficiency of such as machine is low they may well be competitive with other types of machines for use in rural areas of developing countries. Many solar adsorption machines combine the solar collector and adsorbent bed into one unit to improve simplicity of design and reduce thermal losses. Hence the solar collector generates refrigerant during the day and acts as the adsorber at night when cold production is achieved [3]. The solar collector itself consists of the adsorbent material covered by a transparent material such as glass. This utilises the heat

trapping effect caused by the selective transmittance of glass and other transparent materials to increase the temperature inside the collector. Hence solar heat enters the solar collector through the glass at a greater rate than it can escape increasing the temperature of the adsorbent bed. Bougard and Boussemaere [3] also comment that the maximum temperature attainable within the bed can be increased by utilising devices such as selective coatings and vacuum insulation. An example of such a selective coating is "Maxorb", as used by several researchers [52, 53, 55]. Vacuum insulation while effective also tends to be prohibitively expensive for developing country applications. Critoph [55] also investigated the use of a transparent polycarbonate honeycomb insulation but did not find it to be cost effective. When the cost and availability was compared to the predicted increases in performance toughened float glass was used in preference to low iron glass [55, 56]. The efficiency of the solar collector will depend on a number of environmental factors such as ambient temperature, solar radiation and percentage of diffuse radiation as well as system parameters such as mass flow rate and refrigerant properties [3]. Evacuated tube collectors achieve far higher solar COPs than flat plate collectors [3] although this is at the expense of increasing system cost.

Critoph [5] examines energy efficiency and the COP of solar refrigeration machines. For a solar driven system, the main cost of the system is due to the collectors while the fuel costs are zero. Hence improving COP may reduce the collector size required and hence reduce overall system cost. However, if increased COP is achieved at the expense of system simplicity and reliability then it may be counter productive. Critoph [5] has also investigated the progress made on solar thermal refrigeration systems. A number of researchers have produced intermittent solar thermal adsorption systems for ice production based on both chemisorption utilising calcium chloride-ammonia and physical adsorption utilising activated carbon-methanol, but with limited commercial success. There are few examples of solar thermal systems designed for large quantities of ice production in the region of 100–1000 kg of ice per day apart from a couple of liquid absorption systems driven by solar or biomass heat. However, problems arise when adapting the simple intermittent adsorption cycle for production of large quantities of ice due to the large inventory of adsorbent and

adsorbate required. Critoph and Gong [31] calculate that to produce 100 kg of ice through one cycle (as would be the case for a solar thermal system operating on a diurnal cycle) using a carbon-ammonia pair would require approximately 250 kg of active carbon occupying a volume of approximately 500 litres. Scaling this up to a 1 tonne per day ice maker would clearly make the system far too large. Hence some form of rapid cycling needs to be employed in order to increase the cooling powers achieved and reduce the adsorbent-adsorbate inventory required. For producing in excess of 1 tonne of ice per day Critoph and Tarbaghia [57] conclude that the solar powered Platen-Munters diffusion absorption system is a good option.

A small solar powered solid adsorption refrigerator was built and evaluated by Critoph using an active carbon-ammonia pair [55, 56]. Farber [58] built a solar powered ammonia-water absorption refrigerator where the collector and ammonia generator were combined in one unit. Continuous cooling was achieved while a virtually constant rate of ice production was achieved during the day. Grenier et al [52] present their results for a solar powered solid adsorption cold store based on the zeolite-water pair. They describe the zeolite-water and active carbon-methanol pairs as being the most promising for solar cooling. Another solar powered zeolite-water adsorption system was built by Hinotani et al [36] and incorporated heat pipes into the design to enhance heat transfer. The zeolite-water adsorption pair appears to be a popular choice for solar cooling. According to Meunier [43] the zeolite 13X-water pair appears to be well suited to solar cooling applications through both low and high technology. Meunier et al [59] discuss the testing of solar powered solid adsorption refrigeration systems based on both the zeolite-water and active-carbon methanol pairs. The active-carbon methanol pair is utilised in an ice maker to produce 30 kg of ice per day. It is stated that if the solar COP could be increased there would be a significant possibility of developing larger systems capable of producing up to 1000 kg of ice per day [59]. Meunier et al [59] also highlight the fact that careful sizing of the solar reactor is of great importance due to the multiple functions it performs. The solar reactor collects solar heat during the day and transfers it to the adsorbent bed for desorption while during the night the collector re-adsorbs refrigerant vapour and rejects the heat to the

surroundings. As an alternative to the conventional adsorption pairs, Sakoda and Suzuki [41] used a silica gel-water pair for solar cooling with the water providing a large enthalpy of vaporisation and silica gel being a commonly used desiccant. Additionally Swartman [60] has carried out a comprehensive literature survey of solar refrigeration systems based on vapour compression and liquid absorption cycles since 1936. Solar powered vapour compression systems were found to have low efficiencies and high fabrication costs. Worsøe-Schmidt [14] applied the calcium chloride-ammonia pair to solar solid sorption refrigeration as it was considered the best pair in terms of simplicity and thermal efficiency. The solar collector and ammonia absorber were combined together to reduce thermal losses. Based on this chemisorption pair the Danish company Kaptan ApS subsequently manufactured an intermittent cycle adsorption refrigerator.

In conclusion, a number of solar powered refrigeration systems have been built operating on both absorption and adsorption cycles. Possible suggested applications include vaccine storage and food preservation. Systems have been utilised for both cold production above 0°C and for ice production up to approximately 30 kg per day. However, solar adsorption refrigeration systems capable of producing much larger quantities of ice in the region of 1 tonne per day have not yet been achieved.

2.6 Numerical Modelling

Prior to building an adsorption system it is desirable to be able to predict the required system geometries, thermodynamic behaviour and performance. However, due to the complex nature of heat and mass transfers as well as adsorption and desorption processes, adsorption systems do not lend themselves to analytical solution. Hence, a numerical model is required based on a number of simplifying assumptions to predict system operation. From the data supplied by the numerical model the experimental rig can then be manufactured. However, the numerical model then needs to be validated against experimental data if the results obtained are to have any significance. For numerical modelling most researchers have chosen to use a one or two dimensional implicit finite difference model utilising a Crank-Nicholson scheme.

Before numerically modelling an adsorption system the basic equations and assumptions about the system behaviour need to be developed. According to Aittomäki and Härkönen [27] when modelling a solid adsorption cycle the following should be considered: the flow of vapour between the adsorbent and adsorbate vessels, the flow of vapour in the void regions between the adsorbent granules, vapour diffusion inside the adsorbent granules, the adsorption and desorption processes and associated heat effects as well as the heat transfer within the adsorbent bed. The physical processes within the adsorbent bed are complex involving simultaneous heat and mass transfers. The system becomes increasingly complex as the quantities such as heat capacity, density and thermal conductivity will vary with the amount adsorbed. This is highlighted by Härkönen and Aittomäki [15] when they state that the specific heat capacities will vary during the adsorption and desorption periods. A number of assumptions can be made in order to simplify the governing equations such as assuming constant bed pressure during adsorption and desorption processes if the sizes of the evaporator and condenser are large enough [27]. Aittomäki and Härkönen [27] chose to use an implicit finite difference method to solve the resulting set of governing system equations.

In terms of discretising the set of governing system equations the implicit finite difference technique appears to be the method favoured by most researchers. However, in modelling the sorption in a metal hydride Spinner [37] discusses the use of a control volume discretisation method with the Crank-Nicholson scheme. Critoph [32] modelled an adsorption cycle using a one dimensional finite difference program. In order to model the system, mass flow and heat transfer equations were required for the adsorbent and adsorbate together with a number of simplifying assumptions and boundary conditions. Critoph [24] presents the governing equations for heat and mass transfer used in the model. These equations describe conservation of mass, heat transfer, total mass of refrigerant, sorption heat load and heat input to the fluid (unsteady flow energy equation). These equations were then discretised and solved iteratively. Pressure at evaporation and condensation was assumed constant. At times when the pressure was changing it was

calculated by a Newton-Raphson iteration. Critoph [32] also assumed the velocity of the gas entering the adsorbent bed to be constant.

The numerical modelling of adsorption systems is also discussed by Douss et al [19]. They indicate that several approaches are possible in modelling the system, described as "black box", "white box" and "grey box" techniques. The "black box" approach, where the process is poorly understood, ignores the details of heat and mass transfer within the system. In contrast to this the "white box" approach requires complete understanding of the system to construct a detailed model of the process. The "grey box" approach lies somewhere between the above two extremes where a certain understanding of the system enables a simplified model to be constructed. The numerical code developed by Douss et al [19] follows the "white box" approach in describing as precisely as possible the operation of the system. For the numerical model assumptions of component homogeneity, leading to a set of ordinary differential equations, and thermodynamic equilibrium in each component were made. The subsequent set of equations were solved using an implicit finite differencing method. The roots of the non-linear finite difference equations were found using the Newton-Raphson method.

Grenier et al [52] produced a one dimensional numerical model based on a number of simplifying assumptions for a solar powered cold store. The set of equations developed were solved using a Crank-Nicholson semi-implicit finite difference method. Computational modelling indicated that the solar COP for the system was zero below a certain threshold value of daily solar input while increasing to maximum above this threshold value.

In performing a theoretical analysis on an adsorbent reactor Hajji and Khalloufi [21] made simplifying assumptions such as constant pressure of the vapour phase, continual thermodynamic equilibrium and constant temperature of the heat transfer fluid. Following the development of the governing equations, boundary and initial conditions, system energy analysis and sorption rates, an explicit finite difference method was used.

Härkönen and Aittomäki [15] state that two dimensional modelling of the heat transfer is necessary in order to observe the effect of bed thickness on process efficiency. This also makes it possible to analyse the behaviour of the propagating temperature front. The governing partial differential equations for heat transfer were solved using an implicit finite difference method.

The process of numerical modelling is also discussed by Karagiorgas and Meunier [20]. The system of governing equations were again solved numerically using a finite difference method with a Crank-Nicholson scheme. Newton's method was then applied to resolve the system of non-linear equations produced. The numerical model does not allow for temperature inhomogeneities inside the solid adsorption reactor.

A numerical model for non-isothermal multi-component adsorption is presented by Nagel and Kluge [61]. The diffusion model for mass transfers allows for both macropore diffusion and diffusion in the adsorbed phase. The numerical solution developed involves using both the collocation and spline methods. This appears to be a different approach to that followed by other researchers. The subsequent system equations were developed based on a number of modelling assumptions.

Two methods of numerically modelling the adsorption in solar powered solid adsorption units are discussed by Passos et al [62]. The uniform temperature and concentration model, as used by Sakoda and Suzuki [41], involves using equations for state, kinetics and global heat balance. The model uses ordinary differential equations only and is unable to predict the influence of other factors such as fins within the bed. The uniform pressure model analyses the temperature inhomogeneities within the adsorbent bed and is able to predict the influence of structures such as fins within the bed, since the numerical simulation is two dimensional, although resistances to mass transfer are neglected. The model proposed by Passos et al [62] utilises the uniform pressure model with the addition of a linear driving force (LDF) equation to account for resistance to mass transfer within the adsorbent. A finite element numerical method was employed to model the system.

Tamainot-Telto and Critoph [30] have also developed a finite difference numerical model for an adsorption generator based on mass and energy conservation equations. This two dimensional model again utilises finite differencing with the Crank-Nicholson scheme. The model takes heat transfers into account, the adsorbent bed is assumed to be at a uniform pressure while resistances to mass transfer are ignored. It is also stated that the model behaviour is controlled by transient heat transfer in conjunction with heat, mass and sorption equilibrium equations.

Sun et al [39] produced a one dimensional numerical model for an adsorbent bed including heat and mass transfers in conjunction with the Ergun law describing the flow of adsorbate inside the adsorber. The Ergun equation was applied to determine the flow velocity within the adsorbent bed. A number of simplifying assumptions are made such as one dimensionality, adsorbent homogeneity, local equilibrium of the solid and gaseous phases, ideal behaviour of the gaseous phase, neglected mass dispersion of the gaseous phase while certain other parameters are assumed to remain constant. The governing equations, boundary and initial conditions are developed and the governing equations are re-written in dimensionless form. The resulting set of partial differential equations were solved by a finite difference method using the Crank-Nicholson scheme. Further work on finite difference methods applied to sorption systems is presented by Sun and Meunier [63]. A solution adaptive gridding technique (SAG) and a four point quadratic upstream differencing scheme (QUDS) are proposed for resolving sudden temperature and concentration variations. When devising a mathematical model a number of mechanisms such as heat and mass transfer, heat conduction and mass diffusion as well as additional physical properties need to be taken into consideration. Two main difficulties which may be encountered when modelling the dynamics of fixed adsorbent beds using finite differences include resolution of the convection-diffusion equations and modelling of the coupling between adsorbate components [63]. The implicit Crank-Nicholson scheme is selected by Sun and Meunier [63] as explicit schemes tend to suffer from severe stability limitations. However, it is also mentioned that although implicit schemes tend to be more accurate and

unconditionally stable they require the inversion of generally large matrices which is computationally intensive.

In conclusion, in numerically modelling sorption systems the vast majority of researchers have discretised the governing set of partial differential equations using a finite differencing method with a Crank-Nicholson scheme. Implicit methods tend to be preferred to explicit methods as they are more accurate and stable albeit more computationally intensive. Simplifying assumptions such as constant temperature or constant pressure allow the system equations to be simplified considerably. The results from various numerical models have been partially validated by the cited researchers and have been found to be in good agreement with their experimental findings.

2.7 Conclusions

On the basis of the literature review, a number of different possibilities have been identified for producing an adsorption system to meet with the requirements of the research specification. In general the review suggests the use of monolithic adsorbents, thermal conductivity intensification devices, rapid thermal cycling and multi-bed operation as routes to achieving increased specific cooling powers.

References

[1] **Douss, N., Meunier, F.**, Effect of Operating Temperatures on the Coefficent of Performance of Active Carbon-Methanol Systems, Heat Recovery Systems & CHP, Vol. 8, No. 5, pp. 383–392, **1988**.

[2] **Meunier, F., Douss, N.**, Adsorptive Heat Pumps: Active Carbon-Methanol and Zeolite-Water Pairs, CEC/British Gas International Workshop on Adsorption Heat Pumps, pp. 63–72, April **1988**.

[3] **Bougard, J., Boussemaere, C.**, Thermodynamics of Solar Adsorption Refrigerating Machines, Faculté Polytechnique de Mons, Belgium, March **1987**.

[4] **Ülkü, S.**, Adsorption Heat Pumps, Heat Recovery Systems, Vol. 6, No. 4, pp. 277–284, **1986**.

[5] **Critoph, R.E.**, Refrigeration in Developing Countries - The Renewable Options, 1st World Renewable Energy Conference, Reading, UK, **1990**.

[6] **Suzuki, M.**, Application of Adsorption Cooling System to Automobiles, Solid Sorption Refrigeration Symposium Paris, pp. 136–141, 18–20 November **1992**.

[7] **Pons, M., Guilleminot, J.J.**, Design of an Experimental Solar-Powered Solid-Adsorption Ice Maker, JSEE, ASME, Vol. 108, pp. 332–337, November **1986**.

[8] **Jones, J.A.**, Sorption Refrigeration Research at JPL/NASA, Solid Sorption Refrigeration Symposium Paris, pp. 126–135, 18–20 November **1992**.

[9] **Cacciola, G., Restuccia, G.**, Progress on Adsorption Heat Pumps, Heat Recovery Systems & CHP, Vol. 14, No. 4, pp. 409–420, **1994**.

[10] **Passos, E., Meunier, F., Gianola, J.C.**, Thermodynamic Performance Improvement of an Intermittent Solar-Powered Refrigeration Cycle Using Adsorption of Methanol on Activated Carbon, Heat Recovery Systems, Vol. 6, No. 3, pp. 259–264, **1986**.

[11] **Shelton, S.V., Wepfer, W.J., Miles, D.J.**, Ramp Wave Analysis of the Solid/Vapor Heat Pump, Journal of Energy Resources Technology, Vol. 112, pp. 69–78, **1990**.

[12] **Zhu, R., Han, B., Lin, M., Yu, Y.**, Experimental Investigation on an Adsorption System for Producing Chilled Water, International Journal of Refrigeration, Vol. 15, No. 1, pp. 31–34, **1992**.

[13] **Meunier, F.**, Solid Sorption: An Alternative to CFC's, Heat Recovery Systems & CHP, Vol. 13, No. 4, pp. 289–295, **1993**.

[14] **Worsøe-Schmidt, P.**, Solar Refrigeration for Developing Countries Using a Solid-Absorption Cycle, International Journal of Ambient Energy, Vol. 4, No. 3, pp. 115–124, July **1983**.

[15] **Härkönen, M., Aittomäki, A.**, The Principle of Internal Regeneration as Applied to the Adsorption Heat Pump Process, Heat Recovery Systems & CHP, Vol. 11, No. 4, pp. 239–248, **1991**.

[16] **Meunier, F.**, Second Law Analysis of a Solid Adsorption Heat Pump Operating on Reversible Cascade Cycles: Application to the Zeolite-Water Pair, Heat Recovery Systems, Vol. 5, No. 2, pp. 133–141, **1985**.

[17] **Critoph, R.E., Turner, L.H.**, Performance of Ammonia-Activated Carbon and Ammonia-Zeolite Heat Pump Adsorption Cycles, Proceedings of Conference: Pompes a Chaleur Chimiques de Hautes Performances, Perpignan (publ. Lavoisier), pp. 202–211, **1988**.

[18] **Critoph, R.E.**, Performance Limitations of Adsorption Cycles for Solar Cooling, Solar Energy, Vol. 41, No. 1, pp. 21–31, **1988**.

[19] **Douss, N., Meunier, F.E., Sun, L.**, Predictive Model and Experimental Results for a Two-Adsorber Solid Adsorption Heat Pump, Ind. Eng. Chem. Res., Vol. 27, No. 2, pp. 310–316, **1988**.

[20] **Karagiorgas, M., Meunier, F.**, The Dynamics of a Solid-Adsorption Heat Pump Connected with Outside Heat Sources of Finite Capacity, Heat Recovery Systems & CHP, Vol. 7, No. 3, pp. 285–299, **1987**.

[21] **Hajji, A., Khalloufi, S.**, Theoretical and Experimental Investigation of a Constant-Pressure Adsorption Process, International Journal of Heat and Mass Transfer, Vol. 38, No. 18, pp. 3349–3358, **1995**.

[22] **Meunier, F.**, Theoretical Performances of Solid Adsorbent Cascading Cycles Using the Zeolite-Water and Active Carbon-Methanol Pairs: Four Case Studies, Heat Recovery Systems, Vol. 6, No. 6, pp. 491–498, **1986**.

[23] **Groll, M.**, Solid Sorption Machines for CFC-Free Generation of Heat and Cold (An Overview), 1st ISMHT-ASME Heat and Mass Transfer Conference, Bombay, **1994**.

[24] **Critoph, R.E.**, Forced Convection Enhancement of Adsorption Cycles, Heat Recovery Systems & CHP, Vol. 14, No. 4, pp. 343–350, **1994**.

[25] **Groll, M.**, Reaction Beds for Dry Sorption Machines, Solid Sorption Refrigeration Symposium Paris, pp. 207–214, 18–20 November **1992**.

[26] **Turner, L.**, Improvement of Activated Charcoal-Ammonia Adsorption Heat Pumping/Refrigeration Cycles. Investigation of Porosity and Heat/Mass Transfer Characteristics. Graz 3rd International Workshop on Research Activities on Advanced Heat Pumps, pp. 325–334, **1990**.

[27] **Aittomäki, A., Härkönen, M.**, Modelling of Zeolite/Methanol Adsorption Heat Pump Process, Heat Recovery Systems & CHP, Vol. 8, No. 5, pp. 475–482, **1988**.

[28] **Turner, L.**, Improvement of Activated Charcoal-Ammonia Adsorption Heat Pump/Refrigeration Cycles: Investigation of Porosity and Heat/Mass Transfer Characteristics, PhD Thesis, Department of Engineering, University of Warwick **1992**.

[29] **Cacciola, G., Cammarata, G., Fichera, A., Restuccia, G.**, Advances on Innovative Heat Exchangers in Adsorption Heat Pumps, Solid Sorption Refrigeration Symposium Paris, pp. 221–226, 18–20 November **1992**.

[30] **Tamainot-Telto, Z., Critoph, R.E.**, Adsorption Refrigerator Using Monolithic Carbon-Ammonia Pair, International Journal of Refrigeration, Vol. 20, No. 2, pp. 146–155, **1997**.

[31] **Critoph, R.E., Gong, F.**, A Rapid Cycling Ice Maker for use in Developing Countries, Proc. 2nd World Renewable Energy Congress, Reading, pub. Pergamon, pp. 708–714, **1992**.

[32] **Critoph, R.E.**, A Forced Convection Regenerative Cycle Using the Carbon-Ammonia Pair, Solid Sorption Refrigeration Symposium Paris, pp. 80–85, 18–20 November **1992**.

[33] **Guilleminot, J.J., Choisier, A., Chalfen, J.B., Nicolas, S.**, Heat Transfer Intensification in Fixed Bed Adsorbers, Heat Recovery Systems & CHP, Vol. 13, No. 4, pp. 297–300, **1993**.

[34] **Guilleminot, J.J., Gurgel, J.M.**, Heat Transfer Intensification in Adsorbent Beds of Adsorption Thermal Devices, Proceedings of the 12th Annual International Solar Energy Conference, Miami, USA, ASME, New York, pp. 69–74, **1990**.

[35] **Liu, Z.Y., Cacciola, G., Restuccia, G., Giordano, N.**, Fast Simple and Accurate Measurement of Zeolite Thermal Conductivity, Zeolites, Vol. 10, pp. 565–570, July/August **1990**.

[36] **Hinotani, K., Kanatani, K., Matsumoto, K., Kume, M.**, Development of Solar Actuated Zeolite Refrigeration System, Research Centre, Sanyo Electric Co. Ltd., Hirakata, Osaka 573, Japan.

[37] **Spinner, B.**, Application of New Concepts for the Development of Gas Solid Sorption Machines, CNRS-IMP, LEA-SIMAP, University of Perpignan (France), **1996**.

[38] **Mauran, S., Prades, P., L'Haridon, F.**, Heat and Mass Transfer in Consolidated Reacting Beds for Thermochemical Systems, Heat Recovery Systems & CHP, Vol. 13, No. 4, pp. 315–319, **1993**.

[39] **Sun, L.M., Ben Amar, N., Meunier, F.**, Numerical Study on Coupled Heat and Mass Transfers in an Adsorber with External Fluid Heating, Heat Recovery Systems & CHP, Vol. 15, No. 1, pp. 19–29, **1995**.

[40] **Critoph, R.E., Vogel, R.**, Possible Adsorption Pairs for use in Solar Cooling, International Journal of Ambient Energy, Vol. 7, No. 4, pp. 183–190, October **1986**.

[41] **Sakoda, A., Suzuki, M.**, Fundamental Study on Solar Powered Adsorption Cooling System, Journal of Chemical Engineering of Japan, Vol. 17, No. 1, pp. 52–57, **1984**.

[42] **Douss, N., Meunier, F.**, Experimental Study of Cascading Adsorption Cycles, Chem. Eng. Sci., Vol. 44, pp. 225–235, **1989**.

[43] **Meunier, F.**, Research and Development Toward New Thermochemical Cycles for Cold Production from Solar Energy Using Solid Adsorbents, Journal of Solar Energy Research, Vol. 1, Part. 1, pp. 23–35, **1983**.

[44] **Meunier, F., Mischler, B.**, Solar Cooling Through Cycles Using Microporous Solid Adsorbents, Sun 2, Vol. 1, pp. 676–680, **1979**.

[45] **Bougard, J.**, Thermodynamical and Technical Problems in Solar Adsorption Refrigeration, Science et Technique du Froid, Part 1, pp. 25–33, **1986**.

[46] **Critoph, R.E.**, Evaluation of Alternative Refrigerant-Adsorbent Pairs for Refrigeration Cycles, Applied Thermal Engineering, Vol. 16, No. 11, pp. 891–900, **1996**.

[47] **Jüntgen, H.**, New Applications for Carbonaceous Adsorbents, Carbon, Vol. 15, pp. 273–277, **1977**.

[48] **McEnaney, B., Masters, K.J.**, Assessment of Adsorption in Microporous Carbons, Thermochimica Acta, 82, pp. 81–102, **1984**.

[49] **Manual of Symbols and Terminology**, Appendix 2, Part 1, Colloid and Surface Chemistry, Pure and Applied Chemistry, Vol. 31, p. 578, **1972**.

[50] **McEnaney, B.**, Adsorption and Structure in Microporous Carbons, Based on a plenary review lecture given at "Carbon '86", Baden-Baden FRG., 30th June **1986**.

[51] **Critoph, R.E.**, Assessment of Chemical Surface Modifications on the Porosity of Active Carbons for Heat Pump Use, Phase I/II, Internal Report, University of Warwick, **1989**.

[52] **Grenier, Ph., Guilleminot, J.J., Meunier, F., Pons, M.**, Solar Powered Solid Adsorption Cold Store, Journal of Solar Energy Engineering, Vol. 110, pp. 192–197, August **1988**.

[53] **Boussemaere, C., Bougard, J.**, Solar Thermal Refrigerator for Vaccine Storage and Icemaking, Intersol '85, Proceedings of the 9th Biennial Congress of the I.S.E.S, Montreal, Canada, Pergammon Press, **1985**.

[54] **World Health Organisation**, Standard Performance Specifications and Standard Test Procedures for Cold Chain Equipment, January **1988**.

[55] **Critoph, R.E.**, An Ammonia Carbon Solar Refrigerator for Vaccine Cooling, Renewable Energy, 5, Part I, pp. 502–508, **1994**.

[56] **Critoph, R.E.**, Laboratory Testing of an Ammonia Carbon Solar Refrigerator, Proc. ISES Solar World Congress, Budapest, p. 6, August **1993**.

[57] **Critoph, R.E., Tarbaghia, T.M.**, Solar Powered Platen-Munters (Electrolux) Refrigeration Cycle for Large Scale Refrigeration, Proc. Int. Conf. on Applications of Solar and Renewable Energy, Cairo, pub. ISES, p. 6, April **1992**.

[58] **Farber, E.A.**, Design and Performance of a Compact Solar Refrigeration System, International Solar Energy Conference, Paper No. 6158, **1970**.

[59] **Meunier, F., Grenier, Ph., Guilleminot, J.J., Pons, P.**, Solar Powered Refrigeration Using Intermittent Solid Adsorption Cycles, Laboratoire de Thermodynamique des Fluides, UA CNRS 874.

[60] **Swartman, R.K et al**, Survey of Solar-Powered Refrigeration, ASME Paper 73-WA/SOL-6, New York, ASME, **1973**.

[61] **Nagel, G., Kluge, G.**, Modelling of Non-Isothermal Multi-Component Adsorption in Non-Adiabatic Fixed Beds, Hungarian Journal of Industrial Chemistry, Vol. 15, pp. 68–71, **1987**.

[62] **Passos, E.F., Escobedo, J.F., Meunier, F.**, Simulation of an Intermittent Adsorptive Solar Cooling System, Solar Energy, Vol. 42, No. 2, pp. 103–111, **1989**.

[63] **Sun, L.M., Meunier, F.**, An Improved Finite Difference Method for Fixed-Bed Multicomponent Sorption, AIChE Journal, Vol. 37, No. 2, pp. 244–254, February **1991**.

Chapter 3

Theory

3.1 Introduction

In the following chapter the adsorption equations of state and thermodynamic relationships applied during the research are presented together with an example of a general adsorption cycle. The adsorption equations enable the concentration of adsorbate in the adsorbent material to be calculated. The Dubinin-Astakhov (D-A) equation, given in equation (3.8), is applied in the predictive numerical model discussed in Chapter 5.

3.2 Principles of Adsorption

Adsorption is a process by which the molecules of a vapour or liquid form a bond at the surface interface with a solid material and in so doing increase the concentration of the molecular species at the interface. The solid material is known as the adsorbent and the vapour or liquid that is adsorbed onto the solid surface is known as the adsorbate. The two types of adsorption are chemical adsorption (chemisorption) and physical adsorption. Chemical adsorption involves a chemical reaction between the adsorbent and adsorbate forming chemical species which are held in place by strong molecular bonds. However, as the chemical sorption process takes place throughout the medium, it may also be categorised as a class of *ab*sorption which is more commonly associated with liquid/vapour systems. The enthalpy of chemical adsorption is relatively high and of the same order of magnitude as the energy of the chemical reaction. The extent of chemical adsorption depends on both the properties of the adsorbent and adsorbate. Physical adsorption

involves the attraction of the polar adsorbate molecules to the surface of the adsorbent where the adsorbate molecules are held in place by weak van der Waals bonds. The enthalpy of physical adsorption is considerably lower than that for chemisorption and is of the same order of magnitude as the enthalpy of vaporisation. Since condensation also involves the formation of weak van der Waals bonds, physical adsorption may be viewed as analogous to a condensation process. The extent of physical adsorption is primarily dependent on the properties of the adsorbent such as internal structure, porosity and internal surface area. Microporous physical adsorbents such as activated carbon and zeolites have large internal surface areas and porosities that allow large adsorbate concentrations to be achieved.

3.3 Adsorption Equations of State

There are a number of equations which have been developed to describe the nature of adsorption in microporous adsorbents. Some equations treat adsorption as a purely surface process, whether monolayer or multilayer, without taking the pore volume of the adsorbent into account. Other more sophisticated approaches treat microporous adsorption as a volumetric process governed by potentials acting within the pore.

3.3.1 The Langmuir Equation

The equation proposed by Langmuir in 1916 provides a theoretical relationship between the mass of adsorbate, temperature and pressure, expressed by Bougard [1] as:

$$\theta = \frac{m}{m_{max}} = \frac{bP}{1+bP} \tag{3.1}$$

where:

θ is the fraction of internal porous surface covered

m is the mass of adsorbed gas

m_{max} is the maximum mass of adsorbed gas

b is the adsorption coefficient, a function of temperature and the adsorbent-adsorbate pair

P is the pressure in the adsorbent (N m^{-2})

The Langmuir equation assumes that the adsorbed molecules form a monolayer over the internal surface of the adsorbent and do not interact with each other. It is assumed that there are fixed adsorption sites over the internal surface of the adsorbent possessing the same enthalpy of adsorption and that each site can accommodate only one molecule of adsorbate. The adsorption process is treated as a purely surface phenomenon.

3.3.2 The Branauer, Emmett, Teller (BET) Equation

The Branauer-Emmett-Teller (BET) equation also gives a theoretical relationship between mass of adsorbate, temperature and pressure, expressed as [1]:

$$\theta = \frac{m}{m_{max}} = \frac{c\left(\frac{P}{(P_{sat})_T}\right)\left(1-\left(\frac{P}{(P_{sat})_T}\right)^n\right)}{\left(1-\frac{P}{(P_{sat})_T}\right)\left(1-\frac{P}{(P_{sat})_T}+c\left(\frac{P}{(P_{sat})_T}\right)\right)} \tag{3.2}$$

where:

c is a constant

n is the number of molecular layers

P_{sat} is the saturation pressure of the adsorbate (N m^{-2}) at temperature T (K)

The BET equation is an extension of the Langmuir equation where multilayer rather than monolayer adsorption is allowed to occur over the internal surface of the adsorbent. However, the adsorption process is still treated as a purely surface phenomenon.

3.3.3 The Dubinin-Radushkevich Equation

In contrast to the Langmuir and BET equations which treat adsorption as a purely surface phenomenon consisting of the build up of one or many molecular layers, the equation

developed by Dubinin and Radushkevich [2] describes adsorption as a volume pore filling process. The internal surface of the adsorbent is described as a plane over which there is a variation in potential energy, where adsorption sites are characterised as regions of maximum potential energy. If all the adsorption sites are at the same potential energy level then the surface is considered to be homogeneous whereas if there are variations in the potential energies of the adsorption sites the surface is considered heterogeneous. Heterogeneous surfaces are commonly found for adsorbents such as activated carbons.

The Dubinin-Radushkevich equation, which relates concentration to pressure and temperature is:

$$V = V_0 \exp\left(-B\left(\frac{RT}{\beta}\ln\frac{P_{sat}}{P}\right)^2\right) \tag{3.3}$$

where:

V is the micropore volume filled by the adsorbate (m^3)

V_0 is the maximum micropore volume available or limiting micropore volume (m^3)

B is a function of the micropore structure

R is the adsorbate gas constant ($J\ kg^{-1}K^{-1}$)

T is the temperature (K)

β is the affinity coefficient

P is the pressure in the adsorbent ($N\ m^{-2}$)

P_{sat} is the saturation pressure of the adsorbate ($N\ m^{-2}$) at temperature T (K)

The value of the coefficient B decreases as the microporosity of the adsorbent increases. The value of the affinity coefficient β is obtained empirically from the properties of the adsorbate only. It is calculated as the ratio of adsorbate volume to adsorbed reference gas volume (usually benzene) under the same conditions. Critoph [3] provides details of β for a

range of adsorbates, determined by the methods suggested by Smíšek and Černý [4], with a value for ammonia with respect to benzene given as 0.28.

Critoph and Turner [5] found that experimental porosity data for the ammonia-carbon pair could be fitted by a simpler form of equation (3.3) with no loss of accuracy, as expressed by:

$$x = x_0 \exp\left(-k\left(T \ln\frac{P_{sat}}{P}\right)^2\right) \tag{3.4}$$

where:

x is the concentration (kg kg^{-1})

x_0 is the maximum concentration or limiting concentration (kg kg^{-1})

k is a constant

Specifying a linear relationship between saturation pressure and saturation temperature as:

$$\ln P_{sat} = a - \frac{c}{T_{sat}} \tag{3.5}$$

Specifying a linear relationship between pressure and temperature along an isostere as:

$$\ln P = a - \frac{c'}{T} \tag{3.6}$$

where:

a is a constant

c is a constant

c' is a constant

Substituting equation (3.5) and equation (3.6) into equation (3.4) yields the final modified form of the D-R equation:

$$x = x_0 \exp\left(-K\left(\frac{T}{T_{sat}} - 1\right)^2\right) \tag{3.7}$$

where:

K is a constant

T_{sat} is the saturation temperature of the adsorbate (K) at the system pressure P

3.3.4 The Dubinin-Astakhov Equation

The Dubinin-Astakhov (D-A) equation [6] is a more general form of the D-R equation where the index of the power two is replaced by a variable index n. This allows an improved correlation with experimental data to be obtained. The modified D-A equation developed from equation (3.7) is thus:

$$x = x_0 \exp\left(-K\left(\frac{T}{T_{sat}} - 1\right)^n\right) \tag{3.8}$$

where:

n is a constant

The D-A equation has been found to offer a high degree of flexibility and accuracy in determining the concentration within activated carbon adsorbents utilising constants obtained empirically. When applied to the monolithic activated carbon type LM127 the standard error of estimate is 0.0019 [7].

3.4 Thermodynamic Relationships

3.4.1 The Clausius-Clapeyron Equation

The Clausius-Clapeyron equation provides the relationship between the enthalpy of vaporisation and the pressure and temperature of a material.

The Gibbs free energy is defined as:

$$G = H - TS \tag{3.9}$$

The definition of enthalpy is:

$$H = U + PV \tag{3.10}$$

Substituting equation (3.10) into equation (3.9) gives:

$$G = U + PV - TS \tag{3.11}$$

Differentiating equation (3.11) gives:

$$dG = dU + PdV + VdP - TdS - SdT \tag{3.12}$$

From the first and second laws of thermodynamics:

$$\begin{aligned} Q &= dU + PdV = TdS \\ \therefore\ & dU + PdV - TdS = 0 \end{aligned} \tag{3.13}$$

Substituting equation (3.13) into equation (3.12) gives:

$$dG = VdP - SdT \tag{3.14}$$

With respect to the transition of a liquid phase to a gas phase where the gas phase is assumed to behave as an ideal gas, for an initial equilibrium condition between the gas phase and the liquid phase:

$$\Delta G = G_g - G_f = 0 \tag{3.15}$$

For an increase in system pressure and a corresponding increase in temperature to maintain equilibrium, equation (3.14) may be re-written for the gas and liquid phases:

$$dG_g = V_g dP - S_g dT \tag{3.16}$$

$$dG_f = V_f dP - S_f dT \tag{3.17}$$

To remain at equilibrium after the system pressure and temperature change, equation (3.15) still holds and hence:

$$G_g + dG_g = G_f + dG_f \tag{3.18}$$

Subtracting equation (3.15) from equation (3.18) and substituting in equations (3.16) and (3.17) gives:

$$V_g dP - S_g dT = V_f dP - S_f dT \tag{3.19}$$

Rearranging equation (3.19) and substituting in specific entropy and specific volume gives:

$$\frac{dP}{dT} = \frac{s_g - s_f}{v_g - v_f} \tag{3.20}$$

The enthalpy of vaporisation for an internally reversible isothermal process is:

$$h_v \equiv h_g - h_f = T\left(s_g - s_f\right) \tag{3.21}$$

For an ideal gas (as assumed initially):

$$v_g = \frac{RT}{P} \tag{3.22}$$

Assuming that the liquid specific volume v_f is negligible compared to the gas specific volume v_g ($v_f << v_g$ such that $v_f \cong 0$) and substituting equation (3.21) and equation (3.22) into equation (3.20) gives:

$$\frac{dP}{dT} = \frac{h_v P}{RT^2} \tag{3.23}$$

Equation (3.23) expresses the rate of change of equilibrium vapour pressure with equilibrium temperature, which may be re-written as:

$$h_v = \frac{dP}{dT}\left(\frac{RT^2}{P}\right) \tag{3.24}$$

or, as the Clausius-Clapeyron equation:

$$\frac{d(\ln P)}{dT} = \frac{h_v}{RT^2} \tag{3.25}$$

3.4.2 Enthalpy of Vaporisation

Assuming that at the phase change between liquid and gas the equilibrium temperature is the saturation temperature, equation (3.24) becomes:

$$h_v = \frac{dP}{dT_{sat}}\left(\frac{RT_{sat}^2}{P}\right) \tag{3.26}$$

and equation (3.25) becomes:

$$\frac{d(\ln P)}{dT_{sat}} = \frac{h_v}{RT_{sat}^2} \tag{3.27}$$

Integrating equation (3.27), assuming h_v is constant with saturation temperature gives:

$$\ln P = C - \frac{h_v}{RT_{sat}} \tag{3.28}$$

Equation (3.27) indicates that a plot of $\ln P$ against $-1/T_{sat}$ should be a straight line with gradient h_v/R. A plot of $\ln P$ against $-1/T_{sat}$ for pure ammonia is shown in Figure 3.1.

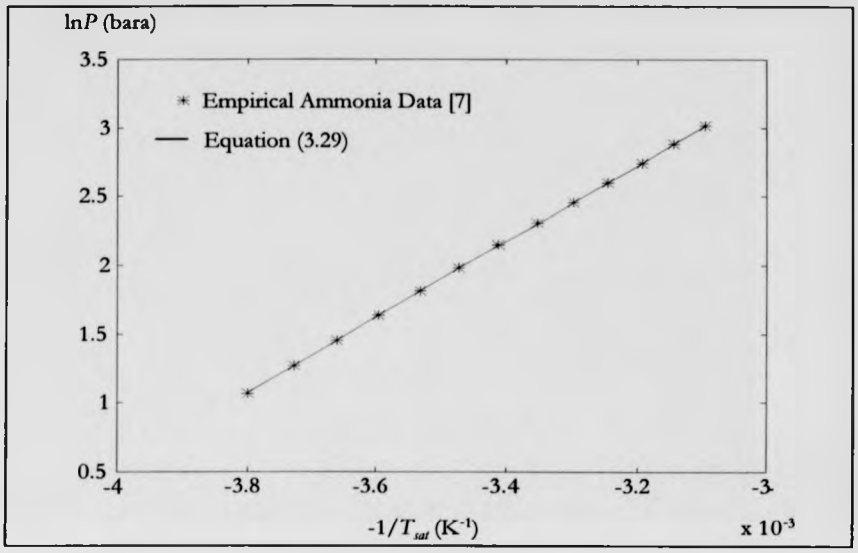

Figure 3.1: Pressure ($\ln P$) against Saturation Temperature ($-1/T_{sat}$) for Saturated Liquid Ammonia

Over a saturation temperature range from -10°C to +50°C a straight line fit through the data points in Figure 3.1 gives:

$$\ln P = 11.541 - \frac{2754.5}{T_{sat}} \tag{3.29}$$

Hence:

$$A = 2754.5 = \frac{h_v}{R}$$
$$\therefore h_v = RA \tag{3.30}$$

where:

A is the line gradient

However, the result in equation (3.30) is only valid when assuming that the enthalpy of vaporisation h_v does not vary with saturation temperature.

Using the relationship given in equation (3.21), the value of h_r for pure ammonia as a function of saturation temperature was calculated by applying the following equations derived from published empirical data [8]:

$$h_f = \left(423.50 + \left(4.584 \times T_{sat}\right) + \left(0.002472 \times T_{sat}^2\right)\right) \times 10^3 \tag{3.31}$$

$$h_g = \left(1685.16 + \left(1.017 \times T_{sat}\right) - \left(0.008106 \times T_{sat}^2\right)\right) \times 10^3 \tag{3.32}$$

where:

T_{sat} is the ammonia saturation temperature (°C)

3.4.3 Enthalpy of Adsorption

The enthalpy of adsorption can be defined in the same way as the enthalpy of vaporisation in the Clausius-Clapeyron. Re-writing equation (3.24) for a constant concentration condition at the adsorbent-gas phase interface during a change in pressure and temperature:

$$h_{ads} = \left.\frac{dP}{dT}\right|_x \left(\frac{RT^2}{P}\right) \tag{3.33}$$

For a constant concentration (x = constant), the T/T_{sat} term in the D-A equation is also constant and hence:

$$\left.\frac{dT_{sat}}{dT}\right|_x = \frac{T_{sat}}{T} \tag{3.34}$$

Therefore:

$$\left.\frac{dP}{dT}\right|_x = \frac{dP}{dT_{sat}} \cdot \frac{dT_{sat}}{dT} = \frac{dP}{dT_{sat}} \cdot \frac{T_{sat}}{T} \tag{3.35}$$

Substituting equation (3.35) into equation (3.33) gives:

$$h_{ads} = \frac{dP}{dT_{sat}} \left(\frac{RTT_{sat}}{P}\right) \tag{3.36}$$

Where the specific gas constant R is obtained from equation (3.22) at the required pressure and temperature.

Rearranging equation (3.26) to give dP/dT_{sat} :

$$\frac{dP}{dT_{sat}} = \frac{h_r P}{RT_{sat}^2} \tag{3.37}$$

Substituting equation (3.37) into equation (3.36) gives the enthalpy of adsorption in terms of enthalpy of vaporisation, temperature and saturation temperature, thus:

$$h_{ads} = h_r\left(\frac{T}{T_{sat}}\right) \tag{3.38}$$

Substituting equation (3.30) into equation (3.38) gives:

$$h_{ads} = RA\left(\frac{T}{T_{sat}}\right) \tag{3.39}$$

Rewriting equation (3.33) in the form of the Clausius-Clapeyron equation:

$$\left.\frac{d(\ln P)}{dT}\right|_{x} = \frac{h_{ads}}{RT^2} \tag{3.40}$$

Integrating equation (3.40), assuming h_r is constant with temperature, and thus along an isostere (x = constant) from equation (3.38) h_{ads} is also constant with temperature:

$$\ln P = C - \frac{h_{ads}}{RT} \tag{3.41}$$

Equation (3.41) indicates that a plot of $\ln P$ against $-1/T$ should be a straight line with gradient h_{ads}/R.

3.5 Adsorption Cycle Processes

The general adsorption cycle is presented in Figure 3.2 (a Clausius-Clapeyron or p-T-x diagram) superimposed on the total isostere plot for the ammonia-LM127 carbon

adsorption pair. The heating and cooling cycle processes are shown on the p-T-x diagram between points 1–4. An evaporating saturation temperature of 0°C (4.3 bara) and condensing saturation temperature of 30°C (11.7 bara) are shown.

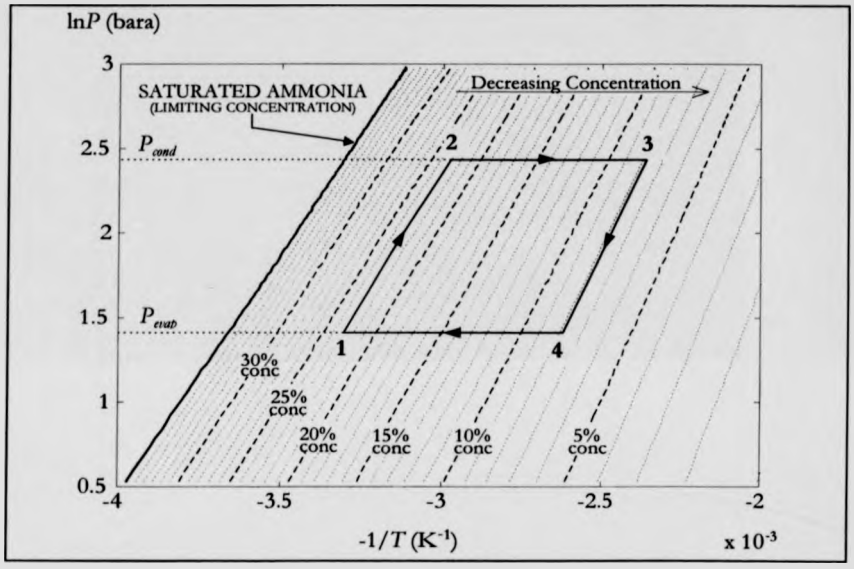

Figure 3.2: Ammonia-LM127 Carbon Isostere Plot with Thermodynamic Cycle

(i) 1 → 2 - Isosteric Heating Process

During this process sensible heating of the carbon and adsorbed ammonia at constant volume takes place. The generator pressure increases from the evaporating pressure (P_{evap}) to the condensing pressure (P_{cond}). The mass in the generator is considered to remain constant while moving up the isostere until the condensing pressure is reached, although the concentration may decrease slightly if ammonia is able to be desorbed into any void volume present in the system.

(ii) 2 → 3 - Isobaric Heating Process

During this process sensible heating of the carbon and adsorbed ammonia phase continues at constant pressure whilst additional heat is required (heat of generation or desorption) to

desorb the ammonia from the generator. The mass of ammonia in the generator is no longer constant and the concentration decreases as the temperature increases from the lower generating temperature of 63°C to the upper generating temperature of 150°C.

(iii) $3 \rightarrow 4$ - Isosteric Cooling Process

During this process heat is rejected from the generator as sensible cooling of the carbon and adsorbed ammonia at constant volume takes place. The generator pressure decreases from the condensing pressure (P_{cond}) to the evaporating pressure (P_{evap}).The mass in the generator is considered to remain constant while moving down the isostere until the evaporating pressure is reached, although the concentration may increase slightly if ammonia is able to be adsorbed from any void volume present in the system.

(iv) $4 \rightarrow 1$ - Isobaric Cooling Process

During this process heat is rejected from the generator as sensible cooling of the carbon and adsorbed ammonia phase continues at constant pressure whilst additional heat is rejected (heat of adsorption) as ammonia is adsorbed. The mass of ammonia in the generator is no longer constant and the concentration increases as the temperature decreases from the initial adsorption temperature of 108°C to the final adsorption temperature (ambient heat rejection temperature) of 30°C.

3.6 Conclusions

The general theory relating to the research area has been covered with particular emphasis on the principles of adsorption and the equations that describe the adsorbent pore filling process. The thermodynamic relationships and equations relating to the enthalpy of vaporisation and enthalpy of adsorption have also been derived.

References

[1] **Bougard, J.**, Thermodynamical and Technical Problems in Solar Adsorption Refrigeration, Science et Technique du Froid, Part 1, pp. 25–33, **1986**.

[2] **Dubinin, M.M., Radushkevich, L.V.**, Equation of the Characteristic Curve of Activated Charcoal, Doklady Akad Nauk S.S.S.R, Vol. 55, pp. 327–329, **1947**.

[3] **Critoph, R.E.**, Performance Limitations of Adsorption Cycles for Solar Cooling, Solar Energy, Vol. 41, No. 1, pp. 21–31, **1988**.

[4] **Smíšek, M., Černý, S.**, Active Carbon-Manufacture, Properties and Applications, Elsevier, New York, **1970**.

[5] **Critoph, R.E., Turner, L.H.**, Performance of Ammonia-Activated Carbon and Ammonia-Zeolite Heat Pump Adsorption Cycles, Proceedings of Conference: Pompes a Chaleur Chimiques de Hautes Performances, Perpignan (publ. Lavoisier), pp. 202–211, **1988**.

[6] **Dubinin, M.M., Astakhov, V.A.**, Adv. Chem. Ser. 102, 69, **1970**.

[7] **Tamainot-Telto, Z., Critoph, R.E.**, Monolithic Carbon for Sorption Refrigeration and Heat Pump Applications, submitted to Applied Thermal Engineering.

[8] **International Institute of Refrigeration**, Thermodynamic and Physical Properties of Ammonia R717, ISBN: 2-903633-11-8, **1981**.

Chapter 4

Adsorption Generator Design Philosophy

4.1 Introduction

Although the research specification provides a guide to the overall generator design there are still a range of viable solutions that fulfil the research criteria. Hence, it is necessary to define the generator design more precisely before commencing the numerical modelling. The generator design confirms the overall generator geometry and structure as well as the materials that will be employed in the final design.

4.2 Generator Structure

The overall design criterion for the adsorption generator was for implementation in an experimental rig with a view to producing a heat driven ice maker suitable for use in developing countries. With this in mind, the size, simplicity and raw material costs of the generator were major factors in guiding the design.

For an adsorption cycle, during the heating phase of the cycle, adsorbate is driven out of the generator, condensed and stored in an evaporator whilst during the cooling phase of the cycle the adsorbate boils in the evaporator under low pressure as it is re-adsorbed into the generator. This boiling process produces the cooling effect, equal to the mass of adsorbate multiplied by its enthalpy of vaporisation. The cooling power is dependent on the

mass of adsorbate that is desorbed/adsorbed and the time it takes to complete a thermodynamic cycle. Hence, the more rapidly a given mass of adsorbate can be desorbed and re-adsorbed the greater the cooling power that can be realised.

Although a number of different approaches are available for increasing the rate at which heat can be delivered and extracted from adsorbent beds, many of them are not suitable for a developing country application because they are either too complex to implement or involve the use of expensive materials and manufacturing processes. Hence, after weighing up a number of the available options against the requirements for a design suitable for manufacture in a developing country, a cylindrical adsorption generator was selected consisting of layers of adsorbent material sandwiched between metal discs in a laminate structure, as shown in Figure 6.4. This was considered to offer a good potential for rapid thermal cycling of the adsorbent whilst also offering a relatively simple method of manufacture, low cost of materials and robustness of generator internal structure.

Having specified the general generator geometry the method of heating and cooling the generator was then considered. Four different options were considered, heating and cooling externally, heating and cooling internally, heating externally and cooling internally, heating internally and cooling externally. Heating and cooling internally was discounted because of the poor heat transfer area available compared to external methods. Heating externally and cooling internally and heating internally and cooling externally both offered the advantage of separating the heating and cooling loops entirely with the option of using different heat transfer fluids for heating and cooling. However, the low heat transfer area available for internal heating/cooling as well as the greater complexity of manufacture made both of these options less desirable. Therefore, it was decided that the generator should be both heated and cooled externally.

For external heating and cooling two different approaches were considered. The first approach was to separate the heating and cooling loops by winding a spiral pair of rectangular section tubing around the outside of the cylindrical laminate shell, one tube containing the heating heat transfer fluid and the other containing the cooling heat transfer

fluid. Although this approach again offered the possibility of separating the heating and cooling loops and thus heat transfer fluids it was thought to be too complex. Additionally the heat transfer would be compromised by the thermal contact resistance between the heating/cooling loop tube and the outside of the laminate shell as well as the reduced heat transfer area available as a result of splitting the heating and cooling loops. A variation on this idea was to mill a spiral pair of channels directly into the laminate shell wall and sleeve the channels with another close tolerance shell passing over the length of the generator and welded in place along the spiral path of the channels. However, although this would have provided increased heat transfer between the heating and cooling loops and the laminate shell, the idea was not pursued as it was considered too complex. Additionally, the thicker laminate shell wall required to accommodate the heat transfer channels would increase the sensible heating/cooling and thermal mass to be cycled over the complete thermodynamic cycle reducing efficiency and increasing cycle times. The second approach considered was to heat or cool the generator by respectively condensing or boiling a heat transfer fluid directly on the external laminate shell wall. This method was chosen as it offers the advantages of utilising the entire external surface area of the laminate shell for heating and cooling to provide good heat transfer while also being simpler to implement than individual spiral tube pairs. However, this method necessitates utilising the same heat transfer fluid for both the heating and cooling phases of the thermodynamic cycle.

4.3 Generator Materials

The key materials utilised within the generator are the adsorbent and the adsorbate and their selection characterises the manner in which the generator will operate with respect to factors such as cycling time, system pressure, concentration swing and specific cooling power. A review of the possible adsorbents and adsorbates as well as the choices governing their use was presented in Section 2.4. The adsorbate will not only be present (at a certain concentration) within the generator but also throughout the remainder of the system condenser-receiver-evaporator loop. The other material choices are related to the generator shell containing the laminate and the heat transfer discs utilised within the laminate.

Factors affecting choice of adsorbent:

- Thermal Conductivity
- Specific Heat Capacity
- Porosity
- Permeability
- Compatibility (with other materials)
- Stability (over many cycles)
- Availability
- Cost

Factors affecting choice of adsorbate:

- Enthalpy of Vaporisation
- Vapour Pressure
- Molecular Weight
- Polarity (small polar molecules)
- Viscosity
- Diffusivity
- Flammability
- Corrosiveness
- Compatibility (with other materials)
- Stability (no chemical decomposition)
- Toxicity
- Environmental Friendliness
- Availability
- Legal Restrictions
- Cost

Due to their cost chemical adsorbents such as calcium chloride were not considered to be suitable for a developing country application. In addition to this, chemical adsorbents pose difficulties associated with corrosion and poor adsorbent physical stability as a result of volume changes that take place during the adsorption and desorption processes. The poor physical stability of the chemical adsorbents was of particular concern for a rapid cycling system where the adsorbent may experience several adsorption and desorption processes over a short period of time.

Physical adsorbents are generally neutral and chemically unreactive and so present no long term corrosion difficulties. They also maintain a constant volume during the adsorption and desorption processes which allows for greater physical stability and robustness compared to chemical adsorbents, particularly when applied in a rapid cycling system.

The three main physical adsorbents considered were activated carbon, zeolites (both natural and synthetic) and silica gels. The final choice of adsorbent material was made by assessing the benefits and drawbacks of each adsorbent material in relation to the intended developing country application.

For the adsorption generators, an activated carbon adsorbent, type LM127, manufactured by Sutcliffe Carbons Ltd was selected. In a monolithic form this activated carbon has good porosity, permeability and thermal conductivity characteristics. The Sutcliffe Carbons activated carbon LM127 is of an advanced formulation incorporating a binding material and manufactured to a consistent specification. However, in a developing country, a less costly activated carbon could be manufactured from locally available starting materials such as wood, soft fruit stones (peaches, apricots, etc.), coconut shell or other carbon based organic precursor. In this way the activated carbon could be manufactured directly in the country of use, thus saving on the expense of importing a far more expensive product from overseas.

The final choice of adsorbate was made by assessing the benefits and drawbacks of each adsorbate with regard to factors such as enthalpy of vaporisation, thermal stability and vapour pressure over the operating temperature range.

Based on the above criteria, ammonia was selected as the most suitable adsorbate for use in conjunction with the monolithic activated carbon adsorbent. Ammonia is readily available, thermally stable and can be used over a wide temperature range. However, ammonia is also toxic, flammable in certain concentrations with air and incompatible with copper. Therefore, stainless steel was selected for all of the pressure vessels (condenser, receiver, evaporator) and pipe-work that would come into contact with ammonia. For a developing country application, mild steel provides a lower cost alternative to stainless steel which is also resistant to corrosive attack from ammonia. However, for use outdoors, particularly in a humid environment, mild steel would need to be painted or lacquered externally to prevent it from rusting. Although ammonia is toxic, the presence of ammonia

can be detected in very small concentrations allowing the user to become aware of any leaks in the system very quickly.

The greater the enthalpy of vaporisation the greater the cooling that can be achieved per unit mass of adsorbate that is desorbed and adsorbed through each thermodynamic cycle. Although water has a greater enthalpy of vaporisation than ammonia, and would therefore appear to be a better choice as an adsorbate, it is not suitable for use in an ice making system unless precautions are taken, such as the addition of ethylene glycol (anti-freeze), to prevent it from freezing in the evaporator. The vapour pressure of ammonia is greater than atmospheric pressure over the system operating temperature range while the vapour pressure for water or methanol will drop below atmospheric pressure at points in the system operating temperature range and at ambient temperature. For good reliability, the system should be as leak proof as possible so that the adsorption and desorption processes take place in the absence of air. If there are any small leaks in the system utilising ammonia, although some adsorbate will be lost, the system should continue operating with a reduced ammonia inventory. In contrast to this, for a system utilising water or methanol, any small leaks will allow air to be sucked into the system and prevent continued operation. Additionally, for an ice making system utilising water as the adsorbate, the vapour pressures involved are so low (high vacuum) that high technology solutions are required to prevent pressure losses within the system.

Stainless steel, type 304 or type 316, was selected for the generator shell, laminate shell, condenser, receiver, evaporator and connecting pipe-work. Stainless steel is both resistant to corrosion in the presence of ammonia and able to withstand the pressures encountered in the system which may be as great as 20 bar in the ammonia condenser.

Aluminium was selected as a suitable material for the discs within the laminate, with a thermal conductivity of 204 $W\,m^{-1}K^{-1}$. A high thermal conductivity for the disc in the radial direction is desirable in order to allow heat to be conducted into and out of the centre of the laminate as rapidly as possible. A compliant soft annealed aluminium foil was chosen to provide good thermal contact between the disc and the internal wall of the laminate shell

and between the disc and the monolithic carbon. A good thermal contact, and thus low thermal contact resistance, facilitates an increased rate of heat transfer into and out of the laminate during heating and cooling cycles and consequently more rapid thermal cycling. The thermal contact may be improved by ensuring close contact, with a minimal air gap, between the aluminium discs and the laminate shell internal wall and the aluminium discs and the adjacent monolithic carbon layers.

4.4 Conclusions

An adsorption generator design based on a cylindrical laminate structure was selected by consideration of the design criteria for a system suitable for use in developing countries. This laminate consists of alternate layers of activated carbon adsorbent and aluminium contained within a stainless steel shell. The laminate shell located within the generator will be heated and cooled externally by condensing steam and boiling water under low pressure respectively. All pressure vessels in contact with the ammonia adsorbate will be manufactured from stainless steel to avoid any corrosion problems.

Chapter 5

Numerical Modelling

5.1 Introduction

Having evaluated a number of possible adsorption generator structures, a novel cylindrical carbon-aluminium laminate structure was thought to offer the most promising possibilities, both in terms of specific cooling powers attainable and suitability for future production and utilisation in developing countries. However, before manufacturing the laminate, it was decided that a numerical model of the system should be constructed in order to arrive at an optimal generator geometry with respect to design parameters such as carbon layer thickness, aluminium layer thickness and laminate diameter.

5.2 Material Properties

In order to develop a numerical model for the system it was initially necessary to obtain accurate thermophysical data for material properties such as thermal conductivity, density and specific heat capacity. For the aluminium and stainless steel components of the generators such data is readily available from published texts [1]. The thermophysical data for the materials used in the generator is presented in Table 5.1.

Material	Thermal Conductivity (k) ($W\ m^{-1}K^{-1}$)	Density (ρ) ($kg\ m^{-3}$)	Specific Heat (Cp) ($J\ kg^{-1}K^{-1}$)
Stainless Steel	54	7833	465
Aluminium	204	2700	900
Ammonia	n/a	equation (5.64)	4734
LM127 Carbon	equation (5.1)	750	equation (5.7)

Table 5.1: Material Properties

Thermophysical data for the activated carbon provided by Sutcliffe Carbons Ltd has been published by Tamainot-Telto and Critoph [2]. This data includes polynomial equations derived from measured experimental data. These equations were used directly in the numerical model. Coefficients describing the carbon porosity characteristics were also used directly within the numerical model for calculating the generator concentration.

5.2.1 Carbon Thermal Conductivity

For an adsorption generator operating between two temperature levels, during each complete thermodynamic cycle the adsorbate is desorbed from the generator during the heating half-cycle and re-adsorbed into the generator during the cooling half-cycle. The cooling power obtained depends on the mass of adsorbent in the system, the concentration swing obtained over the cycle, the adsorbate enthalpy of vaporisation and the cycling time. Assuming the same concentration swing and adsorbate enthalpy of vaporisation, to deliver the same cooling power a system operating on a diurnal heating/cooling cycle would require a far larger adsorbent-adsorbate inventory than a comparable system operating on a rapid cycling regime of the order of minutes. Hence, a rapid cycling system has the advantage of smaller system volume and lower raw material costs, which is an important consideration for a developing country application. However, in order to realise short cycling times, good heat transfer is required at the interface between the activated carbon and the aluminium discs and stainless steel shell as well as within the activated carbon itself.

For a granular carbon, grain discontinuities and the small contact area between grain boundaries reduces heat transfer. The porosity of the carbon in conjunction with the poor heat transfer at grain boundaries limits the maximum thermal conductivity that is possible.

Monolithic carbons tend to exhibit an increased thermal conductivity as a result of the greater contact area between grain boundaries and increased bulk density of the material. The monolithic carbon used in the generators was provided by Sutcliffe Carbons Ltd and classified as type LM127; a coarse powder activated carbon. The thermal conductivity for the activated carbon, as arrived at by Tamainot-Telto and Critoph [2] is given by:

$$k_c = 0.8379 - (0.0008 \times T) \tag{5.1}$$

where:

k_c is the carbon thermal conductivity (W $m^{-1}K^{-1}$)

T is the carbon temperature (K)

The stated accuracy of equation (5.1) is $\pm 7\%$.

5.2.2 Carbon Density

For the LM127 activated carbon, Tamainot-Telto and Critoph [2] measured a density of 750 kg m^{-3}. This is 50% greater than the bulk density of an ordinary granular carbon, such as type 208C, which has a measured bulk density of 500 kg m^{-3}. The increased density of the monolithic carbon allows the generator volume to be reduced for a given mass of adsorbent. This should allow cost savings to be made in the raw material required to manufacture the sorption generator, which is an important consideration for a possible developing country application. The higher density should also provide an improved thermal contact path within the carbon and a corresponding increase in thermal conductivity. However, the increased carbon density will tend to reduce the permeability and may lead to a significant pressure drop through the carbon.

5.2.3 Carbon Porosity

Within the numerical model, the modified Dubinin-Astakhov equation was applied in order to calculate the mean generator concentration for a known set of nodal temperatures and generator saturation temperature at each time step. For the LM127 activated carbon a set of

Dubinin coefficients obtained empirically from experimental data were required in order to accurately model the porosity and adsorption characteristics of the carbon in the presence of the ammonia adsorbate. This data was obtained from the porosity data for the activated carbon LM127 presented by Tamainot-Telto and Critoph [2] using the porosimeter developed by Critoph [3] at the University of Warwick

The porosimeter was used to calculate the ammonia concentration within a sample of carbon, as the ratio of adsorbate to adsorbent, by applying the relationship:

$$x = \frac{M_a}{M_c} \tag{5.2}$$

where:

x is the ammonia concentration (kg NH_3 kg^{-1}Carbon)

M_a is the mass of ammonia within the sample (kg)

M_c is the mass of the carbon sample (kg)

The ammonia concentration predicted theoretically by the modified Dubinin-Astakhov equation is:

$$x = x_0 \exp\left(-K\left(\frac{T}{T_{sat}} - 1\right)^n\right) \tag{5.3}$$

where:

x_0 is the limiting concentration corresponding to maximum ammonia concentration under saturation conditions

K is a constant

n is a constant

T/T_{sat} is the ratio of adsorbent temperature (K) to adsorbate saturation temperature (K)

The Dubinin coefficients (x_0, K, n) for the sample were then obtained by equating the experimentally obtained concentration with that predicted theoretically by the Dubinin-Astakhov equation and obtaining the best fit by the method of least mean squares.

Tamainot-Telto and Critoph [2] found the concentration using the monolithic carbon to be approximately 30% higher that that obtainable with ordinary granular carbon, such as type 208C provided by Sutcliffe Carbons Ltd. The maximum concentration (x_0) was also found to be approximately 0.36 kg/kg for the monolithic carbon LM127 and approximately 0.29 kg/kg for the granular carbon 208C.

The Dubinin coefficients for the activated carbon LM127-ammonia pair, as arrived at by Tamainot-Telto and Critoph [2] are:

$x_0 = 0.3629$

$K = 3.6571$

$n = 0.9400$

$SEE = 0.0019$ (standard error of estimate)

These coefficients were used in the numerical model to calculate generator concentrations at each time step, concentration swings over the complete heating and cooling cycle and hence specific cooling power.

5.2.4 Carbon Permeability

The permeability of the monolithic carbon is of particular interest when considering the pressure losses that will occur within the generator while desorbing and adsorbing at times of maximum adsorbate flow rate. For the generators used in the experimental rig, the radial pressure drop through the carbon is of more importance than the axial pressure drop as adsorbate only flows in and out of the carbon in the radial direction. The aluminium discs between each carbon layer within the laminate prevent the axial flow of ammonia through the carbon.

Axial and radial permeability tests were carried out by Tamainot-Telto and Critoph [2] using a specially designed test rig. Permeability data is presented for a sample monolithic carbon disc of 76 mm diameter and 10 mm thickness. The samples were tested by measuring the pressure drop across the sample disc at a specified gas (air or argon) volume flow rate. It is stated that as the samples tested are porous, for radial flow the Ergun model [4, 5] may be applied in the form:

$$-\frac{dP}{dr} = \frac{\mu_g}{K_r} v_r + B_r \rho_g v_r^2 \tag{5.4}$$

where:

dP/dr is the pressure gradient across the sample (N m^{-3})

μ_g is the gas dynamic viscosity (N $m^{-2}s$)

ρ_g is the gas density (kg m^{-3})

v_r is the radial gas velocity (m s^{-1})

K_r is the radial permeability (m^2)

B_r is the radial material shape factor (m^{-1})

The permeability K_r and the shape factor B_r for the activated carbon LM127 under conditions of diverging radial flow are:

$K_r = 35.39 \times 10^{-14}$ m^2

$B_r = 0.44 \times 10^8$ m^{-1}

The pressure drop within the generator will be of greatest concern under conditions of diverging radial flow when the generator is in the adsorption phase of the sorption cycle. During this cooling phase the generator saturation pressure is considerably lower than during the desorption phase, the gas density will also be lower and for a given mass flow rate the flow velocity will be correspondingly larger. Hence, there will be a greater pressure

drop within the generator which will act to reduce cycle efficiency and specific cooling power.

The anisotropic nature of the monolithic carbon is highlighted in the data presented by Tamainot-Telto and Critoph [2] where for the coarse powder LM127 activated carbon a radial permeability approximately ten times larger than the axial permeability is presented. This anisotropic permeability characteristic is attributed to the manufacturing process employed in compressing the carbon powder in the axial direction to form monolithic carbon discs.

The axial or radial pressure drop within the generator for a gas with a dynamic viscosity less than 3×10^{-5} N m^{-2}s, such as ammonia, flowing through it may be calculated by applying [2]:

$$\Delta P = \frac{RT\mu_g \dot{m}_r}{2\pi\Delta\zeta_{gen} P_m}.\log\left(\frac{r_i}{r_o}\right)\left[\frac{1}{K} + B\frac{\left(\frac{1}{r_o}-\frac{1}{r_i}\right)}{2\pi\Delta\zeta_{gen}.\log\left(\frac{r_i}{r_o}\right)}\left(\frac{\dot{m}_r}{\mu_g}\right)\right] \tag{5.5}$$

$$\mu_a = \left(\left(0.0040\times T\right) - 0.1658\right)\times 10^{-5} \tag{5.6}$$

where:

$\Delta P = P_2 - P_1$ is the pressure drop within the generator (N m^{-2})

$P_m = \left(P_1 + P_2\right)/2$ is the mean carbon pressure (N m^{-2})

μ_a is the ammonia dynamic viscosity (N m^{-2}s) with T in Kelvin (K)

T is the generator temperature (K)

R (~ 488 for ammonia) is the specific gas constant (J kg^{-1}K^{-1})

$\Delta\zeta_{gen}$ is the total generator length (m)

$\dot{m}_r$ is the radial gas mass flow rate (kg s^{-1})

r_o is the generator outside radius (m)

r_i is the generator inside radius (m)

K is the carbon permeability (m^2)

B is the shape factor (m^{-1})

For operating parameters relevant to the current generators [6, 7]; radial ammonia mass flow rate of 0.001 kg s^{-1} which is consistent with a maximum mean specific cooling power of approximately 1 kW kg^{-1} of adsorbent, generator diameter of 50 mm and generator length of 1 metre, the pressure drop within the generator may be calculated. Tamainot-Telto and Critoph [2] found that the pressure drop through the generator was higher when operating with lower gas pressures. However, they calculated a radial pressure drop of only 50 mbar for a generator using the monolithic carbon LM127. Hence, even when the generator is operating in the cooling phase of the cycle where ammonia is re-adsorbed into the carbon and gas pressures are low, the radial pressure drop is still negligible compared to the ammonia saturation pressure.

5.2.5 Carbon Void Volume

For a granular carbon, the void volume created between the carbon grains constitutes a major percentage of the total carbon volume and must be taken into consideration when performing a numerical analysis of the carbon adsorption and desorption. However, for a monolithic carbon, if the carbon is assumed to be continuous and homogeneous, the void volume may be regarded as negligible within the carbon structure itself. Hence, the sorption properties will be completely defined by the porosity characteristics of the carbon as stated by the Dubinin-Astakhov (D-A) equation. The D-A equation will not encompass the void volume created by the carbon macropores although this may be neglected and still produce good accuracy. However, when modelling pipe-work and valves in addition to the carbon generator itself, a void volume term within the program may be necessary to provide greater modelling accuracy and an improved fit with experimental data.

5.2.6 Carbon Effective Specific Heat

For the carbon adsorbent in the absence of ammonia adsorbate, the specific heat may be expressed as a function of temperature. The specific heat obtained by Restuccia [8] for the activated carbon LM127 using a scanning differential calorimeter is given by:

$$Cp_c = 34.685 + (2.811 \times T) \tag{5.7}$$

where:

Cp_c is the carbon specific heat (J $kg^{-1}K^{-1}$)

T is the carbon temperature (K)

For an adsorbent-adsorbate pair the specific heat will not only be a function of temperature, but also the concentration and pressure. Hence the specific heat is also a function of the path taken by the thermodynamic cycle. The complete thermodynamic cycle may be idealised as a four stage process, two isosteric (constant concentration) phases and two isobaric (constant pressure) phases. The effective specific heat will be seen to vary during the isobaric phases of the thermodynamic cycle where the generator concentration is changing due to adsorption or desorption compared to the isosteric phases of the thermodynamic cycle where the concentration remains constant.

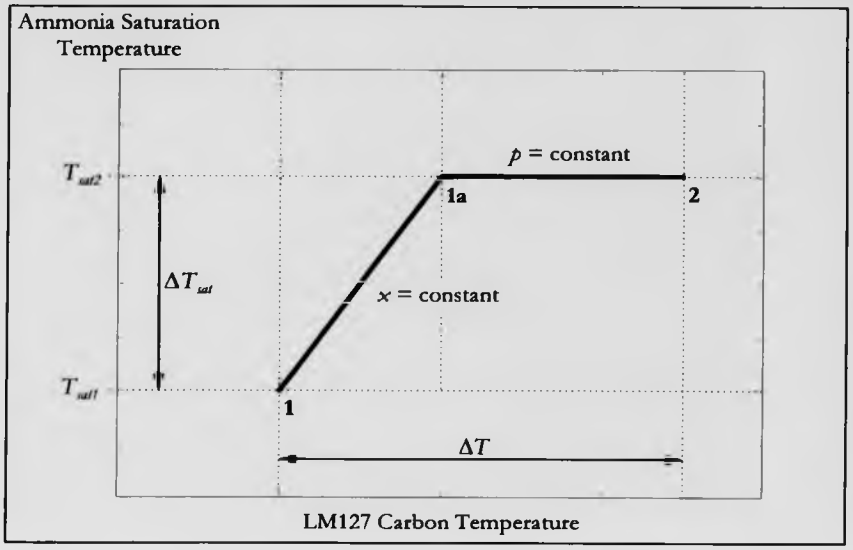

Figure 5.1: Clausius-Clapeyron Diagram Between Points 1 and 2 in the Thermodynamic Process Path

The effective specific heat of the carbon-ammonia pair may be evaluated by referring to the Clausius-Clapeyron diagram in Figure 5.1. From geometrical considerations it can be shown [9] that:

$$T_{sat1}T_{1a} = T_{sat2}T_1 \tag{5.8}$$

$$\therefore T_{1a} = \frac{T_{sat2}T_1}{T_{sat1}} = T_1\left(\frac{\Delta T_{sat} + T_{sat1}}{T_{sat1}}\right) = T_1\left(\frac{\Delta T_{sat}}{T_{sat1}} + 1\right) \tag{5.9}$$

Evaluating the heat input (q) for a unit mass from 1 - 1a (constant concentration):

$$\Delta q_{1\to 1a} = \left(Cp_c + x_1 Cp_a\right)\left(T_{1a} - T_1\right) \tag{5.10}$$

Substituting equation (5.9) into equation (5.10):

$$\Delta q_{1\to 1a} = \left(Cp_c + x_1 Cp_a\right)\left(\frac{T_1 \cdot \Delta T_{sat}}{T_{sat1}}\right) = T_1\left(Cp_c + x_1 Cp_a\right)\left(\frac{\Delta T_{sat}}{T_{sat1}}\right) \tag{5.11}$$

Evaluating the heat input (q) for a unit mass from 1a - 2 (constant pressure):

$$\Delta q_{1a\to 2} = \left(Cp_c + x_1 Cp_a\right)\left(T_2 - T_{1a}\right) - \frac{\partial x.h_v T_1}{T_{sat1}} \tag{5.12}$$

Alternatively, substituting in the enthalpy of adsorption from equation (3.38) into equation (5.12) gives:

$$\Delta q_{1a\to 2} = \left(Cp_c + x_1 Cp_a\right)\left(T_2 - T_{1a}\right) - \partial x.h_{adi} \tag{5.13}$$

where:

x_1 is the ammonia concentration at 1 (kg NH_3 kg^{-1}Carbon)

Cp_a is the ammonia specific heat (J $kg^{-1}K^{-1}$)

T is the temperature (K)

T_{sat} is the saturation temperature (K) at the ammonia pressure

h_v is the specific enthalpy of vaporisation (kJ kg^{-1})

h_{adi} is the specific enthalpy of adsorption (kJ kg^{-1})

Differentiating the modified D-A equation, presented in equation (5.3), to give the rate of concentration change with respect to temperature at constant saturation temperature:

$$\left(\frac{\partial x}{\partial T}\right)_{T_{sat}} = \left(x_0 \exp\left(-K\left(\frac{T_1}{T_{sat1}} - 1\right)^n\right) \times \left(-\frac{Kn}{T_{sat1}}\right)\left(\frac{T_1}{T_{sat1}} - 1\right)^{n-1}\right) \tag{5.14}$$

$$\therefore \left(\frac{\partial x}{\partial T}\right)_{T_{sat}} = \left(-\frac{Knx_1}{T_{sat1}}\right)\left(\frac{T_1}{T_{sat1}} - 1\right)^{n-1} \tag{5.15}$$

Now from 1a - 2:

$$\partial x = \left(\left(T_2 - T_{1a} \right) \left(-\frac{Knx_1}{T_{sat1}} \right) \left(\frac{T_1}{T_{sat1}} - 1 \right)^{n-1} \right) \tag{5.16}$$

Substituting equation (5.16) into equation (5.12) yields:

$$\begin{aligned} \Delta q_{1a \to 2} &= \left(Cp_c + x_1 Cp_a \right) \left(T_2 - T_{1a} \right) \\ &+ \left(\left(T_2 - T_{1a} \right) \left(\frac{h_v T_1}{T_{sat1}} \right) \left(\frac{Knx_1}{T_{sat1}} \right) \left(\frac{T_1}{T_{sat1}} - 1 \right)^{n-1} \right) \end{aligned} \tag{5.17}$$

Adding equation (5.11) to equation (5.17) gives:

$$\begin{aligned} \Delta q_{1 \to 2} &= T_1 \left(Cp_c + x_1 Cp_a \right) \left(\frac{\Delta T_{sat}}{T_{sat1}} \right) + \left(Cp_c + x_1 Cp_a \right) \left(T_2 - T_{1a} \right) \\ &+ \left(\left(T_2 - T_{1a} \right) \left(\frac{h_v T_1}{T_{sat1}} \right) \left(\frac{Knx_1}{T_{sat1}} \right) \left(\frac{T_1}{T_{sat1}} - 1 \right)^{n-1} \right) \end{aligned} \tag{5.18}$$

Substituting equation (5.9) into equation (5.18) and rearranging gives:

$$\begin{aligned} \Delta q_{1 \to 2} &= \left(Cp_c + x_1 Cp_a \right) \left(T_2 - T_1 \right) \\ &+ \left(\left(\frac{h_v T_1}{T_{sat1}} \right) \left(\frac{Knx_1}{T_{sat1}} \right) \left(\frac{T_1}{T_{sat1}} - 1 \right)^{n-1} \right) \left(T_2 - T_1 \left(1 + \frac{\Delta T_{sat}}{T_{sat1}} \right) \right) \end{aligned} \tag{5.19}$$

Let:

$$Cp^A = Cp_c + x_1 Cp_a \tag{5.20}$$

Let:

$$Cp^B = \left(\left(\frac{h_v T_1}{T_{sat1}} \right) \left(\frac{Knx_1}{T_{sat1}} \right) \left(\frac{T_1}{T_{sat1}} - 1 \right)^{n-1} \right) \tag{5.21}$$

Substituting equations (5.20) and (5.21) into equation (5.19) gives:

$$\Delta q_{1\to 2} = Cp^{A}\left(T_2 - T_1\right) + Cp^{B}\left(T_2 - T_1\left(1 + \frac{\Delta T_{sat}}{T_{sat1}}\right)\right) \tag{5.22}$$

Now:

$$\overline{Cp}_{1\to 2} = \frac{\Delta q_{1\to 2}}{\Delta T_{1\to 2}} \tag{5.23}$$

Therefore:

$$\begin{aligned}\overline{Cp}_{1\to 2} &= Cp^{A} + Cp^{B}\left(\frac{T_2}{T_2 - T_1} - \frac{T_1}{T_2 - T_1}\left(1 + \frac{\Delta T_{sat}}{T_{sat1}}\right)\right)\\ &= Cp^{A} + Cp^{B}\left(1 - \left(\frac{T_1}{T_2 - T_1}\right)\left(\frac{\Delta T_{sat}}{T_{sat1}}\right)\right)\\ &= Cp^{A} + Cp^{B} - \frac{Cp^{B}.\Delta T_{sat}.T_1}{\Delta T.T_{sat1}}\end{aligned} \tag{5.24}$$

Let:

$$Cp^{C} = Cp^{A} + Cp^{B} \tag{5.25}$$

Let:

$$Cp^{D} = \frac{Cp^{B}.\Delta T_{sat}.T_1}{T_{sat1}} \tag{5.26}$$

Let:

$$Cp^{E} = \frac{Cp^{D}}{Cp^{C}} \tag{5.27}$$

The effective specific heat utilised in the governing energy balance equations is then:

$$\overline{Cp}_{1\to 2} = Cp^{C} - \frac{Cp^{D}}{\Delta T} \tag{5.28}$$

where:

$\Delta T = T_{i,j}^{n+1} - T_{i,j}^{n}$ is the temperature difference at node i, j over a time-step Δt.

5.3 Governing System Equations

In order to model the transient heat and mass transfer within the generator, a series of equations were developed to describe the physical behaviour of the system in terms of heat fluxes, energy storage and adsorption/desorption processes. This generator itself consists of a porous monolithic carbon adsorbent, sandwiched in between aluminium discs to form a carbon-aluminium laminate. This laminate is contained by, and is in close physical contact with, a stainless steel shell. This shell is heated externally by condensing steam and cooled externally by boiling water at low saturation pressure.

Within the adsorbent micropores (< 2 nm) the monolithic carbon will contain adsorbed ammonia in a condensed state. The larger mesopores (2 nm - 50 nm) and macropores (> 50 nm) will contain ammonia in the vapour phase. For a granular carbon there will also be a significant volume of gaseous ammonia within the intergranular voids. However, within a monolithic carbon the presence of gaseous ammonia within any voids present may be assumed to be negligible.

The physical governing equations which describe the transient heat conduction and mass transfer within the generator are:

(i) The heat transfer equation

(ii) The mass transfer equation

(iii) The adsorption equation of state

5.3.1 Heat Transfer Equation

The generalised three dimensional heat equation in cylindrical polar coordinates, applicable to modelling the generator heat transfer is given by:

$$\frac{1}{\alpha}\frac{\partial T}{\partial t} = \frac{\partial^2 T}{\partial r^2} + \frac{1}{r}\frac{\partial T}{\partial r} + \frac{1}{r^2}\frac{\partial^2 T}{\partial \theta^2} + \frac{\partial^2 T}{\partial z^2} + \frac{\dot{H}}{k} \tag{5.29}$$

$$\alpha = \frac{k}{\rho . Cp} \tag{5.30}$$

where:

$\dot{H}$ is the internal heat generation rate per unit volume (W m^{-3})

α is the thermal diffusivity ($m^2 s^{-1}$)

k is the thermal conductivity of the material (W $m^{-1} K^{-1}$)

ρ is the material density (kg m^{-3})

Cp is the specific heat capacity of the material (J $kg^{-1} K^{-1}$)

For a two dimensional case in the r-z plane with cylindrical polar coordinates in the absence of internal heat generation, equation (5.29) reduces to:

$$\frac{1}{\alpha}\frac{\partial T}{\partial t} = \frac{\partial^2 T}{\partial r^2} + \frac{1}{r}\frac{\partial T}{\partial r} + \frac{\partial^2 T}{\partial z^2} \tag{5.31}$$

However, in this form it is assumed that the thermal conductivity k is constant. For the adsorption generator model this is not the case. Although it is perfectly possible to use equation (5.31) to derive the system finite difference equations, for the present case a better starting point is offered by the one dimensional Fourier heat equation:

$$\dot{Q}_x = -kA\frac{\partial T}{\partial x} \tag{5.32}$$

where:

$\dot{Q}_x$ is the rate of heat flow in the x direction (W)

A is the area normal to the direction of heat flow (m^2)

$\partial T/\partial x$ is the temperature gradient in the x direction (K m^{-1})

For transient conditions the rate of temperature rise for a given control volume of material will be determined by:

$$\dot{Q} = mCp\frac{\partial T}{\partial t} = \rho VCp\frac{\partial T}{\partial t} \tag{5.33}$$

where:

$\dot{Q}$ is the rate of heat flow into the control volume (W)

m is the mass of material (kg)

V is the control volume (m^3)

$\partial T/\partial t$ is the rate of temperature change (K s^{-1})

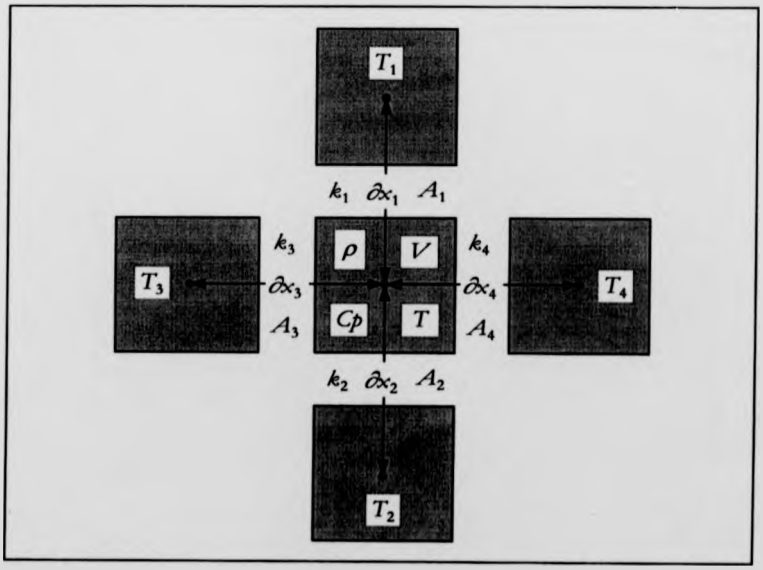

Figure 5.2: Two Dimensional Control Volume

For the control volume (central square) shown in Figure 5.2, equating equations (5.32) and (5.33) in an energy balance for a two dimensional problem with heat flows into the control volume in four directions in the absence of internal heat generation gives:

$$\rho V Cp \frac{\partial T}{\partial t} = -k_1 A_1 \frac{\partial T_1}{\partial x_1} - k_2 A_2 \frac{\partial T_2}{\partial x_2} - k_3 A_3 \frac{\partial T_3}{\partial x_3} - k_4 A_4 \frac{\partial T_4}{\partial x_4} \qquad (5.34)$$

Equivalent finite difference equations are obtained by discretising the two dimensional heat equation (5.31) directly and by discretising the energy balance equation (5.34).

5.3.2 Mass Transfer Equation

If the permeability of the adsorbent is sufficiently high, a uniform pressure distribution throughout the generator can be assumed. From the permeability data for the carbon type LM127, it has been calculated (see Section 5.2.4) that even at the highest adsorbate mass flow rates likely to be encountered, the pressure drop within the generator will only be of the order of 50 mbar. Hence, for modelling purposes, compared to the generator evaporating saturation pressure (4.3 bara at 0°C) and condensing saturation pressure (15.5 bara at 40°C), the pressure drop within the generator may be considered to be zero. If the monolithic carbon is also assumed to be continuous and homogeneous, the physical governing equations reduce to the heat transfer equation and the adsorption equation of state. Mass transfer is then governed by pressure gradients across the system, between the generators and system components such as the condenser, receiver and evaporator. Thus, the generator pressures are completely described by the temperature and concentration calculations.

5.3.3 Adsorption Equations of State

The Dubinin-Radushkevich (D-R) and Dubinin-Astakhov (D-A) equations which describe the volumetric pore filling in microporous adsorbents are defined in equations (3.3) and (3.8) respectively. The D-A equation was applied within the numerical model to predict the mean generator concentration at each time step and thus the specific cooling power. The constants used in the D-A equation are presented in Section 5.2.3.

5.3.4 Simplifying Assumptions

A number of simplifying assumptions have been made in developing the numerical model for the adsorption generator as listed below:-

(i) The monolithic carbon is stationary, homogeneous and isotropic.

(ii) The initial temperature distribution within the generator is uniform.

(iii) The pressure distribution within the generator is uniform at each point in time.

(iv) Void volume can be neglected as there are no intergranular voids, the mass of gaseous ammonia in the mesopores and macropores is negligible and the remaining void volume within the generator, before the check valves, is small enough to be ignored.
Also, the volume of ammonia in the mesopores and macropores is implicity taken into account in the Dubinin coefficients obtained from porosity measurements.

(v) The internal heat transfer coefficient between the aluminium discs and the monolithic carbon, the stainless steel shell and the monolithic carbon and the stainless steel shell and the aluminium discs is infinite, assuming perfect contact - supported by the carbon micrographs presented in Section 6.3.4.

5.4 Finite Difference Models

Exact analytical solutions to the governing partial differential equations (PDEs) are only possible for simplified cases with regular geometries and stable boundary conditions. Some analytical solutions, such as those presented in the "Heisler" charts may be available for greatly simplified one dimensional problems. However, for more complex problems involving two or three dimensions, transient boundary conditions, and for the present case also adsorption and desorption processes, an alternative solution approach is required.

Finite difference methods allow the governing PDEs and boundary conditions to be replaced by a set of algebraic equations which lend themselves to a numerical solution. These algebraic finite difference equations approximate to the governing partial differential

equations, replacing a continuous problem domain with a discrete problem domain where the dependent variables are solved at grid points (nodes) within the domain. The accuracy of these finite difference equations is determined by factors such as the truncation error between the governing PDEs and their finite difference representation, the size of grid spacing used to define the space steps and for transient problems the size of the time step utilised. Accuracy may also be compromised by round-off errors in the numerical solution, governed by the number of digits to which solution variables can be represented. A finite differencing scheme is said to be consistent if the truncation error tends to zero as the grid is refined and the space steps become smaller. For transient problems where the solution is marched forward in time, depending on the finite difference discretisation scheme selected, stability criteria will impose limits on the size of the space steps and time steps that can be applied in order to achieve a converged solution. For solution convergence, any errors generated due to factors such as truncation and round-off should not be allowed to grow from one time step to another.

The two main finite difference methods for transient conduction problems are based on explicit or implicit solution procedures although there are other finite differencing schemes which have been developed as a compromise between these two approaches. Explicit schemes evaluate the solution variable at the new time level in terms of other known variables. Hence, there is only one unknown in the finite difference equation which can be evaluated directly from other known solution variables. The solution at each node within the computational domain can then be calculated by sweeping through the nodes in sequence. In this way the solution can be marched forward in time from a specified set of boundary conditions. However, the stability criteria for explicit schemes tend to limit the size of the time-step which may be applied for a given grid refinement with greater refinement (for improved accuracy) demanding smaller time-steps and thus increased computing time to march the solution forward to a given point in time. In contrast to this, implicit schemes evaluate the solution variable at the new time level in terms of other unknown variables. This generates a set of algebraic equations for all the nodes in the computational domain which must be solved simultaneously in order to evaluate the new

solution variable at each node. The advantage of implicit schemes in that they are unconditionally stable for any time-step value, with the scheme accuracy improving as the time-step is reduced. However, although an implicit scheme may give an equivalent accuracy to an explicit scheme while using a larger time-step, the additional computational procedures required to solve the simultaneous set of algebraic equations at the new time level for the implicit scheme may negate any computational speed advantage realised through using a larger time-step.

5.4.1 Finite Difference Grid Generation

In order to construct a numerical model for the adsorption generator, a schematic of a unit cell was isolated from the generator as a whole. This unit cell, presented in Figure 5.3 shows a single layer of the adsorbent generator. For clarity, the unit cell will be described in terms of north, south, east and west directions.

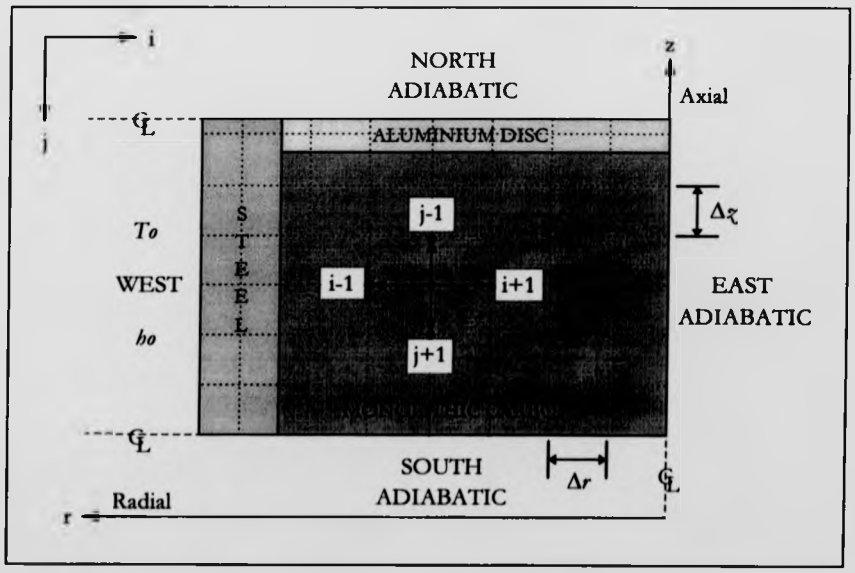

Figure 5.3: Numerical Unit Cell Schematic

where:

To is the external steam condensing temperature or water boiling temperature (K)

ho is the external convective heat transfer coefficient ($W\ m^{-2}K^{-1}$)

- The **north** face of the unit cell is a line of symmetry through a half thickness of the aluminium disc and is defined as an adiabatic boundary.
- The **south** face of the unit cell is a line of symmetry through a half thickness of the monolithic carbon layer and is defined as an adiabatic boundary.
- The **east** face of the unit cell is the generator line of axial symmetry and is defined as an adiabatic boundary.
- The **west** face of the unit cell is the external wall of the generator, exposed to condensing steam and boiling water under low pressure and is defined as a convective boundary.

The unit cell has a finite difference grid superimposed on it to break the continuous problem domain down into a series of nodes at discrete locations. Nodes are located by the use of the subscripts *i* and *j*. Applying cylindrical polar coordinates, nodes in the *i* direction are separated by space-steps Δr and nodes in the *j* direction are separated by space-steps Δz. The size of the space steps Δr and Δz are allowed to vary in the *i* and *j* directions, between the carbon and the shell wall or carbon and the aluminium fin for instance. A control volume is defined around each node with interfaces between each adjacent node in the north, south, east and west direction.

The conduction areas normal to the direction of heat flow at the node control volume interfaces, with respect to a node *i, j* are given by:

$$A_N = r_{i,j}\left(\Delta l_W + \Delta l_E\right) + \left(\frac{\left(\Delta l_W\right)^2 - \left(\Delta l_E\right)^2}{2}\right) \qquad (5.35)$$

$$A_S = r_{i,j}\left(\Delta l_W + \Delta l_E\right) + \left(\frac{\left(\Delta l_W\right)^2 - \left(\Delta l_E\right)^2}{2}\right) \tag{5.36}$$

$$A_E = \left(r_{i,j} - \Delta l_E\right)\left(\Delta l_N + \Delta l_S\right) \tag{5.37}$$

$$A_W = \left(r_{i,j} + \Delta l_W\right)\left(\Delta l_N + \Delta l_S\right) \tag{5.38}$$

The cell control volume is:

$$V_{i,j} = \left(r_{i,j}\left(\Delta l_W + \Delta l_E\right) + \left(\frac{\left(\Delta l_W\right)^2 - \left(\Delta l_E\right)^2}{2}\right)\right)\left(\Delta l_N + \Delta l_S\right) \tag{5.39}$$

where:

$r_{i,j}$ is the radius from the unit cell axial line of symmetry to a node i,j

Δl_N is the length in the north direction from node i,j to the control volume interface

Δl_S is the length in the south direction from node i,j to the control volume interface

Δl_E is the length in the east direction from node i,j to the control volume interface

Δl_W is the length in the west direction from node i,j to the control volume interface

In general, the heat transfer coefficients between a node i,j and adjacent nodes in the north, south, east and west directions are given by:

$$u_N = \frac{k_N}{\Delta z_N} \tag{5.40}$$

$$u_S = \frac{k_S}{\Delta z_S} \tag{5.41}$$

$$u_E = \frac{k_E}{\Delta r_E} \tag{5.42}$$

$$u_W = \frac{k_W}{\Delta r_W} \tag{5.43}$$

where:

k_N is the thermal conductivity in the north direction from a node i, j

k_S is the thermal conductivity in the south direction from a node i, j

k_E is the thermal conductivity in the east direction from a node i, j

k_W is the thermal conductivity in the west direction from a node i, j

Δz_N is the space-step in the north direction from a node i, j

Δz_S is the space-step in the south direction from a node i, j

Δr_E is the space-step in the east direction from a node i, j

Δr_W is the space-step in the west direction from a node i, j

The heat transfer coefficient between a node i, j (node 1) and adjacent nodes (node 2) across an interface between two materials such as steel-carbon, aluminium-carbon and steel-aluminium, in the north, south, east and west directions, using an electrical resistance analogy is given by:

$$u_{N,S,E,W} = \frac{1}{\frac{1}{u_{material\,1}} + \frac{1}{u_{interface}} + \frac{1}{u_{material\,2}}} \tag{5.44}$$

where:

$u_{material\,1}$ is the heat transfer coefficient between node 1 and the interface (W $m^{-2}K^{-1}$)

$u_{material\,2}$ is the heat transfer coefficient between node 2 and the interface (W $m^{-2}K^{-1}$)

$u_{interface}$ is the interface heat transfer coefficient at the material junction area between node 1 and node 2 (W $m^{-2}K^{-1}$)

The material heat transfer coefficients are evaluated by dividing the material conductivity at node 1 or node 2 by the distance between the interface and node 1 or node 2 respectively. The interface heat transfer coefficient will depend on the degree of thermal contact between the two materials. The pressure, surface roughness and the characteristics of any fluid filling the void at the interface will all affect the interface heat transfer coefficient. If the contact between the two materials is assumed to be perfect, the contact resistance will be zero and the interface heat transfer coefficient infinite.

The remaining unit cell boundary heat transfer coefficients are given by:

North Adiabatic Boundary: $u_N = 0$

South Adiabatic Boundary: $u_S = 0$

East Adiabatic Boundary: $u_E = 0$

West Convective Boundary: $u_W = ho$

5.4.2 Finite Difference Schemes

Both explicit and implicit schemes were considered for the numerical model of the adsorption generator. Various schemes were assessed [10, 11] based on accuracy, stability, ease of implementation and computational speed of execution. Implicit schemes were discounted mainly due to their additional programming complexity compared to explicit schemes. Additionally, doubts were raised as to the computational speed improvement that could be achieved with an implicit scheme particularly in the presence of adsorption and desorption processes. Therefore, two different explicit finite differencing schemes were implemented; the alternating direction explicit finite difference scheme and the simple explicit finite difference scheme.

The computer model employing the alternating direction explicit scheme was written in C and compiled and executed on Sun Sparc/Ultrasparc Unix workstations. The later computer model, written to predict to performance of the experimental rig and using the simple explicit scheme was written mainly in C but with the addition of some C++

routines. This model was written, compiled and run using Microsoft Visual C++ on a PC running Microsoft Windows 95.

5.4.2.1 Alternating Direction Explicit Finite Difference Scheme

The alternating direction explicit (ADE) finite difference scheme used in the numerical model was proposed by Barakat and Clark [11, 12]. This scheme was chosen because of its relative programming simplicity compared to implicit schemes while also being unconditionally stable, offering the possibility of using larger time-steps than possible with the simple explicit scheme so as to reduce computing times and speed up analysis.

In this method two solution variables are calculated at each node at a given time level. The solution variable p is calculated by sweeping through the numerical domain from bottom left hand corner node to top right hand corner node. At the same time level the solution variable q is calculated by sweeping through the numerical domain in the opposite direction from top right hand corner node to bottom left hand corner node. The two solution variables are then averaged at that time level to give the new temperature at each node. The time then marches forward by time-step Δt and the process is repeated.

Taking equation (5.34), the two dimensional energy balance PDE as the starting point, the finite difference equations for the solution variables p and q at an internal node may be developed based on the Barakat and Clark alternating direction explicit scheme.

For the p solution variable:

$$\rho_{i,j} V_{i,j} Cp_{i,j} \left(\frac{p_{i,j}^{n+1} - p_{i,j}^{n}}{\Delta t} \right) = \left(\begin{array}{l} \dfrac{k_N A_N}{\Delta z_N} \left(p_{i,j-1}^{n} - p_{i,j}^{n} \right) + \dfrac{k_S A_S}{\Delta z_S} \left(p_{i,j+1}^{n+1} - p_{i,j}^{n+1} \right) \\ + \dfrac{k_E A_E}{\Delta r_E} \left(p_{i+1,j}^{n} - p_{i,j}^{n} \right) + \dfrac{k_W A_W}{\Delta r_W} \left(p_{i-1,j}^{n+1} - p_{i,j}^{n+1} \right) \end{array} \right) \tag{5.45}$$

$$p_{i,j}^{n+1} = p_{i,j}^{n} + \left(\frac{\Delta t}{\rho_{i,j} V_{i,j} Cp_{i,j}} \right) \left(\begin{array}{l} \dfrac{k_N A_N}{\Delta z_N} \left(p_{i,j-1}^{n} - p_{i,j}^{n} \right) + \dfrac{k_S A_S}{\Delta z_S} \left(p_{i,j+1}^{n+1} - p_{i,j}^{n+1} \right) \\ + \dfrac{k_E A_E}{\Delta r_E} \left(p_{i+1,j}^{n} - p_{i,j}^{n} \right) + \dfrac{k_W A_W}{\Delta r_W} \left(p_{i-1,j}^{n+1} - p_{i,j}^{n+1} \right) \end{array} \right) \tag{5.46}$$

Rearranging to gather $p_{i,j}^{n+1}$ coefficients on LHS:

$$p_{i,j}^{n+1}\left(1+\left(\frac{\Delta t}{\rho_{i,j}V_{i,j}Cp_{i,j}}\right)\left(\begin{array}{l}\dfrac{k_S A_S}{\Delta z_S}\\ +\dfrac{k_W A_W}{\Delta r_W}\end{array}\right)\right)$$
$$= p_{i,j}^{n}+\left(\frac{\Delta t}{\rho_{i,j}V_{i,j}Cp_{i,j}}\right)\left(\begin{array}{l}\dfrac{k_N A_N}{\Delta z_N}\left(p_{i,j-1}^{n}-p_{i,j}^{n}\right)+\dfrac{k_S A_S}{\Delta z_S}\left(p_{i,j+1}^{n+1}\right)\\ +\dfrac{k_E A_E}{\Delta r_E}\left(p_{i+1,j}^{n}-p_{i,j}^{n}\right)+\dfrac{k_W A_W}{\Delta r_W}\left(p_{i-1,j}^{n+1}\right)\end{array}\right) \quad (5.47)$$

$$p_{i,j}^{n+1}=\frac{\begin{array}{l}p_{i,j}^{n}\left(\dfrac{\rho_{i,j}V_{i,j}Cp_{i,j}}{\Delta t}\right)+\dfrac{k_N A_N}{\Delta z_N}\left(p_{i,j-1}^{n}-p_{i,j}^{n}\right)\\ +\dfrac{k_S A_S}{\Delta z_S}\left(p_{i,j+1}^{n+1}\right)+\dfrac{k_E A_E}{\Delta r_E}\left(p_{i+1,j}^{n}-p_{i,j}^{n}\right)+\dfrac{k_W A_W}{\Delta r_W}\left(p_{i-1,j}^{n+1}\right)\end{array}}{\dfrac{k_S A_S}{\Delta z_S}+\dfrac{k_W A_W}{\Delta r_W}+\dfrac{\rho_{i,j}V_{i,j}Cp_{i,j}}{\Delta t}} \quad (5.48)$$

Substituting in the effective specific heat coefficients from equations (5.25) and (5.27):

$$p_{i,j}^{n+1}=\frac{\begin{array}{l}\left(p_{i,j}^{n}+Cp_{i,j}^{E(p)}\right)\left(\dfrac{\rho_{i,j}V_{i,j}Cp_{i,j}^{C(p)}}{\Delta t}\right)+\dfrac{k_N A_N}{\Delta z_N}\left(p_{i,j-1}^{n}-p_{i,j}^{n}\right)\\ +\dfrac{k_S A_S}{\Delta z_S}\left(p_{i,j+1}^{n+1}\right)+\dfrac{k_E A_E}{\Delta r_E}\left(p_{i+1,j}^{n}-p_{i,j}^{n}\right)+\dfrac{k_W A_W}{\Delta r_W}\left(p_{i-1,j}^{n+1}\right)\end{array}}{\dfrac{k_S A_S}{\Delta z_S}+\dfrac{k_W A_W}{\Delta r_W}+\dfrac{\rho_{i,j}V_{i,j}Cp_{i,j}^{C(p)}}{\Delta t}} \quad (5.49)$$

where:

$Cp_{i,j}^{C(p)}$ is the effective specific heat coefficient C at node i,j for the p solution variable

$Cp_{i,j}^{E(p)}$ is the effective specific heat coefficient E at node i,j for the p solution variable

For the q solution variable:

$$\rho_{i,j}V_{i,j}Cp_{i,j}\left(\frac{q_{i,j}^{n+1}-q_{i,j}^{n}}{\Delta t}\right)=\left(\begin{array}{l}\dfrac{k_N A_N}{\Delta z_N}\left(q_{i,j-1}^{n+1}-q_{i,j}^{n+1}\right)+\dfrac{k_S A_S}{\Delta z_S}\left(q_{i,j+1}^{n}-q_{i,j}^{n}\right)\\ +\dfrac{k_E A_E}{\Delta r_E}\left(q_{i+1,j}^{n+1}-q_{i,j}^{n+1}\right)+\dfrac{k_W A_W}{\Delta r_W}\left(q_{i-1,j}^{n}-q_{i,j}^{n}\right)\end{array}\right) \tag{5.50}$$

$$q_{i,j}^{n+1}=q_{i,j}^{n}+\left(\frac{\Delta t}{\rho_{i,j}V_{i,j}Cp_{i,j}}\right)\left(\begin{array}{l}\dfrac{k_N A_N}{\Delta z_N}\left(q_{i,j-1}^{n+1}-q_{i,j}^{n+1}\right)+\dfrac{k_S A_S}{\Delta z_S}\left(q_{i,j+1}^{n}-q_{i,j}^{n}\right)\\ +\dfrac{k_E A_E}{\Delta r_E}\left(q_{i+1,j}^{n+1}-q_{i,j}^{n+1}\right)+\dfrac{k_W A_W}{\Delta r_W}\left(q_{i-1,j}^{n}-q_{i,j}^{n}\right)\end{array}\right) \tag{5.51}$$

Rearranging to gather $q_{i,j}^{n+1}$ coefficients on LHS:

$$\begin{aligned}&q_{i,j}^{n+1}\left(1+\left(\frac{\Delta t}{\rho_{i,j}V_{i,j}Cp_{i,j}}\right)\left(\begin{array}{l}\dfrac{k_N A_N}{\Delta z_N}\\ +\dfrac{k_E A_E}{\Delta r_E}\end{array}\right)\right)\\ &=q_{i,j}^{n}+\left(\frac{\Delta t}{\rho_{i,j}V_{i,j}Cp_{i,j}}\right)\left(\begin{array}{l}\dfrac{k_N A_N}{\Delta z_N}\left(q_{i,j-1}^{n+1}\right)+\dfrac{k_S A_S}{\Delta z_S}\left(q_{i,j+1}^{n}-q_{i,j}^{n}\right)\\ +\dfrac{k_E A_E}{\Delta r_E}\left(q_{i+1,j}^{n+1}\right)+\dfrac{k_W A_W}{\Delta r_W}\left(q_{i-1,j}^{n}-q_{i,j}^{n}\right)\end{array}\right)\end{aligned} \tag{5.52}$$

$$q_{i,j}^{n+1}=\frac{\begin{array}{l}q_{i,j}^{n}\left(\dfrac{\rho_{i,j}V_{i,j}Cp_{i,j}}{\Delta t}\right)+\dfrac{k_N A_N}{\Delta z_N}\left(q_{i,j-1}^{n+1}\right)\\ +\dfrac{k_S A_S}{\Delta z_S}\left(q_{i,j+1}^{n}-q_{i,j}^{n}\right)+\dfrac{k_E A_E}{\Delta r_E}\left(q_{i+1,j}^{n+1}\right)+\dfrac{k_W A_W}{\Delta r_W}\left(q_{i-1,j}^{n}-q_{i,j}^{n}\right)\end{array}}{\dfrac{k_N A_N}{\Delta z_N}+\dfrac{k_E A_E}{\Delta r_E}+\dfrac{\rho_{i,j}V_{i,j}Cp_{i,j}}{\Delta t}} \tag{5.53}$$

Substituting in the effective specific heat coefficients from equations (5.25) and (5.27):

$$q_{i,j}^{n+1} = \frac{\left(q_{i,j}^{n} + Cp_{i,j}^{E(q)}\right)\left(\frac{\rho_{i,j} V_{i,j} Cp_{i,j}^{C(q)}}{\Delta t}\right) + \frac{k_N A_N}{\Delta z_N}\left(q_{i,j-1}^{n+1}\right) + \frac{k_S A_S}{\Delta z_S}\left(q_{i,j+1}^{n} - q_{i,j}^{n}\right) + \frac{k_E A_E}{\Delta r_E}\left(q_{i+1,j}^{n+1}\right) + \frac{k_W A_W}{\Delta r_W}\left(q_{i-1,j}^{n} - q_{i,j}^{n}\right)}{\frac{k_N A_N}{\Delta z_N} + \frac{k_E A_E}{\Delta r_E} + \frac{\rho_{i,j} V_{i,j} Cp_{i,j}^{C(q)}}{\Delta t}} \tag{5.54}$$

where:

$Cp_{i,j}^{C(q)}$ is the effective specific heat coefficient C at node i, j for the q solution variable

$Cp_{i,j}^{E(q)}$ is the effective specific heat coefficient E at node i, j for the q solution variable

The temperature at node i, j is then:

$$T_{i,j}^{n+1} = \frac{p_{i,j}^{n+1} + q_{i,j}^{n+1}}{2} \tag{5.55}$$

Additional finite difference equations were developed at the unit cell convective and adiabatic boundaries by the same method as shown above. For adiabatic boundary conditions heat conduction terms became zero in equation (5.34). For convective boundary conditions conduction terms were replaced with heat transfer terms. In total, eighteen finite difference equations were developed, nine p sweep equations and nine q sweep equations. Of each set of nine equations, four defined corner nodes, four defined edge nodes and the remaining equation defined all the internal nodes as given in equations (5.49) and (5.54).

The alternating direction explicit model was used to determine the optimal generator geometry in terms of carbon thickness, aluminium thickness and generator diameter. Although the scheme is stated to be unconditionally stable [11, 12], the model was found to diverge if the time-step applied was too great. Several attempts were made at developing a stability criterion for the scheme but none were successful, possibly due to the added complexity of modelling adsorption and desorption processes and utilising unequal Δr and Δz grid spacings. However, the scheme did allow a time-step of a factor of 5–10 greater than that permissible with the simple explicit scheme to be applied without the model

diverging. Although, the computed results were satisfactory, the time taken to run each parametric simulation was too great even using Sun UltraSparc workstations.

Therefore, after having used the alternating direction explicit model to arrive at the desired generator geometry another model was developed to predict the performance of the experimental rig. The results of the parametric simulations are presented in Figure 5.4.

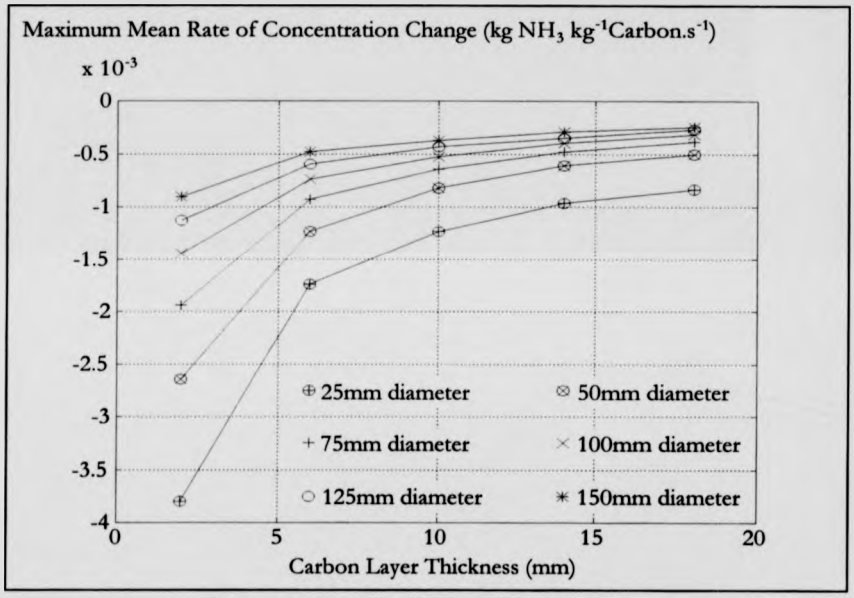

Figure 5.4: ADE Generator Geometry Plots

(Aluminium Layer Thickness 10% of Carbon Layer Thickness)

The maximum mean rate of concentration change was used as a figure of merit as it is equivalent to the maximum specific cooling power. It is apparent that for a constant carbon layer thickness the maximum mean rate of concentration change increases (greater rate of desorption) as the diameter of the carbon is reduced from 150mm to 25mm. For a constant diameter of carbon the maximum mean rate of concentration change increases as the carbon layer thickness is reduced from 18mm to 2mm. Further simulations indicated a negligible improvement in rate of desorption when the aluminium layer thickness was increased from 10% of carbon layer thickness to 25% of carbon layer thickness. The results

indicate that for the best performance the diameter and thickness of the carbon layers should be as small as possible. However, manufacturing limitations may well restrict the minimum dimensions that are practicable.

5.4.2.2 Simple Explicit Finite Difference Scheme

The simple explicit (SE) finite difference scheme was chosen because of its relative ease of programming and modification while also providing good numerical accuracy. The numerical model based on this scheme utilises a coarser grid than that applied with the ADE scheme, allowing larger time-steps to be implemented and computing times to be reduced correspondingly.

With the simple explicit method, the solution variable T is calculated by sweeping through the nodes in sequence from a known set of initial nodal temperatures and boundary conditions. The nodal temperatures at each new time level are evaluated in terms of the nodal temperatures calculated at the previous time level. In this manner, the solution marches forward in time, by time-step Δt, evolving from the temperature distribution specified initially.

Taking equation (5.34), the two dimensional energy balance PDE as the starting point, the finite difference equation for the temperature solution variable T may be developed based on the simple explicit scheme. This scheme applies forward differencing in time and central differencing in space.

$$\rho_{i,j} V_{i,j} Cp_{i,j} \left(\frac{T_{i,j}^{n+1} - T_{i,j}^{n}}{\Delta t} \right) = \left(\begin{array}{l} \dfrac{k_N A_N}{\Delta z_N} \left(T_{i,j-1}^{n} - T_{i,j}^{n} \right) + \dfrac{k_S A_S}{\Delta z_S} \left(T_{i,j+1}^{n} - T_{i,j}^{n} \right) \\ + \dfrac{k_E A_E}{\Delta r_E} \left(T_{i+1,j}^{n} - T_{i,j}^{n} \right) + \dfrac{k_W A_W}{\Delta r_W} \left(T_{i-1,j}^{n} - T_{i,j}^{n} \right) \end{array} \right) \tag{5.56}$$

Substituting in equations (5.40), (5.41), (5.42), (5.43) for heat transfer coefficients gives:

$$\rho_{i,j} V_{i,j} Cp_{i,j} \left(\frac{T_{i,j}^{n+1} - T_{i,j}^{n}}{\Delta t} \right) = \left(\begin{array}{l} u_N A_N \left(T_{i,j-1}^{n} - T_{i,j}^{n} \right) + u_S A_S \left(T_{i,j+1}^{n} - T_{i,j}^{n} \right) \\ + u_E A_E \left(T_{i+1,j}^{n} - T_{i,j}^{n} \right) + u_W A_W \left(T_{i-1,j}^{n} - T_{i,j}^{n} \right) \end{array} \right) \tag{5.57}$$

Rearranging and solving for $T_{i,j}^{n+1}$ gives:

$$T_{i,j}^{n+1} = T_{i,j}^{n} + \left(\frac{\Delta t}{\rho_{i,j} V_{i,j} Cp_{i,j}}\right)\begin{pmatrix} u_N A_N\left(T_{i,j-1}^{n} - T_{i,j}^{n}\right) + u_S A_S\left(T_{i,j+1}^{n} - T_{i,j}^{n}\right) \\ + u_E A_E\left(T_{i+1,j}^{n} - T_{i,j}^{n}\right) + u_W A_W\left(T_{i-1,j}^{n} - T_{i,j}^{n}\right) \end{pmatrix} \tag{5.58}$$

Substituting in the effective specific heat coefficients from equations (5.25) and (5.27):

$$T_{i,j}^{n+1} = \left(T_{i,j}^{n} + Cp_{i,j}^{E}\right) + \left(\frac{\Delta t}{\rho_{i,j} V_{i,j} Cp_{i,j}^{C}}\right)\begin{pmatrix} u_N A_N\left(T_{i,j-1}^{n} - T_{i,j}^{n}\right) + u_S A_S\left(T_{i,j+1}^{n} - T_{i,j}^{n}\right) \\ + u_E A_E\left(T_{i+1,j}^{n} - T_{i,j}^{n}\right) + u_W A_W\left(T_{i-1,j}^{n} - T_{i,j}^{n}\right) \end{pmatrix} \tag{5.59}$$

The common result for the two dimensional simple explicit scheme stability with uniform thermal conductivity and equal grid spacing is:

$$\alpha \frac{\Delta t}{(\Delta x)^2} \leq 0.25 \tag{5.60}$$

For stability, to avoid divergent behaviour, the coefficient of $T_{i,j}^{n}$ in equation (5.58) must be positive. Therefore grouping together $T_{i,j}^{n}$ coefficients, for stability:

$$\left(1 - \left(\frac{\Delta t}{\rho_{i,j} V_{i,j} Cp_{i,j}}\left(u_N A_N + u_S A_S + u_E A_E + u_W A_W\right)\right)\right) \geq 0 \tag{5.61}$$

Rearranging for Δt:

$$\Delta t \leq \frac{\rho_{i,j} V_{i,j} Cp_{i,j}}{u_N A_N + u_S A_S + u_E A_E + u_W A_W} \tag{5.62}$$

Replacing the heat transfer coefficients (u) with thermal conductivities (k) and substituting in the thermal diffusivity (α), equation (5.62) reduces to the result for the simple explicit scheme stability presented in equation (5.60).

Equation (5.59) applies to all of the nodes within the unit cell, whether they are internal nodes, boundary nodes or corner nodes. The heat transfer coefficient terms (u) are defined throughout the unit cell to include simple conduction terms between nodes, combinations

of conductivity and interface heat transfer coefficients and the heat transfer coefficients at the convective and adiabatic boundaries.

5.4.3 System Starting Conditions

For both of the explicit schemes selected, starting conditions must be specified at the initial time level *n* for the program to march forward from in time. For the initial simulations used to determine the generator geometry all of the nodes within the unit cell were set to 323 K at the start of the heating half-cycle to approximate to the generator mean temperature (at the end of a cooling half-cycle) after having completed several heating and cooling thermodynamic cycles. This quasi-steady-state corresponds to an evaporator saturation temperature of 0°C and a bed concentration of approximately 0.17. For the validation computer simulations all of the nodes within the unit cell were set to the generator internal thermocouple temperature measured experimentally. This was considered to be a good approximation since at the end of a cooling half-cycle the generator would be expected to be in thermal equilibrium with the surroundings and the carbon temperature throughout the generator to be virtually uniform.

5.4.4 Boundary Conditions

For the generator under the influence of external heating and cooling, three out of the four (north, south, east) unit cell boundaries were set as adiabatic boundaries as they represent lines of symmetry and thus have no heat flow across them. The western boundary of the unit cell was defined as a convective boundary with a variable heat transfer coefficient. Typical heat transfer coefficients applied at the boundary were 1000 W $m^{-2}K^{-1}$ for the heating phase and 500 W $m^{-2}K^{-1}$ for the cooling phase.

The boundary conditions governing the path of the thermodynamic cycle are defined by the evaporator saturation pressure, condenser saturation pressure, the system mass of ammonia at the start of heating and cooling, the generator external heating and cooling source and sink temperatures and either the required concentration change during the heating and cooling half-cycles or the required heating and cooling half-cycle times.

5.4.4.1 Constant Mass Boundary Condition

When modelling the heating or cooling of the generator while moving along an isostere (line of constant concentration) the mass of ammonia in the system was held constant. The mass of ammonia was evaluated at two points in the thermodynamic cycle, at the start of the heating phase and at the start of the cooling phase. During these isosteric processes the generator check valves are both closed isolating the generator from the evaporator and condenser. The generator then behaves as a closed system and so the total mass of ammonia (adsorbed ammonia and gaseous ammonia) remains constant. Thus, at the start of a heating half-cycle with the pressure equal to the evaporator saturation pressure, the initial mass of ammonia in the generator was calculated by summing the mass of ammonia at each carbon node over the unit cell:

$$m_a = \sum_{carbon}\left(\left(x_{i,j}\rho_c V_{i,j}\right)+\left(\rho_{a_{i,j}} V_{i,j}\psi\right)\right) \tag{5.63}$$

For a perfect gas, assuming the carbon and gaseous ammonia are in thermal equilibrium:

$$\rho_{a_{i,j}} = \frac{P_{sat}}{R_a T_{i,j}} \tag{5.64}$$

where:

m_a is the mass of ammonia in the unit cell (kg)

$x_{i,j}$ is the concentration at node i, j from the modified D-A equation (kg NH_3 kg^{-1}Carbon)

ρ_c is the carbon density (kg m^{-3})

$\rho_{a_{i,j}}$ is the ammonia density at node i, j (kg m^{-3})

ψ is the void fraction (m^3 void volume m^{-3} unit cell volume)

P_{sat} is the saturation pressure (N m^{-2})

$R_a \sim 488$ is the ammonia specific gas constant (J $kg^{-1}K^{-1}$)

If the void fraction is considered to be negligible, the density at each carbon node is a constant and the mass of ammonia in the generator is only a function of the generator concentration. Since the Dubinin coefficients in the D-A equation are evaluated based on this assumption, it is consistent and accurate. The ammonia saturation pressure and temperature are assumed to be uniform throughout the generator at any given time level.

Within the model, at the start of the computation, having evaluated the initial mass of ammonia in the generator using equation (5.63) a first guess for a new value of the generator saturation temperature is made by either incrementing the previous saturation temperature for a heating half-cycle, or decrementing the previous saturation temperature for a cooling half-cycle thus:

$$T_{sat\sim guess1}^{n+1} = T_{sat}^{n} \pm \Delta T_{sat} \tag{5.65}$$

The model then evaluates the new nodal temperatures and concentrations. The new mass in the generator is then calculated by applying equation (5.63) and the result compared with the initial mass of ammonia in the generator. If the absolute value of the mass error between the initial mass value and the new mass value is less than the defined mass tolerance the program marches on to the next time-step. If however the mass error is too great, another guess is made for the saturation temperature by incrementing or decrementing the previous first value guessed for saturation temperature thus:

$$T_{sat\sim guess2}^{n+1} = T_{sat\sim guess1}^{n+1} \pm \Delta T_{sat} \tag{5.66}$$

A second mass error is then evaluated based on the second guessed value for the saturation temperature utilising the nodal temperatures calculated from the first guessed value for saturation temperature. A Newton-Raphson iteration [13] is then performed using the first and second calculated mass errors and saturation temperature guesses until a value for the saturation temperature is arrived at which satisfies the mass tolerance criterion and allows the model to march on to the next time level. Following the first guess for saturation temperature increment or decrement, the subsequent values are then based on the

increment or decrement value which satisfied the mass tolerance criterion at the previous time level. This results in a faster convergence of the Newton-Raphson iteration.

5.4.4.2 Constant Pressure Boundary Condition

The constant mass condition is maintained during the heating phase while moving along an isostere between the evaporator saturation pressure and the condenser saturation pressure. Once the generator has reached the condenser saturation pressure and the check valve has opened the constant mass condition is no longer applicable, and the generator starts to desorb ammonia at constant pressure. The isobaric (constant pressure) desorption process continues until either a heating half-cycle time limit has been reached or a specified concentration change Δx has been achieved. Conversely, the constant mass condition is maintained during the cooling phase while moving along an isostere between the condenser saturation pressure and the evaporator saturation pressure. Once the generator has reached the evaporator saturation pressure and the check valve has opened the constant mass condition is no longer applicable and the generator starts to adsorb ammonia at constant pressure. Again, the isobaric adsorption process continues until either a cooling half-cycle time limit has been reached or a specified concentration change Δx has been achieved. During the isobaric cycle processes the mass of ammonia in the generator is still calculated. However, the difference between the ammonia mass at the new time level $(n+1)$ and the old time level (n) is no longer an error but the mass of ammonia entering or leaving the generator. For the experimental rig which utilises two generators operating 180^o out of phase, the heating and cooling half-cycle times are identical to provide symmetrical operation and semi-continuous cooling.

5.5 Solution Procedures

A number of solution procedures were performed at each time level in order to evaluate the pertinent generator variables such as temperature, pressure, concentration, cooling power, heating power and coefficient of performance (COP).

5.5.1 Calculation of Generator Temperature

The temperatures at each node within the unit cell were calculated by applying equation (5.55) for the initial geometry prediction simulations and equation (5.59) for the later generator performance and prediction simulations. In each case, having determined the discrete carbon temperature at each node, the mean carbon temperature was calculated by summing the nodal temperatures over the unit cell:

$$T_c = \frac{\sum_{carbon}\left(T_{i,j}^{n+1}\rho_c V_{i,j}\right)}{m_c} \tag{5.67}$$

$$m_c = \sum_{carbon}\left(\rho_c V_{i,j}\right) \tag{5.68}$$

where:

T_c is the mean carbon temperature (K)

m_c is the mass of carbon in the unit cell (kg)

5.5.2 Calculation of Generator Pressure

The generator pressure was evaluated at each time-step by applying equation (3.29), which for pure ammonia relates the pressure to the saturation temperature. For the isobaric processes the saturation temperature was defined by the condenser saturation temperature or evaporator saturation temperature. For the isosteric cycle processes the saturation temperature was obtained by a mass balance technique, as described in Section 5.4.4.1.

5.5.3 Calculation of Generator Concentration

The concentrations at each node within the unit cell were calculated by applying equation (5.3), the modified D-A equation. Having determined the discrete ammonia concentration at each node, the mean ammonia concentration was calculated by summing the nodal concentrations over the unit cell:

$$x_a = \frac{\sum_{carbon}\left(x_{i,j}^{n+1}\rho_c V_{i,j}\right)}{m_c} \tag{5.69}$$

where:

x_a is the mean ammonia concentration (kg NH_3 kg^{-1}Carbon)

5.5.4 Calculation of Specific Cooling Power

The specific cooling power for the generator is given by:

$$\dot{q}_{cooling} = \frac{\left(x_a^{t_{cool}+\Delta t_{cool}} - x_a^{t_{cool}}\right)\left(h_g - h_f\right)}{t_{cycle}} \tag{5.70}$$

where:

$\dot{q}_{cooling}$ is the specific cooling power (W kg^{-1})

t_{cool} is the time at the start of the cooling half-cycle (s)

Δt_{cool} is the cooling half-cycle duration (s)

h_g is the specific enthalpy of ammonia vapour leaving the evaporator (kJ kg^{-1})

h_f is the specific enthalpy of ammonia liquid leaving the condenser (kJ kg^{-1})

t_{cycle} is the total cycle time (s)

5.5.5 Calculation of Specific Heating Power

The specific heating power for the generator is given by:

$$\dot{q}_{heating} = \frac{Q_{heating}}{m_c . t_{cycle}} \tag{5.71}$$

$$Q_{heating} = \sum_{t=t_{heat}+\Delta t_{heat}}^{t=t_{heat}} \left(\sum_{\substack{convective \\ boundary}} \left(h_o A_W \left(T_o - T_{i,j}^{n+1} \right) \Delta t \right) \right) \tag{5.72}$$

$$t_{cycle} = \Delta t_{cool} + \Delta t_{heat} \tag{5.73}$$

where:

$\dot{q}_{heating}$ is the specific heating power (W kg^{-1})

$Q_{heating}$ is the heat energy (J)

t_{heat} is the time at the start of the heating half-cycle (s)

Δt_{heat} is the heating half-cycle duration (s)

T_e is the external heat transfer fluid temperature (K)

5.5.6 Calculation of Coefficient of Performance (COP)

The COP for the generator is given by:

$$COP = \frac{\dot{q}_{cooling}}{\dot{q}_{heating}} \tag{5.74}$$

For the simulation runs used to predict the generator performance and optimal geometry, based on a defined initial temperature distribution, several unsteady cycles were predicted by the model before $\dot{q}_{cooling}$, $\dot{q}_{heating}$ and *COP* converged to steady-cyclic values.

The ideal Carnot COP for the generator is given by:

$$COP_{carnot} = \frac{T_{evap}\left(T_{max} - T_{cond}\right)}{T_{max}\left(T_{cond} - T_{evap}\right)} \tag{5.75}$$

where:

T_{evap} is the evaporator temperature (K)

T_{cond} is the condenser temperature (K)

T_{max} is the maximum generating temperature (K)

5.6 Conclusions

Two transient conduction numerical models have been developed; one using an alternating direction explicit finite differencing scheme and the other using a simple explicit finite differencing scheme. The alternating direction explicit model was applied to determine the optimal generator laminate geometry. The results of the parametric simulations indicate that for maximum specific cooling power or maximum mean rate of concentration change as a figure of merit the laminate carbon layers should be as thin as possible with a laminate diameter as small as possible. However, in practice the minimum carbon layer dimensions may well be dictated by manufacturing limitations. The numerical simulations also indicate a negligible improvement when increasing the aluminium layer thickness from 10% of the carbon layer thickness to 25% of the carbon layer thickness. The simple explicit model was validated against data from the experimental rig (see Chapter 9) and then applied to predicting the possible future performance of the system (see Chapter 10).

References

[1] **Parrish, A.**, Mechanical Engineer's Reference Book, 11th Edition, Butterworths, London, **1973**.

[2] **Tamainot-Telto, Z., Critoph, R.E.**, Monolithic Carbon for Sorption Refrigeration and Heat Pump Applications, submitted to Applied Thermal Engineering.

[3] **Critoph, R.E.**, Evaluation of Alternative Refrigerant-Adsorbent Pairs for Refrigeration Cycles, Applied Thermal Engineering, 16 (11), pp. 891–900, **1996**.

[4] **Bird, R.B., Stewart, W.E., Lightfoot, E.N.**, Transport Phenomena, John Wiley & Sons, New York, **1960**.

[5] **Kiavany, M.**, Principles of Heat Transfer in Porous Media, 2nd Edition, Springer-Verlag, New York, **1995**.

[6] **Critoph, R.E., Tamainot-Telto, Z., Davies, G.N.L.**, Design of an Adsorption Generator Utilising a Novel Carbon-Aluminium Laminate, Proc. HPC Int. Conf. Nottingham (UK), pp. 349–358, **1997**.

[7] **Critoph, R.E., Tamainot-Telto, Z., Davies, G.N.L.**, The Use of Monolithic Carbon-Aluminium Laminates in the Adsorption Refrigeration Generators to Enhance the Effective Conductivity and Power Density, Proc. FOA6 Int. Conf., Giens (France), **1998**.

[8] **Restuccia, G.**, Private Communication, **1997**.

[9] **Haseler, L.E., et al.**, Absorption Cycle Heat Pumps for Domestic Heating, AERE-G 104R, AERE Harwell, **1978**.

[10] **Roberts, D.L., Selim, M.S.**, Comparative Study of Six Explicit and Two Implicit Finite Difference Schemes for Solving One-Dimensional Parabolic Partial Differential Equations, International Journal for Numerical Methods in Engineering, Vol. 20, pp. 817–844, **1984**.

[11] **Anderson, D.A., Tannehill, J.C., Pletcher, R.H.**, Computational Fluid Mechanics and Heat Transfer, McGraw-Hill, p. 119, **1984**.

[12] **Barakat, H.Z., Clark, J.A.**, On the Solution of the Diffusion Equations by Numerical Methods, Journal of Heat Transfer, pp. 421–427, November **1966**.

[13] **Minkowycz, W.J., Sparrow, E.M., Schneider, G.E., Pletcher, R.H.**, Handbook of Numerical Heat Transfer, John Wiley & Sons, pp. 6–8, **1988**.

Chapter 6

Experimental Apparatus

6.1 Introduction

The experimental rig was designed in order to evaluate the cooling that could be achieved utilising the carbon-aluminium laminate generator. Although at inception developing country considerations were taken in account, the experimental rig itself was designed primarily as a "laboratory" test rig to allow greater flexibility of operation. Hence, a number of expensive components were used that would be inappropriate for a final cooling system to be used in a developing country. For a developing country design a compromise would need to be reached between component cost and system efficiency while also taking into account the availability of manufacturing and maintenance facilities.

6.2 Experimental Rig Design

6.2.1 General Layout

A schematic of the experimental rig is presented in Figure 6.1. The experimental rig consists of two adsorption generators, steam boiler, water condenser, ammonia condenser, ammonia receiver, ammonia evaporator and a series of pneumatically operated ball valves and electrically operated solenoid valves.

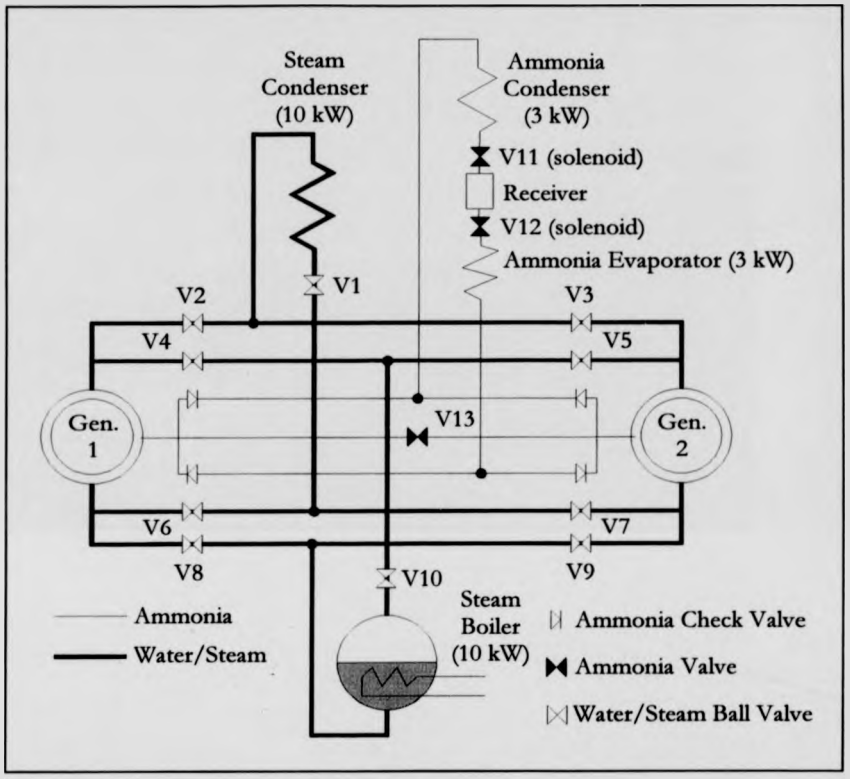

Figure 6.1: Experimental Rig Schematic Layout

The generators (Gen.1 & Gen.2) are connected through a series of valves to both a water loop for heating and cooling and an ammonia loop for adsorbate mass transfer. The steam required for external heating of the generator shells by condensing heat transfer is produced in a boiler situated below both generators. Generator cooling is achieved utilising water boiling under low pressure in the generator pressure vessel to reject heat through the water condenser situated above both generators. Ammonia is desorbed at the condensing pressure from the generator being heated and is driven out of the generator through a check valve under the influence of the pressure gradient developed between the generator and the ammonia condenser. The condensed ammonia liquid then passes through two ammonia solenoid valves, which define the receiver control volume, and down into the evaporator. The two ammonia valves (V11, V12) and receiver perform the function of an

expansion valve and are amenable to computer control. Cooling is achieved as the ammonia boils under reduced pressure in the evaporator and passes back through a check valve into the cooled generator, again driven by the pressure gradient between the evaporator and the cooled generator. The system is designed for a maximum heat input at the steam boiler of 10 kW and for a cooling load at the evaporator of up to 3 kW.

6.2.2 Generators

The generator design utilises a "tube in tube" thermosyphon construction with the carbon-aluminium laminate shell located within a larger steam pressure vessel, the complete unit being referred to as the generator.

On the ammonia side of the generator steam pressure vessel a grade 304 stainless steel slip on flange compliant to BS4504 [1] was welded in place. A length of half inch stainless steel tubing was inserted through a hole drilled in a compatible blind flange in grade 316 stainless steel, also compliant to BS4504, and welded in place. One end of the tubing was connected via Swagelok to the carbon-aluminium laminate shell with the other end of tube facilitating connection to the ammonia loop. The flange assembly allows the carbon-aluminium laminate shell to be inserted easily into the steam pressure vessel and sealed in place by tightening the cap head bolts on the flange to form a gas tight seal.

On the water/steam side of the generator steam pressure vessel, a stainless steel end plate was welded in place into which copper fittings were silver soldered to allow connection to the water loop. The top fitting was connected to the water loop as a vapour inlet/outlet to carry steam from the boiler into the pressure vessel during the heating phase and carry water vapour out of the pressure vessel into the steam condenser during the cooling phase. The bottom fitting was connected to the water loop as a liquid inlet/outlet to carry water out of the pressure vessel and back to the boiler during the heating phase and to carry water into the pressure vessel from the water condenser during the cooling phase.

Liquid level floats were connected between the top and bottom water loop fittings on each generator pressure vessel. These stainless steel liquid level floats, supplied by Applications Engineering Ltd, contain a magnet which in conjunction with a reed switch

allows the liquid level in the generator pressure vessels to be determined. Additionally, both generators and liquid level assemblies were insulated with glass fibre to minimise thermal losses to the environment. A schematic diagram of the generator assembly is presented in Figure 6.2.

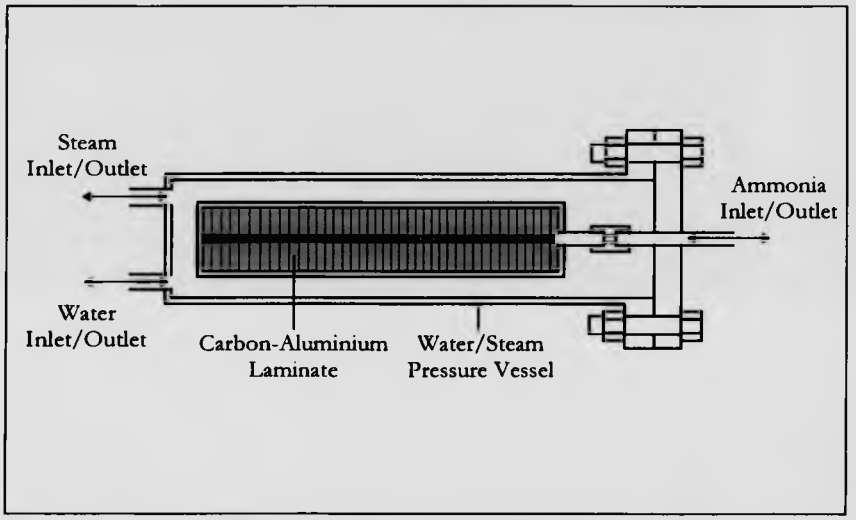

Figure 6.2: Generator Cross Sectional Schematic

6.2.3 Heaters

Cartridge heaters supplied by Watlow Ltd were utilised within the experimental rig to supply the cooling load within the evaporator and to generate steam within the boiler. A 230 V/3 kW cartridge heater with a K type thermocouple was utilised within the evaporator and a 415 V/10 kW cartridge heater with a K type thermocouple was utilised within the boiler. The thermocouples were fitted in situ by Watlow Ltd along the midway length of each cartridge heater and allowed the heater surface temperature and power to be monitored and controlled. The heater temperatures were controlled to a specified value utilising CAL 9900 PID type temperature controllers (manufactured by CAL). To protect the cartridge heater within the evaporator from corrosion, the heater was inserted within an aluminium thermowell with close tolerances between the heater surface and thermowell

inside wall to minimise the thermal contact resistance due to any air gap. Hence, with a low thermal contact resistance the heater could be operated at the design power rating without any need to down rate the heater to prevent burn-out.

6.2.4 Water Loop

The water loop consists of copper pipe-work connecting the generators to the water boiler and water condenser through a series of ball valves (V1–V10). All connections within the water loop were either welded or silver soldered to provide a hermetically air tight system even under vacuum conditions. However, air leaks into the water loop continued to be a persistent problem which proved difficult to eradicate due to the presence of micro-leaks. The water loop was sucked down to vacuum to remove any air in the system before commencing an experimental run, and also at stages during the experimental run to ensure there was no air in the system. Due to the partial pressure of the air component present, any air leaks were found to compromise the water boiling process under low pressure and cooling heat transfer achieved during the cooling half-cycle. Thus, the minimum generator temperature that could be attained was greater than expected and consequently the amount of cooling achieved over the complete thermodynamic cycle was reduced. For a future design, the problem of air leakage could be minimised by reducing the number of joints in the water loop and employing either welded joints or a gas tight connection system such as Swagelok.

6.2.4.1 Control Valves

Spring return pneumatically actuated three piece carbon steel ball valves (V1–V10) provided by Fpeco Group Ltd were applied around the water loop for controlling the water flow between the boiler, steam condenser and generators. The valves are rated to 22 bar/220°C, well in excess of the specified maximum steam saturation temperature and pressure of 10 bar at 180°C. These valves proved to be one of the most expensive components on the experimental rig. For a final developing country system they could be replaced with a less costly spool valve design to change between the various heating and cooling states. Each

valve is normally open and so fails open for safety should the power supply to the pneumatic actuators be disrupted. To insure against air leakage into the system, each ball valve contains a PTFE seal to provide a good seal against vacuum. Being of a three piece construction with socket weld ends, the valves were dismantled while the copper pipe-work was silver soldered in place and then re-assembled, to prevent any thermal damage to the PTFE seals. Solenoid valves are utilised to control the pneumatic (80 psi) supply to each ball valve pneumatic actuator. Hence, applying voltage to the solenoid valve opens the pneumatic supply to the actuator and closes the ball valve, removing the voltage then returns the ball valve through the spring return to the initial open state.

The open or closed state of each ball valve around the water loop for each of the cycle heating, cooling and regeneration processes is presented in Table 6.1.

Valve No. / Process	V1	V2	V3	V4	V5	V6	V7	V8	V9	V10
Heat Generator 1 and Cool Generator 2	0	1	0	0	1	1	0	0	1	0
Fill Generator 1 with Water	0	1	1	1	1	1	1	0	1	1
Regenerative Heat from Generator 1 †	1	1	1	0	0	0	0	1	1	1
Cool Generator 1 and Heat Generator 2	0	0	1	1	0	0	1	1	0	0
Fill Generator 2 with Water	0	1	1	1	1	1	1	1	0	1
Regenerative Heat from Generator 2 †	1	1	1	0	0	0	0	1	1	1

0 OPEN

1 CLOSED

† Boiler and evaporator cartridge heaters off during heat regeneration processes

Table 6.1: Water Loop Valve States (including optional heat regeneration)

The four main steps in the thermodynamic cycle are heating generator 1 while cooling generator 2, filling generator 1 with water, cooling generator 1 while heating generator 2 and filling generator 2 with water. For symmetrical operation, the first two steps are of the

same duration as the last two steps so that the heating half-cycle duration is equal to the cooling half-cycle duration. For heat regeneration two additional steps are included following the water filling processes - regenerative heat from generator 1 and regenerative heat from generator 2.

6.2.4.2 Steam Boiler

The steam boiler is situated at the bottom of the experimental rig, as indicated in Figure 6.1, beneath both generators. The boiler itself is fabricated from a 1020 mm length of thick walled grade 304 stainless steel pipe with outside diameter 73 mm and wall thickness 2.1 mm and has a water capacity of approximately 3.8 litres. The boiler is capable of producing steam up to 200°C and is insulated with a glass fibre jacket to minimise thermal losses. The water inlet and steam outlet are silver soldered into a welded end plate at one end of the boiler. The 10 kW cartridge heater passes through a welded end plate at the opposite end of the boiler (near the base to ensure that it is always covered with water) and is secured in place with a Swagelok compression fitting. A pressure relief valve is located in parallel with the boiler with a cracking pressure of 10 bar to maintain the steam pressure within the design limit.

6.2.4.3 Steam Condenser

The steam condenser provided by Occo Coolers Ltd is a stainless steel compact steam/water heat exchanger of a spiral internal construction designed to operate at sub-atmospheric pressures. The heat is rejected at the water condenser into a flow of cooling water provided by the departmental cooling tower. The steam condenser has a power rating of approximately 10 kW and a condensing temperature rating of up to 200°C.

6.2.5 Ammonia Loop

The ammonia loop consists of grade 316 stainless steel tubing connecting the ammonia inlet/outlet from each generator to the ammonia condenser, receiver and evaporator. The generators are also connected to each other through a manual ball valve (V13) which allows the option of heat regeneration between the generators at the end of each half-cycle. Two

solenoid valves (V11, V12) are utilised between the condenser and the evaporator in order to control the flow of ammonia and limit the pressure rise in the evaporator. All connections within the ammonia loop are made with Swagelok compression fittings to prevent any leak of ammonia from the system.

6.2.5.1 Control Valves

Seven valves are employed within the ammonia loop. Four manual check valves are utilised to connect the generators to the condenser and the evaporator, a ¼" NPT manual ball valve (V13) manufactured by Alco Valves Ltd is inserted between the two generators. Two Danfoss refrigeration solenoid valves (V11, V12) are placed in series between the condenser and evaporator with their operation determined by the ammonia condenser pressure and controlled from the WorkBench software. Once the condensing pressure has been reached the solenoid valves open and close in the sequence presented in Figure 6.3.

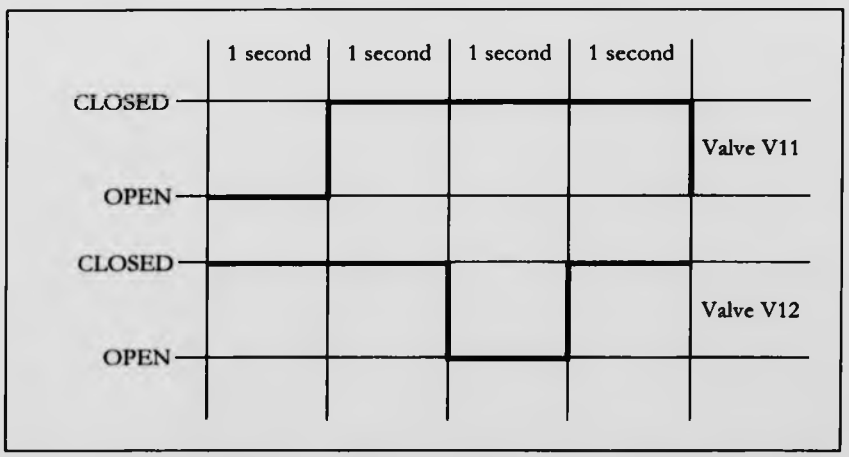

Figure 6.3: Ammonia Solenoid Valves Control Sequence

Hence, once the ammonia condensing pressure has been reached the solenoid valves, V11 and V12, open and close in a defined sequence over a fixed four second period of time. In the first stage V11 is open and V12 is closed allowing condensed ammonia to collect in the receiver. In the second stage V11 closes isolating the condensed ammonia in the receiver.

In the third stage V12 opens allowing the condensed ammonia to flow down into the evaporator. The high pressure liquid ammonia flashes when V12 is opened and so the effect on the ammonia refrigerant is exactly as if it had been through a conventional expansion valve. In the fourth stage V12 closes and at the end of the four second time period V11 returns to the original open state. The net effect is to both control the condenser pressure (down to the minimum allowed by the coolant flow) and to meter the liquid ammonia refrigerant down into the evaporator.

The open or closed state of each valve around the ammonia loop for each of the cycle heating, cooling and regeneration processes is presented in Table 6.2.

Valve No. / Process	V11	V12	V13
Heat Generator 1 and Cool Generator 2	1/0	1/0	1
Fill Generator 1 with Water	1/0	1/0	0
Regenerative Heat from Generator 1 †	1/0	1/0	1
Cool Generator 1 and Heat Generator 2	1/0	1/0	1
Fill Generator 2 with Water	1/0	1/0	0
Regenerative Heat from Generator 2 †	1/0	1/0	1

0 OPEN
1 CLOSED
† Boiler and evaporator cartridge heaters off during heat regeneration processes

Table 6.2: Ammonia Loop Valve States (including optional heat regeneration)

The 1/0 states for valves V11 and V12 represent the change in valve states while liquid ammonia is passing from the receiver into the evaporator as shown in Figure 6.3. The valve V13 allows ammonia mass transfer to occur between generator 1 and generator 2 during the water filling processes.

6.2.5.2 Ammonia Condenser

The ammonia condenser provided by Occo Coolers Ltd is a compact ammonia/water heat exchanger of a spiral internal construction designed to operate at ammonia saturation pressures up to 25 bara. It is of a stainless steel construction with internal neoprene baffles to avoid corrosion compatibility problems in the presence of ammonia. The heat is rejected at the ammonia condenser into a flow of cooling water provided by the departmental cooling tower. A pressure relief valve is located in parallel with the condenser with a cracking pressure of 20 bar to maintain the ammonia pressure within design limits. The ammonia condenser has a power rating of approximately 3 kW and an ammonia condensing temperature rating of up to 50°C.

6.2.5.3 Ammonia Receiver

A small ammonia receiver, fabricated from stainless steel tubing, is situated between the condenser and the evaporator with a control volume of 28 cm^3 defined by solenoid valves V11 and V12. This receiver section controls the flow of liquid ammonia into the evaporator with the valve control sequence presented in Figure 6.3.

6.2.5.4 Ammonia Evaporator

The ammonia evaporator is situated beneath both generators at the bottom of the experimental rig on the same level as the water boiler. The evaporator itself is fabricated from a 800 mm length of thick walled grade 304 stainless steel pipe with outside diameter 73 mm and wall thickness 2.1 mm and has an ammonia capacity of approximately 3 litres. The evaporator is insulated with a glass fibre jacket to minimise thermal losses and improve the measurement accuracy of the thermal load provided by the heater. The ammonia inlet and outlet are welded in place through the stainless steel end plate, which is in turn welded into the stainless steel pipe. The 3 kW cartridge heater is located within an aluminium thermowell which screws into a thread tapped into the welded end plate at the opposite end of the evaporator. This is located near to the base of the evaporator to ensure that it is always covered with ammonia and does not boil dry. Two sight glasses are also screwed

into threads tapped in the heater end plate in order to allow the amount of ammonia present in the evaporator to be visually assessed.

6.3 Carbon-Aluminium Laminate

The carbon-aluminium laminate is crucial to the rapid cycling performance of the experimental rig and the overall level of cooling achieved. Having decided on the laminate structure and geometry it was necessary to determine a practical method of manufacture. The four main processes involved were manufacture of the aluminium discs, pressing of the laminate, laminate pyrolysis and final finishing before installation in the generator pressure vessel on the experimental rig. A schematic of the desired cross-section through the laminate is presented with dimensions in Figure 6.4.

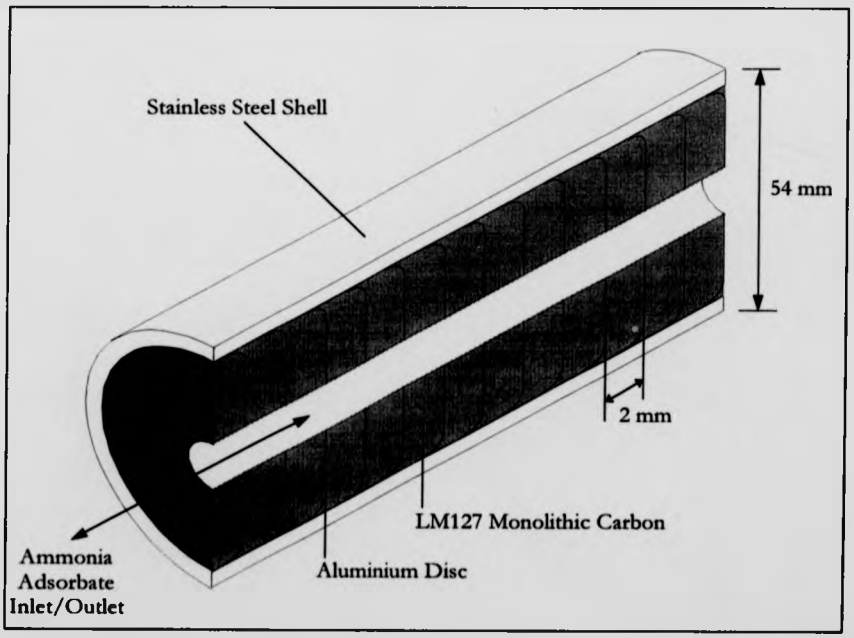

Figure 6.4: Carbon-Aluminium Laminate Cross-Sectional Schematic

6.3.1 Aluminium Discs

Before constructing the full two metre length of laminate, a number of test laminates were manufactured with the assistance and equipment of Sutcliffe Carbons Ltd. While compressing each carbon and aluminium layer it was noted that when the pressure was removed the "clad" aluminium discs would spring back thus disrupting and cracking the carbon layer. This phenomenon was attributed to the mechanical properties of the aluminium and the build up of air pressure beneath the disc. Hence, it was decided that a softer annealed aluminium should be utilised which would plastically deform under load pressure forming a good carbon-aluminium contact interface without springing back and disturbing the carbon layer when the pressure was removed. Additionally, it was decided that a hole should be punched at the centre of the disc to enable improved bonding between adjacent carbon layers and to provide a route for air pressure release at the end of the compression process.

A soft annealed 0.2 mm thickness 10/50 aluminium foil supplied by Multifoil Ltd was selected as a suitable starting material for the discs. The material was cut into one thousand squares on a guillotine and a 52.80 mm circle of aluminium punched out from each square utilising a manual fly-press. A 10 mm hole was then punched out of the centre of each aluminium disc. A hole was required up through the centre of the laminate in order to allow the ammonia adsorbate to pass in and out of the generator during adsorption and desorption processes while also providing a route for air pressure release at the end of each compression process. Although a hole could have been drilled through the aluminium at a later stage once the laminate had been pyrolysed, it was thought that the drilling procedure would probably tear the aluminium foil thus disturbing the regular carbon layers in the vicinity of the hole. The flat aluminium discs were then formed into a dish shape with a flat base and a lip. Seamless grade PN40 stainless steel tubing purchased from Tubesales Ltd with external diameter 53.98 mm and wall thickness 1.59 mm giving a nominal inside diameter of 50.80 mm was selected to contain the laminate. However, in practice the average internal diameter was measured as 51.10 mm and thus the total disc diameter was set at this value. The lip was formed by passing the flat discs through a die with a plunger to

form a lip height of 1.8 mm. It was hoped that by this process the aluminium discs would form an interference fit with the inside wall of the stainless steel laminate shell resulting in a low thermal contact resistance at the wall-disc interface. The cutting and forming process to produce each disc involved the use of grease to prevent the manufacturing tools from seizing. There was a possibility that this grease might poison the carbon if not removed from the discs, although in all probability it would have been decomposed during the pyrolysis process. Initially, an ultrasonic bath and acetone solvent were employed to remove the grease, but this method was found to be slow and unsatisfactory. Methylated spirits were also found to be unsatisfactory as the purple dye left a residue on the discs. Therefore, a cleaning method was selected where the discs were washed manually in pure methanol and then dried in a fume cupboard.

6.3.2 Laminate Pressing

The carbon-aluminium laminate was compressed in situ within the stainless steel shell with a force of 32 tonnes (equivalent to a pressure of 152 MNm^{-2}) utilising the departmental "Amsler" press. The stainless steel shell was constrained within a mild steel die designed to withstand the pressure encountered during the compression process and prevent radial distortion. Initially a solid mild steel die was utilised with a lubricating paste between the die and laminate shell wall. However, after having produced a 500 mm length of laminate, the shell could not be pushed out of the die without buckling and deformation occurring. Therefore, a split die design was manufactured consisting of four pairs of split mild steel blocks, with each block 250 mm x 70 mm x 137.5 mm, held together with four M30 grade 12-9 high tensile cap head bolts, stacked one on top of the other with a centre hole to accommodate the laminate stainless steel shell. The whole die assemble was secured together with M16 studding passing from a base plate to a top plate. The hole diameter in the top plate was dimensioned at 51.5 mm to allow the aluminium discs and plunger sufficient clearance to enter the shell while preventing the shell from moving vertically during the compression process. A photograph of the split die assembly is presented in Figure 6.5.

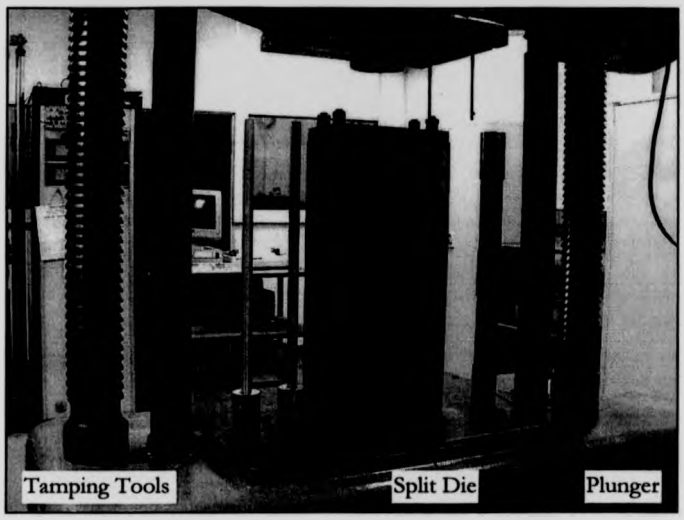

Figure 6.5: Split Die Assembly

Four laminate sections were produced, each with a shell length of approximately 500 mm. Any space between the stainless steel shell and the top plate of the split die assembly was filled with a tube spacer to prevent the laminate shell from moving vertically during the compression process. To form the laminate, a layer of aluminium was pushed down to the bottom of the shell with a hand plunger followed by approximately 6.2 g of LM127 carbon powder which was tamped down with a flat faced hand plunger. This was designed to give a carbon layer thickness of approximately 2 mm after the compression process. This procedure was repeated in order to build up ten carbon-aluminium layers before the compression process. Compressing ten layers at the same time was found to give the same laminate density as compressing one layer at a time whilst also significantly speeding up the manufacturing process.

A 600 mm tool steel plunger supplied by Hardwick Engineering Ltd was employed in order to transmit the load from the press to the carbon-aluminium laminate. This plunger was lowered down into the shell to rest on top of the final carbon layer. The press was then raised up until a force of 32 tonnes was achieved. This force was maintained for approximately 60 seconds before being reduced gradually to zero. The whole process was

repeated approximately twenty times until the laminate had been built up to fill the shell. The laminate shell was then released from the split die and left to dry out gradually in air. The compression data for each of the four laminate sections detailing the carbon layer masses is presented in Appendix IV.

6.3.3 Laminate Pyrolysis

The four compressed laminate sections were left to dry over the course of a two week period. Each laminate section was then placed on a lathe and a 5 mm hole drilled along the axial centre line, concentric with the holes in the centre of the aluminium discs through the length of the laminate. The carbon powder itself was still very moist at this stage and thus drilling was a slow process with the flute on the drill bit having to be cleared of carbon at regular intervals. The hole through the laminate was necessary not only to allow flow of ammonia into and out of the laminate during adsorption and desorption processes but also to provide a channel for gases driven out of the laminate during the pyrolysis process. Without the hole through the laminate there was the possibility that steam and other pyrolysis gases could become trapped within the carbon-aluminium layers during the pyrolysis process and be released explosively under high pressure thus destroying the laminate.

The four laminate sections were sent to Sutcliffe Carbons Ltd to be pyrolysed in their temperature controlled oven. The LM127 carbon consists of an activated carbon incorporating a polymer binder developed by Sutcliffe Carbons Ltd. When this carbon is compressed the company believe the binder acts as a lubricant allowing the carbon grains to slip over each other until they interlock to form a solid block. In the pyrolysis process the carbon is heated in an inert atmosphere at a temperature between 500°C and 650°C in order to pyrolyse the binder and fix the carbon as a solid monolithic block. During the pyrolysis process, water within the carbon is vaporised and driven out as steam while the carbon binder consolidates the compressed carbon powder into a solid monolithic carbon. Sutcliffe Carbons Ltd suggest that higher curing temperatures yield improved binding and a stronger monolithic block. However, since the upper end of the pyrolysis temperature

range approaches the melting point of the pure aluminium discs, lower curing temperatures were applied to the laminate sections. During the pyrolysis process there was the possibility that differential expansion of the stainless steel shell and aluminium discs might cause the laminate to distort while shear stresses caused the carbon to break up. However, the pyrolysed test samples showed no evidence of disruption to the regular carbon structure.

6.3.4 Internal Structure

Two test samples 65 mm in length were produced utilising the "Amsler" press to evaluate the effectiveness of the manufacturing process and consider possible improvements. Each of these samples was potted in a slow curing transparent epoxy resin and cut in half along the centre axis on a band saw to reveal the cross-sectional structure of the laminate.

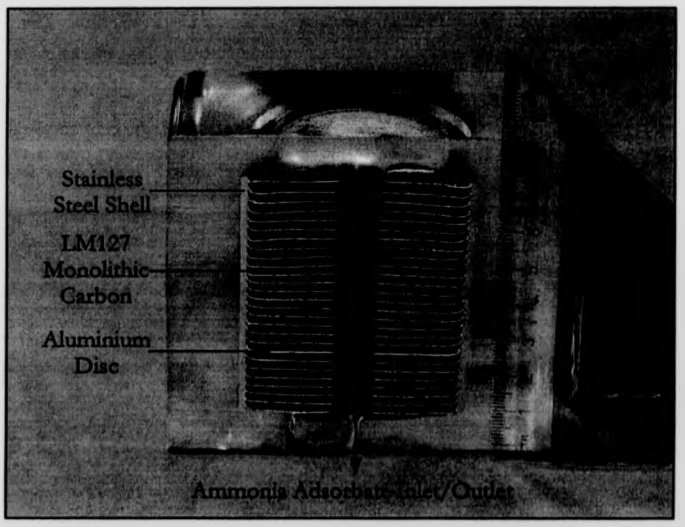

Figure 6.6: Carbon-Aluminium Laminate Axial Cross-Section

A photograph of one of the laminate cross-sections is presented in Figure 6.6 which highlights the regular laminate internal structure. The carbon layer thickness is consistent throughout the cross-section with no sign of disruption following the pyrolysis process.

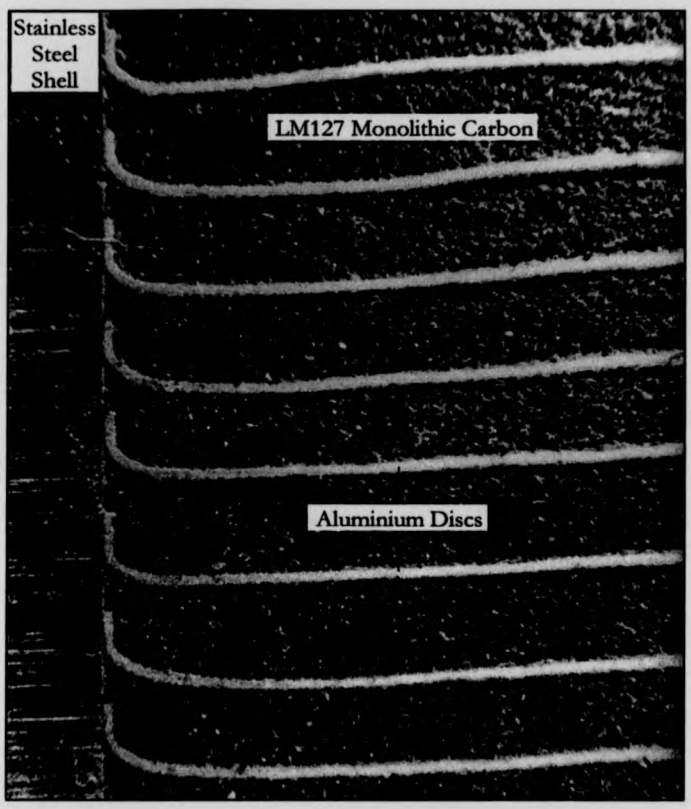

Figure 6.7: Laminate Internal Structure

A photograph of the carbon-aluminium internal structure is presented in Figure 6.7. There appears to be good material contact between the aluminium discs and carbon layers suggesting a significant improvement in the effective thermal conductivity of the carbon should be realised.

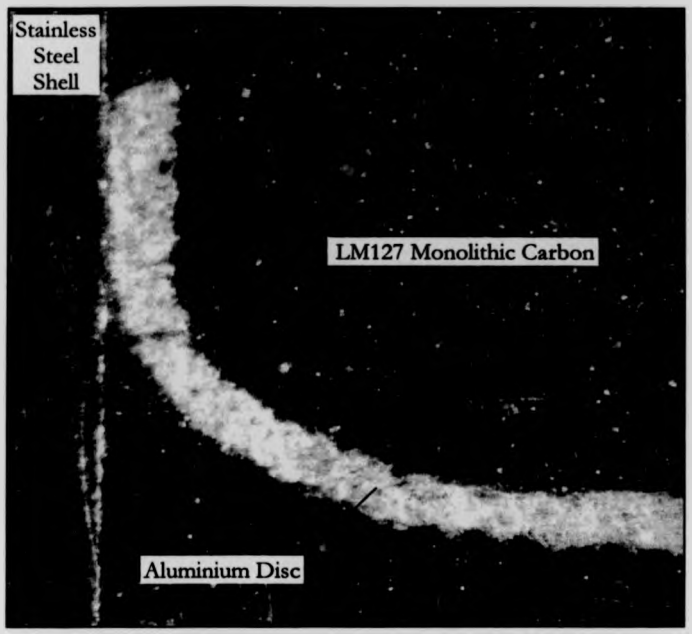

Figure 6.8: Magnified View of Aluminium Disc Contact Interface

A photograph of a magnified region of the laminate cross-section in the vicinity of the aluminium disc and shell wall interface is presented in Figure 6.8. The material contact between the aluminium disc and the internal shell wall appears to be very good with no apparent void regions suggesting a low thermal contact resistance and thus a high interface heat transfer coefficient.

6.3.5 Laminate Assembly

In order to produce the completed adsorption generators it was necessary to connect two 500 mm laminate sections together to form a complete one metre length before insertion into the generator steam pressure vessels on the experimental rig. This was achieved by forming a butt joint between the two laminate sections and welding a collar around both sections at the interface. End caps were also welded at either end of the one metre laminate section with a length of stainless steel tube at the centre of one end plate to allow the

ammonia into and out of the carbon through the centre hole along the laminate axis. All welding was performed in an inert argon atmosphere to inhibit combustion of the carbon at the weld points.

6.3.6 Laminate Characteristics

The number of layers, length and mass distribution for each of the four laminate sections is given in Appendix IV. The average laminate characteristics, based on the four laminate sections manufactured, are presented in Table 6.3.

Component	Mass per unit length ($kg\ m^{-1}$)	Proportion (%)
Aluminium Discs	0.474	11.5
LM127 Activated Carbon	1.526	37.2
Stainless Steel Shell	2.109	51.3

Table 6.3: Laminate Average Mass Distribution

For a one metre length of laminate the average total mass is 4.109 kg. The average number of carbon-aluminium layers 430 per metre giving a mean carbon-aluminium layer thickness of approximately 2.3 mm. Hence, taking the aluminium disc thickness as unchanged at 0.2 mm, the carbon layer is 5% thicker than originally specified.

The proportion of aluminium in the laminate by mass is only 11.5%. Hence, the aluminium is able to increase the effective thermal conductivity of the monolithic carbon without a major increase in the effective thermal mass.

6.4 Experimental Rig Construction

The experimental rig was built around a Dexion framework to provide flexibility in the design and to allow modifications to be carried out more quickly. Photographs of the final working experimental rig are presented in Figure 6.9 and Figure 6.10.

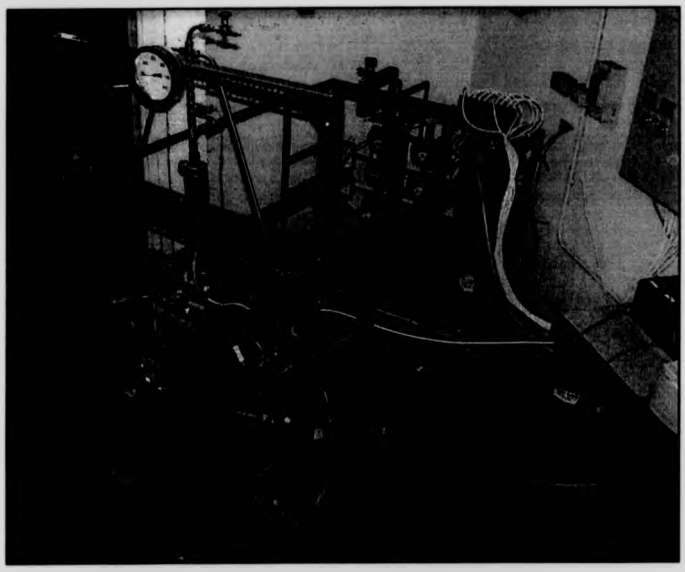

Figure 6.9: Main View of Experimental Rig

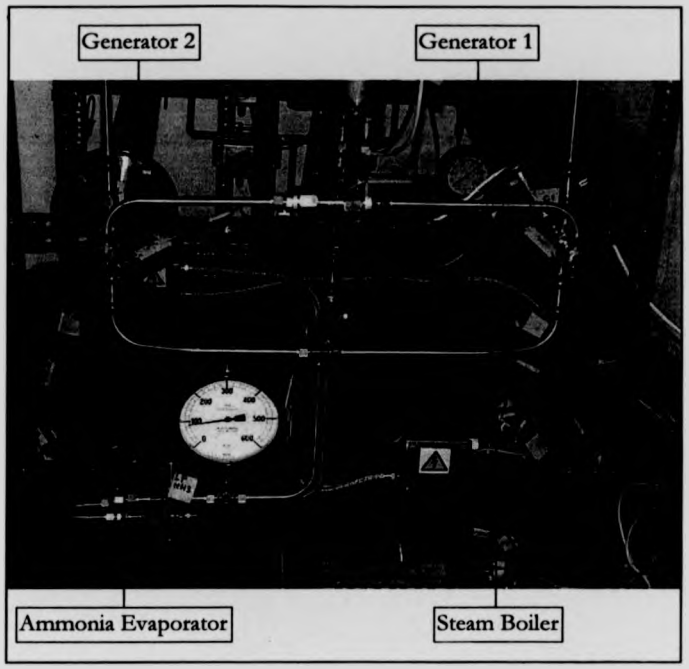

Figure 6.10: Close-up View of Main Rig Components

Once the basic Dexion framework with dimensions 1.5 m x 1.0 m x 1.0 m had been assembled, the water boiler, ammonia evaporator and both adsorption generator outer shells were placed within the rig framework. The remainder of the rig construction was performed around these four main components. Each of the ten pneumatically actuated ball valves to be used within the water loop were disassembled and copper fittings silver soldered directly into the weld sockets. The ball valves were then reassembled and installed on the rig framework. The water condenser was then inserted and the water loop connected between generator outer pressure vessels, ball valves and the water boiler and condenser utilising standard 15 mm plumbing copper to BS 1306 [2]. Once all of the water loop pipe-work was assembled, it was silver soldered in situ on the rig. This proved to be a major difficulty particularly with respect to obtaining gas tight joints. Hence, a better option in

future would be to either assemble the copper pipe-work off the rig where it is easier to manipulate or select Swagelok type compression fittings instead.

The ammonia loop was connected together with half inch stainless steel tubing to BS 3605 [3] between the generator flanges, ammonia evaporator, ammonia condenser and valves utilising Swagelok stainless steel compression fittings. This proved to be far quicker than had been the case with the water loop. A safety pressure relief valve with a cracking pressure of 20 bar was inserted in parallel with the condenser with the valve exit connected through tubing into a water tank.

The finished laminate sections were inserted into the generator pressure vessels on the experimental rig with a spacer at one end of the laminate, consisting of three short lengths of tubing at 120° intervals connected with wire around the circumference, to support and maintain the laminate concentric within the water pressure vessel. The stainless steel tube at the end of the laminate was connected with an in line Swagelok compression fitting to the stainless steel tube passing through the blind flange and into the ammonia loop. The whole assembly was then secured in place by tightening the bolts on the generator flange to form a gas tight seal between a gasket and the flange faces.

6.5 System Instrumentation

Once the construction of the experimental rig had been completed, thermocouples, pressure transducers and pressure gauges were added to the rig to allow the system pressures and temperatures to be monitored, controlled and logged on the computer.

6.5.1 Thermocouples

In order to monitor system temperatures, K type thermocouples supplied by TC Ltd were attached to the experimental rig. The temperature accuracy of the thermocouples was ±0.5 °C. A 1 mm diameter stainless steel sheathed thermocouple was placed in the centre of both carbon-aluminium laminates to measure the carbon internal temperature. Thermocouples were also attached to the outside base of both generator pressure vessels to measure the water temperature and to the outside base of the evaporator shell to measure

the evaporator temperature. The boiler heater temperature and the evaporator heater temperature were monitored utilising the K type thermocouples provided on the cartridge heaters.

6.5.2 Pressure Transducers and Gauges

Transinstruments 2000 A-G-B40-01-A00A gauge pressure transducers with a 0–40 bar range, a resolution of 0.40 bar mV^{-1} and an accuracy of $\pm 1.0\%$ were applied to monitor the ammonia pressure in both carbon-aluminium laminates. Druck PDCR 920 absolute pressure transducers with a 0–35 bar range, a resolution of 0.35 bar mV^{-1} and an accuracy of $\pm 1.5\%$ were applied to monitor the pressure in the ammonia condenser and evaporator. Gauge pressure transducers purchased from RS Components Ltd with a 0–10 bar range, a resolution of 0.10 bar mV^{-1} and an accuracy of $\pm 1.0\%$ were applied to monitor the water/steam pressure in both generator pressure vessels. Two mechanical pressure gauges were also utilised on the experimental rig to give a direct visual indication of the water pressure in the boiler and the ammonia pressure in the condenser.

6.5.3 Data Acquisition and Control

Two Strawberry Tree DATAshuttles (DA-16-8-TC-AO) were employed to acquire the data from the thermocouples, pressure transducers and liquid level floats on the experimental rig and control the state of the pneumatically actuated ball valves on the water loop and solenoid valves on the ammonia loop. The stated accuracy of the DATAshuttles is $\pm 0.3\,^{\circ}C$ on temperature and $\pm 25\mu V \pm 0.05\%$ of reading on voltage. The control process and data logging was performed utilising the dedicated WorkBench software running on a standard 486/Win 3.11 PC operating in conjunction with the DATAshuttles. All of the experimental data was logged at one second intervals (sampling frequency of 1 Hz per channel) and written to local hard-disk for processing and analysis at a later stage. The ammonia condensing pressure was monitored through the WorkBench software to instruct the ammonia solenoid valves to operate in sequence (presented in Figure 6.3) once a specified condensing pressure had been attained, thus allowing a controlled mass of condensed

ammonia to pass down into the evaporator. The change in the pneumatic valve states on the water loop was controlled according to the desired heating/cooling half-cycle time.

6.6 Experimental Rig Testing and Commissioning

Before performing any experimental testing the experimental rig was tested to ensure safe and correct operation. In the first instance, the water loop was pressure tested by filling the loop completely with water, closing the valve at the bottom of the loop and applying water pressure at the top of the loop. Water was chosen rather than air for pressure testing since it is essentially an incompressible fluid and hence the boundary work required to compress water between two pressure levels may be assumed to be negligible. Hence, any sudden failure in the pipe-work would not result in a dangerous explosive decompression. In contrast to this, for a compressible fluid such as air considerable energy would be stored in the form of compressive boundary work with the possibility of an explosive release of pressure during a pipe-work failure. Numerous leaks at the silver soldered joints between pipe-work where highlighted following the initial pressure testing. However, after many of the joints were re-soldered the leakage problem was reduced to that of micro-leaks which proved difficult to eradicate. Therefore, when the water loop was sucked down to vacuum by the vacuum pump, a gradual increase in system pressure back to atmospheric pressure was seen over a period of two to three days. The ammonia loop was tested for leaks by connecting it to a cylinder containing compressed argon. Any leaks were detected by applying a detergent solution to the pipe-work joints and visually inspecting for foaming and gas bubble formation. Any leaks detected were easily eradicated by tightening the relevant screwthread or Swagelok compression fitting.

All the pneumatically actuated ball valves and solenoid valves were connected up to the power supplies, DATAshuttles and computer to verify their operation. The outputs from the rig thermocouples and pressure transducers were also verified. Once all the control, instrumentation and data logging systems had been checked for correct operation preliminary experimental runs were able to commence.

6.7 Conclusions

From numerical simulations and practical manufacturing considerations a laminate radius of 25.4 mm, carbon layer thickness of 2 mm and aluminium layer thickness of 0.2 mm was selected for the carbon-aluminium laminate. The carbon-aluminium layers were compressed in groups of ten at a pressure of 152 MNm^{-2} to build up the complete laminate structure. Observation of pyrolysed test laminate samples under the microscope, presented in Figures 6.7 and 6.8, revealed an internal structure that showed good contact between the aluminium discs and stainless steel shell and between the aluminium discs and carbon layers, suggesting good heat transfer in these regions. Four laminate sections, each approximately 500 mm long, were fabricated and welded together in pairs to form the one metre long laminate sections utilised within the adsorption generators. Manufacture of the laminate sections was found to be very labour intensive. However, for a developing country the issue would in all probability not be the cost/time of labour but the capital cost of the raw materials used within the generator. A cost breakdown of a one metre length of laminate is presented in Table 6.4.

Component	Quantity Required (for 1 m length)	Material Cost	Component Cost (for 1 m length)
Aluminium Discs	455	£41.55/thousand	£18.91
LM127 Carbon	2.7 kg (wet)	£2.00/kg	£5.40
Stainless Steel Shell	1 metre	£56.59/metre	£56.59
Total Cost for 1 metre Length of Carbon-Aluminium Laminate:			**£80.90**

Table 6.4: Carbon-Aluminium Laminate Costing

It is apparent the greatest material cost involved in the laminate is the stainless steel shell which represents 70% of the total cost. However, this could be readily replaced with a cheaper alternative such as mild steel which while not possessing the desirable corrosion characteristics of stainless steel would reduce the total generator cost considerably.

The complete experimental rig was considerably more expensive and complex than initially envisaged resulting in a prototype system suitable for evaluating the concepts involved rather than a final system suitable for use directly in a developing country environment.

References

[1] **British Standards Institution: BS 4504**, Circular Flanges for Pipes, Valves and Fittings (PN Designated), Section 3.1, Specification for Steel Flanges, **1989**.

[2] **British Standards Institution: BS 1306**, Specification for Copper and Copper Alloy Pressure Piping Systems, **1975**.

[3] **British Standards Institution: BS 3605**, Austenitic Stainless Steel Pipes and Tubes for Pressure Purposes, Part 1, Specification for Seamless Tubes, **1991**.

Chapter 7

Experimental Procedure

7.1 Introduction

Prior to commencing experimental runs it was necessary to set the mass of water and ammonia in the system. The water loop was then sucked down to vacuum to remove any air present in the copper pipework and enable efficient generator cooling through water boiling under low pressure. The experimental data was acquired and logged automatically on the computer throughout each experimental run.

7.2 System Initialisation

7.2.1 Setting System Water Mass

The water level float reed switches on both generators were placed at the mid-way height in order to set the water level in both generators to half cover the laminate shell. The valves at the top and bottom of the water loop were then opened. All of the ball valves around the water loop were maintained in their normally open state. The bottom of the water loop was then connected, via a length of flexible plastic tubing, to a vessel containing distilled water. The water was allowed into the water loop and the signal from the reed switches monitored to determine the correct filling level. Once the half way level had been attained for both generators the bottom water valve was closed to isolate the water loop from the distilled water vessel.

7.2.2 Vacuum Pumping Water Loop

Once the water loop had been filled, the valve at the top of the loop was connected to a vacuum pump. The pressure in the water loop was then monitored using the WorkBench software until the pressure had dropped to the water saturation pressure at ambient temperature.

Throughout the experimental runs the water loop was intermittently re-connected to the vacuum pump to remove any air that may have entered the system through microleaks in the copper pipework.

7.2.3 Charging Ammonia Loop

The ammonia loop was charged from a cylinder of compressed ammonia in conjunction with a vacuum pump. The solenoid valves (V11, V12) and the ball valve (V13), as shown in Figure 6.1, were set in the open state, the valve at the bottom of the loop was closed and the valve at the top of the loop opened. The top valve was then connected to the vacuum pump to remove any air present. Once the loop pressure reached a stable minimum value the vacuum pump was disconnected and the ammonia cylinder connected. The ammonia was then allowed into the loop until the evaporator was half full of ammonia liquid, as judged visually from the sight glasses located on the evaporator end plate. The top valve was then closed to isolate the system from the ammonia cylinder which was then disconnected. No ammonia leaks were apparent from the ammonia loop over the complete experimental period.

7.3 Data Logging

The data from the experimental rig was acquired and logged by computer implementing the instrumentation and equipment discussed in Section 6.5. For each experimental run the following parameters were logged or calculated:

1. Time Elapsed (seconds)
2. Steam Boiler Temperature (K)

3. Ammonia Evaporator Temperature	(K)
4. Internal Laminate Temperature (Generators 1 & 2)	(K)
5. External Generator Base Temperature (Generators 1 & 2)	(K)
6. Water Pressure (Generators 1 & 2)	(bar)
7. Ammonia Pressure (Generators 1 & 2)	(bar)
8. Ammonia Evaporator Pressure (Low Pressure)	(bar)
9. Ammonia Condenser Pressure (High Pressure)	(bar)
10. Calculated Concentration (Generators 1 & 2)	(kg NH_3 kg^{-1}Carbon)
11. Ammonia Solenoid Valve States (V11 & V12)	(0 volts ≡ Open, 5 volts ≡ Closed)

All of the above data was automatically logged or calculated at one second intervals throughout the duration of the experimental run. The experimental data was displayed directly on screen as it was acquired so as to highlight any trends in the data and allow the progress of the run to be monitored. The generator water pressure during cooling was followed particularly closely with the water loop re-connected to the vacuum pump to remove any air from the system if the water pressure appeared to be too high or the generator cooling was inadequate during the adsorption phase. The data obtained was stored on local hard disc and analysed at a later stage using Matlab.

Several thermodynamic cycles were logged during each experimental run in order to obtain consistent data from cycle to cycle. During the first two or three logged cycles there was a considerable variation in the rig parameters recorded, such as pressure and temperature. Once the rig had achieved a dynamic thermal equilibrium, the cycles recorded were far more consistent and consequently exhibited less variation from cycle to cycle. Any change in the system settings between cycles, such as removing air from the water loop with the vacuum pump, was evident by the pronounced effect on the subsequent data recorded. Therefore, after connecting the water loop to the vacuum pump a further one or two cycles were required before the experimental rig achieved a new dynamic thermal equilibrium.

7.4 System Cycling Times

The system cycling times were defined through the Workbench control software. For the first sets of experimental data 15 minute half-cycle times were employed resulting in a total thermodynamic cycle time, including the valve change-over and water filling processes, of approximately 1840 seconds. On later experimental runs this half-cycle time was reduced to 10 minutes in order to evaluate any improvement in the specific cooling power achieved.

Chapter 8

Experimental Results and Performance Analysis

8.1 Introduction

Several sets of experimental data were logged and analysed for various external heating temperatures and cycle times. During each experimental run, several heating and cooling cycles were recorded in order to obtain repeatable data under conditions of dynamic equilibrium. The experimental data obtained from one experimental run with a heating and cooling half-cycle time of 10 minutes (600 seconds) is presented in the following sections. The total half-cycle time is 620 seconds; this corresponds to a heating or cooling half-cycle time of 600 seconds and a generator water filling time of 20 seconds.

8.2 Generator Heating and Cooling Cycles

8.2.1 Generator Temperature Cycles

The laminate internal temperature variation with time for generator 1 and generator 2, as recorded by the thermocouple situated at the centre of the laminate, is presented in Figure 8.1. For generators 1 and 2, the steam supplied by the boiler allows a maximum laminate temperature of approximately 140°C while during the thermosyphon cooling phase the minimum laminate temperature is approximately 40°C. Good thermal matching between the generators is indicated by the similarity between the two temperature profiles.

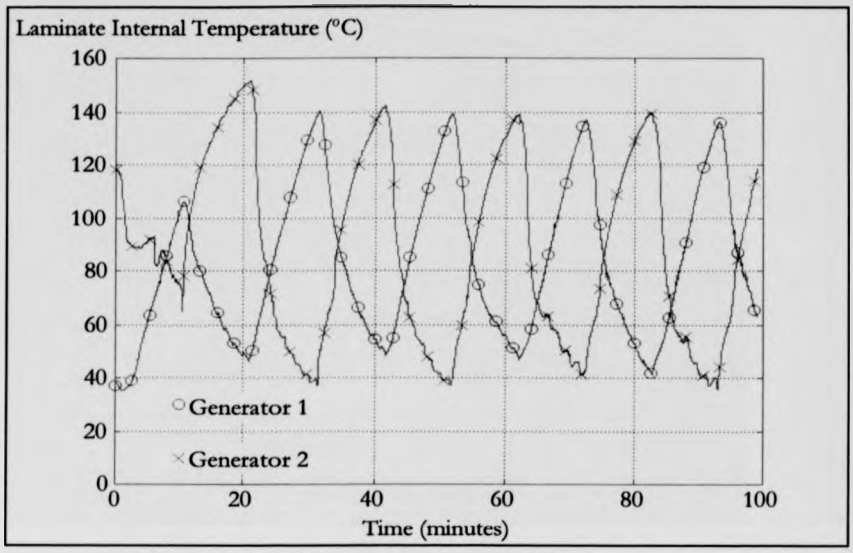

Figure 8.1: Generator 1 and Generator 2 Temperature Cycles

The variation of laminate internal temperature and generator steam pressure vessel saturation temperature with time for generator 1 is presented in Figure 8.2. After the first complete thermal cycle, both temperature profiles repeat from cycle to cycle. During the heating half-cycles the water saturation temperature calculated from the shell pressure is greater than the laminate internal temperature as would be expected for a heat flow into the laminate. During the cooling half-cycle the reverse is true with a water saturation temperature less than the laminate internal temperature consistent with a heat flow out of the laminate. At the end of the heating half-cycles the temperature difference between the steam in the generator pressure vessel and the centre of the laminate is approximately 10°C. At the end of the cooling half-cycles the temperature difference between the steam in the generator pressure vessel and the centre of the laminate varies between 0°C and 4°C.

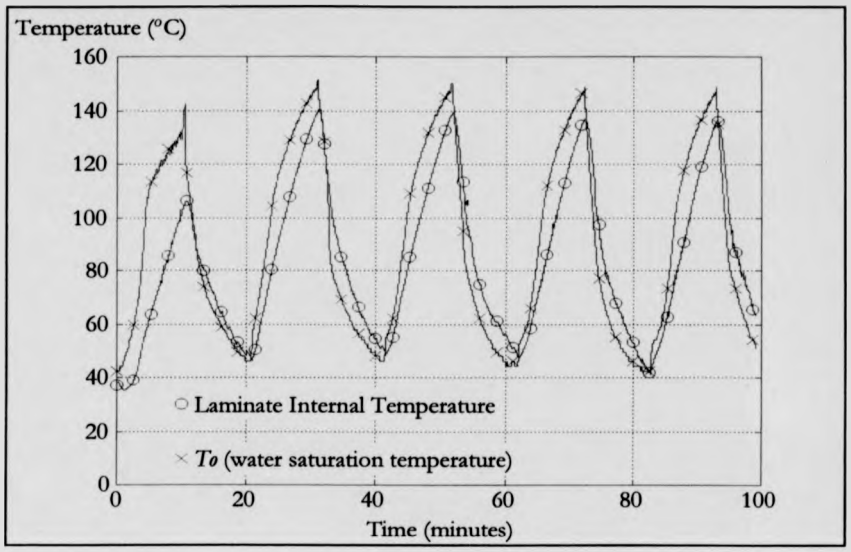

Figure 8.2: Generator 1 - Laminate and Water/Steam Saturation Temperature Cycles

For clarity, the boiler temperature and generator pressure vessel temperature as measured by the external thermocouple for generator 1, over the same temperature and time ranges as above, are presented separately in Figure 8.3. Rather than having an ideal constant value, the boiler temperature has a saw-tooth profile which varies between approximately 75°C and 150°C. This is due to the cooling effect of the water from the cooled generator flowing back into the boiler. The boiler temperature increases during each heating half-cycle as it approaches the temperature specified by the PID controller. At the end of each heating half-cycle water from the boiler is pumped up into the pressure vessel of the generator about to be cooled. The boiler is then connected to the generator which has completed a cooling half-cycle and is about to be heated. During this process a volume of cooled water flows down from the cooled generator into the boiler rapidly lowering the boiler temperature. The boiler temperature then increases again during the subsequent heating half-cycle as a result of further heat input from the cartridge heater.

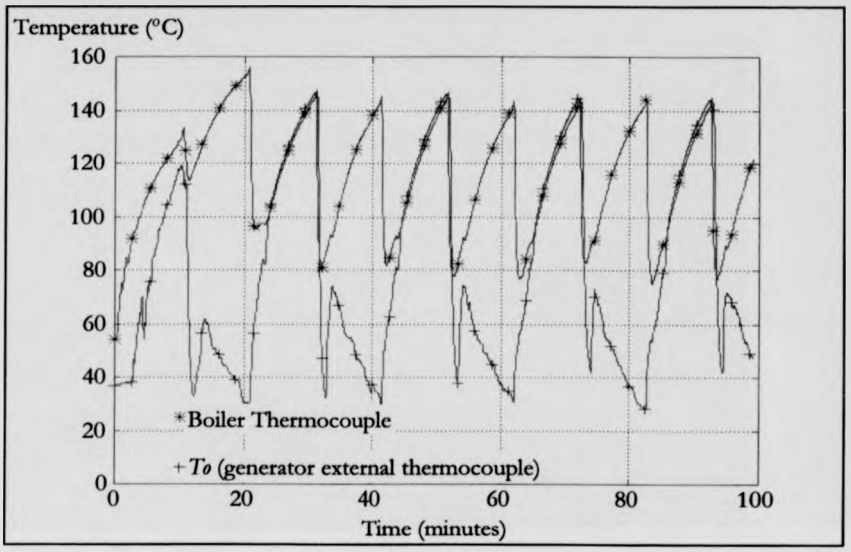

Figure 8.3: Generator 1 - Boiler and External Thermocouple Temperature Cycles

For the heating half-cycles the boiler thermocouple, generator pressure vessel external thermocouple and pressure vessel saturation temperature profiles all follow each other closely. However, for the cooling half-cycles the pressure vessel temperatures obtained from the external thermocouple and saturation temperature differ considerably. At the start of each cooling half-cycle there is a dramatic decrease in the temperature measured by the generator external thermocouple at approximately the same time as the decrease in boiler temperature at the half-cycle change-over time. This is believed to be due to sub-cooled liquid water flowing into the generator pressure shell from the water condenser resulting in a sudden decrease in temperature as measured by the thermocouple. The temperature then increases as a new thermal equilibrium point is established. The cooling process then continues with water boiling around the laminate in the pressure shell.

8.2.2 Generator Pressure Cycles

The laminate saturation pressure variation with time for generator 1 and generator 2 is presented in Figure 8.4. For generators 1 and 2, the minimum and maximum median

saturation pressures are approximately 5 bara and 13 bara respectively, as controlled by the WorkBench software. The comparable permeability of both generator laminates is indicated by the similarity between the two pressure profiles. The pressure profiles for generator 1 and 2 also indicate good cycle to cycle repeatability.

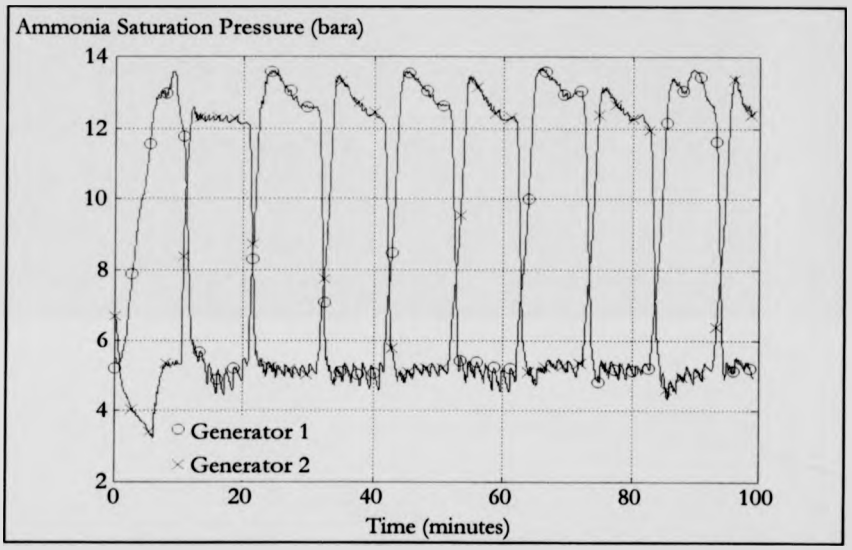

Figure 8.4: Generator 1 and Generator 2 Pressure Cycles

For both generators 1 and 2, the operation of the ammonia check valves is highlighted by the fluctuations in the saturation pressure during the (ideally isobaric) adsorption and desorption processes. During the desorption period of the heating half-cycles the generator ammonia saturation pressure decreases by approximately 1 bar between the beginning and end of the desorption period as the mass flow of ammonia leaving the generator decreases resulting in a corresponding reduction in the pressure drop through the check valves and a reduction in generator saturation pressure. During the adsorption period of the cooling half-cycles there is a sudden jump in the laminate saturation pressure each time the check valve cracks open and the laminate is connected up to the evaporator. The check valve closes when the pressure differential across it is insufficient to overcome the valve spring

tension. The saturation pressure continues to decrease as the bed is cooled further until the pressure differential across the check valve is sufficient to allow the check valve to crack open again.

The variation of the generator 1 ammonia pressure, ammonia condenser pressure and ammonia evaporator pressure with time is presented in Figure 8.5.

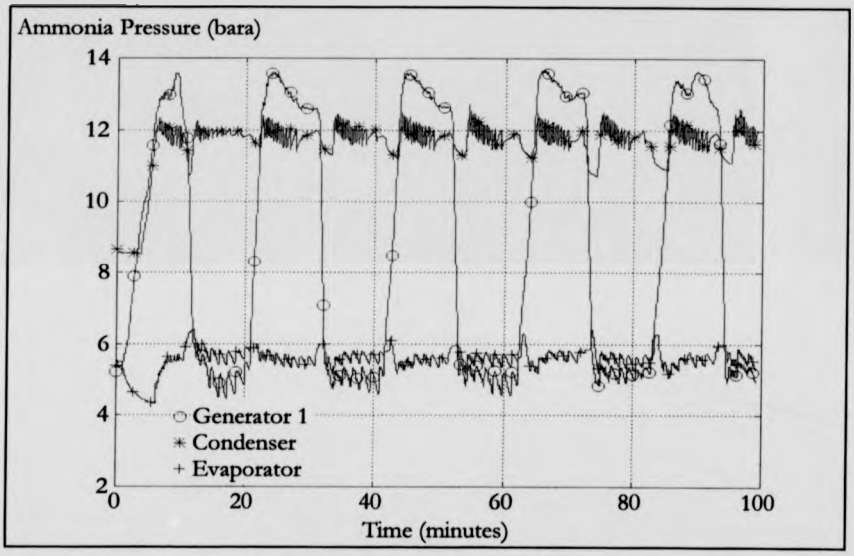

Figure 8.5: Generator 1 Laminate, Ammonia Condenser and Evaporator Pressure Cycles

Taking the median data value over the 10–100 minute condenser and evaporator pressure ranges gives:

Evaporating Pressure, $P_{evap} = 5.62$ bara

Condensing Pressure, $P_{cond} = 11.84$ bara

Evaporating Temperature, $T_{evap} = 7.5\,^{\circ}C$

Condensing Temperature, $T_{cond} = 30.5\,^{\circ}C$

During the heating half-cycle desorption period the generator saturation pressure is approximately 1.1 bar greater than the condenser pressure whilst during the cooling half-

cycle adsorption period the generator saturation pressure is approximately 0.55 bar less than the evaporator pressure. These pressure differences represent a pressure loss of approximately 10% and are as a result of the pressure drops created by the pipe-work and check valves between the generator, evaporator and condenser. The pressure drop is, in general terms assuming density remains constant, proportional to a constant multiplied by the flow velocity squared. Hence, for a given mass flow rate and rate of concentration change, the pressure drop will be greatest when the ammonia density is lowest as is the case during the heating half-cycle where high temperature ammonia is desorbed from the laminate. Conversely, the pressure drop will be lowest when the ammonia density is greatest as is the case during the cooling half-cycle where low temperature ammonia is adsorbed into the laminate. The pressure drop between the generator and condenser decreases over the desorption period as the massflow and rate of concentration change decreases. The fluctuations in the condenser and evaporator pressure are due to the control volume of condensed ammonia passing from the condenser via the receiver to the evaporator. On each occasion the ammonia solenoid valve control sequence allows a control volume of condensed ammonia into the evaporator the condenser pressure decreases and the evaporator pressure increases. Apart from these small pressure fluctuations, the evaporating pressure and the condensing pressure are both quasi constant over the time period presented.

8.2.3 Generator Concentration Cycles

The generator concentrations were calculated by applying the D-A equation given in equation (3.8) with ammonia saturation temperature calculated from the experimental ammonia saturation pressure by applying equation (3.29). The laminate concentration variation with time for generator 1 and generator 2 is presented in Figure 8.6.

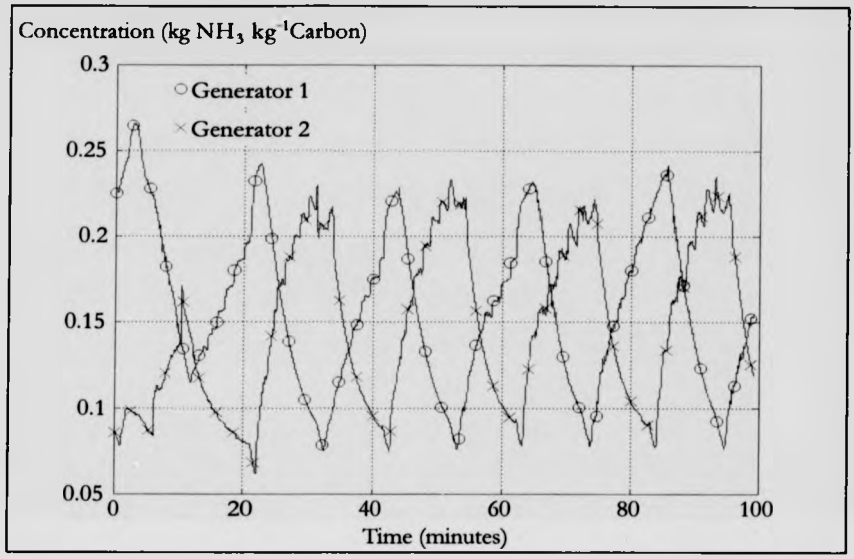

Figure 8.6: Generator 1 and Generator 2 Ammonia Concentration Cycles

For generators 1 and 2, the minimum and maximum concentrations are approximately 0.08 kg NH_3 kg^{-1}Carbon and 0.24 kg NH_3 kg^{-1}Carbon respectively giving a maximum concentration change over each complete thermodynamic cycle of approximately 0.16 kg NH_3 kg^{-1}Carbon (a concentration swing of 16%). As a general estimate, a concentration swing of greater than 10% may be considered acceptable. During each heating and cooling half-cycle the plots are almost linear indicating a constant mean rate of concentration change over the desorption and adsorption processes. The mean rate of concentration change for both generators correlate well, particularly during cooling, suggesting close geometric similarity between the generators. As would be expected for identical heating and cooling half cycle times, the mean rate of concentration change during cooling is the same as during heating. However, during the heating half-cycle the concentration change is negative (desorption) as the ammonia concentration decreases when the generator is heated. Conversely, during the cooling half-cycle the concentration

change is positive (adsorption) as the ammonia concentration increases when the generator is cooled.

8.2.4 Generator Clausius-Clapeyron Diagram

A Clausius-Clapeyron diagram based on successive laminate internal temperature and laminate saturation pressure cycles for generator 1 and generator 2 is presented in Figure 8.7.

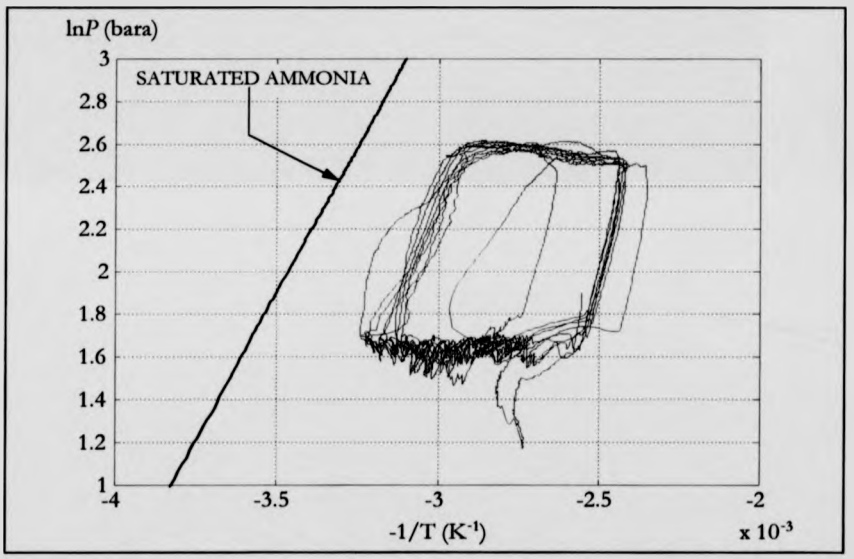

Figure 8.7: Generator 1 and Generator 2 Clausius-Clapeyron Diagram

This Clausius-Clapeyron cycle determined from experimental data closely resembles the idealised cycle presented in Figure 3.2. The idealised cycle consists of two isosteric and two isobaric processes with sudden and definite transitions from isosteric to isobaric processes and vice versa. In contrast to this, the experimental Clausius-Clapeyron diagram indicates that the actual thermodynamic cycle possesses smooth curved transitions between cycle processes. The fact that the cycles for both generator 1 and generator 2 are superimposed

on top of one another indicates that the generators have similar properties with repeatable data obtained from cycle to cycle at the selected working conditions.

8.2.5 Generator Heat Capacity and Specific Heat

The heat capacity (thermal mass) variation of the carbon-aluminium laminate (carbon/aluminium discs/stainless steel shell) and the carbon only with internal laminate temperature is presented in Figure 8.8. The curves shown are for the fourth heating half-cycle logged for generator 1 up to a maximum generating temperature of approximately 135°C.

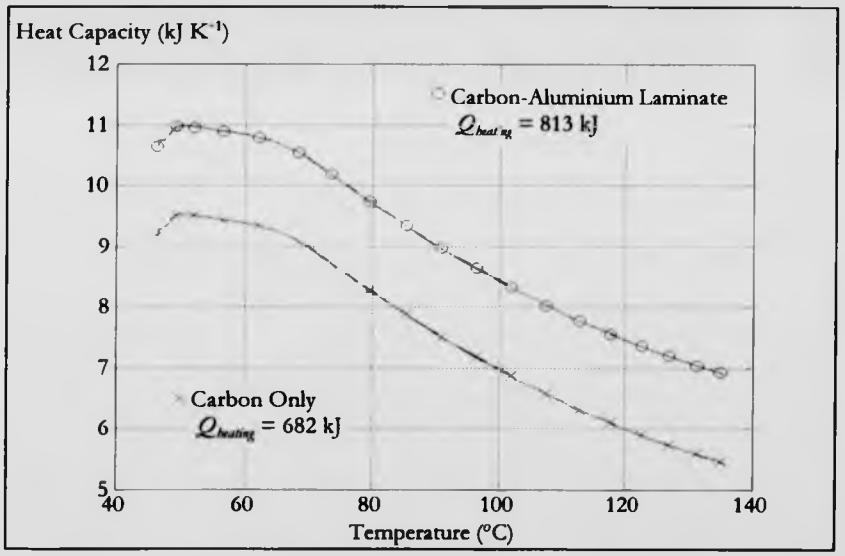

Figure 8.8: Generator 1 - Heat Capacities and Heat Inputs for a Heating Half-Cycle

It has been assumed that the carbon effective specific heat is a function of temperature whilst the specific heat of the aluminium and steel remain constant with temperature. Hence, both curves have the same shape but are displaced from each other in the y-axis by a constant heat capacity value. Additionally, it is assumed that the temperature is uniform throughout the laminate with the carbon, aluminium and stainless steel in thermal

equilibrium at any given time. The heat capacity curves reach a maximum value at approximately 50°C which corresponds to a heating duration of 40 seconds. The maximum heat capacity occurs at the point of maximum mean rate of concentration change where the rate of ammonia desorbed from the laminate is greatest. The heat capacity then decreases with increasing laminate temperature and time through the heating half-cycle as progressively less ammonia is desorbed and the maximum mean rate of concentration change is reduced. Integrating under the heat capacity curves between the minimum and maximum laminate internal temperature limits gives the heat input over the duration of the heating half-cycle.

For the carbon only the heat input is given by:

$$Q_{in,car} = \int_{T_{min}}^{T_{max}} \left(M_c \left(Cp_c(T) + xCp_a - h_{ads} \left(\frac{\partial x}{\partial T} \right)_{P_{sat}} \right) \right) dT \qquad (8.1)$$

For the carbon-aluminium laminate (carbon/aluminium discs/stainless steel shell) the heat input is given by:

$$Q_{in,lam} = \int_{T_{min}}^{T_{max}} \left(M_c \left(Cp_c(T) + xCp_a - h_{ads} \left(\frac{\partial x}{\partial T} \right)_{P_{sat}} \right) + M_{alum} Cp_{alum} + M_{steel} Cp_{steel} \right) dT \qquad (8.2)$$

where:

T_{min} is the minimum laminate temperature achieved by water/steam cooling loop (°C)

T_{max} is the maximum laminate temperature achieved by water/steam heating loop (°C)

$M_c = 1.586$ is the generator 1 laminate mass of carbon (kg)

$M_{alum} = 0.489$ is the generator 1 laminate mass of aluminium (kg) → see Appendix IV

$M_{steel} = 2.183$ is the generator 1 laminate mass of steel (kg)

$Cp_c(T) = 34.685 + (2.811 \times T)$ is the carbon specific heat (J $kg^{-1}K^{-1}$) with T in Kelvin

$Cp_a \sim 4734$ is the ammonia specific heat (J $kg^{-1}K^{-1}$)

Cp_{alum} ~ 900 is the aluminium specific heat (J $kg^{-1}K^{-1}$)

Cp_{steel} ~ 465 is the steel specific heat (J $kg^{-1}K^{-1}$)

x is the concentration (kg NH_3 kg^{-1}Carbon)

h_{ads} is the enthalpy of adsorption (J kg^{-1})

$(\partial x/\partial T)_{P_{sat}}$ is the rate of concentration change with carbon temperature at constant saturation pressure (kg NH_3 kg^{-1}Carbon K^{-1})

For the carbon only the heat input over the heating half-cycle is 682 kJ. For the complete carbon-aluminium laminate assembly the additional thermal mass provided by the aluminium discs and stainless steel shell increases the heat input requirement over the heating half-cycle by 19% to a value of 813 kJ.

Dividing the heat capacity for the carbon only and the heat capacity for the carbon-aluminium laminate by the total mass of carbon and total mass of laminate respectively gives the mean effective specific heat curves presented in Figure 8.9.

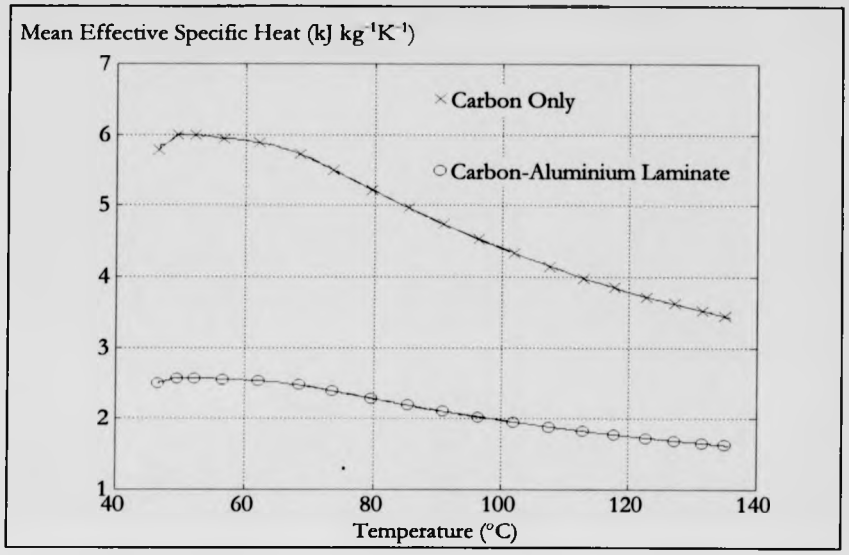

Figure 8.9: Generator 1 - Mean Effective Specific Heats for a Heating Half-Cycle

8.3 Heating Power

The heating power may be expressed as:

$$P_{heating} = \frac{Q_{heating}}{t_{cycle}} \tag{8.3}$$

where:

$P_{heating}$ is the heating power (W)

$Q_{heating}$ is the heat input to the laminate (J)

t_{cycle} is the total cycle time (s)

Therefore, with reference to Figure 8.8, the heating power for the carbon only is:

$$P_{heating,car} = \frac{682 \times 10^3}{1240} = 550 \text{ W}$$

With reference to Figure 8.8, the heating power for the carbon-aluminium laminate is:

$$P_{heating,lam} = \frac{813 \times 10^3}{1240} = 656 \text{ W}$$

Both of the above heating powers are taken over the complete cycle duration rather than over the heating half-cycle duration. They represent the heating power for one generator only. The heating power values for the complete rig would therefore be twice the heating power values quoted above.

8.4 Cooling Power

The cooling power may be expressed as:

$$P_{cooling} = \frac{\Delta x_{cooling} M_c (h_{gc} - h_{fc})}{t_{cyc}} \tag{8.4}$$

where:

$P_{cooling}$ is the cooling power (W)

$\Delta x_{cooling}$ is the change in concentration during the cooling half-cycle (kg NH_3 kg^{-1}Carbon)

h_{gc} is the specific enthalpy of ammonia vapour leaving the evaporator (J kg^{-1})

h_{fc} is the specific enthalpy of ammonia liquid leaving the condenser (J kg^{-1})

The specific enthalpy of ammonia liquid leaving the condenser is calculated by applying equation (3.31) at the condenser temperature, $T_{cond} = 30.5\,°C$. The specific enthalpy of ammonia vapour leaving the evaporator is calculated by applying equation (3.32) at the evaporator temperature, $T_{evap} = 7.5\,°C$.

Therefore, with reference to the fourth concentration cycle of generator 1 in Figure 8.6, the cooling power is:

$$P_{cooling} = \frac{(0.237 - 0.078) \times 1.586 \times (1692 - 566) \times 10^3}{1240} = 229 \text{ W}$$

The specific cooling power per unit mass of carbon is then:

$$P_{sp,cooling,car} = \frac{P_{cooling}}{M_c} = \frac{229}{1.586} = 144 \text{ W kg}^{-1}$$

The specific cooling power per unit mass of laminate is:

$$P_{sp,cooling,lam} = \frac{P_{cooling}}{M_c + M_{abem} + M_{steel}} = \frac{229}{1.586 + 0.489 + 2.183} = 54 \text{ W kg}^{-1}$$

The cooling power is calculated over the complete cycle duration rather than over the cooling half-cycle duration and represents the cooling power provided by one generator only. The cooling power value for the complete rig would therefore be twice the 229 W cooling power value quoted above.

During the cooling process ammonia boils in the evaporator and is re-adsorbed into the carbon-aluminium laminate. The average mass flow rate of ammonia returning to the generator during cooling is given by:

$$\dot{m} = \frac{\Delta x_{cooling} M_c}{\Delta t_{cool}} \tag{8.5}$$

where:

$\dot{m}$ is the average ammonia mass flow rate (g s^{-1})

Δt_{cool} is the cooling half-cycle duration (s)

Therefore, with reference to the fourth concentration cycle of generator 1 in Figure 8.6, the average ammonia mass flow rate is:

$$\dot{m} = \frac{(0.237 - 0.078) \times 1586}{620} = 0.41 \text{ g s}^{-1}$$

8.5 Coefficient of Performance

The coefficient of performance (COP) is a measure of the experimental rig efficiency. The cooling COP for the carbon only is:

$$COP_{car} = \frac{P_{cooling}}{P_{heating,car}} = \frac{229}{550} = 0.42$$

The cooling COP for the complete carbon-aluminium laminate is:

$$COP_{lam} = \frac{P_{cooling}}{P_{heating,lam}} = \frac{229}{656} = 0.35$$

The ideal Carnot COP is:

$$COP_{carnot} = \frac{T_{evap}\left(T_{max} - T_{cond}\right)}{T_{max}\left(T_{cond} - T_{evap}\right)} = \frac{280.65(408.15 - 303.65)}{408.15(303.65 - 280.65)} = 3.12$$

8.6 Summary of Performance Results

The experimental rig performance results including the cooling power, heating power and cooling coefficient of performance for both the carbon adsorbent only and the complete carbon-aluminium laminate are presented in Table 8.1.

$P_{heating,car}$ (W)	$P_{heating,lam}$ (W)	$P_{cooling}$ (W)	$P_{sp,cooling}$ (W kg^{-1}car)	COP
550	656	229	144	0.35

Table 8.1: Adsorption Cooling Rig Performance (Generator 1)

($T_{evap} = 7.5\,°C$, $T_{cond} = 30.5\,°C$, $T_{max} = 135\,°C$, $t_{cycle} = 1240$ seconds)

The data presented in Table 8.1 is for one generator only. The heating power required for the complete laminate is some 19% greater than for the carbon alone due to the additional thermal mass presented by the aluminium discs and stainless steel shell. For the complete operational rig the heating powers for the carbon and for the laminate would be twice the values given in Table 8.1; 1.1 kW and 1.3 kW respectively. In the same manner, the semi-continuous cooling power provided by the experimental rig would be 0.46 kW for two generators behaving identically but operating 180° out of phase. The specific cooling power and COP remain as the values given in Table 8.1 irrespective of the number of adsorption

generators employed. The value calculated for specific cooling power of 144 W kg^{-1} is a considerable improvement over the specific cooling powers obtained previously in the range 30–60 W kg^{-1} for experimental rigs utilising both granular and monolithic carbons.

8.7 Conclusions

Several sets of experimental data were obtained from the experimental rig for various generating temperatures and cycling times. For the experimental results presented, the specific cooling power per unit mass of carbon is 144 W kg^{-1} with a COP of 0.35 and a half-cycle time of 620 seconds. This gives a total cooling power for the experimental rig (cycling two generators) of 458 W. The specific cooling power of 144 W kg^{-1} is considerably lower than the value of 500 W kg^{-1} initially calculated when determining the optimal generator geometry. However, the higher value is based on a heating half-cycle time a factor in excess of twenty times less than the 620 seconds used experimentally. For the experimental rig in its present form the thermal mass of the system, including the generator pressure shell, flanges, and the water heat transfer fluid, prevents such short half-cycle times from being utilised. Additionally, the time required to fill each generator before the cooling half-cycle and the poorer heat transfer observed during the cooling phase makes the use of half-cycle times of the order of 30 seconds totally impractical at the present time.

Chapter 9

Numerical Model Validation

9.1 Introduction

Three sets of experimental data have been analysed utilising the simple explicit numerical model described in Chapter 5. The results from these validation runs are presented in the following sections for temperature, pressure and concentration. In each of the validation cases the "driving" external temperature outside the laminate unit cell in the numerical model was provided by either the experimental water/steam pressure vessel thermocouple or the water/steam pressure vessel saturation temperature. In this manner the temperature input data for the numerical model was provided directly from the experimental data rather than by a theoretical step input, polynomial equation or exponential function within the model. The external heat transfer coefficients during heating and cooling were varied initially to give the best numerical results. External heat transfer coefficients during heating of 1000 $W m^{-2}K^{-1}$ and during cooling of 500 $W m^{-2}K^{-1}$ were found to give the best correlation between the numerical model and the experimental data. Therefore, all of the final validation runs utilising the water/steam pressure vessel saturation temperature were carried out with an external heat transfer coefficient during heating of 1000 $W m^{-2}K^{-1}$ and an external heat transfer coefficient during cooling of 500 $W m^{-2}K^{-1}$

9.2 Generator Heating and Cooling Validations

9.2.1 Generator Temperature Validation

The temperature validation (laminate internal temperature) for experimental data set 1 based on the generator water/steam pressure vessel thermocouple driving temperature is presented in Figure 9.1. The first validation run was carried out with an external heat transfer coefficient during heating of 1000 $W\,m^{-2}K^{-1}$ and an external heat transfer coefficient during cooling of 500 $W\,m^{-2}K^{-1}$. During the heating half cycle the numerical model predicts a mean carbon internal temperature approximately 4°C greater than the experimental value. During the first 300 seconds of the cooling half-cycle the numerical model is in good agreement with the experimental data. However, beyond this time the predicted temperature decreases at a greater rate than the experimental value to a temperature almost 10°C lower than the experimental value at a total elapsed time of 1500 seconds. This temperature discrepancy is due in part to the external thermocouple driving temperature which decreases rapidly in the same region. The rapid reduction in the temperature measured by the thermocouple may be due, as mentioned in Chapter 8, to sub-cooled liquid from the steam/water condenser flowing into the generator pressure vessel at the start of the cooling half-cycle. However, the complete physical mechanism for the temperature reduction is not fully understood.

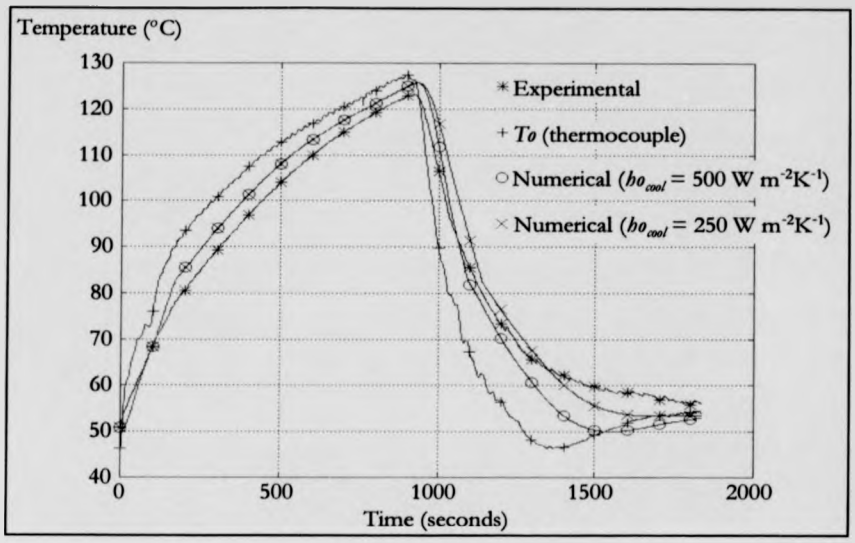

Figure 9.1: Experimental Data Set 1 - Temperature Validation Based on Generator Pressure Vessel External Thermocouple Driving Temperature

Therefore, in order to achieve an improved match between the numerical model and the experimental data during the cooling half-cycle a further validation run was carried out with an external heat transfer coefficient during heating of 1000 W $m^{-2}K^{-1}$ and a reduced external heat transfer coefficient during cooling of 250 W $m^{-2}K^{-1}$. This was done in order to reduce the rate of temperature decrease during the cooling half-cycle predicted by the model. During the heating half-cycle the results are identical to those obtained previously as the external heat transfer coefficients are the same. During the cooling half-cycle the predicted temperature curve has been displaced upwards resulting in a slightly improved correlation between numerical and experimental data. The predicted temperature is approximately 5°C lower than the experimental value at a total elapsed time of 1600 seconds, which is comparable with the temperature error seen during heating. However, although the gradient of the numerically predicted temperatures matches the experimental closely during heating, beyond a time of approximately 1200 seconds during the cooling half-cycle the gradient and shape of the numerically predicted temperatures do not follow

those seen experimentally. Validation runs utilising even lower external heat transfer coefficients during cooling produced curves of the same shape but displaced further upwards during the cooling half-cycle. Cooling external heat transfer coefficients less than 250 W $m^{-2}K^{-1}$ were felt to be physically unrealistic, particularly for water boiling within the generator pressure vessel over the surface of the laminate shell.

In order to improve the correlation between the numerical model and the experimental data the water/steam pressure vessel saturation temperature was selected as the driving temperature input for the numerical model rather than the water/steam pressure vessel thermocouple temperature. The temperature validation for experimental data set 1 based on the generator water/steam pressure vessel saturation temperature is presented in Figure 9.2. During the heating half cycle the numerical model again predicts a mean carbon internal temperature approximately 4°C greater than the experimental value. There is also a good match between the numerical and experimental during the cooling half-cycle with a numerical temperature approximately 6°C less than the experimental value at the end of the cooling half-cycle. In general the shape of the numerical and experimental curves are very similar, with the model over-predicting the internal carbon temperature during heating and under-predicting the internal carbon temperature during cooling. For the cooling half-cycle the numerical results obtained using the pressure vessel saturation temperature (presented in Figure 9.2) give a better fit to the experimental data than the results obtained using the pressure vessel thermocouple (presented in Figure 9.1).

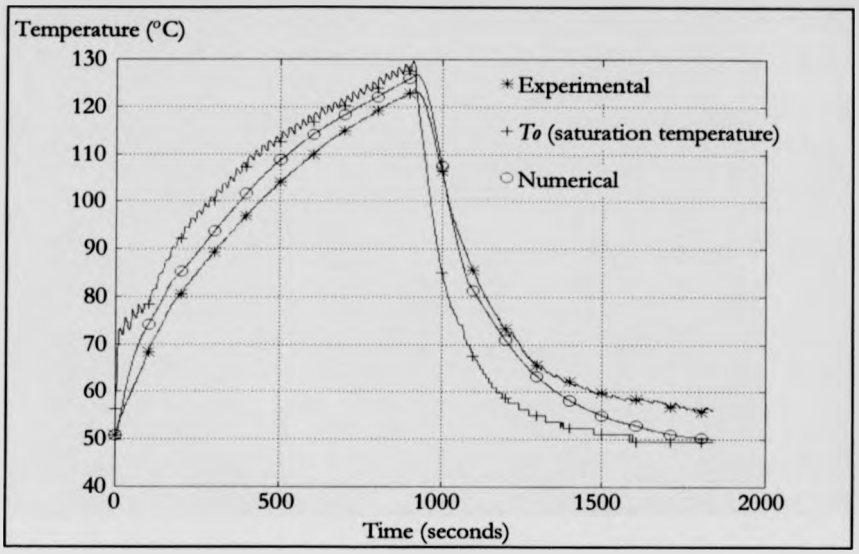

Figure 9.2: Experimental Data Set 1 - Temperature Validation Based on Generator Water/Steam Saturation Driving Temperature

The temperature validation for experimental data set 2 based on the generator water/steam pressure vessel saturation temperature is presented in Figure 9.3. During the heating half cycle the numerical model predicts a mean carbon internal temperature approximately 3°C greater than the experimental value. During the cooling half-cycle there is a very good match between the numerical and experimental temperature profiles with a numerical temperature only 2.5°C less than the experimental value at the end of the cooling half-cycle. The similarity of the two temperature profiles suggests that the external heat transfer coefficients selected for heating and cooling are near optimal for this validation case.

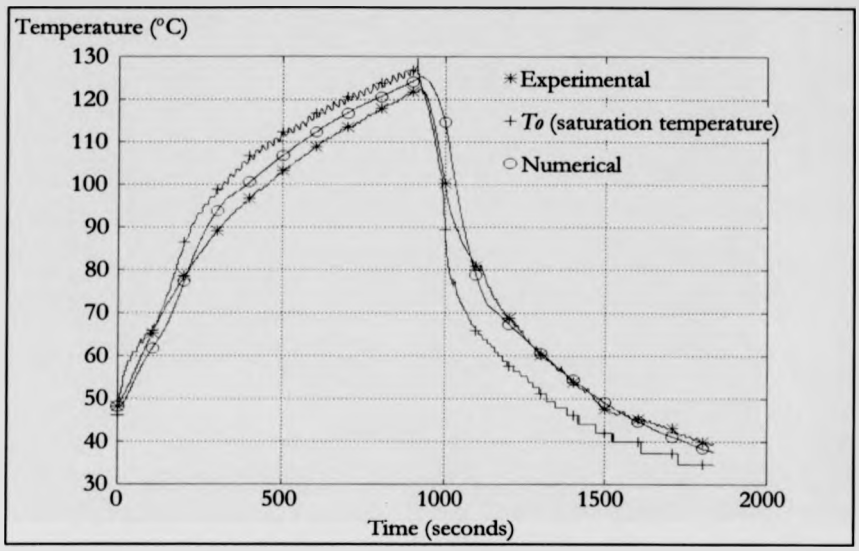

Figure 9.3: Experimental Data Set 2 - Temperature Validation Based on Generator Water/Steam Saturation Driving Temperature

The temperature validation for experimental data set 3 based on the generator water/steam pressure vessel saturation temperature is presented in Figure 9.4. The numerical model predicts a mean carbon internal temperature approximately 6°C greater than the experimental value at the end of the heating half-cycle. During the cooling half-cycle, rather than the numerical model under predicting the carbon temperature as seen in the previous cases, the numerical model predicts a carbon temperature approximately 6°C greater than the experimental value at the end of the cooling half-cycle. However, the general shape of the numerical and experimental temperature curves are in good agreement.

All of the numerically predicted temperature curves presented in Figures 9.2/3/4 have similar overall profiles compared to the temperature data obtained experimentally suggesting that the numerical model is valid for evaluating the temperature performance of the carbon-aluminium laminate over the range of input driving temperatures investigated. The discrepancies in the numerical and experimental temperatures highlight the difficulty involved in assigning constant external heat transfer coefficients during heating and cooling

within the model to physical processes which are considerably more complex. This is particularly true during the generator cooling phase where the physical processes taking place within the water/steam pressure vessel are not fully understood.

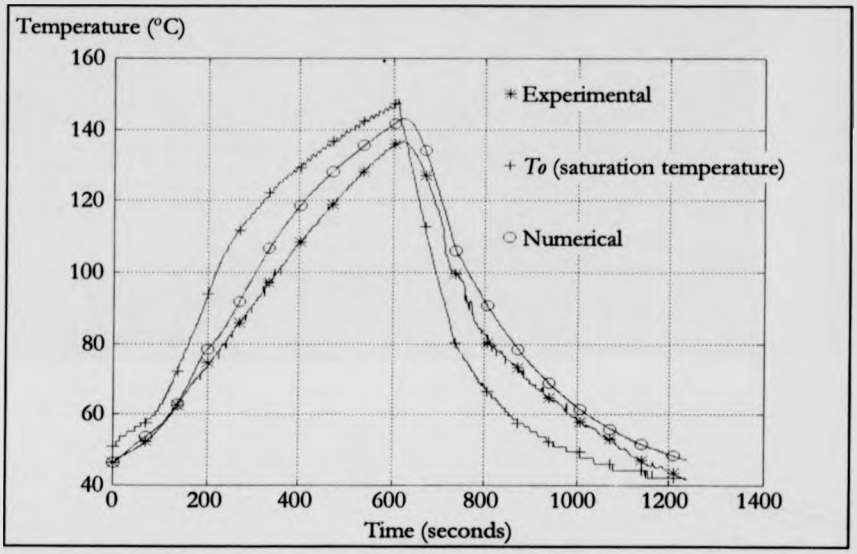

Figure 9.4: Experimental Data Set 3 - Temperature Validation Based on Generator Water/Steam Saturation Driving Temperature

9.2.2 Generator Pressure Validation

The pressure validation for experimental data set 1 based on the generator water/steam pressure vessel thermocouple driving temperature is presented in Figure 9.5. The initial validation run was carried out with an external heat transfer coefficient during heating of 1000 $W\,m^{-2}K^{-1}$ and an external heat transfer coefficient during cooling of 500 $W\,m^{-2}K^{-1}$. The numerical model isobaric boundary conditions were determined by evaluating the median experimental pressure value for the isobaric desorption phase during the heating half-cycle and the isobaric adsorption phase during the cooling half-cycle.

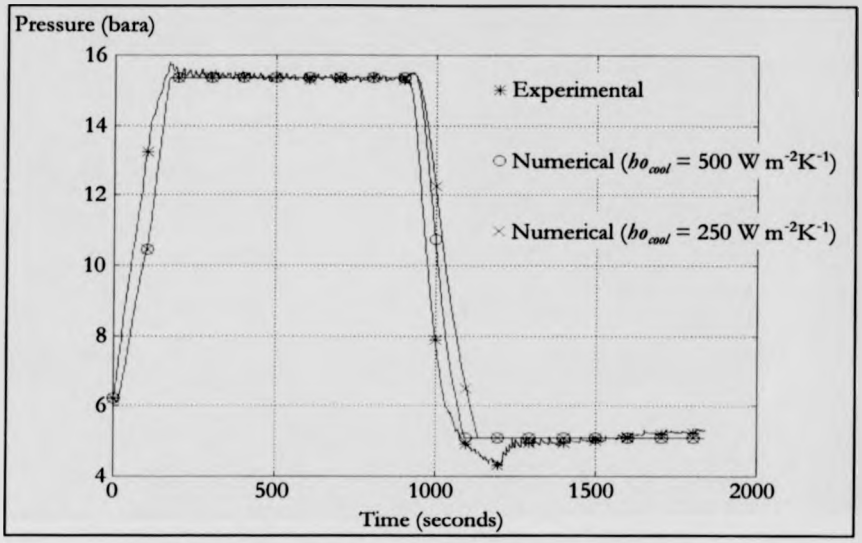

Figure 9.5: Experimental Data Set 1 - Pressure Validation Based on Generator Pressure Vessel External Thermocouple Driving Temperature

During the heating half cycle the rate of pressure rise within the laminate predicted by the numerical model compares well with that seen experimentally. However, the numerical data during this bed pressurisation process lags the experimental data in time by approximately 40 seconds. Hence, during this initial laminate pressurisation process the pressure predicted by the numerical model is approximately 2.5 bar less than that seen experimentally at the same point in time. The numerical model requires approximately 15 seconds longer to reach the condensing pressure than experimental laminate. There is obviously a good correlation at the condensing pressure between the numerical model and the experimental data as the model isobaric condition is obtained directly from the median experimental pressure value. The slight "bump" in the numerical pressure at the end of the isobaric desorption process is due to the model switching from an isobaric boundary condition to an isosteric boundary condition between the heating and cooling half-cycles. Hence, any heat conducted into the carbon from the stainless steel shell after the cycle change-over from heating to cooling will result in a slight increase in the predicted pressure while the

mean concentration is kept constant. During the cooling half cycle the rate of pressure reduction within the laminate predicted by the numerical model again compares well with that seen experimentally. A time lag of approximately 40 seconds is still apparent between the numerical and experimental results. The numerically predicted pressure is 2.5 bar greater than the experimental pressure at 1000 seconds. The numerical model requires approximately 10 seconds longer to reach the evaporating pressure than experimental laminate. The numerical results during the cooling half-cycle with a reduced external heat transfer coefficient of 250 $W\,m^{-2}K^{-1}$ indicate that the time lag between the numerical and experimental results essentially doubles to approximately 80 seconds and gives a numerical pressure discrepancy of 4.2 bar at 1000 seconds. With the reduced external heat transfer coefficient the numerical model requires approximately 50 seconds longer to reach the evaporating pressure than the experimental laminate.

The pressure validation for experimental data set 1 based on the generator water/steam pressure vessel saturation temperature is presented in Figure 9.6. During the heating half cycle the rate of pressure rise within the laminate predicted by the numerical model compares extremely well with that seen experimentally. Over the first 70 seconds of the heating half-cycle the numerical and experimental results are superimposed on one another. However, the numerical model still requires approximately 15 seconds longer to reach the condensing pressure than the experimental laminate. During the cooling half cycle the rate of pressure reduction within the laminate predicted by the numerical model again compares well with that seen experimentally. There is a time lag of approximately 20 seconds between the numerical and experimental results during this pressure reduction process. The numerically predicted pressure during this cooling phase is 1.4 bar greater than the experimental pressure at 1000 seconds. However, the numerical model reaches the evaporating pressure at the same point in time as the experimental laminate.

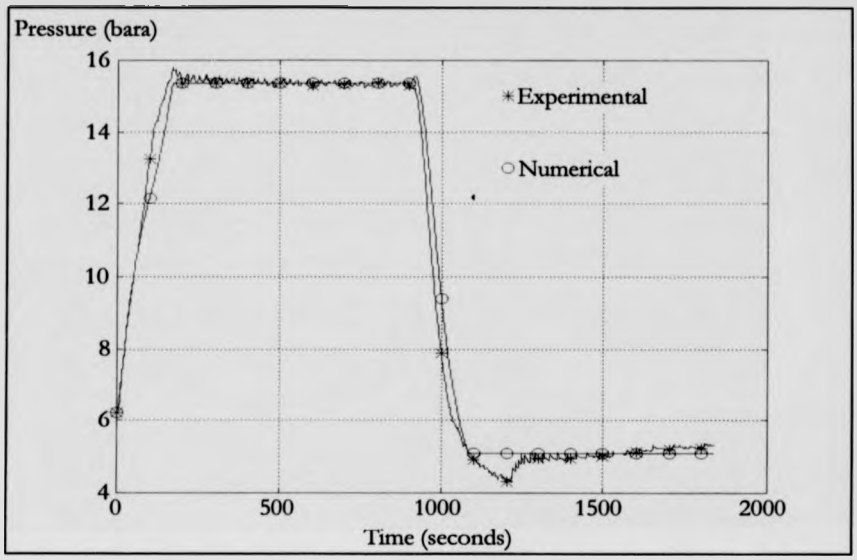

Figure 9.6: Experimental Data Set 1 - Pressure Validation Based on Generator Water/Steam Saturation Driving Temperature

During both the heating half-cycle and the cooling half-cycle the numerical results obtained using the saturation temperature (presented in Figure 9.6) give a better fit to the experimental data than the results obtained using the pressure vessel thermocouple (presented in Figure 9.5).

The pressure validation for experimental data set 2 based on the generator water/steam pressure vessel saturation temperature is presented in Figure 9.7. There is a large discrepancy between the numerical and experimental results during the laminate pressurisation process. The numerical results lag the experimental results in time during the laminate pressurisation process by approximately 90 seconds over the 8–10 bara pressure range. The numerical model requires twice as long as the experimental results to reach a pressure of 9 bara. The numerically predicted pressure during this heating phase is 3.2 bar less than the experimental pressure at 100 seconds. However, the numerical model reaches the condensing pressure at the same point in time as the experimental laminate. During the cooling half cycle the rate of pressure reduction within the laminate predicted by the

numerical model is similar to that observed experimentally. There is a time lag of approximately 50 seconds between the numerical and experimental results during this generator pressure reduction process. The numerically predicted pressure for this cooling phase is approximately 4.9 bar greater than the experimental pressure at 1000 seconds.

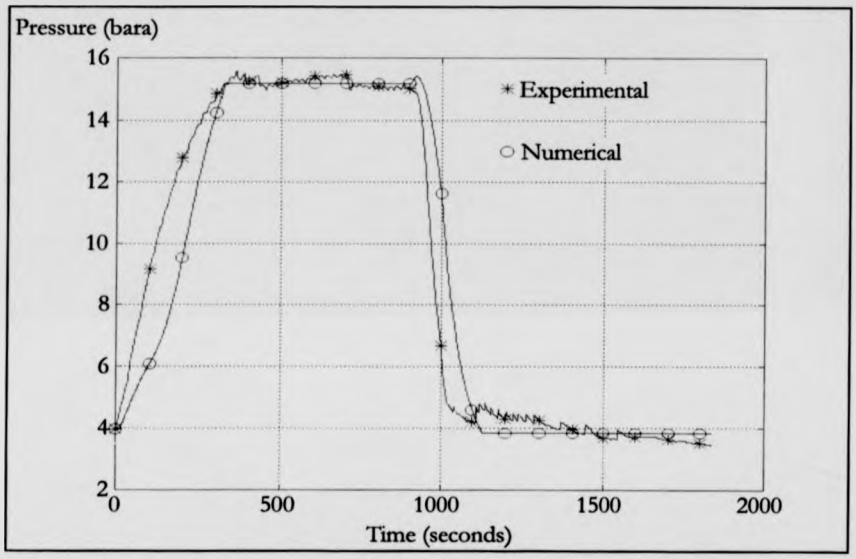

Figure 9.7: Experimental Data Set 2 - Pressure Validation Based on Generator Water/Steam Saturation Driving Temperature

The pressure validation for experimental data set 3 based on the generator water/steam pressure vessel saturation temperature is presented in Figure 9.8. The rate of pressure rise predicted by the numerical model is very similar to that observed experimentally. During the laminate pressurisation process the numerical results lag the experimental results in time by approximately 45 seconds. The numerically predicted pressure during this heating phase is approximately 2.1 bar less than the experimental pressure at 100 seconds. The numerical model requires approximately 30 seconds longer to reach the condensing pressure than experimental laminate. During the cooling half cycle the rate of pressure reduction within the laminate predicted by the numerical model is also similar to that observed

experimentally. There is a time lag of approximately 30 seconds between the numerical and experimental results during this generator pressure reduction process. The numerically predicted pressure for this cooling phase is approximately 2.4 bar greater than the experimental pressure at 700 seconds. The numerical model requires approximately 20 seconds longer to reach the evaporating pressure than experimental laminate.

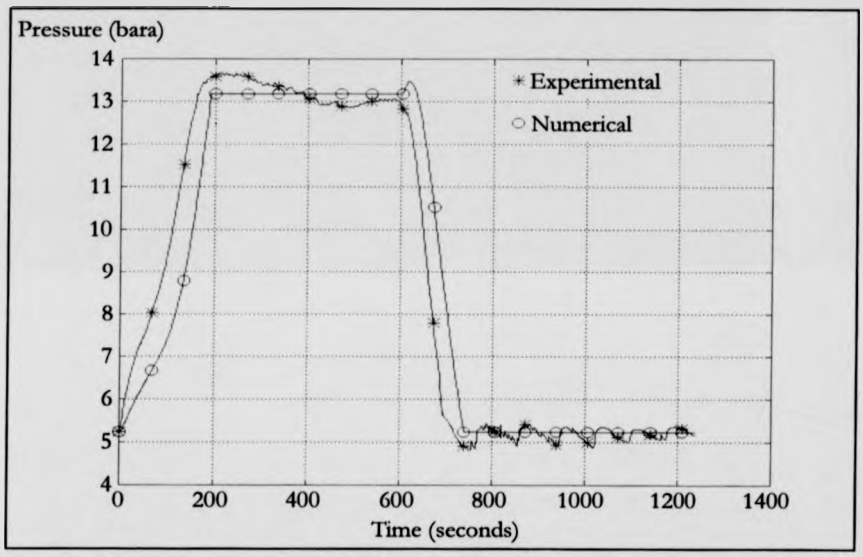

Figure 9.8: Experimental Data Set 3 - Pressure Validation Based on Generator Water/Steam Saturation Driving Temperature

Overall the numerical model has predicted the rate of pressure change adequately for both the heating and cooling half-cycles but there are time lags inherent in the numerical pressure response which lead to large discrepancies between the numerical and experimental results. All of the numerically predicted pressure curves presented in Figures 9.6/7/8 have similar overall profiles compared to the pressure data obtained experimentally. This suggests that the numerical model is valid for evaluating the global pressure performance of the carbon-aluminium laminate although time lags may limit the accuracy of the instantaneous pressure values calculated.

9.2.3 Generator Concentration Validation

The concentration validation for experimental data set 1 based on the generator water/steam pressure vessel thermocouple driving temperature is presented in Figure 9.9.

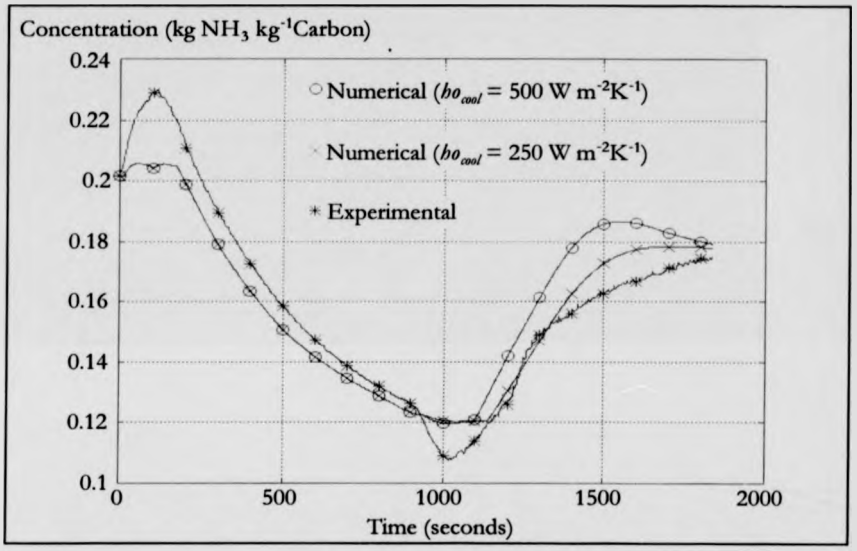

Figure 9.9: Experimental Data Set 1 - Concentration Validation Based on Generator Pressure Vessel External Thermocouple Driving Temperature

The initial validation run was carried out with an external heat transfer coefficient during heating of 1000 W $m^{-2}K^{-1}$ and an external heat transfer coefficient during cooling of 500 W $m^{-2}K^{-1}$. The numerical concentration presented is the mean value for the internal carbon nodes of the unit cell rather than the mean value for all the carbon nodes in the unit cell. Hence, during the isosteric cycle processes where the total mean concentration remains constant the concentration calculated by the numerical model for the internal nodes is still able to vary. Since the concentration is a function of the laminate temperature and ammonia saturation pressure the same discrepancies noted in the previous figures between the numerical and experimental data will be apparent. At the beginning of the heating half-cycle the numerical concentration does not increase in the same way as that determined

from experimental data, as ammonia is desorbed from the warmer outer part of the laminate and re-adsorbed in the cooler regions at the centre the laminate. During the remainder of the heating half cycle the rate of concentration decrease within the laminate predicted by the numerical model compares well with that seen experimentally. At the beginning of the cooling half-cycle the numerical concentration does not decrease in the same way as that determined from experimental data, as ammonia is desorbed from the warmer regions at the centre the laminate and re-adsorbed in the cooler outer part of the laminate. The numerical concentration determined for the cooling half-cycle does not follow the same profile as the experimental concentration data. The numerical concentration reaches a maximum value during cooling at a time of 1535 seconds and then starts to decrease again which appears to be physically unrealistic. The numerical data during the cooling half-cycle with an external heat transfer coefficient of 250 $W\,m^{-2}K^{-1}$ results in an improved fit between the numerical and experimental data. However, the numerical data still does not follow the same profile as the experimental data.

The concentration validation for experimental data set 1 based on the generator water/steam pressure vessel saturation temperature is presented in Figure 9.10. At the beginning of both the heating and cooling half-cycles the numerical concentration does not increase or decrease respectively in the same manner as the experimental data. However, the numerical concentration profiles calculated for both heating and cooling half-cycles correlate well with the experimental results. During the heating half-cycle desorption phase the numerical concentration is approximately 0.010 less than the experimental value while during the cooling half-cycle adsorption phase the numerical concentration is greater than the experimental value reaching a value of approximately 0.013 greater than the experimental concentration at the end of the cooling half-cycle.

For the cooling half-cycle the numerical results obtained using the saturation temperature (presented in Figure 9.10) give a better fit to the experimental data than the results obtained using the pressure vessel thermocouple (presented in Figure 9.9).

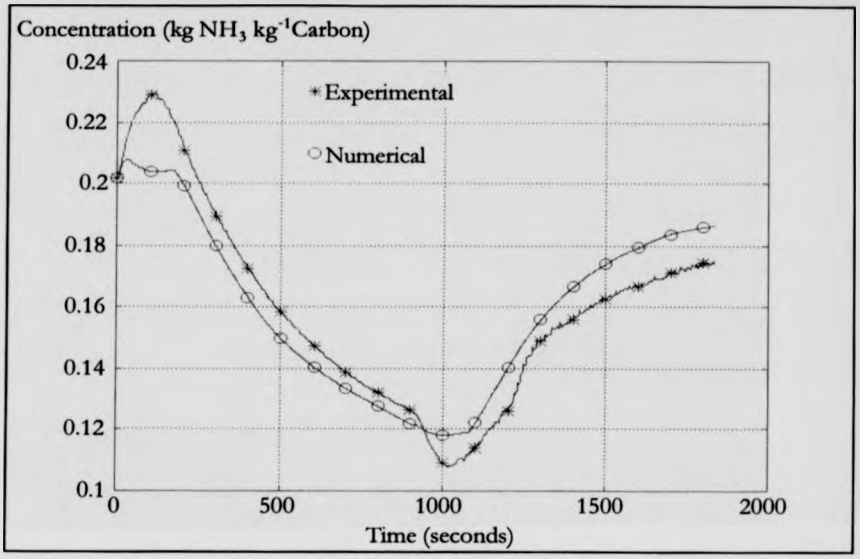

Figure 9.10: Experimental Data Set 1 - Concentration Validation Based on Generator Water/Steam Saturation Driving Temperature

The concentration validation for experimental data set 2 based on the generator water/steam pressure vessel saturation temperature is presented in Figure 9.11. At the beginning of the heating half-cycle the experimental concentration peaks at 0.20 while the numerical concentration remains virtually constant at a value of 0.17. During the heating half-cycle desorption phase the numerical concentration profile is approximately 0.010 less than the experimental value. At the start of the cooling half-cycle the numerical concentration remains virtually constant while the experimental value falls to almost 0.10. The two concentration curves then follow each other closely with the numerical concentration reaching a value of approximately 0.012 greater than the experimental concentration at the end of the cooling half-cycle.

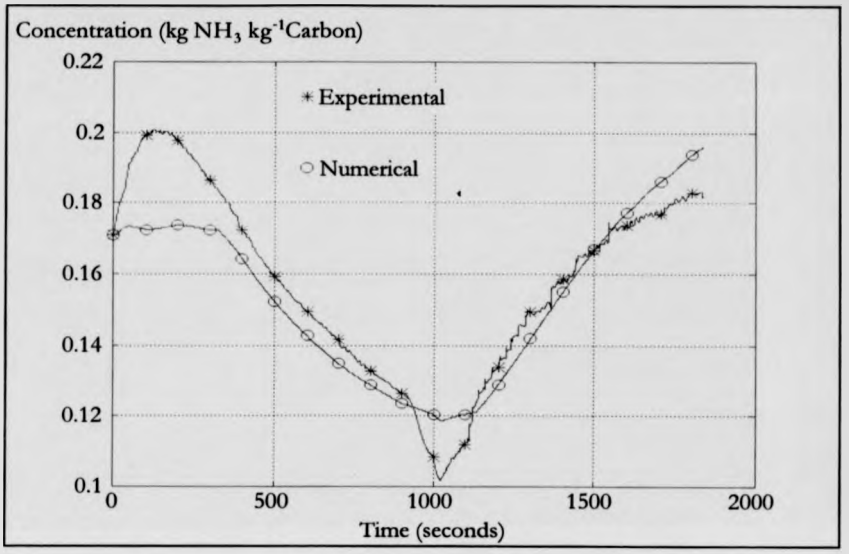

Figure 9.11: Experimental Data Set 2 - Concentration Validation Based on Generator Water/Steam Saturation Driving Temperature

The concentration validation for experimental data set 3 based on the generator water/steam pressure vessel saturation temperature is presented in Figure 9.12. At the beginning of the heating half-cycle the experimental concentration peaks at 0.23 while the numerical concentration remains virtually constant at a value of 0.20. During the heating half-cycle desorption phase the numerical concentration is approximately 0.016 less than the experimental. At the start of the cooling half-cycle the numerical concentration remains virtually constant while the experimental value falls to slightly less than 0.08. The two concentration curves then follow each other closely with the numerical concentration reaching a value of approximately 0.015 less than the experimental concentration at the end of the cooling half-cycle. The numerical concentration remains lower than the experimental for the complete thermodynamic cycle. This is consistent with the numerical temperature which remains greater than the experimental for the complete thermodynamic cycle, as highlighted in Figure 9.4.

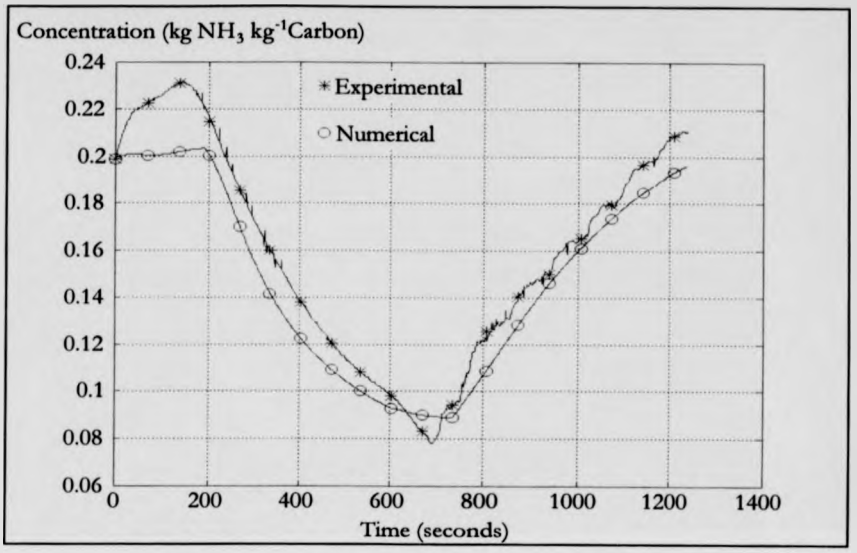

Figure 9.12: Experimental Data Set 3 - Concentration Validation Based on Generator Water/Steam Saturation Driving Temperature

All of the numerically predicted concentration curves presented in Figures 9.10/11/12 have similar overall profiles compared to the concentration data obtained experimentally. However, the peaks and troughs in the experimental concentration profiles at the beginning of the heating and cooling half-cycles are not resolved by the numerical model. This may be due to limiting assumptions within the model or unknown thermal factors acting on the thermocouple at the half-cycle change over times.

9.3 Experimental and Numerical Performance

The experimental and numerical performance results including the heating power, cooling power, specific cooling power and cooling coefficient of performance for both the carbon adsorbent only and the complete carbon-aluminium laminate are presented in Table 9.1. The numerical results are based on the data presented in Section 9.2 for the numerical model applying the water/steam pressure vessel saturation temperature as the model

"driving" temperature. The results listed for experimental data set 3 are identical to those presented in Table 8.1.

Data	Parameter	$P_{heating,car}$ (W)	$P_{heating,lam}$ (W)	$P_{cooling}$ (W)	$P_{sp,cooling}$ (W kg^{-1}car)	*COP*
Data Set 1	Experimental	310	367	86	54	0.23
	Numerical (T_{sat})	213	250	55	38	0.22
	Ratio (Exp/Num)	1.46	1.47	1.56	1.42	1.05
Data Set 2	Experimental	309	367	109	69	0.30
	Numerical (T_{sat})	177	215	62	44	0.29
	Ratio (Exp/Num)	1.75	1.71	1.76	1.57	1.03
Data Set 3	Experimental	550	656	229	144	0.35
	Numerical (T_{sat})	409	479	136	95	0.28
	Ratio (Exp/Num)	1.34	1.37	1.68	1.52	1.25

Table 9.1: Experimental and Numerical Performance Results

The heating powers predicted by the numerical model are less than the heating powers calculated from experimental data for each of the three data sets. The experimental heating power is calculated by integrating the thermal mass of the carbon only or the complete laminate between minimum and maximum heating temperature limits assuming the same temperature change occurs throughout the carbon or laminate. The numerical heating power is calculated by summing the heat inputs across a defined boundary into the laminate unit cell or carbon only throughout the heating half-cycle duration. The numerical model uses a total mass of carbon in the laminate, based on volume and density, of 1.433 kg. The total mass of carbon in the laminate determined experimentally is 1.586 kg. Hence there is a 10% discrepancy in carbon mass between the experimental and the numerical. A combination of these factors explains the difference between the numerical and experimental heating powers calculated.

The cooling powers and specific cooling powers predicted by the numerical model are also less than the cooling powers calculated from experimental data for each of the three data sets. The experimental and numerical cooling powers are both calculated in the same way, based on concentration change, carbon mass and enthalpy of vaporisation. The

numerical model determines the change in the mean concentration between the start and finish of the cooling half-cycle. For the isosteric cycle processes the mean concentration remains constant. The experimental concentration change is based on the temperature measured by the thermocouple at the centre of the carbon and therefore assumes that all of the carbon is at the thermocouple temperature. The experimental concentration curves indicate a peak in the concentration at the start of the heating half cycle and a trough in the concentration at the start of the cooling half-cycle. These peaks and troughs serve to accentuate the observed concentration swing. The temperature and pressure validation curves indicate a good correlation between the experimental and numerical data. However, the concentration is very sensitive to small temperature and pressure variations and this may account for the larger concentration swing indicated in the experimental data. The increased concentration swing and greater mass of carbon results in a larger calculated experimental cooling power. The percentage difference between the numerical and experimental specific cooling powers is less than the percentage difference between the experimental and numerical cooling powers since the 10% mass difference is no longer a consideration and the specific cooling powers will therefore be primarily a function of the concentration swing.

The experimental and numerical COP values for data sets 1 and 2 agree well with each other giving experimental/numerical ratios close to unity. This may be attributed to similar differences between the experimental and numerical results for both the heating power and the cooling power. Hence, if the ratio of the cooling power to heating power remains constant for both the experimental and numerical results the COP values will be the same. There is a larger difference between the experimental and numerical COP values for data set 3 with a consequent increase in the experimental/numerical ratio to 1.25.

9.4 Conclusions

The numerical model was validated by comparison with experimental temperature, pressure, concentration and performance data. For the validation results presented, in general the numerical model demonstrates a good correlation with the experimental data.

The numerical model has been validated for simulation and prediction of the present generator behaviour utilising an external heat transfer coefficient during heating of 1000 W $m^{-2}K^{-1}$ and an external heat transfer coefficient during cooling of 500 W $m^{-2}K^{-1}$. However, the performance data with respect to heating power, cooling power, specific cooling power and coefficient of performance is in general lower for the numerical model than the values calculated from the experimental data. Therefore, the experimental data leads to a specific cooling power of 144 W kg^{-1} and a total cooling power for the rig of 458 W while the numerical model gives a specific cooling power of 95 W kg^{-1} and a total cooling power for the rig of only 272 W. The difference in specific cooling power may be accounted for by referring to the experimental and numerical Clausius-Clapeyron diagrams. For the experimental case the Clausius-Clapeyron diagram, presented in Figure 8.7, has smooth curved transitions between cycle processes whereas the numerical Clausius-Clapeyron diagram (thermodynamic cycle), presented in Figure 3.2, has sudden and definite transitions between cycle processes. Hence, for the experimental case the concentration "overshoots" at the end of the heating and cooling half-cycles leading to a greater change in mean concentration and a greater calculated experimental specific cooling power. The difference in cooling power may then be directly attributed to the 10% difference between the experimental and numerical carbon masses, with a numerical carbon mass (based on unit cell volume and measured carbon density) of 1.433 kg and an experimental carbon mass (determined empirically) of 1.586 kg.

Chapter 10

Numerical Performance Prediction

10.1 Introduction

In order to improve the performance of the present experimental rig, particularly with respect to specific cooling power, the current water loop for heating and cooling will be replaced. During heating steam will be condensed on the outer surface of the laminate shell. It is hoped that this steam will be provided at a constant and stable temperature rather than varying in a saw-tooth manner with time as is presently the case. During cooling a series of heat pipes containing pentane will be utilised in order to reduce the thermal mass of the generator and improve the rate of heat transfer.

The numerical model has been validated against the experimental data from the present version of the experimental rig which utilises water/steam for heating and cooling. The intention is now to apply the numerical model to the proposed future version of the experimental rig - heating with steam and cooling with pentane contained in a series of heat pipes. It must be stressed that this not to predict the performance of the present experimental rig but rather an idealised, and hopefully improved, future version of the experimental rig. The purpose in doing this is to apply the numerical model to confirm the effect of cycle time and generating temperature on performance. It is hoped that by simulating the effect of key parameters on an idealised version of the present experimental rig the possible future improvements in performance may be highlighted.

With this in mind, predictions have been carried out with the validated numerical model at generating temperatures of $To_{heat} = 150\,^{\circ}C$ and $To_{heat} = 200\,^{\circ}C$ during heating and

To_{cool} = 40 °C during cooling with total cycling times of 1800 seconds, 1200 seconds, 600 seconds and 300 seconds in order to assess the possible future performance of the carbon-aluminium laminate under the new heating and cooling regime. The heat transfer areas and thermal mass of stainless steel in the numerical model have been modified accordingly to represent the desired new heating and cooling arrangement. For the new heating and cooling design it is hoped that the heat transfer during the cooling phase will be comparable to the heat transfer in the heating phase. Hence, for the numerical predictions an external heat transfer coefficient of 1000 W $m^{-2}K^{-1}$ was selected for both the heating and cooling half-cycles. All of the predictions are based on an evaporating temperature, T_{evap} = 0 °C and a condensing temperature, T_{cond} = 40 °C.

10.2 Generator Heating and Cooling Predictions

10.2.1 Generator Temperature Prediction

The temperature prediction for a 15 minute half-cycle time is presented in Figure 10.1. For both the 150°C and 200°C generating temperatures the predicted internal carbon temperature rises rapidly during the heating half-cycle reaching a steady state value, in thermal equilibrium with the external driving temperature, after approximately 300 seconds. During the cooling half-cycle the predicted decrease in internal carbon temperature is almost as rapid reaching the external cooling temperature of 40°C approximately 400 seconds after the cycle change-over.

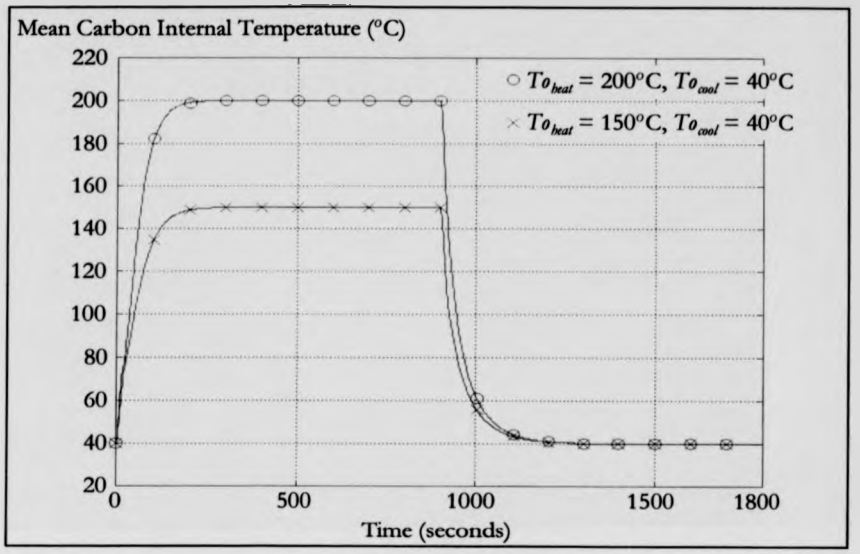

Figure 10.1: Generator Mean Carbon Internal Temperature - 15 Minute Half-Cycle Time

The temperature prediction for a 10 minute half-cycle time is presented in Figure 10.2. The heating and cooling rates are identical to those seen in Figure 10.1. For both the 150°C and 200°C generating temperatures the predicted internal carbon temperature reaches a steady state value, in thermal equilibrium with the external driving temperature, after approximately 300 seconds. In the same manner, for the external cooling temperature of 40°C the predicted internal carbon temperature reaches a steady state value, in thermal equilibrium with the external driving temperature, after approximately 400 seconds. A reduction in the half-cycle time will not have any effect on the cycle performance until it impinges on either the heating or cooling time for the predicted internal carbon temperature to reach a steady state value with the external temperature.

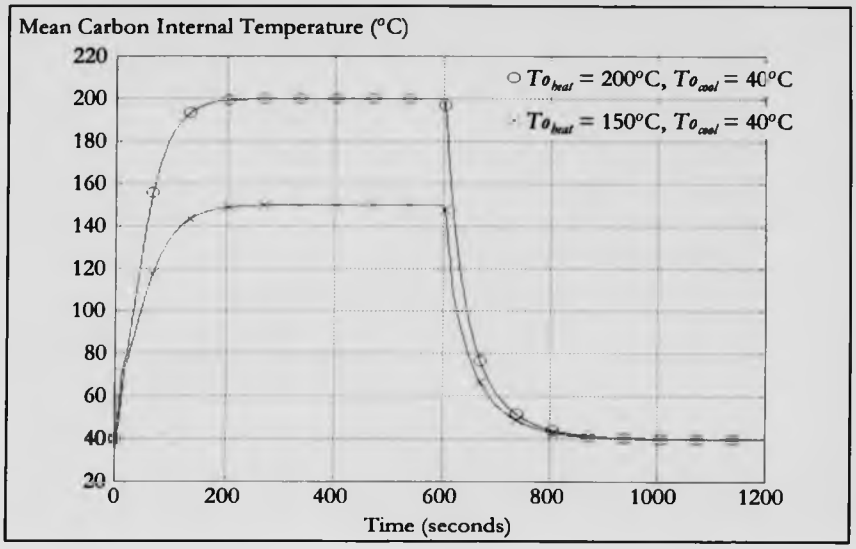

Figure 10.2: Generator Mean Carbon Internal Temperature - 10 Minute Half-Cycle Time

The temperature prediction for a 5 minute half-cycle time is presented in Figure 10.3. For both the 150°C and 200°C generating temperatures the predicted internal carbon temperature reaches a steady state value, in thermal equilibrium with the external driving temperature at the end of the heating half-cycle. However, for the external cooling temperature of 40°C the internal carbon temperature for both prediction cases fails to reach the steady state value at the end of the cooling half-cycle. The internal carbon temperature predicted for the 150°C generating temperature case at the end of the cooling half-cycle is 40.71°C. The internal carbon temperature predicted for the 200°C generating temperature case at the end of the cooling half-cycle is 40.93°C.

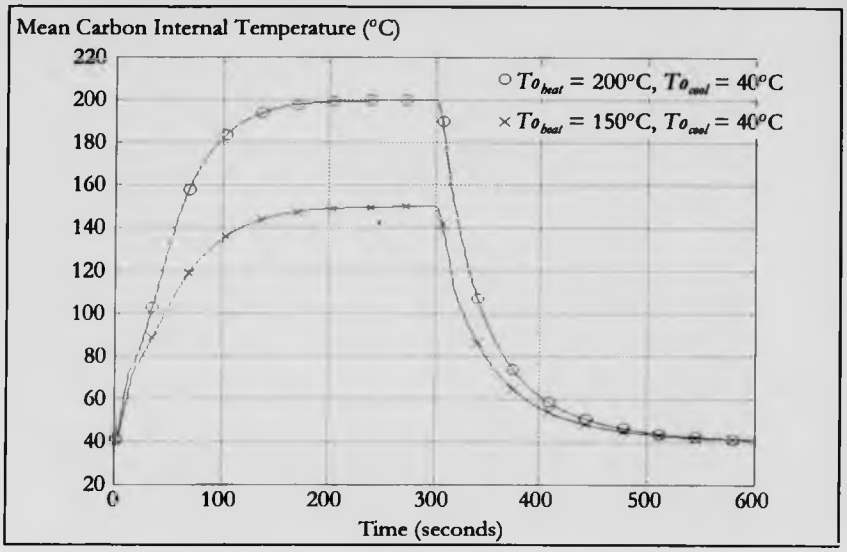

Figure 10.3: Generator Mean Carbon Internal Temperature - 5 Minute Half-Cycle Time

The temperature prediction for a 2½ minute half-cycle time is presented in Figure 10.4. Due to the short heating half-cycle time the internal carbon temperature for either case fails to reach the steady state value, in thermal equilibrium with the external driving temperature. The internal carbon temperature predicted for the 150°C generating temperature case at the end of the heating half-cycle is 145.99°C. The internal carbon temperature predicted for the 200°C generating temperature case at the end of the heating half-cycle is 196.39°C. For the external cooling temperature of 40°C the internal carbon temperature for both prediction cases also fails to reach the steady state value at the end of the cooling half-cycle. The internal carbon temperature predicted for the 150°C generating temperature case at the end of the cooling half-cycle is 46.91°C. The internal carbon temperature predicted for the 200°C generating temperature case at the end of the cooling half-cycle is 49.23°C.

Hence, the reduced half-cycle time has the effect of reducing the overall temperature swing experienced by the carbon during the thermodynamic cycle. However, the specific cooling power or coefficient of performance are better indicators of cycle performance than temperature swing alone.

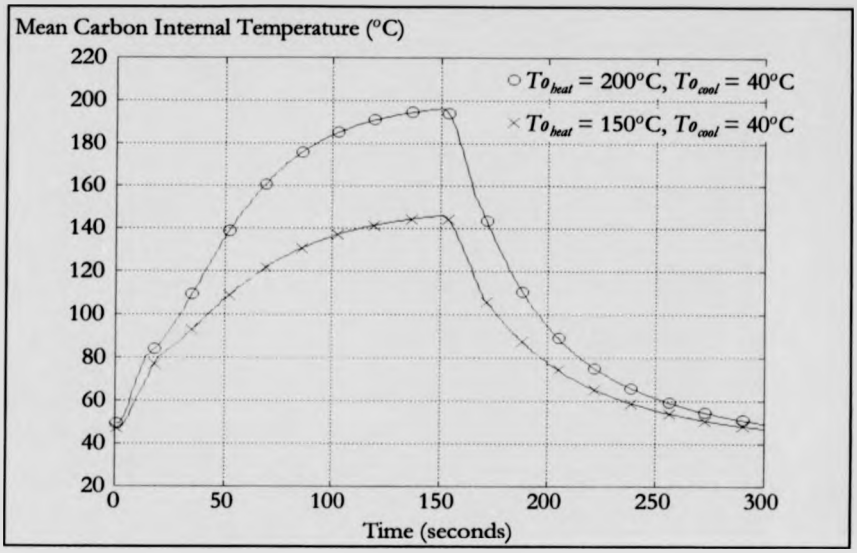

Figure 10.4: Generator Mean Carbon Internal Temperature - 2½ Minute Half-Cycle Time

10.2.2 Generator Pressure Prediction

The pressure prediction for a 15 minute half-cycle time is presented in Figure 10.5. For both the 150°C and 200°C generating temperatures the predicted generator pressure rises rapidly to the condensing pressure of 15.56 bara during the heating half-cycle and falls rapidly to the evaporating pressure of 4.29 bara during the cooling half-cycle. For the 150°C generating temperature case, the generator pressure reaches the condensing pressure 18 seconds after the start of the heating half-cycle and reaches the evaporating pressure 19 seconds after the start of the cooling half-cycle. For the 200°C generating temperature case, the generator pressure reaches the condensing pressure 12 seconds after the start of the heating half-cycle cycle and reaches the evaporating pressure 14 seconds after the start of the cooling half-cycle.

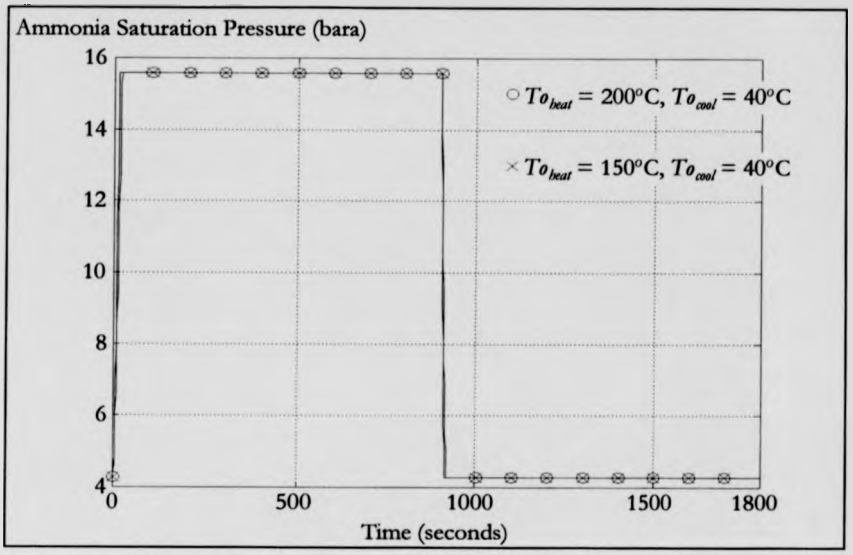

Figure 10.5: Generator Ammonia Saturation Pressure - 15 Minute Half-Cycle Time

The pressure prediction for a 10 minute half-cycle time is presented in Figure 10.6. For both the 150°C and 200°C generating temperatures the predicted generator pressure rises rapidly to the condensing pressure of 15.56 bara during the heating half-cycle and falls rapidly to the evaporating pressure of 4.29 bara during the cooling half-cycle. The times to reach the condensing pressure and the evaporating pressure for both prediction cases are identical to those seen for the previous case with a half-cycle time of 15 minutes.

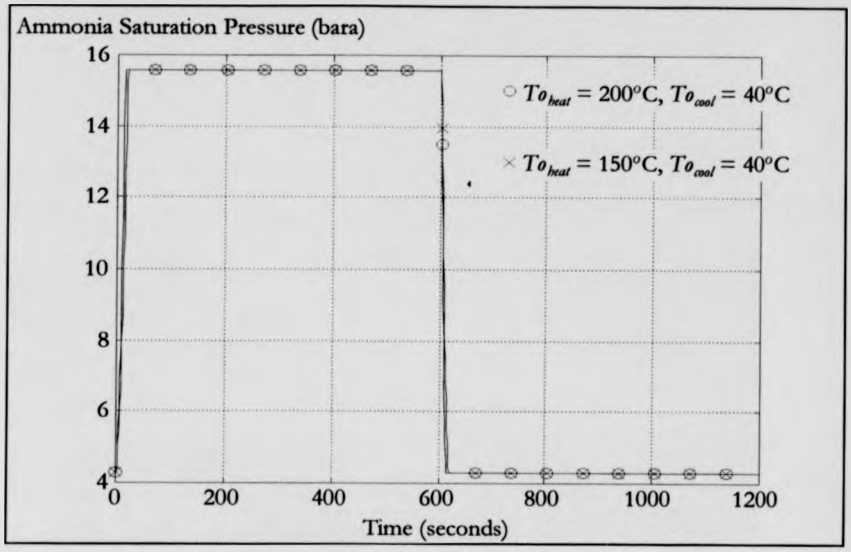

Figure 10.6: Generator Ammonia Saturation Pressure - 10 Minute Half-Cycle Time

The pressure prediction for a 5 minute half-cycle time is presented in Figure 10.7. For both the 150°C and 200°C generating temperatures the predicted generator pressure rises rapidly to the condensing pressure of 15.56 bara during the heating half-cycle and falls rapidly to the evaporating pressure of 4.29 bara during the cooling half-cycle. The times to reach the condensing pressure and the evaporating pressure for both prediction cases are identical (for numerical data written to file at one second intervals) to those seen for the previous cases with half-cycle times of 10 minutes and 15 minutes.

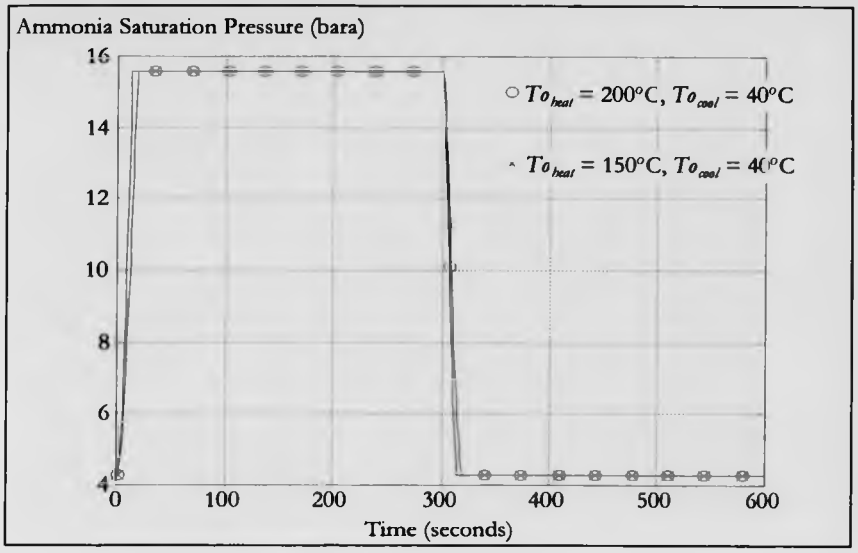

Figure 10.7: Generator Ammonia Saturation Pressure - 5 Minute Half-Cycle Time

The pressure prediction for a 2½ minute half-cycle time is presented in Figure 10.8. For both the 150°C and 200°C generating temperatures the predicted generator pressure rises rapidly to the condensing pressure of 15.56 bara during the heating half-cycle and falls rapidly to the evaporating pressure of 4.29 bara during the cooling half-cycle. For the 150°C generating temperature case, the generator pressure reaches the condensing pressure 19 seconds after the start of the heating half-cycle and reaches the evaporating pressure 20 seconds after the start of the cooling half-cycle. For the 200°C generating temperature case, the generator pressure reaches the condensing pressure 13 seconds after the start of the heating half-cycle cycle and reaches the evaporating pressure 14 seconds after the start of the cooling half-cycle.

Hence, reducing the half-cycle time from 15 minutes to 5 minutes has no apparent effect on the times required for the generator to reach the condensing pressure after the start of the heating half-cycle and to reach the evaporating pressure after the start of the cooling half-cycle. For the 150°C generating temperature case, reducing the half-cycle time to 2½ minutes has the effect of increasing the time required to reach the evaporating and

condensing pressures after the half-cycle change over points by one second. For the 200°C generating temperature case, reducing the half-cycle time to 2½ minutes has the effect of increasing the time required to reach the condensing pressure after the start of the heating half-cycle by one second. The time to reach the evaporating pressure after the start of the cooling half-cycle remains the same as for the 5 minute, 10 minute and 15 minute half-cycle times. Overall the rate of generator pressure increase and decrease appears to be essentially independent of the half-cycle time over the 2½ minute to 15 minute range. Increasing the generating pressure from 150°C to 200°C results in a 5–6 second decrease in the time required to reach the condensing or evaporating pressure after the half-cycle change over point.

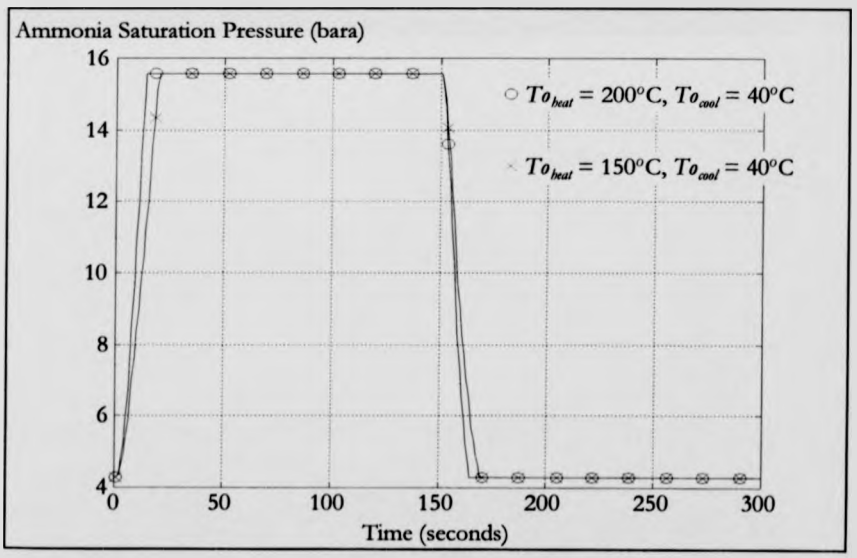

Figure 10.8: Generator Ammonia Saturation Pressure - 2½ Minute Half-Cycle Time

10.2.3 Generator Concentration Prediction

The mean internal concentration prediction for a 15 minute half-cycle time is presented in Figure 10.9. For the 150°C generating temperature case the concentration rises rapidly at the start of the heating half-cycle to a value of 0.232. The concentration then decreases to a

value of 0.092 approximately 300 seconds after the start of the heating half-cycle as ammonia is desorbed from the generator at constant pressure. At the start of the cooling half-cycle the mean internal concentration falls rapidly to a value of 0.077. The concentration then increases to a value of 0.199 approximately 400 seconds after the start of the cooling half-cycle as ammonia is adsorbed back into the generator at constant pressure. For the 200°C generating temperature case the concentration rises rapidly at the start of the heating half-cycle to a value of 0.238. The concentration then decreases to a value of 0.052 approximately 300 seconds after the start of the heating half-cycle as ammonia is desorbed from the generator at constant pressure. At the start of the cooling half-cycle the mean internal concentration falls rapidly to a value of 0.039. The concentration then increases to a value of 0.199 approximately 400 seconds after the start of the cooling half-cycle as ammonia is adsorbed back into the generator at constant pressure. The peaks and troughs in the concentration profile may be attributed to ammonia adsorption at the cooler internal nodes of the carbon-aluminium laminate at the start of the heating half-cycle and ammonia desorption from the warmer internal nodes of the carbon-aluminium laminate at the start of the cooling half-cycle, in both cases under conditions of constant total adsorbed ammonia mass within the generator.

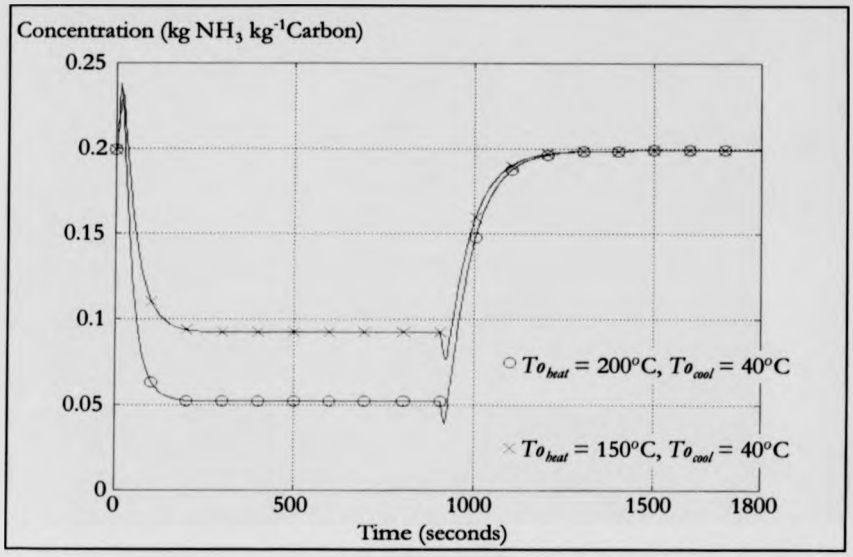

Figure 10.9: Generator Ammonia Concentration - 15 Minute Half-Cycle Time

The mean internal concentration prediction for a 10 minute half-cycle time is presented in Figure 10.10. For both the 150°C and 200°C generating temperature cases the concentration values and times required to reach the stated concentrations are identical to those seen in Figure 10.9. This is to be expected as the temperature and pressure ranges for the 10 minute and 15 minute half-cycle times were also found to be identical.

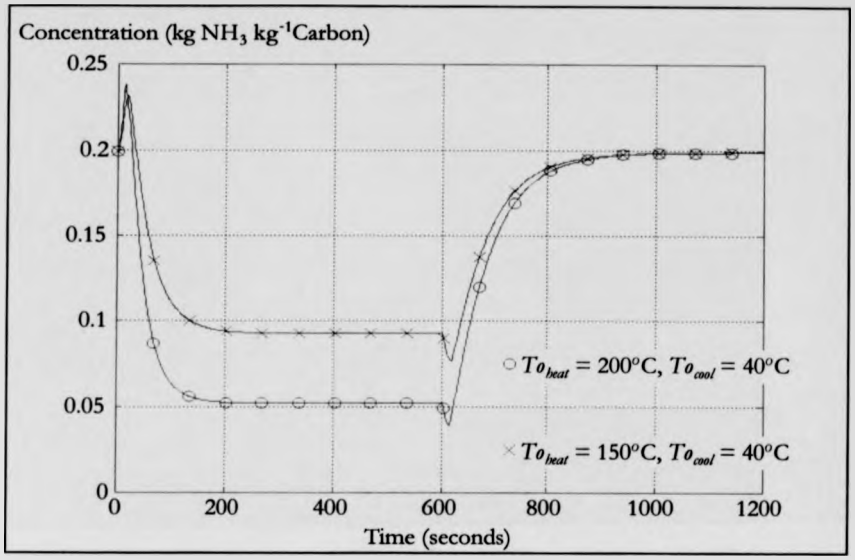

Figure 10.10: Generator Ammonia Concentration - 10 Minute Half-Cycle Time

The mean internal concentration prediction for a 5 minute half-cycle time is presented in Figure 10.11. For the 150°C generating temperature case the concentration rises rapidly at the start of the heating half-cycle to a value of 0.230. The concentration then decreases to a value of 0.092 at the end of the heating half-cycle as ammonia is desorbed from the generator at constant pressure. At the start of the cooling half-cycle the mean internal concentration falls rapidly to a value of 0.077. The concentration then increases to a value of 0.197 at the end of the cooling half-cycle as ammonia is adsorbed back into the generator at constant pressure. For the 200°C generating temperature case the concentration rises rapidly at the start of the heating half-cycle to a value of 0.235. The concentration then decreases to a value of 0.052 at the end of the heating half-cycle as ammonia is desorbed from the generator at constant pressure. At the start of the cooling half-cycle the mean internal concentration falls rapidly to a value of 0.039. The concentration then increases to a value of 0.196 at the end of the cooling half-cycle as ammonia is adsorbed back into the generator at constant pressure.

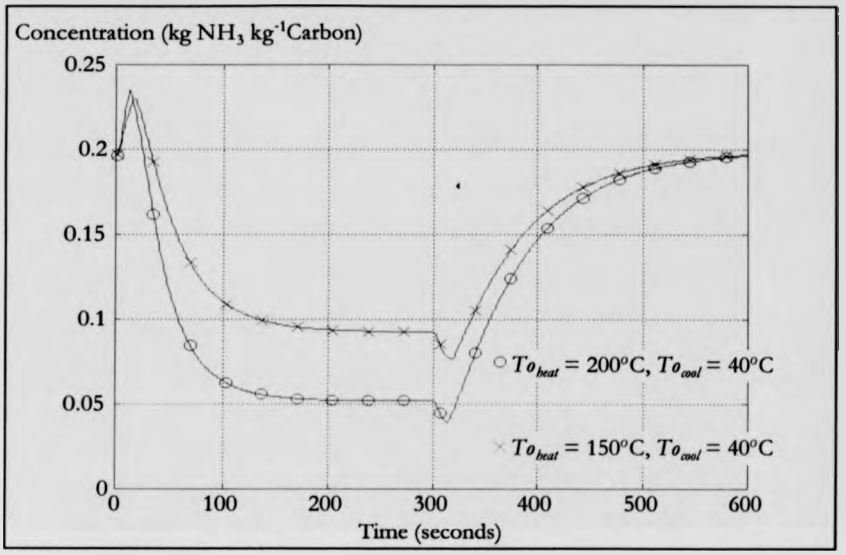

Figure 10.11: Generator Ammonia Concentration - 5 Minute Half-Cycle Time

The mean internal concentration prediction for a 2½ minute half-cycle time is presented in Figure 10.11. For the 150°C generating temperature case the concentration rises rapidly at the start of the heating half-cycle to a value of 0.214. The concentration then decreases to a value of 0.097 at the end of the heating half-cycle as ammonia is desorbed from the generator at constant pressure. At the start of the cooling half-cycle the mean internal concentration falls rapidly to a value of 0.080. The concentration then increases to a value of 0.180 at the end of the cooling half-cycle as ammonia is adsorbed back into the generator at constant pressure. For the 200°C generating temperature case the concentration rises rapidly at the start of the heating half-cycle to a value of 0.213. The concentration then decreases to a value of 0.054 at the end of the heating half-cycle as ammonia is desorbed from the generator at constant pressure. At the start of the cooling half-cycle the mean internal concentration falls rapidly to a value of 0.041. The concentration then increases to a value of 0.174 at the end of the cooling half-cycle as ammonia is adsorbed back into the generator at constant pressure.

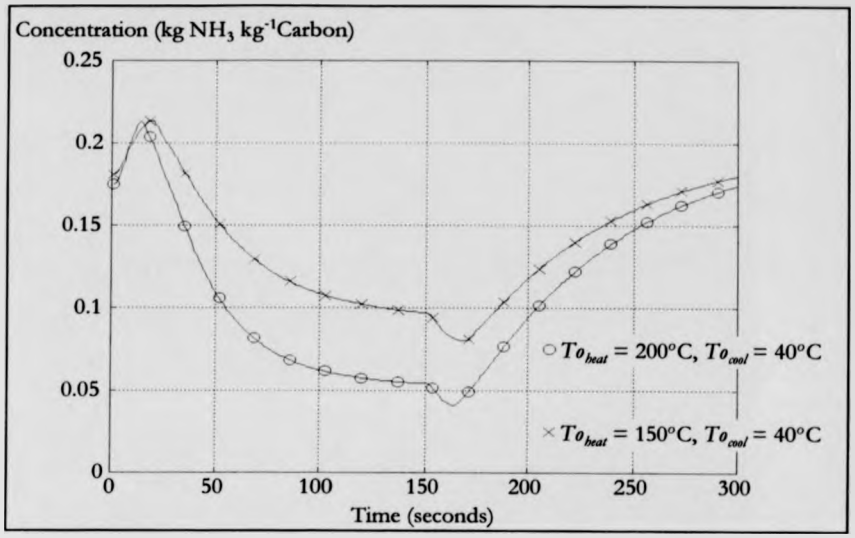

Figure 10.12: Generator Ammonia Concentration - 2½ Minute Half-Cycle Time

10.3 Generator Performance Prediction

The generator performance prediction results including heating power, cooling power, specific cooling power and cooling coefficient of performance for the carbon only and the complete carbon-aluminium laminate at generating temperatures of 150°C and 200°C and half-cycle times of 2½ minutes, 5 minutes, 10 minutes and 15 minutes are presented in Table 10.1.

Half-Cycle Time	To_{heat} (°C)	$P_{heating,car}$ (W)	$P_{heating,lam}$ (W)	$P_{cooling}$ (W)	$P_{sp,cooling}$ (W kg^{-1}car)	*COP*
2 ½ minutes	150	1616	2554	458	320	0.18
	200	2342	3715	651	455	0.18
5 minutes	150	901	1385	269	188	0.19
	200	1280	1984	372	260	0.19
10 minutes	150	455	698	137	95	0.20
	200	645	998	189	132	0.19
15 minutes	150	303	465	91	64	0.20
	200	430	665	126	88	0.19

Table 10.1: Generator Performance Prediction Results

The predicted heating power, cooling power and specific cooling power at 150°C and 200°C all increase as the half-cycle time decreases from 15 minutes to 2½ minutes. As the half-cycle time decreases the cooling coefficient of performance remains relatively constant. For a given half-cycle time, the heating power, cooling power and specific cooling power all increase from a generating temperature of 150°C to a generating temperature of 200°C. At the same half-cycle time and generating temperature the heating power required is greater for the complete laminate than it is for the carbon only due to the additional thermal mass provided by the aluminium discs and the stainless steel shell. Overall the results indicate than in order to achieve the greatest specific cooling power the cycling time should be as short as possible and the generating temperature as high as possible. For the present numerical predictions this suggests a system operating on a rapid cycling regime with a half cycle time of 150 seconds and an external driving temperature of 200°C. Under these conditions the numerical model predicts a specific cooling power per unit mass of carbon of 455 W kg^{-1}.

10.4 Conclusions

The performance of a modified future version of the current experimental rig was evaluated at elevated generating temperatures of 150°C and 200°C for total cycle times of 300 seconds, 600 seconds, 1200 seconds and 1800 seconds. These numerical prediction

results suggest that for a generating temperature of 200°C and a half-cycle time of 150 seconds the specific cooling power per unit mass of carbon for a future experimental rig could be increased to 455 W kg^{-1} with a COP of 0.18. This predicted specific cooling power approaches the value of 500 W kg^{-1} arrived at in the initial generator geometry numerical simulations but with a far more practicable half-cycle time. However, for a "real world" experimental case the specific cooling power will generally be less than that predicted numerically because of additional thermal masses and heat losses not accounted for in the numerical model. The specific cooling power value of 455 W kg^{-1} is still considerably lower than the desired target "holy grail" specific cooling power of 1 kW kg^{-1}. However, with a smaller diameter or thinner layer laminate, specific cooling powers approaching 1 kW kg^{-1} may still be attainable.

It is desirable to maximise the specific cooling power as far as possible so as to reduce the adsorbent inventory and containing vessel volume required for a given cooling power and therefore minimise capital costs. The importance of the COP is related to the cost of the heat input source. Therefore, for a developing country with a plentiful supply of solar heat or biofuel a low overall COP value need not be of such great importance.

Chapter 11

Conclusions

The main objective of the current research was to design, build and evaluate a rapid cycling heat driven adsorption cooling system, utilising a novel monolithic adsorbent material with enhanced effective thermal conductivity, suitable for refrigeration and ice production in developing countries.

Many of the previous adsorption cooling designs have employed granular adsorbent materials operating on a diurnal cycle. These systems require a large adsorbent inventory to provide a given cooling power and hence have a high overall capital cost. Additionally if only a single mass of adsorbent material is thermally cycled the cooling is intermittent.

The present research was conducted with a view to improving on previous designs and for eventual application in a developing country. The specific areas of interest during the current work were:

- Application of an adsorbent material with enhanced effective thermal conductivity
  (to increase the rate of heat transfer into and out of the adsorbent)

- Rapid cycling of the adsorbent material on a time-scale of minutes rather than hours/days
  (to increase the cooling power and specific cooling power)

- Utilisation of two adsorption generators operating 180^{o} out of phase
  (to provide semi-continuous rather than intermittent cooling)

An experimental rig has been constructed employing two monolithic carbon-aluminium laminate generators operating 180° out of phase so as to provide semi-continuous cooling. These generators have been operated under a rapid cycling regime down to a half-cycle time of 600 seconds giving a maximum specific cooling power of 144 W kg^{-1} and a cooling coefficient of performance of 0.35.

A numerical model based on a simple explicit finite differencing scheme has been validated for use in predicting the temperature, pressure and concentration performance of the experimental rig. Numerical prediction results confirm that higher generating temperatures and reduced cycling times yield greater specific cooling powers. Specific cooling powers approaching 0.5 kW kg^{-1} may be attainable with modified generators utilising heat pipes containing pentane rather than water boiling under low pressure during cooling.

The broad objectives of the research have been achieved although further work is still required to refine and build on the present system in order to make it better suited for direct application in a developing country.

Chapter 12

Recommendations

Although the present experimental rig has acceptable performance, it does have a number of shortcomings both in terms of the specific cooling power available and the suitability of the rig in its present form for use in developing countries.

On the present water loop design the number of valves required could be reduced by employing a spool valve to change between cycle heating, cycle cooling and regeneration states. This would greatly simplify the water loop construction and reduce the overall cost as well as delivering improving reliability with a reduced component count.

The water saturation pressure during the cooling half-cycle drops to approximately 0.1 bara resulting in the problem of air leakage into the system. This could be rectified by utilising a heat transfer fluid such as pentane which has a saturation pressure which is greater than atmospheric over the range of temperatures under consideration. However, this obviously poses an increased safety risk as pentane is highly flammable.

In the present system the thermal mass of the water heat transfer fluid leads to an increased sensible heat load during each cycle thus reducing cycle efficiency. Additionally, the thermal mass of the water results in a time lag which has a deleterious effect on cycling time and specific cooling power. A significant improvement in specific cooling power could be realised by replacing the present design for laminate heating and cooling with a series of heat pipes arranged along the length of the laminate. By utilising a system of heat pipes the heating and cooling heat transfer fluids may be completely separated. Heat pipes would also reduce the thermal mass cycled, thus reducing the cycling time required to achieve a given

concentration swing. In addition to this, with careful design the micro-leak problems experienced with the present water loop could be eradicated with a system employing heat pipes.

The present design utilises a combination of stainless steel and copper components to meet the requirements of tensile strength and corrosion resistance. For a developing country design many of these components, such as the generators, boiler and evaporator could be fabricated from suitably dimensioned mild steel to reduce cost. The external surfaces of the mild steel components could then be lacquered or painted to prevent surface oxidation. Cartridge heaters are used to provide the cooling load to the evaporator and heat input to the steam boiler. In a real world application the cooling load would obviously be related to the intended application, such as ice production. The value of the COP for the present system is such that for an electrical heat input it is not competitive compared to more efficient technologies such as the vapour compression cycle. However, for a developing country application the system could be adapted to harness alternative heat sources derived from biofuels or solar collectors. Hence, the performance of the system could be re-evaluated using a biofuel/solar driven boiler instead of the electrically powered one used at present.

The experimental rig consumes an overall volume of approximately 1.5 m^3 which is predominately empty space. Although when "installed in the field" rig size is in all probability not a major issue for a developing country, steps could be taken in the future to make the experimental rig more compact while maintaining or improving on the present levels of performance. The replacement of the ten pneumatically actuated ball valves used at present on the water loop with a compact spool valve design should help to reduce the overall rig volume required. For an idealised end design, the system could be reduced to a user optimised "black box", appropriate to the environment in which the system is being applied, where the end user is simply required to supply a heat input, a cooling load, a method of rejecting waste heat and an electrical input to power any control systems.

Bibliography

Adams, J.A., Rogers, D.F., Computer-Aided Heat Transfer Analysis, McGraw-Hill, New York, **1973**.

Adamson, A.W., A Textbook of Physical Chemistry, 2nd Edition, Academic Press, **1979**.

Aittomäki, A., Härkönen, M., Modelling of Zeolite/Methanol Adsorption Heat Pump Process, Heat Recovery Systems & CHP, Vol. 8, No. 5, pp. 475–482, **1988**.

Anderson, D.A., Tannehill, J.C., Pletcher, R.H., Computational Fluid Mechanics and Heat Transfer, 2nd Edition, McGraw-Hill, p. 119, **1984**.

Backstrom, M., The Theory of the Evaporator Working by Diffusion, Kylteknisk Tidskrift, pp. 22–26, **1954**.

Barakat, H.Z., Clark, J.A., On the Solution of the Diffusion Equations by Numerical Methods, Journal of Heat Transfer, pp. 421–427, November **1966**.

Bird, R.B., Stewart, W.E., Lightfoot, E.N., Transport Phenomena, John Wiley & Sons, New York, **1960**.

Bougard, J., Boussemaere, C., Thermodynamics of Solar Adsorption Refrigerating Machines, Faculté Polytechnique de Mons, Belgium, March **1987**.

Bougard, J., Thermodynamical and Technical Problems in Solar Adsorption Refrigeration, Science et Technique du Froid, Part 1, pp. 25–33, **1986**.

Boussemaere, C., Bougard, J., Solar Thermal Refrigerator for Vaccine Storage and Icemaking, Intersol '85, Proceedings of the 9th Biennial Congress of the I.S.E.S, Montreal, Canada, Pergammon Press, **1985**.

British Standards Institution: BS 1306, Specification for Copper and Copper Alloy Pressure Piping Systems, **1975**.

British Standards Institution: BS 3605, Austenitic Stainless Steel Pipes and Tubes for Pressure Purposes, Part 1, Specification for Seamless Tubes, **1991**.

British Standards Institution: BS 4504, Circular Flanges for Pipes, Valves and Fittings (PN Designated), Section 3.1, Specification for Steel Flanges, **1989**.

Burchell, T.D., Carbon Materials for Advanced Technologies, Pergamon, pp. 303–340, **1999**.

Cacciola, G., Cammarata, G., Fichera, A., Restuccia, G., Advances on Innovative Heat Exchangers in Adsorption Heat Pumps, Solid Sorption Refrigeration Symposium Paris, pp. 221–226, 18–20 November **1992**.

Cacciola, G., Restuccia, G., Progress on Adsorption Heat Pumps, Heat Recovery Systems & CHP, Vol. 14, No. 4, pp. 409–420, **1994**.

Case, J., Chilver, L., Ross, C.T.F., Strength of Materials and Structures: with an introduction to finite element methods, 3rd Edition, Edward Arnold, **1993**.

Çengel, Y.A., Boles, M.A., Thermodynamics: An Engineering Approach, McGraw-Hill, **1989**.

Critoph, R.E., An Ammonia Carbon Solar Refrigerator for Vaccine Cooling, Renewable Energy, 5, Part I, pp. 502–508, **1994**.

Critoph, R.E., Laboratory Testing of an Ammonia Carbon Solar Refrigerator, Proc. ISES Solar World Congress, Budapest, p. 6, August **1993**.

Critoph, R.E., Evaluation of Alternative Refrigerant-Adsorbent Pairs for Refrigeration Cycles, Applied Thermal Engineering, Vol. 16, No. 11, pp. 891–900, **1996**.

Critoph, R.E., Assessment of Chemical Surface Modifications on the Porosity of Active Carbons for Heat Pump Use, Phase I/II, Internal Report, University of Warwick, **1989**.

Critoph, R.E., Gong, F., A Rapid Cycling Ice Maker for use in Developing Countries, Proc. 2nd World Renewable Energy Congress, Reading, pub. Pergamon, pp. 708–714, **1992**.

Critoph, R.E., Tarbaghia, T.M., Solar Powered Platen-Munters (Electrolux) Refrigeration Cycle for Large Scale Refrigeration, Proc. Int. Conf. on Applications of Solar and Renewable Energy, Cairo, pub. ISES, p. 6, April **1992**.

Critoph, R.E., Vogel, R., Possible Adsorption Pairs for use in Solar Cooling, International Journal of Ambient Energy, Vol. 7, No. 4, pp. 183–190, October **1986**.

Critoph, R.E., Performance Limitations of Adsorption Cycles for Solar Cooling, Solar Energy, Vol. 41, No. 1, pp. 21–31, **1988**.

Critoph, R.E., Turner, L.H., Performance of Ammonia-Activated Carbon and Ammonia-Zeolite Heat Pump Adsorption Cycles, Proceedings of Conference: Pompes a Chaleur Chimiques de Hautes Performances, Perpignan (publ. Lavoisier), pp. 202–211, **1988**.

Critoph, R.E., Refrigeration in Developing Countries - The Renewable Options, 1st World Renewable Energy Conference, Reading, UK, **1990**.

Critoph, R.E., A Forced Convection Regenerative Cycle Using the Carbon-Ammonia Pair, Solid Sorption Refrigeration Symposium Paris, pp. 80–85, 18–20 November **1992**.

Critoph, R.E., Forced Convection Enhancement of Adsorption Cycles, Heat Recovery Systems & CHP, Vol. 14, No. 4, pp. 343–350, **1994**.

Critoph, R.E., "Towards One Tonne Per Day Solar Ice Maker", Proc. IVth World Renewable Energy Congress, Denver (USA), pp. 626–631, **1996**.

Critoph, R.E., Tamainot-Telto, Z., Davies, G.N.L., Design of an Adsorption Generator Utilising a Novel Carbon-Aluminium Laminate, Proc. HPC Int. Conf. Nottingham (UK), pp. 349–358, **1997**.

Critoph, R.E., Tamainot-Telto, Z., Davies, G.N.L., The Use of Monolithic Carbon-Aluminium Laminates in the Adsorption Refrigeration Generators to Enhance the Effective Conductivity and Power Density, Proc. FOA6 Int. Conf., Giens (France), **1998**.

Critoph, R.E., Rapid Cycling Solar/Biomass Powered Adsorption Refrigeration System, Renewable Energy, Vol. 16, pp.673–678, **1999**.

Critoph, R.E., Tamainot-Telto, Z., Davies, G.N.L., Adsorption Refrigerator Using a Monolithic Carbon-Aluminium Laminate Adsorbent and Ammonia Refrigerant, Proc. International Sorption Heat Pump Conference, Munich (Germany), pp. 349–353, **1999**.

Croft, D.R., Lilley, D.G., Heat Transfer Calculations Using Finite Difference Equations, Applied Science Publishers Ltd., London, **1977**.

Croft, D.R., Stone, J.A.R, Heat Transfer Calculations Using Finite Difference Equations, PAVIC Publications, **1989**.

Douss, N., Meunier, F., Experimental Study of Cascading Adsorption Cycles, Chem. Eng. Sci., Vol. 44, pp. 225–235, **1989**.

Douss, N., Meunier, F., Effect of Operating Temperatures on the Coefficent of Performance of Active Carbon-Methanol Systems, Heat Recovery Systems & CHP, Vol. 8, No. 5, pp. 383–392, **1988**.

Douss, N., Meunier, F.E., Sun, L., Predictive Model and Experimental Results for a Two-Adsorber Solid Adsorption Heat Pump, Ind. Eng. Chem. Res., Vol. 27, No. 2, pp. 310–316, **1988**.

Dubinin, M.M., Astakhov, V.A., Adv. Chem. Ser. 102, 69, **1970**.

Dubinin, M.M., Radushkevich, L.V., Equation of the Characteristic Curve of Activated Charcoal, Doklady Akad Nauk S.S.S.R, Vol. 55, pp. 327–329, **1947**.

Dusinberre, G.M., Heat-Transfer Calculations by Finite Differences, International Textbook Company, **1961**.

Farber, E.A., Design and Performance of a Compact Solar Refrigeration System, International Solar Energy Conference, Paper No. 6158, **1970**.

Fried, V., Hameka, H.F., Blukis, U., Physical Chemistry, Macmillan, **1977**.

Gere, J.M., Timoshenko, S.P., Mechanics of Materials, 3rd SI Edition, Chapman & Hall, **1991**.

Grenier, Ph., Guilleminot, J.J., Meunier, F., Pons, M., Solar Powered Solid Adsorption Cold Store, Journal of Solar Energy Engineering, Vol. 110, pp. 192–197, August **1988**.

Groll, M., Solid Sorption Machines for CFC-Free Generation of Heat and Cold (An Overview), 1st ISMHT-ASME Heat and Mass Transfer Conference, Bombay, **1994**.

Groll, M., Reaction Beds for Dry Sorption Machines, Solid Sorption Refrigeration Symposium Paris, pp. 207–214, 18–20 November **1992**.

Guilleminot, J.J., Gurgel, J.M., Heat Transfer Intensification in Adsorbent Beds of Adsorption Thermal Devices, Proceedings of the 12th Annual International Solar Energy Conference, Miami, USA, ASME, New York, pp. 69–74, **1990**.

Guilleminot, J.J., Choisier, A., Chalfen, J.B., Nicolas, S., Heat Transfer Intensification in Fixed Bed Adsorbers, Heat Recovery Systems & CHP, Vol. 13, No. 4, pp. 297–300, **1993**.

Hajji, A., Khalloufi, S., Theoretical and Experimental Investigation of a Constant-Pressure Adsorption Process, International Journal of Heat and Mass Transfer, Vol. 38, No. 18, pp. 3349–3358, **1995**.

Härkönen, M., Aittomäki, A., The Principle of Internal Regeneration as Applied to the Adsorption Heat Pump Process, Heat Recovery Systems & CHP, Vol. 11, No. 4, pp. 239–248, **1991**.

Harvey, A.B., Study of an Intermittent Regenerative Cycle for Solar Cooling, PhD Thesis, Department of Engineering, University of Warwick, **1990**.

Haseler, L.E., et al., Absorption Cycle Heat Pumps for Domestic Heating, AERE-G 104R, AERE Harwell, **1978**.

Hinotani, K., Kanatani, K., Matsumoto, K., Kume, M., Development of Solar Actuated Zeolite Refrigeration System, Research Centre, Sanyo Electric Co. Ltd., Hirakata, Osaka 573, Japan.

Holman, J.P., Heat Transfer, McGraw-Hill, **1989**.

Hulse, G.E., Freight Car Refrigeration by an Adsorption System Employing Silica Gel, Refrigerating Engineer, Vol. 17, No. 2, **1929**.

Iloeje, O.C., Enibe, S.O., Solar Cooling for Africa: Prospects and Problems, IAEA and UNESCO, International Centre for Theoretical Physics, Internal Report IC/95/345, Miramare-Trieste, October **1995**.

Incropera, F.P., DeWitt, D.P., Fundamentals of Heat and Mass Transfer, 4th Edition, Wiley, **1996**.

International Institute of Refrigeration, Thermodynamic and Physical Properties of Ammonia R717, ISBN: 2-903633-11-8, **1981**.

Jones, J.A., Sorption Refrigeration Research at JPL/NASA, Solid Sorption Refrigeration Symposium Paris, pp. 126–135, 18–20 November **1992**.

Jüntgen, H., New Applications for Carbonaceous Adsorbents, Carbon, Vol. 15, pp. 273–277, **1977**.

Karagiorgas, M., Meunier, F., The Dynamics of a Solid-Adsorption Heat Pump Connected with Outside Heat Sources of Finite Capacity, Heat Recovery Systems & CHP, Vol. 7, No. 3, pp. 285–299, **1987**.

Kemp, M.K., Physical Chemistry: A Step-by-Step Approach, New York: M. Dekker, **1979**.

Kiavany, M., Principles of Heat Transfer in Porous Media, 2nd Edition, Springer-Verlag, New York, **1995**.

Liu, Z.Y., Cacciola, G., Restuccia, G., Giordano, N., Fast Simple and Accurate Measurement of Zeolite Thermal Conductivity, Zeolites, Vol. 10, pp. 565–570, July/August **1990**.

Manual of Symbols and Terminology, Appendix 2, Part 1, Colloid and Surface Chemistry, Pure and Applied Chemistry, Vol. 31, p. 578, **1972**.

Mauran, S., Prades, P., L'Haridon, F., Heat and Mass Transfer in Consolidated Reacting Beds for Thermochemical Systems, Heat Recovery Systems & CHP, Vol. 13, No. 4, pp. 315–319, **1993**.

McEnaney, B., Adsorption and Structure in Microporous Carbons, Based on a plenary review lecture given at "Carbon '86", Baden-Baden FRG., 30th June **1986**.

McEnaney, B., Masters, K.J., Assessment of Adsorption in Microporous Carbons, Thermochimica Acta, 82, pp. 81–102, **1984**.

Meunier, F., Grenier, Ph., Guilleminot, J.J., Pons, P., Solar Powered Refrigeration Using Intermittent Solid Adsorption Cycles, Laboratoire de Thermodynamique des Fluides, UA CNRS 874.

Meunier, F., Mischler, B., Solar Cooling Through Cycles Using Microporous Solid Adsorbents, Sun 2, Vol. 1, pp. 676–680, **1979**.

Meunier, F., Research and Development Toward New Thermochemical Cycles for Cold Production from Solar Energy Using Solid Adsorbents, Journal of Solar Energy Research, Vol. 1, Part. 1, pp. 23–35, **1983**.

Meunier, F., Second Law Analysis of a Solid Adsorption Heat Pump Operating on Reversible Cascade Cycles: Application to the Zeolite-Water Pair, Heat Recovery Systems, Vol. 5, No. 2, pp. 133–141, **1985**.

Meunier, F., Theoretical Performances of Solid Adsorbent Cascading Cycles Using the Zeolite-Water and Active Carbon-Methanol Pairs: Four Case Studies, Heat Recovery Systems, Vol. 6, No. 6, pp. 491–498, **1986**.

Meunier, F., Douss, N., Adsorptive Heat Pumps: Active Carbon-Methanol and Zeolite-Water Pairs, CEC/British Gas International Workshop on Adsorption Heat Pumps, pp. 63–72, April **1988**.

Meunier, F., Solid Sorption: An Alternative to CFC's, Heat Recovery Systems & CHP, Vol. 13, No. 4, pp. 289–295, **1993**.

Miller, E.B., The Development of Silica Gel Refrigeration, The American Society of Refrigerating Engineers, Vol. 17, No. 4, **1929**.

Minkowycz, W.J., Sparrow, E.M., Schneider, G.E., Pletcher, R.H., Handbook of Numerical Heat Transfer, John Wiley & Sons, pp. 6–8, **1988**.

Munyebvu, E., Heat Transfer in Monolithic Charcoals Use in Adsorption Refrigeration Systems, MSc Dissertation, Department of Engineering, University of Warwick, **1994**.

Nagel, G., Kluge, G., Modelling of Non-Isothermal Multi-Component Adsorption in Non-Adiabatic Fixed Beds, Hungarian Journal of Industrial Chemistry, Vol. 15, pp. 68–71, **1987**.

Pappas, C.H., Murray, W.H., Visual C++5: The Complete Reference, McGraw-Hill, **1997**.

Parrish, A., Mechanical Engineer's Reference Book, 11th Edition, Butterworths, London, **1973**.

Passos, E., Meunier, F., Gianola, J.C., Thermodynamic Performance Improvement of an Intermittent Solar-Powered Refrigeration Cycle Using Adsorption of Methanol on Activated Carbon, Heat Recovery Systems, Vol. 6, No. 3, pp. 259–264, **1986**.

Passos, E.F., Escobedo, J.F., Meunier, F., Simulation of an Intermittent Adsorptive Solar Cooling System, Solar Energy, Vol. 42, No. 2, pp. 103–111, **1989**.

Plank, R., Kuprianoff, J., Die kleinkältemaschine, Springer-Verlag, **1960**.

Pons, M., Guilleminot, J.J., Design of an Experimental Solar-Powered Solid-Adsorption Ice Maker, JSEE, ASME, Vol. 108, pp. 332–337, November **1986**.

Reid, R.C., The Properties of Gases and Liquids, 3rd Edition, McGraw-Hill, **1977**.

Restuccia, G., Private Communication, **1997**.

Roberts, D.L., Selim, M.S., Comparative Study of Six Explicit and Two Implicit Finite Difference Schemes for Solving One-Dimensional Parabolic Partial Differential Equations, International Journal for Numerical Methods in Engineering, Vol. 20, pp. 817–844, **1984**.

Rogers, G.F.C., Mayhew, Y.R., Thermodynamic and Transport Properties of Fluids, 4th Edition, Blackwell, **1980**.

Rogers, G.F.C., Mayhew, Y.R., Engineering Thermodynamics Work and Heat Transfer, 3rd Edition, Longman, **1990**.

Ruthven, D.M., Principles of Adsorption and Adsorption Processes, John Wiley & Sons, **1984**.

Ryder, G.H., Strength of Materials, 3rd Edition in SI Units, Macmillan, **1969**.

Sakoda, A., Suzuki, M., Fundamental Study on Solar Powered Adsorption Cooling System, Journal of Chemical Engineering of Japan, Vol. 17, No. 1, pp. 52–57, **1984**.

Shelton, S.V., Wepfer, W.J., Miles, D.J., Ramp Wave Analysis of the Solid/Vapor Heat Pump, Journal of Energy Resources Technology, Vol. 112, pp. 69–78, **1990**.

Simonson, J.R., Engineering Heat Transfer, Macmillan, London, **1975**.

Smíšek, M., Cerný, S., Active Carbon-Manufacture, Properties and Applications, Elsevier, New York, **1970**.

Spinner, B., Application of New Concepts for the Development of Gas Solid Sorption Machines, CNRS-IMP, LEA-SIMAP, University of Perpignan (France), **1996**.

Srivastava, N.C., Eames, I.W., A Review of Developments in Solid-Vapour Adsorption-Refrigeration and Heat-Pump Systems, Journal of the Institute of Energy, pp. 116–127, December **1997**.

Stroud, K.A., Engineering Mathematics, 3rd Edition, Macmillan, **1991**.

Stroud, K.A., Further Engineering Mathematics, 2nd Edition, Macmillan, **1991**.

Sun, L.M., Meunier, F., An Improved Finite Difference Method for Fixed-Bed Multicomponent Sorption, AIChE Journal, Vol. 37, No. 2, pp. 244–254, February **1991**.

Sun, L.M., Ben Amar, N., Meunier, F., Numerical Study on Coupled Heat and Mass Transfers in an Adsorber with External Fluid Heating, Heat Recovery Systems & CHP, Vol. 15, No. 1, pp. 19–29, **1995**.

Suzuki, M., Application of Adsorption Cooling System to Automobiles, Solid Sorption Refrigeration Symposium Paris, pp. 136–141, 18–20 November **1992**.

Swartman, R.K et al, Survey of Solar-Powered Refrigeration, ASME Paper, 73-WA/SOL-6, New York, ASME, **1973**.

Tamainot-Telto, Z., Critoph, R.E., Experimental Investigations of the Permeability of Carbon 208C, Department of Engineering, University of Warwick, Report No. 01-RG/L22119.

Tamainot-Telto, Z., Critoph, R.E., Monolithic Carbon for Sorption Refrigeration and Heat Pump Applications, submitted to Applied Thermal Engineering.

Tamainot-Telto, Z., Critoph, R.E., Adsorption Refrigerator Using Monolithic Carbon-Ammonia Pair, International Journal of Refrigeration, Vol. 20, No. 2, pp. 146–155, **1997**.

Thorpe, R., Heat Transfer by Forced Convection in Beds of Granular Adsorbent Material for Solid Sorption Heat Pumps, PhD Thesis, Department of Engineering, University of Warwick, **1996**.

Turner, L., Improvement of Activated Charcoal-Ammonia Adsorption Heat Pumping/Refrigeration Cycles. Investigation of Porosity and Heat/Mass Transfer Characteristics. Graz 3rd International Workshop on Research Activities on Advanced Heat Pumps, pp. 325–334, **1990**.

Turner, L., Improvement of Activated Charcoal-Ammonia Adsorption Heat Pump/Refrigeration Cycles: Investigation of Porosity and Heat/Mass Transfer Characteristics, PhD Thesis, Department of Engineering, University of Warwick, **1992**.

Ülkü, S., Adsorption Heat Pumps, Heat Recovery Systems, Vol. 6, No. 4, pp. 277–284, **1986**.

University of Warwick - Graduate School, Guide to Examinations for Higher Degrees by Research, September **1996**.

Van Bogaert, G., Adsorption Refrigerator Uses Low-Temperature Waste Heat, Caddet Newsletter, No. 1, pp. 7–9, March **2000**.

White, F.M., Heat and Mass Transfer, Addison-Wesley, **1988**.

World Health Organisation, Standard Performance Specifications and Standard Test Procedures for Cold Chain Equipment, January **1988**.

Worsøe-Schmidt, P., Solar Refrigeration for Developing Countries Using a Solid-Absorption Cycle, International Journal of Ambient Energy, Vol. 4, No. 3, pp. 115–124, July **1983**.

Zhu, R., Han, B., Lin, M., Yu, Y., Experimental Investigation on an Adsorption System for Producing Chilled Water, International Journal of Refrigeration, Vol. 15, No. 1, pp. 31–34, **1992**.

Appendix I

Simple Explicit Program Listing

Simple Explicit 2D Conduction.cpp

```
/*****************************************************************************
*                                                                            *
*          ***   2 Dimensional Transient Heat Conduction Program   ***      *
*                                                                            *
*                          * Simple Explicit Scheme *                        *
*                                                                            *
*     ***   Heating & Cooling Data Read in from Experimental Data File   ***  *
*                                                                            *
*****************************************************************************/

/* preprocessor directives - header files */

#include <fstream.h>
#include <iomanip.h>
#include <stdlib.h>
#include <stdio.h>
#include <errno.h>
#include <math.h>

/* preprocessor directives - symbolic constants */

#define grav 9.81
#define pi 3.14159265359
#define filename "data93_p1.dat"

int main(void)
{
```

```
/* define file pointers */

FILE *f_temp,*f_input,*f_power,*f_var;

/* define variables */

int     countc,counth,dot,dtmaxi,dtmaxj,hour,inrnode,iter,i,j,loop,min;
int     nio,nic,njo,njc,ni,nj,sec,sweeps,subcycle;

double  abstime,cdur,clock,coolpow,cop,cpal,cpnh3,cpst,conc;
double  dt,dtmax,dtmaxold,dtmaxnew,dur,dro,drc,dzo,dzc,hdur,hoheat,hocool;
double  halcar,hstcar,hstal,invhalcar,invhstcar,invhstal,heatpow,heatpowcar,hfnh3,hgnh3;
double  ho,hvnh3,inconc,inrmcar,inrmtempcar,inmnh3,kal,kst,kconst,lconc,lic,lio,ljc,ljo;
double  mtempcar,massflow,masstol,mnh31,mnh32,mnh33,merr1,merr2,merr3,mnh3ads;
double  mcar,nconst,psint,psnew,qin,qincar,rinner,router,rcf1,rcf2,rcf3,rcf4;
double  rhocar,rfile,rhoal,rhost,rtmfile,rnh3,steps,tint,tsint,tsintc,tsold,tsnew,tsnewc;
double  to,tcond,tevap,tsinc,ts1,ts2,time,voidvol,wfile,wscrn,wtmfile,wtmscrn;
double  cfa,cfb,cfc,hfc,hge,po,rhoh2o,dconct,mnh3totnew,mnh3totold,conc1,conc2;
double  spcoolpow,spheatpow,spheatpowcar,copcar,genlength,volfactor;

/* define arrays */

double  an[7][9],as[7][9],ae[7][9],aw[7][9];
double  cpea[7][9],cpeb[7][9],cpec[7][9],cped[7][9],cpee[7][9];
double  cpcar[7][9],dzn[7][9],dzs[7][9],dre[7][9],drw[7][9];
double  dln[7][9],dls[7][9],dle[7][9],dlw[7][9];
double  kn[7][9],ks[7][9],ke[7][9],kw[7][9];
double  rij[9],rho[7][9],rhonh3[7][9],timea[9];
double  told[8][10],tnew[7][9],toldc[7][9],tnewc[7][9];
double  un[7][9],us[7][9],ue[7][9],uw[7][9],v[7][9];
double  x1[7][9],x2[7][9],xold[7][9],xnew[7][9];

/* define material properties */

rhoh2o=1000;
kal=204;
cpal=900;
rhoal=2700;
kst=54;
cpst=465;
rhost=7833;
```

```
rhocar=750;
halcar=1e+12;
hstcar=1e+12;
hstal=1e+12;
invhalcar=0;
invhstcar=0;
invhstal=0;
cpnh3=4734;

/* define heat transfer fluid (water) coefficients */

cfa=2.0096;
cfb=29.0646;
cfc=100.3048;

/* define physical unit cell geometry */

lic=(23.05/1000);          /* carbon radial length (m) */
lio=(1.44/1000);           /* shell wall thickness (m) */
ljc=(1.05/1000);           /* carbon layer semi-thickness (m) */
ljo=(0.1/1000);            /* fin semi-thickness (m) */
rinner=(2.5/1000);         /* generator internal radius */
router=(rinner+lic+lio);   /* shell external radius */
genlength=1;               /* real generator length (m) */

/* define numerical grid */

nio=1;
nic=7;
njo=1;
njc=5;
ni=(nio+nic);
nj=(njo+njc);
drc=(lic/(nic-0.5));
dro=(lio/(nio-0.5));
dzo=(ljo/(njo-0.5));
dzc=(ljc/(njc-0.5));

/* set adiabatic boundary nodes to zero */

for(i=1; i <= ni; i++) {
```

```
        told[0][i]=0;
        told[nj+1][i]=0; }

for(j=1; j <= nj; j++) {
        told[j][ni+1]=0; }

/* set initial, evaporating and condensing temperatures */

printf("\n*** SIMPLE EXPLICIT SCHEME ***\n");

printf("\nEnter the Initial Generator Temperature (K)...\n\n> ");
scanf("%lf",&tint);

printf("\nEnter the Initial Generator Saturation Temperature (K)...\n\n> ");
scanf("%lf",&tsint);

printf("\nEnter the Evaporating Temperature (K)...\n\n> ");
scanf("%lf",&tevap);

printf("\nEnter the Condensing Temperature (K)...\n\n> ");
scanf("%lf",&tcond);

printf("\nEnter the Cooling External Heat Transfer C/f (W/m^2.K)...\n\n> ");
scanf("%lf",&hocool);

printf("\nEnter the Heating External Heat Transfer C/f (W/m^2.K)...\n\n> ");
scanf("%lf",&hoheat);

/* define initial conditions */

tsinc=0.1;
voidvol=0;
masstol=1.0e-12;
tsold=tsint;
tsnew=tsint;
psint=(exp(11.541-(2754.5/tsint)));

for(i=1; i <= ni; i++) {
        for(j=1; j <= nj; j++) {
          told[j][i]=tint;
          toldc[j][i]=(tint-273.15); }}
```

```
/* define dubinin-astakhov parameters */

lconc=0.3629;
kconst=3.6571;
nconst=0.94;
inconc=(lconc*(exp((-1)*kconst*(pow(((tint/tsint)-1),nconst)))));

for(i=(nio+1); i <= ni; i++) {
        for(j=(njo+1); j <= nj; j++) {
          xold[j][i]=inconc; }}

if(lconc == 0) {
        voidvol=0; }

/* define dr & dz arrays */

for(j=1; j <= nj; j++) {
        for(i=1; i <= (nio-1); i++) {
          dre[j][i]=dro; }
        dre[j][nio]=((dro+drc)/2);

        for(i=(nio+1); i <= (ni-1); i++) {
          dre[j][i]=drc; }
        dre[j][ni]=0;
        drw[j][1]=0;

        for(i=2; i <= nio; i++) {
          drw[j][i]=dro; }
        drw[j][(nio+1)]=((dro+drc)/2);

        for(i=(nio+2); i <= ni; i++) {
          drw[j][i]=drc; }}

for(i=1; i <= ni; i++) {
        dzn[1][i]=0;
        for(j=2; j <= njo; j++) {
          dzn[j][i]=dzo; }
        dzn[(njo+1)][i]=((dzc+dzo)/2);

        for(j=(njo+2); j <= nj; j++) {
```

```
        dzn[j][i]=dzc; }

      for(j=1; j <= (njo-1); j++) {
        dzs[j][i]=dzo; }
      dzs[njo][i]=((dzc+dzo)/2);

      for(j=(njo+1); j <= (nj-1); j++) {
        dzs[j][i]=dzc; }
      dzs[nj][i]=0; }

/* define radial positions */

rij[ni]=rinner;
for(i=(ni-1); i>= 1; i--){
      rij[i]=(dre[1][i]+rij[i+1]);}

/* define dl arrays - lengths from node to control volume boundaries */

for(j=1; j <= nj; j++) {
      for(i=1; i <= nio; i++) {
        dle[j][i]=(dro/2); }

      for(i=(nio+1); i <= (ni-1); i++) {
        dle[j][i]=(drc/2); }
      dle[j][ni]=0;
      dlw[j][1]=0;

      for(i=2; i <= nio; i++) {
        dlw[j][i]=(dro/2); }

      for(i=(nio+1); i <= ni; i++) {
        dlw[j][i]=(drc/2); }}

for(i=1; i <= ni; i++) {
      dln[1][i]=0;
      for(j=2; j <= njo; j++) {
        dln[j][i]=(dzo/2); }

      for(j=(njo+1); j <= nj; j++) {
        dln[j][i]=(dzc/2); }
```

```
        for(j=1; j <= njo; j++) {
          dls[j][i]=(dzo/2); }

        for(j=(njo+1); j <= (nj-1); j++) {
          dls[j][i]=(dzc/2); }
        dls[nj][i]=0; }

/* define area arrays */

for(j=1; j <= nj; j++) {
        for(i=1; i <= ni; i++) {
          an[j][i]=(((pow(dlw[j][i],2))-(pow(dle[j][i],2)))/2)+(rij[i]*(dlw[j][i]+dle[j][i]));
          as[j][i]=(((pow(dlw[j][i],2))-(pow(dle[j][i],2)))/2)+(rij[i]*(dlw[j][i]+dle[j][i]));
          ae[j][i]=(rij[i]-dle[j][i])*(dln[j][i]+dls[j][i]);
          aw[j][i]=(rij[i]+dlw[j][i])*(dln[j][i]+dls[j][i]); }}

/* define volume array */

for(i=1; i <= ni; i++) {
        for(j=1; j <= nj; j++) {
          v[j][i]=((((pow(dlw[j][i],2))-(pow(dle[j][i],2)))/2)+(rij[i]
                  *(dlw[j][i]+dle[j][i])))*(dln[j][i]+dls[j][i]); }}

volfactor=((2*pi*genlength)/(ljc+ljo));

/* define conductivity arrays */

for(i=1; i <= nio; i++) {
        for(j=1; j <= nj; j++) {
          kn[j][i]=kst;
          ks[j][i]=kst;
          ke[j][i]=kst;
          kw[j][i]=kst;
          rho[j][i]=rhost; }}

for(i=(nio+1); i <= ni; i++) {
        for(j=1; j <= njo; j++) {
          kn[j][i]=kal;
          ks[j][i]=kal;
          ke[j][i]=kal;
          kw[j][i]=kal;
```

```
        rho[j][i]=rhoal; }}

for(i=(nio+1); i <= ni; i++) {
      for(j=(njo+1); j <= nj; j++) {
        kn[j][i]=(0.8379-(0.0008*told[j][i]));
        ks[j][i]=(0.8379-(0.0008*told[j][i]));
        ke[j][i]=(0.8379-(0.0008*told[j][i]));
        kw[j][i]=(0.8379-(0.0008*told[j][i])); }}

/* define heat transfer arrays */

for(i=1; i <= ni; i++) {
      for(j=1; j <= nj; j++) {
        un[j][i]=(kn[j][i]/dzn[j][i]);
        us[j][i]=(ks[j][i]/dzs[j][i]);
        ue[j][i]=(ke[j][i]/dre[j][i]);
        uw[j][i]=(kw[j][i]/drw[j][i]); }}

for(j=(njo+1); j <= nj; j++) {
      ue[j][nio]=(1/((dro/(2*ke[j][nio]))+(drc/(2*kw[j][nio+1]))+(invhstcar)));
      uw[j][(nio+1)]=(1/((dro/(2*ke[j][nio]))+(drc/(2*kw[j][nio+1]))+(invhstcar))); }

for(i=(nio+1); i <= ni; i++) {
      us[njo][i]=(1/((dzo/(2*ks[njo][i]))+(dzc/(2*kn[njo+1][i]))+(invhalcar)));
      un[(njo+1)][i]=(1/((dzo/(2*ks[njo][i]))+(dzc/(2*kn[njo+1][i]))+(invhalcar))); }

for(j=1; j <= njo; j++) {
      ue[j][nio]=(1/((dro/(2*ke[j][nio]))+(drc/(2*kw[j][nio+1]))+(invhstal)));
      uw[j][(nio+1)]=(1/((dro/(2*ke[j][nio]))+(drc/(2*kw[j][nio+1]))+(invhstal))); }

for(i=1; i <= ni; i++) {
      un[1][i]=0;
      us[nj][i]=0; }

for(j=1; j <= nj; j++) {
      ue[j][ni]=0;
      uw[j][1]=hoheat; }

/* define initial effective specific heats */

for(j=1; j <= nj; j++) {
```

```
        for(i=1; i <= nio; i++) {
          cpec[j][i]=cpst;
          cpee[j][i]=0; }}

for(i=(nio+1); i <= ni; i++) {
        for(j=1; j <= njo; j++) {
          cpec[j][i]=cpal;
          cpee[j][i]=0; }}

/* calculate mass of carbon */

mcar=0;
for(i=(nio+1); i <= ni; i++) {
        for(j=(njo+1); j <= nj; j++) {
          mcar=mcar+(rhocar*v[j][i]); }}

/* calculate mean carbon temperature */

mtempcar=0;
for(i=(nio+1); i <= ni; i++) {
        for(j=(njo+1); j <= nj; j++) {
          mtempcar=mtempcar+((told[j][i]*rhocar*v[j][i])/mcar); }}
mtempcar=(mtempcar-273.15);

/* calculate mean internal nodes temperature */

inrnode=ni;
inrmcar=0;
inrmtempcar=0;
for(j=(njo+1); j <= nj; j++) {
        inrmcar=inrmcar+(rhocar*v[j][inrnode]); }
for(j=(njo+1); j <= nj; j++) {
        inrmtempcar=inrmtempcar+((told[j][inrnode]*rhocar*v[j][inrnode])/inrmcar); }
inrmtempcar=(inrmtempcar-273.15);

/* calculate density of ammonia in voids */

tsintc=(tsint-273.15);

rcf1=((1e-05)*((0.00000068892947*(pow(tsintc,3)))+(0.00009565787857*
        (pow(tsintc,2)))+(0.00844971035705*tsintc)+0.32843436542347));
```

```
rcf2=((1e-02)*((-0.00000052403299*(pow(tsintc,3)))+(-0.00006905794744*
      (pow(tsintc,2)))+(-0.00531432390974*tsintc)-0.18587792629441));

rcf3=(((0.00000140592901*(pow(tsintc,3)))+(0.00017767403458*
      (pow(tsintc,2)))+(0.01203459890161*tsintc)+0.37471284774418));

rcf4=((1e+04)*((-0.00000001416664*(pow(tsintc,3)))+(-0.00000177131542*
      (pow(tsintc,2)))+(-0.00010988317152*tsintc)+0.04572946161140));

rnh3=((rcf1*(pow(tsintc,3)))+(rcf2*(pow(tsintc,2)))+(rcf3*tsintc)+rcf4);

for(i=(nio+1); i <= ni; i++) {
      for(j=(njo+1); j <= nj; j++) {
        rhonh3[j][i]=(((psint*(1e+05))/(rnh3*told[j][i]))*voidvol);
        rho[j][i]=(rhocar+rhonh3[j][i]); }}

/* calculate initial mass of ammonia in generator */

inmnh3=0;
for(i=(nio+1); i <= ni; i++) {
      for(j=(njo+1); j <= nj; j++) {
        inmnh3=inmnh3+((inconc*rhocar*v[j][i])+(rhonh3[j][i]*v[j][i])); }}

/* calculate initial ammonia enthalpy of vaporisation */

hfnh3=((423.498846153846+(4.584407092907*(tsintc))
      +(0.002471878122*(pow((tsintc),2))))*1000);

hgnh3=((1685.15907342657+(1.01716208791*(tsintc))
      -(0.00810606893*(pow((tsintc),2))))*1000);

hvnh3=(hgnh3-hfnh3);

/* determine maximum time step for stability */

for(i=(nio+1); i <= ni; i++) {
      for(j=(njo+1); j <= nj; j++) {
        cpcar[j][i]=(34.685+(2.811*told[j][i]));

        cpea[j][i]=(cpcar[j][i]+(xold[j][i]*cpnh3));
```

```
        cpeb[j][i]=(((hvnh3*told[j][i]*kconst*nconst*xold[j][i])/(pow(tsold,2)))
                *(pow(((told[j][i]/tsold)-1),(nconst-1))));

        cpec[j][i]=(cpea[j][i]+cpeb[j][i]); }}

dtmax=1e+06;
dtmaxold=1e+06;
dtmaxnew=0;
for(j=nj; j>= 1; j--) {
      for(i=ni; i>= 1; i--) {
        dtmaxnew=((rho[j][i]*v[j][i]*cpec[j][i])/((uw[j][i]*aw[j][i])
                +(ue[j][i]*ae[j][i])+(un[j][i]*an[j][i])+(us[j][i]*as[j][i])));

        if((dtmaxnew <= dtmaxold) & (dtmaxnew <= dtmax)) {
                dtmax=dtmaxnew;
                dtmaxi=i;
                dtmaxj=j; }
        dtmaxold=dtmaxnew; }}

/* set modelling parameters */

printf("\nMaximum Permissible Time-step for Stability = %lf\n",dtmax);

printf("\nStability Limited by Node i = %d, j = %d\n",dtmaxi,dtmaxj);

printf("\nEnter the Desired Value for the Time-step...\n\n> ");
scanf("%lf",&dt);

printf("\nEnter the Required Number of Temperature Data Sweeps...\n\n> ");
scanf("%d",&sweeps);

printf("\nEnter the Heating Duration (seconds)...\n\n> ");
scanf("%lf",&hdur);

printf("\nEnter the Cooling Duration (seconds)...\n\n> ");
scanf("%lf",&cdur);

printf("\nEnter the Time Interval Between File Reads & Writes (seconds)...\n\n> ");
scanf("%lf",&rfile);
wfile=rfile;
```

```
printf("\nEnter the Time Interval Between Screen Writes (seconds)...\n\n> ");
scanf("%lf",&wscrn);

/* estimate computation time */

dur=hdur+cdur;
steps=((dur/dt)*sweeps);
clock=(steps/(300.0));
hour=(int)(clock/3600);
min=(int)((clock-(3600*hour))/60);
sec=(int)(clock-(60*min)-(3600*hour));
printf("\nComputation Time Approximately %d hours %d min %d sec\n",hour,min,sec);
printf("_____\n\n\n");

/* set variables */

qin=0;
qincar=0;
conc1=0;
conc2=0;
dconct=0;
massflow=0;
mnh3totold=0;

/* set counters */

dot=0;
abstime=0;
rtmfile=0;
wtmfile=0;
wtmscrn=0;
iter=0;
time=0;
countc=0;
counth=1;
for(i=1; i <= ni; i++) {
      timea[i]=abstime; }
```

```
/* create data files */

ifstream fi_exp(filename);
if(!fi_exp)
        cerr << "Error, cannot open experimental data file for reading\n";

if((f_input=fopen("input.dat","w")) == NULL) {
        printf("Error, cannot open file 'input.dat' for writing\n");
        exit(0); }

if((f_temp=fopen("temp.dat","w")) == NULL) {
        printf("Error, cannot open file 'temp.dat' for writing\n");
        exit(0); }

if((f_var=fopen("var.dat","w")) == NULL) {
        printf("Error, cannot open file 'var.dat' for writing\n");
        exit(0); }

if((f_power=fopen("power.dat","w")) == NULL) {
        printf("Error, cannot open file 'power.dat' for writing\n");
        exit(0); }
fclose(f_power);

/* write initial data to file */

fprintf(f_input," Input Data and Specific Model Parameters\n");
fprintf(f_input," ****************************************\n\n");
fprintf(f_input," Experimental Input Data File: ");
fprintf(f_input,filename);
fprintf(f_input,"\n\n Radial Nodal Positions = ");
for(i=ni; i >= 2; i--) {
        fprintf(f_input,"%9.7lf, ",rij[i]); }
fprintf(f_input,"%9.7lf (m)\n\n",rij[1]);
fprintf(f_input," Timestep (dt) = %lf (sec)                                    \
        \n\n Initial Generator Temperature (tint) = %lf (K)                    \
        \n\n Initial Generator Saturation Temperature (tsint) = %lf (K)        \
        \n\n Evaporating Temperature (tevap) = %lf (K)                         \
        \n\n Condensing Temperature (tcond) = %lf (K)                          \
        \n\n Generator Percentage Void Volume (voidvol) = %5.1lf               \
        \n\n Cooling Heat Transfer c/f (hocool) = %lf (W/m^2.K)                \
        \n\n Heating Heat Transfer c/f (hoheat) = %lf (W/m^2.K)                \
```

```
        \n\n Heat Transfer c/f Steel-Carbon (hstcar) = Infinite (W/m^2.K)          \
        \n\n Heat Transfer c/f Aluminium-Carbon (halcar) = Infinite (W/m^2.K)      \
        \n\n Heat Transfer c/f Steel-Aluminium (hstal) = Infinite (W/m^2.K)        \
        \n\n Number of Data Sweeps (sweeps) = %d                                  \
        \n\n Heating Duration (hdur) = %lf (sec)                                  \
        \n\n Cooling Duration (cdur) = %lf (sec)                                  \
        \n\n Write Period to File (wfile) = %lf (sec)                             \
        \n\n Write Period to Screen (wscrn) = %lf (sec)",dt,tint,tsint,tevap,tcond,voidvol, \
        hocool,hoheat,sweeps,hdur,cdur,wfile,wscrn);

for(i=1; i <= (ni-1); i++) {
        fprintf(f_temp,"%lf, ",timea[i]); }
fprintf(f_temp,"%lf\n",timea[ni]);
for(j=1; j <= nj; j++) {
        for(i=1; i <= (ni-1); i++) {
          fprintf(f_temp,"%lf, ",toldc[j][i]); }
        fprintf(f_temp,"%lf\n",toldc[j][ni]); }

fi_exp >> po;
po=(po-((rhoh2o*grav*0.4)/1e+05));
to=(cfc+(cfb*log(po))+(cfa*(pow(log(po),2))));

fprintf(f_var,"%lf, %lf, %6.2lf, %6.2lf, %lf, %lf, %lf, %14.12lf, %14.12lf, %lf\n",time,
        abstime,mtempcar,inrmtempcar,tsintc,psint,inconc,dconct,massflow,to);

fclose(f_input);fclose(f_temp);fclose(f_var);
fi_exp.seekg(0);

mtempcar=0;
inrmtempcar=0;

/* start of solution time loop */

loop=1;
do {
        time=0;
        subcycle=1;
        ho=hoheat;
        fi_exp >> po;
        po=(po-((rhoh2o*grav*0.4)/1e+05));
        to=(cfc+(cfb*log(po))+(cfa*(pow(log(po),2))));
```

```
to=(to+273.15);

/* set initial mass of ammonia */

inmnh3=0;
for(i=(nio+1); i <= ni; i++) {
  for(j=(njo+1); j <= nj; j++) {
          inmnh3=inmnh3+((xold[j][i]*rhocar*v[j][i])+(rhonh3[j][i]*v[j][i])); }}

/* start of time marching loop */

do {
  iter=iter+1;
  time=time+dt;
  rtmfile=rtmfile+dt;
  wtmfile=wtmfile+dt;
  wtmscrn=wtmscrn+dt;
  abstime=abstime+dt;

  /* read in temperature data from file */

  if(rtmfile >= rfile) {
          fi_exp >> po;
          po=(po-((rhoh2o*grav*0.4)/1e+05));
          to=(cfc+(cfb*log(po))+(cfa*(pow(log(po),2))));
          to=(to+273.15);
          rtmfile=0; }

  /* calculation of generator carbon conductivity & heat transfer */

  for(i=(nio+1); i <= ni; i++) {
          for(j=(njo+1); j <= nj; j++) {
                  kn[j][i]=(0.8379-(0.0008*told[j][i]));
                  ks[j][i]=(0.8379-(0.0008*told[j][i]));
                  ke[j][i]=(0.8379-(0.0008*told[j][i]));
                  kw[j][i]=(0.8379-(0.0008*told[j][i]));

                  un[j][i]=(kn[j][i]/dzn[j][i]);
                  us[j][i]=(ks[j][i]/dzs[j][i]);
                  ue[j][i]=(ke[j][i]/dre[j][i]);
                  uw[j][i]=(kw[j][i]/drw[j][i]); }}
```

```
        /* reset boundary heat transfers */

        for(j=(njo+1); j <= nj; j++) {
            ue[j][nio]=(1/((dro/(2*ke[j][nio]))+(drc/(2*kw[j][nio+1]))+(invhstcar)));
            uw[j][(nio+1)]=(1/((dro/(2*ke[j][nio]))+(drc/(2*kw[j][nio+1]))+(invhstcar))); }

        for(i=(nio+1); i <= ni; i++) {
            us[njo][i]=(1/((dzo/(2*ks[njo][i]))+(dzc/(2*kn[njo+1][i]))+(invhalcar)));
            un[(njo+1)][i]=(1/((dzo/(2*ks[njo][i]))+(dzc/(2*kn[njo+1][i]))+(invhalcar))); }

        for(j=1; j <= njo; j++) {
            ue[j][nio]=(1/((dro/(2*ke[j][nio]))+(drc/(2*kw[j][nio+1]))+(invhstal)));
            uw[j][(nio+1)]=(1/((dro/(2*ke[j][nio]))+(drc/(2*kw[j][nio+1]))+(invhstal))); }

        for(i=1; i <= ni; i++) {
                un[1][i]=0;
                us[nj][i]=0; }

        for(j=1; j <= nj; j++) {
                ue[j][ni]=0;
                uw[j][1]=ho; }

        /* initial guess for tsat */

        if((tsold < tcond) && (subcycle == 1)) {
                tsnew=(tsold+tsinc); }

        if((tsold > tevap) && (subcycle == 2)) {
                tsnew=(tsold-tsinc); }

        if(lconc == 0) {
                tsnew=tsold; }
label_1:
        dot++;
        if(dot == 1000) {
        printf(".");
        dot=0; }

        psnew=(exp(11.541-(2754.5/tsnew)));
```

```
/* calculation to include generator void volume */

tsnewc=(tsnew-273.15);

rcf1=((1e-05)*((0.00000068892947*(pow(tsnewc,3)))+(0.00009565787857
        *(pow(tsnewc,2)))+(0.00844971035705*tsnewc)+0.32843436542347));

rcf2=((1e-02)*((-0.00000052403299*(pow(tsnewc,3)))+(-0.00006905794744
        *(pow(tsnewc,2)))+(-0.00531432390974*tsnewc)-0.18587792629441));

rcf3=(((0.00000140592901*(pow(tsnewc,3)))+(0.00017767403458
        *(pow(tsnewc,2)))+(0.01203459890161*tsnewc)+0.37471284774418));

rcf4=((1e+04)*((-0.00000001416664*(pow(tsnewc,3)))+(-0.00000177131542
        *(pow(tsnewc,2)))+(-0.00010988317152*tsnewc)+0.04572946161140));

rnh3=((rcf1*(pow(tsnewc,3)))+(rcf2*(pow(tsnewc,2)))+(rcf3*tsnewc)+rcf4);

for(i=(nio+1); i <= ni; i++) {
        for(j=(njo+1); j <= nj; j++) {
                rhonh3[j][i]=(((psnew*(1e+05))/(rnh3*told[j][i]))*voidvol);
                rho[j][i]=(rhocar+rhonh3[j][i]); }}

/* set boundary nodes */

for(j=1; j <= nj; j++) {
        told[j][0]=to; }

/* calculate ammonia enthalpy of vaporisation */

hfnh3=((423.498846153846+(4.584407092907*(tsnewc))
        +(0.002471878122*(pow((tsnewc),2))))*1000);

hgnh3=((1685.15907342657+(1.01716208791*(tsnewc))
        -(0.00810606893*(pow((tsnewc),2))))*1000);

hvnh3=(hgnh3-hfnh3);

/* calculation of effective cp coefficients */

for(i=(nio+1); i <= ni; i++) {
```

```
            for(j=(njo+1); j <= nj; j++) {
                    cpcar[j][i]=(34.685+(2.811*told[j][i]));

                    cpea[j][i]=(cpcar[j][i]+(xold[j][i]*cpnh3));

                    cpeb[j][i]=(((hvnh3*told[j][i]*kconst*nconst*xold[j][i])
                            /(pow(tsold,2)))*(pow(((told[j][i]/tsold)-1),(nconst-1))));

                    cpec[j][i]=(cpea[j][i]+cpeb[j][i]);

                    cped[j][i]=((cpeb[j][i]*(tsnew-tsold)*told[j][i])/tsold);

                    cpee[j][i]=((cped[j][i])/(cpec[j][i])); }}

    /* simple explicit transient conduction equation */

    for(i=1; i <= ni; i++) {
            for(j=1; j <= nj; j++) {
                    tnew[j][i]=((told[j][i]+cpee[j][i])
                            +((dt/(rho[j][i]*v[j][i]*cpec[j][i]))
                            *((uw[j][i]*aw[j][i]*(told[j][i-1]-told[j][i]))
                            +(ue[j][i]*ae[j][i]*(told[j][i+1]-told[j][i]))
                            +(un[j][i]*an[j][i]*(told[j-1][i]-told[j][i]))
                            +(us[j][i]*as[j][i]*(told[j+1][i]-told[j][i])))); }}

    /* evaluation of tsat and mass balance */

    if(lconc > 0) {
    if((tsold >= tcond) && (subcycle == 1)) {
            tsold=tcond;
            tsnew=tcond;
            for(i=(nio+1); i <= ni; i++) {
                    for(j=(njo+1); j <= nj; j++) {
                            xnew[j][i]=(lconc*(exp((-1)*kconst*(pow(((tnew[j][i]
                                    /tsnew)-1),nconst)))));
                    }
            }
            goto label_4;
    }

    if((tsold <= tevap) && (subcycle == 2)) {
```

```
            tsold=tevap;
            tsnew=tevap;
            for(i=(nio+1); i <= ni; i++) {
                  for(j=(njo+1); j <= nj; j++) {
                        xnew[j][i]=(lconc*(exp((-1)*kconst*(pow(((tnew[j][i]
                              /tsnew)-1),nconst)))));
                  }
            }
            goto label_4;
}

mnh31=0;
mnh32=0;
mnh33=0;
ts1=tsnew;
if(subcycle == 1) {
      ts2=(ts1+tsinc);
      if(ts1 == ts2) {
            ts2=ts1+0.1; }}

if(subcycle == 2) {
      ts2=(ts1-tsinc);
      if(ts1 == ts2) {
            ts2=ts1-0.1; }}

for(i=(nio+1); i <= ni; i++) {
      for(j=(njo+1); j <= nj; j++) {
            x1[j][i]=(lconc*(exp((-1)*kconst
                  *(pow(((tnew[j][i]/ts1)-1),nconst)))));
            mnh31=mnh31+((x1[j][i]*rhocar*v[j][i])+(rhonh3[j][i]*v[j][i])); }}

merr1=(inmnh3-mnh31);

if(fabs(merr1) <= masstol) {
      for(i=1; i <= ni; i++) {
            for(j=1; j <= nj; j++) {
                  xnew[j][i]=x1[j][i]; }}
      goto label_3; }

if(fabs(merr1) > masstol) {
      for(i=(nio+1); i <= ni; i++) {
```

```
                    for(j=(njo+1); j <= nj; j++) {
                        x2[j][i]=(lconc*(exp((-1)*kconst
                            *(pow(((tnew[j][i]/ts2)-1),nconst)))));
                        mnh32=mnh32+((x2[j][i]*rhocar*v[j][i])+(rhonh3[j][i]
                            *v[j][i])); }}

            merr2=(inmnh3-mnh32);

label_2:
            tsnew=(((merr2*ts1)-(merr1*ts2))/(merr2-merr1));
            for(i=(nio+1); i <= ni; i++) {
                for(j=(njo+1); j <= nj; j++) {
                    xnew[j][i]=(lconc*(exp((-1)*kconst
                        *(pow(((tnew[j][i]/tsnew)-1),nconst)))));
                    mnh33=mnh33+((xnew[j][i]*rhocar*v[j][i])+(rhonh3[j][i]
                        *v[j][i])); }}

            merr3=(inmnh3-mnh33);

            if(fabs(merr3) > masstol) {
                ts1=ts2;
                merr1=merr2;
                ts2=tsnew;
                merr2=merr3;
                mnh33=0;
                goto label_2; }
            goto label_1;
        }

label_3:
        if((tsnew >= tcond) && (subcycle == 1)) {
            tsnew=tcond;
            for(i=(nio+1); i <= ni; i++) {
                for(j=(njo+1); j <= nj; j++) {
                    xnew[j][i]=(lconc*(exp((-1)*kconst
                        *(pow(((tnew[j][i]/tsnew)-1),nconst))))); }}}

        if((tsnew <= tevap) && (subcycle == 2)) {
            tsnew=tevap;
            for(i=(nio+1); i <= ni; i++) {
                for(j=(njo+1); j <= nj; j++) {
```

```
                        xnew[j][i]=(lconc*(exp((-1)*kconst
                                *(pow(((tnew[j][i]/tsnew)-1),nconst))))); }}
        }

label_4:
        tsinc=(tsnew-tsold);
        tsold=tsnew;
        for(i=(nio+1); i <= ni; i++) {
                for(j=(njo+1); j <= nj; j++) {
                        xold[j][i]=xnew[j][i]; }}
        }
        else {
                tsinc=0;
                tsnew=tsint;
                tsold=tsnew;
                for(i=(nio+1); i <= ni; i++) {
                        for(j=(njo+1); j <= nj; j++) {
                                xnew[j][i]=inconc;
                                xold[j][i]=xnew[j][i]; }}
        }

        /* calculate heat into total unit cell and carbon & aluminium only */

        if(time <= hdur) {
                for(j=1; j <= nj; j++) {
                        qin=qin+(uw[j][1]*aw[j][1]*(to-tnew[j][1])*dt);
                        qincar=qincar+(uw[j][nio+1]*aw[j][nio+1]
                                *(tnew[j][nio]-tnew[j][(nio+1)])*dt); }}

        /* calculate mean concentration and mean rate of concentration change */

        for(j=(njo+1); j <= nj; j++) {
                for(i=(nio+1); i <= ni; i++) {
                        mnh3ads=mnh3ads+((lconc*(exp((-1)*kconst
                                *(pow(((tnew[j][i]/tsnew)-1),nconst)))))*(rhocar*v[j][i])); }}

        conc=(mnh3ads/mcar);
        mnh3ads=0;

        if(time <= hdur) {
                dconct=((conc-inconc)/time); }
```

```
else {
        dconct=((conc-conc1)/(time-hdur)); }

/* calculate nodal centigrade temperatures */

if(wtmfile >= wfile) {
for(i=1; i <= ni; i++) {
        for(j=1; j <= nj; j++) {
                tnewc[j][i]=(tnew[j][i]-273.15); }}

/* calculate mean carbon temperature */

for(i=(nio+1); i <= ni; i++) {
        for(j=(njo+1); j <= nj; j++) {
                mtempcar=mtempcar+((tnew[j][i]*rhocar*v[j][i])/mcar); }}
mtempcar=(mtempcar-273.15);

/* calculate mean internal nodes temperature */

for(j=(njo+1); j <= nj; j++) {
        inrmtempcar=inrmtempcar+((tnew[j][inrnode]*rhocar
                *v[j][inrnode])/inrmcar); }
inrmtempcar=(inrmtempcar-273.15);

/* calculate mean massflow (g/s) over file write period */

        for(j=(njo+1); j <= nj; j++) {
                for(i=(nio+1); i <= ni; i++) {
                        mnh3totnew=mnh3totnew+(((lconc*(exp((-1)*kconst
                                *(pow(((tnew[j][i]/tsnew)-1),nconst)))))
                                *(rhocar*v[j][i]))+(rhonh3[j][i]*v[j][i])); }}
        massflow=(((mnh3totnew-mnh3totold)/wtmfile)*1000);
        mnh3totold=mnh3totnew;
        mnh3totnew=0;

/* write data to file & screen */

        if((f_temp=fopen("temp.dat","a")) == NULL) {
                printf("Error, cannot open file 'temp.dat' for appending\n");
                exit(0); }
```

```
        if((f_var=fopen("var.dat","a")) == NULL) {
                printf("Error, cannot open file 'var.dat' for appending\n");
                exit(0); }

        for(i=1; i <= ni; i++) {
                timea[i]=abstime; }

        for(i=1; i <= (ni-1); i++) {
                fprintf(f_temp,"%lf, ",timea[i]); }
        fprintf(f_temp,"%lf\n",timea[ni]);
        for(j=1; j <= nj; j++) {
                for(i=1; i <= (ni-1); i++) {
                        fprintf(f_temp,"%lf, ",tnewc[j][i]); }
                fprintf(f_temp,"%lf\n",tnewc[j][ni]); }

        fprintf(f_var,"%lf, %lf, %6.2lf, %6.2lf, %lf, %lf, %lf, %14.12lf, %14.12lf,
                %lf\n",time,abstime,mtempcar,inrmtempcar,(tsnew-273.15),
                psnew,conc,dconct,massflow,(to-273.15));

        wtmfile=0;
        fclose(f_temp);fclose(f_var);
}

if(wtmscrn >= wscrn) {
        printf("\n\nIteration = %d, Total time elapsed = %lf secs, Tout = %6.2lf
                deg C \nExternal Heat Transfer Coefficient =
                %d\n\n",iter,abstime,(to-273.15),int(ho));

        if(subcycle == 1) {
                printf("Temperature data sweep = %d    Heating cycle =
                        %d\n\n\n",loop,counth); }

        if(subcycle == 2) {
                printf("Temperature data sweep = %d    Cooling cycle =
                        %d\n\n\n",loop,countc); }
        wtmscrn=0;
}

/* reset counters */

mtempcar=0;
inrmtempcar=0;
```

```
/* update temperature array */

for(i=1; i <= ni; i++) {
        for(j=1; j <= nj; j++) {
                told[j][i]=tnew[j][i]; }}

/* assess cycle change-overs */

if((time >= hdur) && (subcycle == 1)) {
        subcycle=2;
        ho=hocool;
        countc++;
        conc1=conc;
        hfc=hfnh3;

        /* set mass in system before cooling */

        inmnh3=0;
        for(i=(nio+1); i <= ni; i++) {
                for(j=(njo+1); j <= nj; j++) {
                inmnh3=inmnh3+((xold[j][i]*rhocar*v[j][i])
                        +(rhonh3[j][i]*v[j][i])); }}
}

if((time >= dur) && (subcycle == 2))  {
        subcycle=1;
        ho=hoheat;
        counth++;
        conc2=conc;
        hge=hgnh3;

        /* set mass in system before heating */

        inmnh3=0;
        for(i=(nio+1); i <= ni; i++) {
                for(j=(njo+1); j <= nj; j++) {
                        inmnh3=inmnh3+((xold[j][i]*rhocar*v[j][i])
                                +(rhonh3[j][i]*v[j][i])); }}
```

```
        /* calculate cooling power, heating power and COP */

        if((f_power=fopen("power.dat","a")) == NULL) {
                printf("Error, cannot open file 'power.dat' for appending\n");
                exit(0); }

        coolpow=(((conc2-conç1)*(hge-hfc)*mcar*volfactor)/dur);
        spcoolpow=(((conc2-conc1)*(hge-hfc))/dur);
        heatpow=((qin*volfactor)/dur);
        spheatpow=(qin/(mcar*dur));
        heatpowcar=((qincar*volfactor)/dur);
        spheatpowcar=(qincar/(mcar*dur));

        if(qin == 0) {
                cop=0; }
        else {
                cop=(spcoolpow/spheatpow); }

        if(qincar == 0) {
                copcar=0; }
        else {
                copcar=(spcoolpow/spheatpowcar); }

fprintf(f_power," Cooling Power, Heating Power and COP results for 1 Generator\n");
fprintf(f_power," ************************************************************\n\n");
fprintf(f_power," Cooling Power (coolpow) = %lf (W)                              \
      \n\n Specific Cooling Power (spcoolpow) = %lf (W/kg)                       \
      \n\n Heating Power (heatpow) = %lf (W)                                     \
      \n\n Specific Heating Power (spheatpow) = %lf (W/kg)                       \
      \n\n Heating Power - Carbon Only (heatpowcar) = %lf (W)                    \
      \n\n Specific Heating Power - Carbon Only (spheatpowcar) = %lf (W/kg)      \
      \n\n COP (cop) = %lf                                                       \
      \n\n COP - Carbon Only (copcar) = %lf",coolpow, spcoolpow,heatpow,         \
      spheatpow,heatpowcar,spheatpowcar,cop,copcar);

      time=0;
      qin=0;
      qincar=0;
      conc1=0;
      conc2=0;
```

```
        fclose(f_power);
        }

      } while(!fi_exp.eof());

      /* start next cycle and read data file from beginning */

      loop++;
      fi_exp.seekg(0);

/* end of solution time loop */

} while (loop <= sweeps);

/* close data files */

fi_exp.close();

/* end of computation */

printf("\n    **** End of Computation ****\n\n");

return 0;

}  /* end of function main */

/*****************************************************************************/
```

Appendix II

Alternating Direction Explicit

Program Listing

Alternating Direction Explicit 2D Conduction.c

```
/*****************************************************************************
*                                                                            *
*          ***   2 Dimensional Transient Heat Conduction Program   ***      *
*                                                                            *
*            *  Barakat & Clark Alternating Direction Explicit Scheme  *     *
*                                                                            *
*****************************************************************************/

/* preprocessor directives */

#include <stdio.h>
#include <stdlib.h>
#include <math.h>
#include <errno.h>

int main(void)
{

/* define file pointers */

 FILE *f1,*f2,*f3,*f4,*f5,*f6,*f7;
```

```
/* define variables */

 int   i,j,nio,nic,nii,njf,njc,ni,nj,wfile,counta,countb,loop,steps,wscrn;
 int   hour,min,sec,simnum,stepin,cycle,subcycle,iter,terminal,host,wall;

 float  dur,dt,zero,voidvol,kal,ljf,tevap,rhocar,rhoal,tint,tcond,tsint;
 float  rinner,router,psint,halal,leni,lic,dro,drc,dri,dzf,dzc,dtg,cpamm;
 float  alpha,dtgm,lio,dtg1,dtg2,dtg3,nconst,ho,bi,tsintc,psintpa,toheat;
 float  tocool,hoheat,hocool,tiheat,ticool,hiheat,hicool,ljc,lii,cpal,lconc;
 float  lenj,ti,to,hi,halcar,kconst,cpcar,conclimit,clock;

 double hpmax,hp1,hp2,utsnew,upsnew,abstime,heatall,heatpall,dtsat,heatcar,mcar;
 double time,heatpcar,dpsat,subtime,tm1,tm2,tm3,qincar,qin,qin1,qin2,qincar1;
 double qincar2,mtempcar,mt1,mt2,mt3,cop,cop2,dconc,dc1,dc2,dconct,dct1,dct2;
 double mnh3ads,inmnh3,lnh3,cpow2,deltaconc,dctmax,inconc,masstol,coolpow;
 double rcf1,rcf2,rcf3,rcf4,ramm,mnh3a,massflow,lcyctm,inmnh3heat,inmnh3cool;

 double pmnh31,pmnh32,pmnh33,pmerr1,pmerr2,pmerr3,pts1,pts2,ppsnew,ptsold;
 double ptsnew,ptsnewc,prcf1,prcf2,prcf3,prcf4,pramm,ptsinc,phgamm,phfamm;

 double qmnh31,qmnh32,qmnh33,qmerr1,qmerr2,qmerr3,qts1,qts2,qpsnew,qtsold;
 double qtsnew,qtsnewc,qrcf1,qrcf2,qrcf3,qrcf4,qramm,qtsinc,qhgamm,qhfamm;

/* define arrays */

 float  kn[17][26],ks[17][26],ke[17][26],kw[17][26],posi[26],posj[26],rij[26];
 float  dzn[17][26],dzs[17][26],dre[17][26],drw[17][26];

 double uold[17][26],unew[17][26],uoldc[17][26],unewc[17][26],rho[17][26];
 double an[17][26],as[17][26],ae[17][26],aw[17][26],v[17][26],temp[17][26];
 double rhoamm[17][26],timea[17];

 double pold[17][26],pnew[17][26],pconc1[17][26],pconc2[17][26],cpcarp[17][26];
 double cpepa[17][26],cpepb[17][26],cpepc[17][26],cpepd[17][26],cpepe[17][26];
 double phvnh3[17][26],pconcold[17][26],pconcnew[17][26];

 double qold[17][26],qnew[17][26],qconc1[17][26],qconc2[17][26],cpcarq[17][26];
 double cpeqa[17][26],cpeqb[17][26],cpeqc[17][26],cpeqd[17][26],cpeqe[17][26];
 double qhvnh3[17][26],qconcold[17][26],qconcnew[17][26];
```

```
/* define number of walls */

 wall=1;
 if(wall > 2)
  wall=1;

/* define boundary conditions */

 tiheat=0;
 ticool=0;
 hiheat=0;
 hicool=0;
 toheat=473;
 tocool=303;
 hoheat=5000;
 hocool=1000;
 halcar=200;

/* define material properties */

 kal=200;
 rhoal=2700;
 rhocar=713;
 cpal=900;
 cpcar=1200;
 cpamm=4734;

/* define geometry */

 simnum=1;

/*
carbon radial length */

 lic=(25.0/1000);

/*
carbon (half) thickness */

 ljc=(1.0/1000);
```

```
/*
fin (half) thickness */

 ljf=(0.1/1000);


/* define numerical grid */

 if(wall == 1) {
  lio=(5.0/1000);
  rinner=0;
  router=(rinner+lic+lio);
  nio=2;
  nic=23;
  njf=2;
  njc=14;
  ni=(nio+nic);
  nj=(njf+njc);
  drc=(lic/(nic-0.5));
  dro=(lio/(nio-0.5));
  dzf=(ljf/(njf-0.5));
  dzc=(ljc/(njc-0.5));
 }
 if(wall == 2) {
  lio=(5.0/1000);
  lii=(5.0/1000);
  rinner=(12.5/1000);
  router=(rinner+lii+lic+lio);
  nio=2;
  nic=21;
  nii=2;
  njf=2;
  njc=14;
  ni=(nio+nic+nii);
  nj=(njf+njc);
  drc=(lic/nic);
  dro=(lio/(nio-0.5));
  dri=(lii/(nii-0.5));
  dzf=(ljf/(njf-0.5));
  dzc=(ljc/(njc-0.5));
 }
```

```
/* define initial conditions */

 conclimit=(-0.1);
 voidvol=0.4;
 masstol=1e-12;
 tint=323.15;
 tcond=323.15;
 tevap=273.15;
 tsint=273.15;
 ptsinc=0.1;
 qtsinc=0.1;
 psint=(exp(11.749-(2823.4/tsint)));

 for(i=1; i <= ni; i++) {
  for(j=1; j <= nj; j++) {
   pold[j][i]=tint;
   qold[j][i]=tint;
   uold[j][i]=tint;
   uoldc[j][i]=(tint-273);
  }
 }
 for(j=1; j <= nj; j++) {
  for(i=1; i <= nio; i++) {
   cpepc[j][i]=cpal;
   cpeqc[j][i]=cpal;
   cpepe[j][i]=0;
   cpeqe[j][i]=0;
  }
  if(wall == 2) {
   for(i=(nio+nic+1); i <= ni; i++) {
    cpepc[j][i]=cpal;
    cpeqc[j][i]=cpal;
    cpepe[j][i]=0;
    cpeqe[j][i]=0;
   }
  }
 }
 for(i=(nio+1); i <= (nio+nic); i++) {
  for(j=1; j <= njf; j++) {
   cpepc[j][i]=cpal;
   cpeqc[j][i]=cpal;
```

```
      cpepe[j][i]=0;
      cpeqe[j][i]=0;
    }
  }
  ptsold=tsint;
  ptsnew=tsint;
  qtsold=tsint;
  qtsnew=tsint;

/* define dubinin-astakhov parameters */

  lconc=0.270;
  kconst=4.3772;
  nconst=1.1965;
  inconc=(lconc*(exp((-1)*kconst*(pow(((tint/tsint)-1),nconst)))));
  for(i=(nio+1); i <= (nio+nic); i++) {
    for(j=(njf+1); j <= nj; j++) {
      pconcold[j][i]=inconc;
      qconcold[j][i]=inconc;
    }
  }

/* define dr & dz arrays */

  for(j=1; j <= nj; j++) {
    for(i=1; i <= (nio-1); i++) {
      dre[j][i]=dro;
    }
    dre[j][nio]=((dro+drc)/2);
    for(i=(nio+1); i <= (nio+nic-1); i++) {
      dre[j][i]=drc;
    }
    if(wall == 2) {
      dre[j][(nio+nic)]=((drc+dri)/2);
      for(i=(nio+nic+1); i <= (ni-1); i++) {
        dre[j][i]=dri;
      }
    }
    dre[j][ni]=0;
    drw[j][1]=0;
    for(i=2; i <= nio; i++) {
```

```
    drw[j][i]=dro;
   }
   drw[j][(nio+1)]=((dro+drc)/2);
   for(i=(nio+2); i <= (nio+nic); i++) {
    drw[j][i]=drc;
   }
   if(wall == 2) {
    drw[j][(nio+nic+1)]=((drc+dri)/2);
    for(i=(nio+nic+2); i <= ni; i++) {
     drw[j][i]=dri;
    }
   }
  }
  for(i=1; i <= ni; i++) {
   dzn[1][i]=0;
   for(j=2; j <= njf; j++) {
    dzn[j][i]=dzf;
   }
   dzn[(njf+1)][i]=((dzc+dzf)/2);
   for(j=(njf+2); j <= nj; j++) {
    dzn[j][i]=dzc;
   }
   for(j=1; j <= (njf-1); j++) {
    dzs[j][i]=dzf;
   }
   dzs[njf][i]=((dzc+dzf)/2);
   for(j=(njf+1); j <= (nj-1); j++) {
    dzs[j][i]=dzc;
   }
   dzs[nj][i]=0;
  }

/* define nodal positions */

  leni=0;
  for(i=1; i <= ni; i++) {
   leni=leni+drw[1][i];
   posi[i]=leni;
   rij[i]=(router-posi[i]);
  }
  lenj=0;
```

```
 for(j=nj; j >= 1; j--) {
  lenj=lenj+dzs[j][1];
  posj[(nj-j+1)]=lenj;
 }

/* define a, v, rho & k arrays */

 for(j=1; j <= nj; j++) {
  for(i=1; i <= ni; i++) {
   an[j][i]=(rij[i]+((drw[j][i]-dre[j][i])/4))*((dre[j][i]+drw[j][i])/2);
   as[j][i]=(rij[i]+((drw[j][i]-dre[j][i])/4))*((dre[j][i]+drw[j][i])/2);
   ae[j][i]=(rij[i]-(dre[j][i]/2))*((dzn[j][i]+dzs[j][i])/2);
   aw[j][i]=(rij[i]+(drw[j][i]/2))*((dzn[j][i]+dzs[j][i])/2);
  }
 }
 for(j=1; j <= nj; j++) {
  for(i=1; i <= ni; i++) {
   v[j][i]=(rij[i]+((drw[j][i]-dre[j][i])/4))*((dre[j][i]+drw[j][i])/2)
        *((dzn[j][i]+dzs[j][i])/2);
  }
 }
 for(j=1; j <= nj; j++) {
  for(i=1; i <= nio; i++) {
   kn[j][i]=kal;
   ks[j][i]=kal;
   ke[j][i]=kal;
   kw[j][i]=kal;
   rho[j][i]=rhoal;
  }
  if(wall == 2) {
   for(i=(nio+nic+1); i <= ni; i++) {
    kn[j][i]=kal;
    ks[j][i]=kal;
    ke[j][i]=kal;
    kw[j][i]=kal;
    rho[j][i]=rhoal;
   }
  }
 }
 for(i=(nio+1); i <= (nio+nic); i++) {
  for(j=1; j <= njf; j++) {
```

```
    kn[j][i]=kal;
    ks[j][i]=kal;
    ke[j][i]=kal;
    kw[j][i]=kal;
    rho[j][i]=rhoal;
   }
  }

/* include 'halal' for heat transfer between fin & walls */

  halal=0;
  if(halal > 0) {
   for(j=1; j <= njf; j++) {
    ke[j][nio]=(halal*dre[j][nio]);
    kw[j][(nio+1)]=(halal*drw[j][(nio+1)]);
    if(wall == 2) {
     ke[j][nio+nic]=(halal*dre[j][(nio+nic)]);
     kw[j][(nio+nic+1)]=(halal*drw[j][(nio+nic+1)]);
    }
   }
  }

/* calculate mass of carbon */

  mcar=0;
  for(j=(njf+1); j <= nj; j++) {
   for(i=(nio+1); i <= (nio+nic); i++) {
    mcar=mcar+(rhocar*v[j][i]);
   }
  }

/* calculate density of ammonia in voids */

  psintpa=(psint*100000);
  tsintc=(tsint-273.15);

  rcf1=((1e-05)*((0.00000068892947*(pow(tsintc,3)))+(0.00009565787857*
     (pow(tsintc,2)))+(0.00844971035705*tsintc)+0.32843436542347));

  rcf2=((1e-02)*((-0.00000052403299*(pow(tsintc,3)))+(-0.00006905794744*
     (pow(tsintc,2)))+(-0.00531432390974*tsintc)-0.18587792629441));
```

```
rcf3=(((0.00000140592901*(pow(tsintc,3)))+(0.00017767403458*
     (pow(tsintc,2)))+(0.01203459890161*tsintc)+0.37471284774418));

 rcf4=((1e+04)*((-0.00000001416664*(pow(tsintc,3)))+(-0.00000177131542*
     (pow(tsintc,2)))+(-0.00010988317152*tsintc)+0.04572946161140));

 ramm=((rcf1*(pow(tsintc,3)))+(rcf2*(pow(tsintc,2)))+(rcf3*tsintc)+rcf4);

 for(i=(nio+1); i <= (nio+nic); i++) {
  for(j=(njf+1); j <= nj; j++) {
   rhoamm[j][i]=(((psintpa)/(ramm*uold[j][i]))*voidvol);
  }
 }

/* calculate initial mass of ammonia in bed */

 inmnh3=0;
 for(i=(nio+1); i <= (nio+nic); i++) {
  for(j=(njf+1); j <= nj; j++) {
   inmnh3=inmnh3+((inconc*rhocar*v[j][i])+(rhoamm[j][i]*v[j][i]));
  }
 }

/* set time step and input initial parameters */

  alpha=(kal/(rhoal*cpal));
  bi=((hoheat*dro)/kal);
  dtg1=((pow((dro*dzf),2))/(2*alpha*(2+bi)*((pow(dzf,2))+(pow(dro,2)))));
  dtg2=((pow((drc*dzf),2))/(2*alpha*(2+bi)*((pow(dzf,2))+(pow(drc,2)))));
  dtg3=((pow((dro*dzc),2))/(2*alpha*(2+bi)*((pow(dzc,2))+(pow(dro,2)))));
  if((dtg1 <= dtg2) && (dtg1 <= dtg3)) {
   dtg=dtg1;
  }
  if((dtg2 <= dtg1) && (dtg2 <= dtg3)) {
   dtg=dtg2;
  }
  if((dtg3 <= dtg1) && (dtg3 <= dtg2)) {
   dtg=dtg3;
  }
  dtgm=(dtg*7.8);
  printf("\nInitial Estimate for the Maximum Timestep is %f\n\n",dtg);
```

```
  printf("First Guess with a Stability Factor of 7.8 is %f\n\n",dtgm);
  printf("Enter the Required Value for the Timestep\n\n");
  scanf("%f",&dt);
  printf("\nEnter the Required Number of Cycles\n\n");
  scanf("%d",&cycle);
  dur=(1e+05*(-(2.38*(pow(conclimit,3)))-(0.38*(pow(conclimit,2)))
      -(0.022*conclimit)-0.0002));
  steps=((dur/dt)*2*cycle);
  printf("\nVery Approximate Number of Time Steps = %d\n\n",steps);
  wfile=(250*2*cycle);
  stepin=(steps/wfile);
  printf("Suggested Interval to Give %d File Writes = %d\n\n",wfile,stepin);
  wfile=0;
  printf("Enter the Time Step Interval Between File Writes\n\n");
  scanf("%d",&wfile);
  printf("\nEnter the Time Step Interval Between Screen Writes\n\n");
  scanf("%d",&wscrn);
  clock=(steps/(8.3));
  hour=(clock/3600);
  min=((clock-(3600*hour))/60);
  sec=(clock-(60*min)-(3600*hour));
  printf("\nComputation Time Approx %d hours %d min %d sec\n\n",hour,min,sec);

/* set counters */

 mtempcar=tint;
 subcycle=1;
 abstime=0;
 subtime=0;
 qin=0;
 qin1=0;
 qin2=0;
 qincar=0;
 qincar1=0;
 qincar2=0;
 mnh3ads=0;
 counta=0;
 countb=0;
 dconc=0;
 lnh3=0;
 iter=0;
```

```
 zero=0;
 time=0;

 for(j=1; j <= nj; j++) {
  timea[j]=abstime;
 }

/* create data files */

 if((f1=fopen("temp.dat","w")) == NULL) {
  printf("Error, cannot open file 'temp.dat' for writing\n");
  exit(0);
 }
 if((f2=fopen("posn.dat","w")) == NULL) {
  printf("Error, cannot open file 'posn.dat' for writing\n");
  exit(0);
 }
 if((f3=fopen("power.dat","w")) == NULL) {
  printf("Error, cannot open file 'power.dat' for writing\n");
  exit(0);
 }
 if((f4=fopen("conc.dat","w")) == NULL) {
  printf("Error, cannot open file 'conc.dat' for writing\n");
  exit(0);
 }
 if((f5=fopen("satn.dat","w")) == NULL) {
  printf("Error, cannot open file 'satn.dat' for writing\n");
  exit(0);
 }

/* write initial data to file */

 for(j=1; j <= (nj-1); j++) {
  fprintf(f1,"%f, ",timea[j]);
 }
 fprintf(f1,"%f\n",timea[nj]);

 for(i=1; i <= (ni-1); i++) {
  for(j=1; j <= (nj-1); j++) {
   fprintf(f1,"%f, ",uoldc[j][i]);
  }
```

```
  fprintf(f1,"%f\n",uoldc[nj][i]);
 }
 for(j=1; j <= (nj-1); j++) {
  fprintf(f1,"%f, ",uoldc[j][ni]);
 }
 fprintf(f1,"%f\n",uoldc[nj][ni]);

 for(i=1; i <= (ni-1); i++) {
  fprintf(f2,"%f, ",posi[i]);
 }
 fprintf(f2,"%f\n",posi[ni]);

 for(i=1; i <= (ni-1); i++) {
  fprintf(f2,"%f, ",posj[i]);
 }
 fprintf(f2,"%f\n",posj[ni]);

 for(i=1; i <= (ni-1); i++) {
  fprintf(f2,"%f, ",rij[i]);
 }
 fprintf(f2,"%f\n",rij[ni]);

 fprintf(f2,"%f, %d, %d, %f",dt,cycle,wfile,conclimit);
 fprintf(f3,"%f, %f, %f, %f, %f, %f, %f\n",zero,zero,zero,mtempcar,
        zero,zero,zero);
 fprintf(f4,"%f, %f, %f, %f, %f, %f, %f\n",zero,zero,zero,mtempcar,
        zero,zero,zero);
 fprintf(f5,"%f, %f, %f, %f, %f, %f\n",zero,zero,zero,mtempcar,zero,zero);
 mtempcar=0;

/* start of solution time loop */

 loop=1;
 do {
  time=0;
  subtime=0;
  subcycle=1;
  if((dconc > conclimit) && (subcycle == 1)) {
   to=toheat;
   ho=hoheat;
   ti=tiheat;
```

```
    hi=hiheat;

/* set mass in system before heating */

    inmnh3heat=0;
    for(i=(nio+1); i <= (nio+nic); i++) {
     for(j=(njf+1); j <= nj; j++) {
      inmnh3heat=inmnh3heat+((((pconcold[j][i]+qconcold[j][i])/2)*rhocar
                  *v[j][i])+(rhoamm[j][i]*v[j][i]));
     }
    }
   }

/* start of time marching loop */

   do {
   iter=iter+1;
   time=time+dt;
   subtime=subtime+dt;
   abstime=abstime+dt;

/*****************************************************************************
*                          * start of barakat & clark ade computation *                          *
*****************************************************************************/

/* calculation of bed carbon conductivity for "p" sweep */

   for(i=(nio+1); i <= (nio+nic); i++) {
    for(j=(njf+1); j <= nj; j++) {
     kn[j][i]=(0.4732-(0.0004*(pold[j][i]-273.15)));
     ks[j][i]=(0.4732-(0.0004*(pold[j][i]-273.15)));
     ke[j][i]=(0.4732-(0.0004*(pold[j][i]-273.15)));
     kw[j][i]=(0.4732-(0.0004*(pold[j][i]-273.15)));
    }
   }
   for(j=(njf+1); j <= nj; j++) {
    ke[j][nio]=(halcar*dre[j][nio]);
    kw[j][(nio+1)]=(halcar*drw[j][(nio+1)]);
    if(wall == 2) {
     ke[j][(nio+nic)]=(halcar*dre[j][(nio+nic)]);
     kw[j][(nio+nic+1)]=(halcar*drw[j][(nio+nic+1)]);
```

```
    }
   }
   for(i=(nio+1); i <= (nio+nic); i++) {
    ks[njf][i]=(halcar*dzs[njf][i]);
    kn[(njf+1)][i]=(halcar*dzn[(njf+1)][i]);
   }

/* initial guess for "p" sweep tsat */

   if((ptsold < tcond) && (subcycle == 1)) {
    ptsnew=(ptsold+ptsinc);
   }
   if((ptsold > tevap) && (subcycle == 2)) {
    ptsnew=(ptsold-ptsinc);
   }

 label_p1:
   ppsnew=((exp(11.749-(2823.4/ptsnew)))*(1e+05));

/* calcuation to include bed void volume for "p" sweep */

   ptsnewc=(ptsnew-273.15);

   prcf1=((1e-05)*((0.00000068892947*(pow(ptsnewc,3)))+(0.00009565787857
         *(pow(ptsnewc,2)))+(0.00844971035705*ptsnewc)+0.32843436542347));

   prcf2=((1e-02)*((-0.00000052403299*(pow(ptsnewc,3)))+(-0.00006905794744
         *(pow(ptsnewc,2)))+(-0.00531432390974*ptsnewc)-0.18587792629441));

   prcf3=(((0.00000140592901*(pow(ptsnewc,3)))+(0.00017767403458
         *(pow(ptsnewc,2)))+(0.01203459890161*ptsnewc)+0.37471284774418));

   prcf4=((1e+04)*((-0.00000001416664*(pow(ptsnewc,3)))+(-0.00000177131542
         *(pow(ptsnewc,2)))+(-0.00010988317152*ptsnewc)+0.04572946161140));

   pramm=((prcf1*(pow(ptsnewc,3)))+(prcf2*(pow(ptsnewc,2)))
          +(prcf3*ptsnewc)+prcf4);

   for(i=(nio+1); i <= (nio+nic); i++) {
    for(j=(njf+1); j <= nj; j++) {
     rhoamm[j][i]=(((ppsnew)/(pramm*pold[j][i]))*voidvol);
```

```
      rho[j][i]=(rhocar+rhoamm[j][i]);
    }
   }

/* calculation of effective cp coefficients for "p" sweep */

   for(i=(nio+1); i <= (nio+nic); i++) {
    for(j=(njf+1); j <= nj; j++) {
     cpcarp[j][i]=(175+(2.245*pold[j][i]));
     phfamm=(423.498846153846+(4.584407092907*(pold[j][i]-273.15))
            +(0.002471878122*(pow((pold[j][i]-273.15),2))));
     phgamm=(1685.15907342657+(1.01716208791*(pold[j][i]-273.15))
            -(0.00810606893*(pow((pold[j][i]-273.15),2))));
     phvnh3[j][i]=(phgamm-phfamm);
     cpepa[j][i]=(cpcarp[j][i]+(pconcold[j][i]*cpamm));
     cpepb[j][i]=(((phvnh3[j][i]*pold[j][i])/ptsold)*(kconst*nconst
              *pconcold[j][i]*((pow(pold[j][i],(nconst-1)))
              /(pow(ptsold,nconst)))));
     cpepc[j][i]=(cpepa[j][i]+cpepb[j][i]);
     cpepd[j][i]=((cpepb[j][i]*(ptsnew-ptsold)*pold[j][i])/ptsold);
     cpepe[j][i]=((cpepd[j][i])/(cpepc[j][i]));
    }
   }

/*****************************************************************************
*          *** marching through "p" equations from bottom left-hand corner ***          *
*****************************************************************************/

   j=nj;
   i=1;

/* node 7 p equation */
   pnew[j][i]=((pold[j][i]+cpepe[j][i])+((dt/(rho[j][i]*v[j][i]*cpepc[j][i]))
            *((ho*aw[j][i]*(to-(pold[j][i])))+(((ke[j][i]*ae[j][i])
            /(dre[j][i]))*(pold[j][(i+1)]-pold[j][i]))+(((kn[j][i]*an[j][i])
            /(dzn[j][i]))*(pold[(j-1)][i]-pold[j][i])))));

   for(i=2; i <= (ni-1); i++) {

/* node 8 p equation */
    pnew[j][i]=((((pold[j][i]+cpepe[j][i])*((rho[j][i]*v[j][i]*cpepc[j][i])
```

```
            /dt))+(((kn[j][i]*an[j][i])/(dzn[j][i]))*(pold[(j-1)][i]
            -pold[j][i]))+(((ke[j][i]*ae[j][i])/(dre[j][i]))*(pold[j][(i+1)]
            -pold[j][i]))+(((kw[j][i]*aw[j][i])/(drw[j][i]))
            *(pnew[j][(i-1)])))/(((kw[j][i]*aw[j][i])/(drw[j][i]))
            +((rho[j][i]*v[j][i]*cpepc[j][i])/dt)));
  }
  i=ni;

/* node 9 p equation */
  pnew[j][i]=((((pold[j][i]+cpepe[j][i])*((rho[j][i]*v[j][i]*cpepc[j][i])
          /dt))+(hi*ae[j][i]*(ti-(pold[j][i])))+(((kw[j][i]*aw[j][i])
          /(drw[j][i]))*(pnew[j][(i-1)]))+(((kn[j][i]*an[j][i])
          /(dzn[j][i]))*(pold[(j-1)][i]-pold[j][i])))/(((kw[j][i]
          *aw[j][i])/(drw[j][i]))+((rho[j][i]*v[j][i]*cpepc[j][i])/dt)));

  for(j=(nj-1); j >= 2; j--) {
   i=1;

/* node 4 p equation */
   pnew[j][i]=((((pold[j][i]+cpepe[j][i])*((rho[j][i]*v[j][i]*cpepc[j][i])
          /dt))+(ho*aw[j][i]*(to-(pold[j][i])))+(((ke[j][i]*ae[j][i])
          /(dre[j][i]))*(pold[j][(i+1)]-pold[j][i]))+(((kn[j][i]*an[j][i])
          /(dzn[j][i]))*(pold[(j-1)][i]-pold[j][i]))+(((ks[j][i]*as[j][i])
          /(dzs[j][i]))*(pnew[(j+1)][i])))/(((ks[j][i]*as[j][i])
          /(dzs[j][i]))+((rho[j][i]*v[j][i]*cpepc[j][i])/dt)));

   for(i=2; i <= (ni-1); i++) {

/* node 5 p equation */
    pnew[j][i]=((((pold[j][i]+cpepe[j][i])*((rho[j][i]*v[j][i]*cpepc[j][i])
          /dt))+(((ke[j][i]*ae[j][i])/(dre[j][i]))*(pold[j][(i+1)]
          -pold[j][i]))+(((kw[j][i]*aw[j][i])/(drw[j][i]))
          *(pnew[j][(i-1)]))+(((kn[j][i]*an[j][i])/(dzn[j][i]))
          *(pold[(j-1)][i]-pold[j][i]))+(((ks[j][i]*as[j][i])
          /(dzs[j][i]))*(pnew[(j+1)][i])))/(((kw[j][i]*aw[j][i])
          /(drw[j][i]))+((ks[j][i]*as[j][i])/(dzs[j][i]))+((rho[j][i]
          *v[j][i]*cpepc[j][i])/dt)));
  }
  i=ni;
```

```
/* node 6 p equation */
    pnew[j][i]=((((pold[j][i]+cpepe[j][i])*((rho[j][i]*v[j][i]*cpepc[j][i])
              /dt))+(hi*ae[j][i]*(ti-(pold[j][i])))+(((kw[j][i]*aw[j][i])
              /(drw[j][i]))*(pnew[j][(i-1)]))+(((kn[j][i]*an[j][i])
              /(dzn[j][i]))*(pold[(j-1)][i]-pold[j][i]))+(((ks[j][i]
              *as[j][i])/(dzs[j][i]))*(pnew[(j+1)][i])))/(((kw[j][i]
              *aw[j][i])/(drw[j][i]))+((ks[j][i]*as[j][i])/(dzs[j][i]))
              +((rho[j][i]*v[j][i]*cpepc[j][i])/dt)));
  }
  j=1;
  i=1;

/* node 1 p equation */
  pnew[j][i]=((((pold[j][i]+cpepe[j][i])*((rho[j][i]*v[j][i]*cpepc[j][i])
            /dt))+(ho*aw[j][i]*(to-(pold[j][i])))+(((ke[j][i]*ae[j][i])
            /(dre[j][i]))*(pold[j][(i+1)]-pold[j][i]))+(((ks[j][i]
            *as[j][i])/(dzs[j][i]))*(pnew[(j+1)][i])))/(((ks[j][i]
            *as[j][i])/(dzs[j][i]))+((rho[j][i]*v[j][i]*cpepc[j][i])/dt)));

  for(i=2; i <= (ni-1); i++) {

/* node 2 p equation */
    pnew[j][i]=((((pold[j][i]+cpepe[j][i])*((rho[j][i]*v[j][i]*cpepc[j][i])
              /dt))+(((ks[j][i]*as[j][i])/(dzs[j][i]))*(pnew[(j+1)][i]))
              +(((kw[j][i]*aw[j][i])/(drw[j][i]))*(pnew[j][(i-1)]))
              +(((ke[j][i]*ae[j][i])/(dre[j][i]))*(pold[j][(i+1)]
              -pold[j][i])))/(((ks[j][i]*as[j][i])/(dzs[j][i]))+((kw[j][i]
              *aw[j][i])/(drw[j][i]))+((rho[j][i]*v[j][i]*cpepc[j][i])/dt)));
  }
  i=ni;

/* node 3 p equation */
  pnew[j][i]=((((pold[j][i]+cpepe[j][i])*((rho[j][i]*v[j][i]*cpepc[j][i])
            /dt))+(hi*ae[j][i]*(ti-(pold[j][i])))+(((kw[j][i]*aw[j][i])
            /(drw[j][i]))*(pnew[j][(i-1)]))+(((ks[j][i]*as[j][i])
            /(dzs[j][i]))*(pnew[(j+1)][i])))/(((kw[j][i]*aw[j][i])
            /(drw[j][i]))+((ks[j][i]*as[j][i])/(dzs[j][i]))+((rho[j][i]
            *v[j][i]*cpepc[j][i])/dt)));

/*****************************************************************************/
```

```
/* evaluation of "p" sweep tsat and mass balance */

  if((ptsold >= tcond) && (subcycle == 1)) {
    ptsold=tcond;
    ptsnew=tcond;
    for(i=(nio+1); i <= (nio+nic); i++) {
      for(j=(njf+1); j <= nj; j++) {
        pconcnew[j][i]=(lconc*(exp((-1)*kconst*(pow(((pnew[j][i]/ptsnew)-1),nconst)))));
      }
    }
    goto label_p4;
  }
  if((ptsold <= tevap) && (subcycle == 2)) {
    ptsold=tevap;
    ptsnew=tevap;
    for(i=(nio+1); i <= (nio+nic); i++) {
      for(j=(njf+1); j <= nj; j++) {
        pconcnew[j][i]=(lconc*(exp((-1)*kconst*(pow(((pnew[j][i]/ptsnew)-1),nconst)))));
      }
    }
    goto label_p4;
  }
  pmnh31=0;
  pmnh32=0;
  pmnh33=0;
  pts1=ptsnew;
  if(subcycle == 1) {
    pts2=(pts1+0.1);
  }
  if(subcycle == 2) {
    pts2=(pts1-0.1);
  }
  for(i=(nio+1); i <= (nio+nic); i++) {
    for(j=(njf+1); j <= nj; j++) {
      pconc1[j][i]=(lconc*(exp((-1)*kconst*(pow(((pnew[j][i]/pts1)-1),nconst)))));
      pmnh31=pmnh31+((pconc1[j][i]*rhocar*v[j][i])+(rhoamm[j][i]*v[j][i]));
    }
  }
  if(subcycle == 1) {
    pmerr1=(inmnh3heat-pmnh31);
  }
```

```
if(subcycle == 2) {
 pmerr1=(inmnh3cool-pmnh31);
}
if(fabs(pmerr1) <= masstol) {
 for(i=1; i <= ni; i++) {
  for(j=1; j <= nj; j++) {
   pconcnew[j][i]=pconc1[j][i];
  }
 }
 goto label_p3;
}
if(fabs(pmerr1) > masstol) {
 for(i=(nio+1); i <= (nio+nic); i++) {
  for(j=(njf+1); j <= nj; j++) {
   pconc2[j][i]=(lconc*(exp((-1)*kconst*(pow(((pnew[j][i]/pts2)-1),nconst)))));
   pmnh32=pmnh32+((pconc2[j][i]*rhocar*v[j][i])+(rhoamm[j][i]*v[j][i]));
  }
 }
 if(subcycle == 1) {
  pmerr2=(inmnh3heat-pmnh32);
 }
 if(subcycle == 2) {
  pmerr2=(inmnh3cool-pmnh32);
 }
label_p2:
 ptsnew=(((pmerr2*pts1)-(pmerr1*pts2))/(pmerr2-pmerr1));
 for(i=(nio+1); i <= (nio+nic); i++) {
  for(j=(njf+1); j <= nj; j++) {
   pconcnew[j][i]=(lconc*(exp((-1)*kconst*(pow(((pnew[j][i]/ptsnew)-1),nconst)))));
   pmnh33=pmnh33+((pconcnew[j][i]*rhocar*v[j][i])+(rhoamm[j][i]*v[j][i]));
  }
 }
 if(subcycle == 1) {
  pmerr3=(inmnh3heat-pmnh33);
 }
 if(subcycle == 2) {
  pmerr3=(inmnh3cool-pmnh33);
 }
 if(fabs(pmerr3) > masstol) {
  pts1=pts2;
  pmerr1=pmerr2;
```

```
      pts2=ptsnew;
      pmerr2=pmerr3;
      pmnh33=0;
      goto label_p2;
     }
     goto label_p1;
    }
 label_p3:
  if((ptsnew >= tcond) && (subcycle == 1)) {
    ptsnew=tcond;
    for(i=(nio+1); i <= (nio+nic); i++) {
      for(j=(njf+1); j <= nj; j++) {
        pconcnew[j][i]=(lconc*(exp((-1)*kconst*(pow(((pnew[j][i]/ptsnew)-1),nconst)))));
      }
    }
  }
  if((ptsnew <= tevap) && (subcycle == 2)) {
    ptsnew=tevap;
    for(i=(nio+1); i <= (nio+nic); i++) {
      for(j=(njf+1); j <= nj; j++) {
        pconcnew[j][i]=(lconc*(exp((-1)*kconst*(pow(((pnew[j][i]/ptsnew)-1),nconst)))));
      }
    }
  }
 label_p4:
  ptsinc=(ptsnew-ptsold);
  ptsold=ptsnew;
    for(i=1; i <= ni; i++) {
      for(j=1; j <= nj; j++) {
        pconcold[j][i]=pconcnew[j][i];
      }
    }

/*****************************************************************************/

/* calculation of bed carbon conductivity for "q" sweep */

   for(i=(nio+1); i <= (nio+nic); i++) {
    for(j=(njf+1); j <= nj; j++) {
      kn[j][i]=(0.4732-(0.0004*(qold[j][i]-273.15)));
      ks[j][i]=(0.4732-(0.0004*(qold[j][i]-273.15)));
```

```
      ke[j][i]=(0.4732-(0.0004*(qold[j][i]-273.15)));
      kw[j][i]=(0.4732-(0.0004*(qold[j][i]-273.15)));
     }
    }
    for(j=(njf+1); j <= nj; j++) {
     ke[j][nio]=(halcar*dre[j][nio]);
     kw[j][(nio+1)]=(halcar*drw[j][(nio+1)]);
     if(wall == 2) {
      ke[j][(nio+nic)]=(halcar*dre[j][(nio+nic)]);
      kw[j][(nio+nic+1)]=(halcar*drw[j][(nio+nic+1)]);
     }
    }
    for(i=(nio+1); i <= (nio+nic); i++) {
     ks[njf][i]=(halcar*dzs[njf][i]);
     kn[(njf+1)][i]=(halcar*dzn[(njf+1)][i]);
    }

/* initial guess for "q" sweep tsat */

    if((qtsold < tcond) && (subcycle == 1)) {
     qtsnew=(qtsold+qtsinc);
    }
    if((qtsold > tevap) && (subcycle == 2)) {
     qtsnew=(qtsold-qtsinc);
    }
   label_q1:
    qpsnew=((exp(11.749-(2823.4/qtsnew)))*(1e+05));

/* calcuation to include bed void volume for "q" sweep */

    qtsnewc=(qtsnew-273.15);

    qrcf1=((1e-05)*((0.00000068892947*(pow(qtsnewc,3)))+(0.00009565787857
          *(pow(qtsnewc,2)))+(0.00844971035705*qtsnewc)+0.32843436542347));

    qrcf2=((1e-02)*((-0.00000052403299*(pow(qtsnewc,3)))+(-0.00006905794744
          *(pow(qtsnewc,2)))+(-0.00531432390974*qtsnewc)-0.18587792629441));

    qrcf3=(((0.00000140592901*(pow(qtsnewc,3)))+(0.00017767403458
          *(pow(qtsnewc,2)))+(0.01203459890161*qtsnewc)+0.37471284774418));
```

```
  qrcf4=((1e+04)*((-0.00000001416664*(pow(qtsnewc,3)))+(-0.00000177131542
        *(pow(qtsnewc,2)))+(-0.00010988317152*qtsnewc)+0.04572946161140));

  qramm=((qrcf1*(pow(qtsnewc,3)))+(qrcf2*(pow(qtsnewc,2)))
        +(qrcf3*qtsnewc)+qrcf4);

  for(i=(nio+1); i <= (nio+nic); i++) {
   for(j=(njf+1); j <= nj; j++) {
    rhoamm[j][i]=(((qpsnew)/(qramm*qold[j][i]))*voidvol);
    rho[j][i]=(rhocar+rhoamm[j][i]);
   }
  }

/* calculation of effective cp coefficients for "q" sweep */

  for(i=(nio+1); i <= (nio+nic); i++) {
   for(j=(njf+1); j <= nj; j++) {
    cpcarq[j][i]=(175+(2.245*qold[j][i]));
    qhfamm=(423.498846153846+(4.584407092907*(qold[j][i]-273.15))
          +(0.002471878122*(pow((qold[j][i]-273.15),2))));
    qhgamm=(1685.15907342657+(1.01716208791*(qold[j][i]-273.15))
          -(0.00810606893*(pow((qold[j][i]-273.15),2))));
    qhvnh3[j][i]=(qhgamm-qhfamm);
    cpeqa[j][i]=(cpcarq[j][i]+(qconcold[j][i]*cpamm));
    cpeqb[j][i]=(((qhvnh3[j][i]*qold[j][i])/qtsold)*(kconst*nconst
          *qconcold[j][i]*((pow(qold[j][i],(nconst-1)))
          /(pow(qtsold,nconst)))));
    cpeqc[j][i]=(cpeqa[j][i]+cpeqb[j][i]);
    cpeqd[j][i]=((cpeqb[j][i]*(qtsnew-qtsold)*qold[j][i])/qtsold);
    cpeqe[j][i]=((cpeqd[j][i])/(cpeqc[j][i]));
   }
  }

/*****************************************************************************
*          *** marching through "q" equations from top right-hand corner ***      *
*****************************************************************************/

  j=1;
  i=ni;
```

```
/* node 3 q equation */
   qnew[j][i]=((qold[j][i]+cpeqe[j][i])+((dt/(rho[j][i]*v[j][i]*cpeqc[j][i]))
              *((((kw[j][i]*aw[j][i])/(drw[j][i]))*(qold[j][(i-1)]
              -qold[j][i]))+(hi*ae[j][i]*(ti-(qold[j][i])))+(((ks[j][i]
              *as[j][i])/(dzs[j][i]))*(qold[(j+1)][i]-qold[j][i])))));

   for(i=(ni-1); i >= 2; i--) {

/* node 2 q equation */
    qnew[j][i]=((((qold[j][i]+cpeqe[j][i])*((rho[j][i]*v[j][i]*cpeqc[j][i])
               /dt))+(((ks[j][i]*as[j][i])/(dzs[j][i]))*(qold[(j+1)][i]
               -qold[j][i]))+(((kw[j][i]*aw[j][i])/(drw[j][i]))
               *(qold[j][(i-1)]-qold[j][i]))+(((ke[j][i]*ae[j][i])/(dre[j][i]))
               *(qnew[j][(i+1)])))/(((ke[j][i]*ae[j][i])/(dre[j][i]))
               +((rho[j][i]*v[j][i]*cpeqc[j][i])/dt)));
   }
   i=1;

/* node 1 q equation */
   qnew[j][i]=((((qold[j][i]+cpeqe[j][i])*((rho[j][i]*v[j][i]*cpeqc[j][i])
              /dt))+(ho*aw[j][i]*(to-(qold[j][i])))+(((ke[j][i]*ae[j][i])
              /(dre[j][i]))*qnew[j][(i+1)])+(((ks[j][i]*as[j][i])/(dzs[j][i]))
              *(qold[(j+1)][i]-qold[j][i])))/(((ke[j][i]*ae[j][i])
              /(dre[j][i]))+((rho[j][i]*v[j][i]*cpeqc[j][i])/dt)));

   for(j=2; j <= (nj-1); j++) {
    i=ni;

/* node 6 q equation */
    qnew[j][i]=((((qold[j][i]+cpeqe[j][i])*((rho[j][i]*v[j][i]*cpeqc[j][i])
               /dt))+(hi*ae[j][i]*(ti-(qold[j][i])))+(((kw[j][i]*aw[j][i])
               /(drw[j][i]))*(qold[j][(i-1)]-qold[j][i]))+(((kn[j][i]*an[j][i])
               /(dzn[j][i]))*(qnew[(j-1)][i]))+(((ks[j][i]*as[j][i])
               /(dzs[j][i]))*(qold[(j+1)][i]-qold[j][i])))/(((kn[j][i]
               *an[j][i])/(dzn[j][i]))+((rho[j][i]*v[j][i]*cpeqc[j][i])/dt)));

    for(i=(ni-1); i >= 2; i--) {

/* node 5 q equation */
     qnew[j][i]=((((qold[j][i]+cpeqe[j][i])*((rho[j][i]*v[j][i]*cpeqc[j][i])
                /dt))+(((ke[j][i]*ae[j][i])/(dre[j][i]))*(qnew[j][(i+1)]))
```

```
            +(((kw[j][i]*aw[j][i])/(drw[j][i]))*(qold[j][(i-1)]
            -qold[j][i]))+(((kn[j][i]*an[j][i])/(dzn[j][i]))
            *(qnew[(j-1)][i]))+(((ks[j][i]*as[j][i])/(dzs[j][i]))
            *(qold[(j+1)][i]-qold[j][i])))/(((ke[j][i]*ae[j][i])
            /(dre[j][i]))+((kn[j][i]*an[j][i])/(dzn[j][i]))+((rho[j][i]
            *v[j][i]*cpeqc[j][i])/dt)));
  }
  i=1;

/* node 4 q equation */
   qnew[j][i]=((((qold[j][i]+cpeqe[j][i])*((rho[j][i]*v[j][i]*cpeqc[j][i])
            /dt))+(ho*aw[j][i]*(to-(qold[j][i])))+(((ke[j][i]*ae[j][i])
            /(dre[j][i]))*(qnew[j][(i+1)]))+(((kn[j][i]*an[j][i])
            /(dzn[j][i]))*(qnew[(j-1)][i]))+(((ks[j][i]*as[j][i])
            /(dzs[j][i]))*(qold[(j+1)][i]-qold[j][i])))/(((ke[j][i]
            *ae[j][i])/(dre[j][i]))+((kn[j][i]*an[j][i])/(dzn[j][i]))
            +((rho[j][i]*v[j][i]*cpeqc[j][i])/dt)));
  }
  j=nj;
  i=ni;

/* node 9 q equation */
  qnew[j][i]=((((qold[j][i]+cpeqe[j][i])*((rho[j][i]*v[j][i]*cpeqc[j][i])
           /dt))+(hi*ae[j][i]*(ti-(qold[j][i])))+(((kw[j][i]*aw[j][i])
           /(drw[j][i]))*(qold[j][(i-1)]-qold[j][i]))+(((kn[j][i]*an[j][i])
           /(dzn[j][i]))*(qnew[(j-1)][i])))/(((kn[j][i]*an[j][i])
           /(dzn[j][i]))+((rho[j][i]*v[j][i]*cpeqc[j][i])/dt)));

  for(i=(ni-1); i >= 2; i--) {

/* node 8 q equation */
   qnew[j][i]=((((qold[j][i]+cpeqe[j][i])*((rho[j][i]*v[j][i]*cpeqc[j][i])
            /dt))+(((kn[j][i]*an[j][i])/(dzn[j][i]))*(qnew[(j-1)][i]))
            +(((ke[j][i]*ae[j][i])/(dre[j][i]))*(qnew[j][(i+1)]))
            +(((kw[j][i]*aw[j][i])/(drw[j][i]))*(qold[j][(i-1)]
            -qold[j][i])))/(((kn[j][i]*an[j][i])/(dzn[j][i]))+((ke[j][i]
            *ae[j][i])/(dre[j][i]))+((rho[j][i]*v[j][i]*cpeqc[j][i])/dt)));
  }
  i=1;
```

```
/* node 7 q equation */
  qnew[j][i]=((((qold[j][i]+cpeqe[j][i])*((rho[j][i]*v[j][i]*cpeqc[j][i])
            /dt))+(ho*aw[j][i]*(to-(qold[j][i])))+(((ke[j][i]*ae[j][i])
            /(dre[j][i]))*(qnew[j][(i+1)]))+(((kn[j][i]*an[j][i])
            /(dzn[j][i]))*(qnew[(j-1)][i])))/(((ke[j][i]*ae[j][i])
            /(dre[j][i]))+((kn[j][i]*an[j][i])/(dzn[j][i]))+((rho[j][i]
            *v[j][i]*cpeqc[j][i])/dt)));

/*****************************************************************************/

/* evaluation of "q" sweep tsat and mass balance */

  if((qtsold >= tcond) && (subcycle == 1)) {
   qtsold=tcond;
   qtsnew=tcond;
   for(i=(nio+1); i <= (nio+nic); i++) {
    for(j=(njf+1); j <= nj; j++) {
     qconcnew[j][i]=(lconc*(exp((-1)*kconst*(pow(((qnew[j][i]/qtsnew)-1),nconst)))));
    }
   }
   goto label_q4;
  }
  if((qtsold <= tevap) && (subcycle == 2)) {
   qtsold=tevap;
   qtsnew=tevap;
   for(i=(nio+1); i <= (nio+nic); i++) {
    for(j=(njf+1); j <= nj; j++) {
     qconcnew[j][i]=(lconc*(exp((-1)*kconst*(pow(((qnew[j][i]/qtsnew)-1),nconst)))));
    }
   }
   goto label_q4;
  }
  qmnh31=0;
  qmnh32=0;
  qmnh33=0;
  qts1=qtsnew;
  if(subcycle == 1) {
   qts2=(qts1+0.1);
  }
  if(subcycle == 2) {
   qts2=(qts1-0.1);
```

```
 }
 for(i=(nio+1); i <= (nio+nic); i++) {
  for(j=(njf+1); j <= nj; j++) {
   qconc1[j][i]=(lconc*(exp((-1)*kconst*(pow(((qnew[j][i]/qts1)-1),nconst)))));
   qmnh31=qmnh31+((qconc1[j][i]*rhocar*v[j][i])+(rhoamm[j][i]*v[j][i]));
  }
 }
 if(subcycle == 1) {
  qmerr1=(inmnh3heat-qmnh31);
 }
 if(subcycle == 2) {
  qmerr1=(inmnh3cool-qmnh31);
 }
 if(fabs(qmerr1) <= masstol) {
  for(i=1; i <= ni; i++) {
   for(j=1; j <= nj; j++) {
    qconcnew[j][i]=qconc1[j][i];
   }
  }
  goto label_q3;
 }
 if(fabs(qmerr1) > masstol) {
  for(i=(nio+1); i <= (nio+nic); i++) {
   for(j=(njf+1); j <= nj; j++) {
    qconc2[j][i]=(lconc*(exp((-1)*kconst*(pow(((qnew[j][i]/qts2)-1),nconst)))));
    qmnh32=qmnh32+((qconc2[j][i]*rhocar*v[j][i])+(rhoamm[j][i]*v[j][i]));
   }
  }
  if(subcycle == 1) {
   qmerr2=(inmnh3heat-qmnh32);
  }
  if(subcycle == 2) {
   qmerr2=(inmnh3cool-qmnh32);
  }
 label_q2:
  qtsnew=(((qmerr2*qts1)-(qmerr1*qts2))/(qmerr2-qmerr1));
  for(i=(nio+1); i <= (nio+nic); i++) {
   for(j=(njf+1); j <= nj; j++) {
    qconcnew[j][i]=(lconc*(exp((-1)*kconst*(pow(((qnew[j][i]/qtsnew)-1),nconst)))));
    qmnh33=qmnh33+((qconcnew[j][i]*rhocar*v[j][i])+(rhoamm[j][i]*v[j][i]));
   }
```

```
    }
    if(subcycle == 1) {
     qmerr3=(inmnh3heat-qmnh33);
    }
    if(subcycle == 2) {
     qmerr3=(inmnh3cool-qmnh33);
    }
    if(fabs(qmerr3) > masstol) {
     qts1=qts2;
     qmerr1=qmerr2;
     qts2=qtsnew;
     qmerr2=qmerr3;
     qmnh33=0;
     goto label_q2;
    }
    goto label_q1;
   }
label_q3:
  if((qtsnew >= tcond) && (subcycle == 1)) {
   qtsnew=tcond;
   for(i=(nio+1); i <= (nio+nic); i++) {
    for(j=(njf+1); j <= nj; j++) {
     qconcnew[j][i]=(lconc*(exp((-1)*kconst*(pow(((qnew[j][i]/qtsnew)-1),nconst)))));
    }
   }
  }
  if((qtsnew <= tevap) && (subcycle == 2)) {
   qtsnew=tevap;
   for(i=(nio+1); i <= (nio+nic); i++) {
    for(j=(njf+1); j <= nj; j++) {
     qconcnew[j][i]=(lconc*(exp((-1)*kconst*(pow(((qnew[j][i]/qtsnew)-1),nconst)))));
    }
   }
  }
label_q4:
  qtsinc=(qtsnew-qtsold);
  qtsold=qtsnew;
  for(i=1; i <= ni; i++) {
   for(j=1; j <= nj; j++) {
    qconcold[j][i]=qconcnew[j][i];
   }
```

```
  }

/*****************************************************************************/

/* calculate new temperatures */

  for(j=1; j <= nj; j++) {
   for(i=1; i <= ni; i++) {
    unew[j][i]=((pnew[j][i]+qnew[j][i])/2);
    unewc[j][i]=(unew[j][i]-273);
   }
  }

/* calculate heat into unit cell and carbon bed */

  if(wall == 1) {
   for(j=1; j <= nj; j++) {
    qin=qin+(ho*aw[j][1]*(to-unew[j][1])*dt);
    qincar=qincar+(halcar*ae[j][nio]*(unew[j][nio]-unew[j][(nio+1)])*dt);
   }
  }
  if(wall == 2) {
   for(j=1; j <= nj; j++) {
    qin1=qin1+(ho*aw[j][1]*(to-unew[j][1])*dt);
    qin2=qin2+(hi*ae[j][ni]*(ti-unew[j][ni])*dt);
    qincar1=qincar1+(halcar*ae[j][nio]*(unew[j][nio]-unew[j][(nio+1)])*dt);
    qincar2=qincar2+(halcar*aw[j][(nio+nic+1)]*(unew[j][(nio+nic+1)]
            -unew[j][(nio+nic)])*dt);
   }
   qin=qin1+qin2;
   qincar=qincar1+qincar2;
  }

/* calculate other significant parameters */

  for(j=1; j <= nj; j++) {
   for(i=1; i <= ni; i++) {
    temp[j][i]=unew[j][i];
   }
  }
  utsnew=((ptsnew+qtsnew)/2);
```

```
    upsnew=(exp(11.749-(2823.4/utsnew)));
    for(j=(njf+1); j <= nj; j++) {
     for(i=(nio+1); i <= (nio+nic); i++) {
      mtempcar=mtempcar+(temp[j][i]*rhocar*v[j][i]);
      mnh3ads=mnh3ads+((lconc*(exp((-1)*kconst*(pow(((temp[j][i]
              /utsnew)-1),nconst)))))*(rhocar*v[j][i]));
      mnh3a=mnh3a+(((lconc*(exp((-1)*kconst*(pow(((temp[j][i]
            /utsnew)-1),nconst)))))*(rhocar*v[j][i]))+(rhoamm[j][i]*v[j][i]));
      lnh3=lnh3+(((phvnh3[j][i]+qhvnh3[j][i])/2)*rhocar*v[j][i]);
     }
    }
    lnh3=(lnh3/mcar);
    mtempcar=(mtempcar/mcar);
    heatall=(qin/(mcar*1000));
    heatpall=(heatall/time);
    heatcar=(qincar/(mcar*1000));
    heatpcar=(heatcar/time);
    massflow=((inmnh3-mnh3a)/time);
    dconc=((mnh3ads/mcar)-inconc);
    dconct=(dconc/time);
    coolpow=((-1)*dconct*lnh3);
    cop=((coolpow*2)/heatpall);
    dtsat=(utsnew-tsint);
    dpsat=(upsnew-psint);
    lcyctm=(abstime-(abstime/cycle));

/* write data to file & screen */

    counta++;
    if(counta == wfile) {
     for(j=1; j <= nj; j++) {
      timea[j]=abstime;
     }
     for(j=1; j <= (nj-1); j++) {
      fprintf(f1,"%f, ",timea[j]);
     }
     fprintf(f1,"%f\n",timea[nj]);
     for(i=1; i <= (ni-1); i++) {
      for(j=1; j <= (nj-1); j++) {
       fprintf(f1,"%f, ",unewc[j][i]);
      }
```

```
      fprintf(f1,"%f\n",unewc[nj][i]);
    }
    for(j=1; j <= (nj-1); j++) {
     fprintf(f1,"%f, ",unewc[j][ni]);
    }
    fprintf(f1,"%f\n",unewc[nj][ni]);
    fprintf(f3,"%f, %f, %f, %f, %f, %f, %f\n",heatpall,heatpcar,coolpow,
          mtempcar,cop,time,abstime);
    fprintf(f4,"%f, %f, %f, %f, %f, %f, %f\n",dconc,dconct,coolpow,mtempcar,
          cop,time,abstime);
    fprintf(f5,"%f, %f, %f, %f, %f, %f\n",dtsat,dpsat,massflow,mtempcar,time,abstime);
    counta=0;
   }
   countb++;
   if(countb == wscrn) {
    printf(" %d\n %f\n\n",iter,abstime);
    if(subcycle == 1) {
     printf("Cycle Number = %d .....Heating !!!\n\n",loop);
    }
    if(subcycle == 2) {
     printf("Cycle Number = %d .....Cooling !!!\n\n",loop);
    }
    countb=0;
   }

/* reset data files 1,3,4,5 for appending during program execution */

 fclose(f1); fclose(f2); fclose(f3); fclose(f4); fclose(f5);

 if((f1=fopen("temp.dat","a")) == NULL) {
  printf("Error, cannot open file 'temp.dat' for appending\n");
  exit(0);
 }
 if((f3=fopen("power.dat","a")) == NULL) {
  printf("Error, cannot open file 'power.dat' for appending\n");
  exit(0);
 }
 if((f4=fopen("conc.dat","a")) == NULL) {
  printf("Error, cannot open file 'conc.dat' for appending\n");
  exit(0);
 }
```

```
 if((f5=fopen("satn.dat","a")) == NULL) {
  printf("Error, cannot open file 'satn.dat' for appending\n");
  exit(0);
 }
/* reset counters */

  mtempcar=0;
  mnh3ads=0;
  mnh3a=0;
  lnh3=0;

/* update temperature arrays */

  for(j=1; j <= nj; j++) {
   for(i=1; i <= ni; i++) {
    uold[j][i]=unew[j][i];
    pold[j][i]=pnew[j][i];
    qold[j][i]=qnew[j][i];
   }
  }

/* assess cycle change-overs */

  if((dconc <= conclimit) && (subcycle == 1)) {
   subcycle=2;
   to=tocool;
   ho=hocool;
   ti=ticool;
   hi=hicool;
   subtime=0;

/* set mass in system before cooling */

   inmnh3cool=0;
   for(i=(nio+1); i <= (nio+nic); i++) {
    for(j=(njf+1); j <= nj; j++) {
     inmnh3cool=inmnh3cool+((((pconcold[j][i]+qconcold[j][i])/2)*rhocar
                *v[j][i])+(rhoamm[j][i]*v[j][i]));
    }
   }
  }
```

```
} while(((dconc > conclimit) && (subcycle == 1)) ||
        ((dconc < 0) && (subcycle == 2)));
 loop++;
/* end of solution time loop */

 } while (loop <= cycle);

/* calculate maximum specific heating power (kw/kg) */

 fclose(f3);
 if((f3=fopen("power.dat","r")) == NULL) {
  printf("Error, cannot open file 'power.dat' for reading\n");
  exit(0);
 }
 hpmax=0;
 hp1=0;
 hp2=0;
 while(fscanf(f3,"%lf, %lf, %lf, %lf, %lf, %lf, %lf\n",&heatpall,&heatpcar,
       &coolpow,&mtempcar,&cop,&time,&abstime)!=EOF) {
  hp2=heatpcar;
  if((hp2 > hp1) && (hp2 > hpmax) && (abstime > lcyctm)) {
   hpmax=hp2;
   mt1=(mtempcar-273);
   tm1=time;
  }
  hp1=hp2;
 }

/* calculate maximum rate of concentration change (kg/kgs) */

 fclose(f4);
 if((f4=fopen("conc.dat","r")) == NULL) {
  printf("Error, cannot open file 'conc.dat' for reading\n");
  exit(0);
 }
 dctmax=0;
 dct1=0;
 dct2=0;
 while(fscanf(f4,"%lf, %lf, %lf, %lf, %lf, %lf, %lf\n",&dconc,&dconct,&coolpow,
      &mtempcar,&cop,&time,&abstime)!=EOF) {
  dct2=dconct;
```

```
   if((dct2 < dct1) && (dct2 < dctmax) && (abstime > lcyctm)) {
     dctmax=dct2;
     cpow2=coolpow;
     mt2=(mtempcar-273);
     cop2=cop;
     tm2=time;
    }
    dct1=dct2;
  }

/* calculate time for 5% concentration change */

  fclose(f4);
  if((f4=fopen("conc.dat","r")) == NULL) {
    printf("Error, cannot open file 'conc.dat' for reading\n");
    exit(0);
  }
  dc1=0;
  dc2=0;
  while(fscanf(f4,"%lf, %lf, %lf, %lf, %lf, %lf, %lf\n",&dconc,&dconct,&coolpow,
        &mtempcar,&cop,&time,&abstime)!=EOF) {
    dc2=dconc;
    if((dc2 <= -0.05) && (dc1 > -0.05) && (abstime > lcyctm)) {
      deltaconc=dc2;
      mt3=((mtempcar*tint)-273);
      tm3=time;
    }
    dc1=dc2;
  }

/* write data to results file */

  if((f6=fopen("results.dat","w")) == NULL) {
    printf("Error, cannot open file 'results.dat' for writing\n");
    exit(0);
  }
  fprintf(f6,"%d, %f, %f, %f, %f, %f, %f, %f, %f, %f, %f, %f",simnum,lic,ljc,ljf,
        hpmax,tm1,tm3,dctmax,mt2,cpow2,cop2,tm2);

  fclose(f1);
  fclose(f2);
```

```
 fclose(f3);
 fclose(f4);
 fclose(f5);
 fclose(f6);

/* write data to comparison file */

 if((f7=fopen("compare.dat","a")) == NULL) {
  printf("Error, cannot open file 'compare.dat' for appending\n");
  exit(0);
 }
 fprintf(f7,"%d, %f, %f, %f, %f, %f, %f, %f, %f, %f, %f, %f",simnum,lic,ljc,ljf,
        hpmax,tm1,tm3,dctmax,mt2,cpow2,cop2,tm2);

 fclose(f7);

/* end of computation */

 printf("\n  **** End of Computation ****\n\n");

 return 0;

}  /* end of function main */

/*****************************************************************************/
```

Appendix III

Laminate Split Die:

Calculations and Drawings

The deflections of the split die outwards in the radial direction and upwards in the axial direction were calculated by applying basic solid mechanics equations. The split die was treated as a beam fixed at both ends subject to a point load at the mid length location. The calculations are based on the dimensions indicated in the split die drawings which follow.

(i) Radial Direction

Half-Depth of Split Die Block (d): 68.75 mm

Radius from Edge of Centre Hole to Outside of Block (r): 43 mm

Distance Between Inside Edges of Bolt Holes (l): 104 mm

Modulus of Elasticity for Steel (E): 200×10^9 N m^{-2}

At a pressure of 10 tonnes/in^2 the loading on each pair of split die bolts is approximately:

$$\text{Load } (W) = 10 \times \left(\frac{54}{25.4}\right) \times \left(\frac{68.75}{25.4}\right) \times 9.81 \times 10^3 = 564.5 \text{ kN (-ve sense)}$$

The second moment of area is given by:

$$I_{yy} = \frac{dr^3}{12}$$

The maximum radial deflection is given by:

$$y_{max} = \frac{-Wl^3}{192EI_{yy}}$$

Therefore:

$$I_{yy} = \frac{68.75 \times (43)^3}{12} = 455509 \text{ mm}^4$$

$$y_{max} = \frac{564.5 \times 10^3 \times (104 \times 10^{-3})^3}{192 \times 200 \times 10^9 \times 455509 \times 10^{-12}} = 0.036 \text{ mm}$$

Hence, even under conditions of maximum load the radial deflection may be considered negligible.

(ii) Axial Direction

Stainless Steel Shell Outside Diameter: 54 mm

Stainless Steel Shell (Nominal) Inside Diameter: 50.8 mm

Top Plate Depth (d): 25 mm

Radius from Edge of Centre Hole to Outside of Block (r): 43 mm

Distance Between Inside Edges of Bolt (Studding) Holes (l): 191 mm

At a pressure of 10 tonnes/in^2 the load acting upwards against half the top plate (two lengths of studding) is approximately:

$$\text{Load } (W) = \frac{10\pi \times \left[\left(\frac{54}{25.4}\right)^2 - \left(\frac{50.8}{25.4}\right)^2\right] \times 9.81 \times 10^3}{8} = 20 \text{ kN (-ve sense)}$$

The second moment of area is given by:

$$I_{xx'} = \frac{rd^3}{12}$$

The maximum axial deflection is given by:

$$y_{max} = \frac{-Wl^3}{192EI_{xx'}}$$

Therefore:

$$I_{xx'} = \frac{43 \times (25)^3}{12} = 55990 \text{ mm}^4$$

$$y_{max} = \frac{20 \times 10^3 \times (191 \times 10^{-3})^3}{192 \times 200 \times 10^9 \times 55990 \times 10^{-12}} = 0.065 \text{ mm}$$

Hence, even under conditions of maximum load the axial deflection may also be considered negligible. Therefore, under the maximum loading conditions the split die deflections in both the radial and axial directions are small enough to prevent any significant plastic deformation of the stainless steel shell and carbon-aluminium laminate.

Split Die Block- All Dimensions in Millimetres, Material: Mild Steel, 3rd Angle Projection

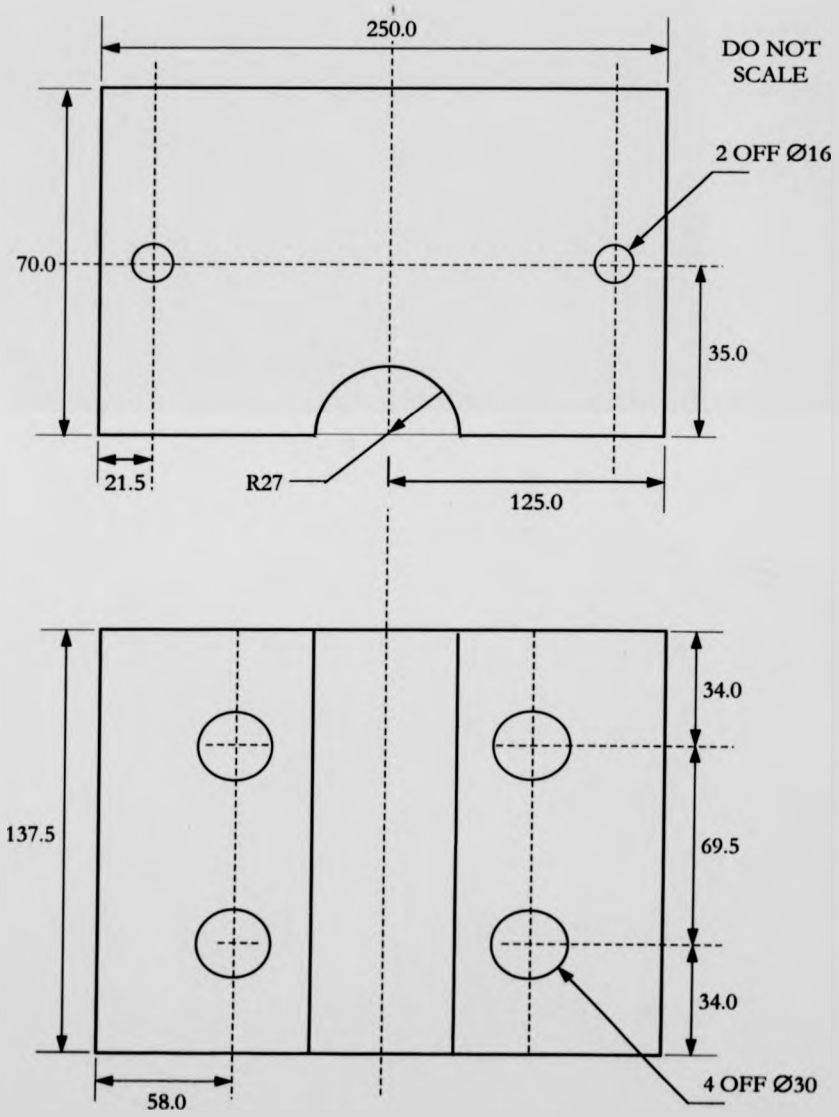

Die Top Plate - All Dimensions in Millimetres, Material: Mild Steel, 3rd Angle Projection

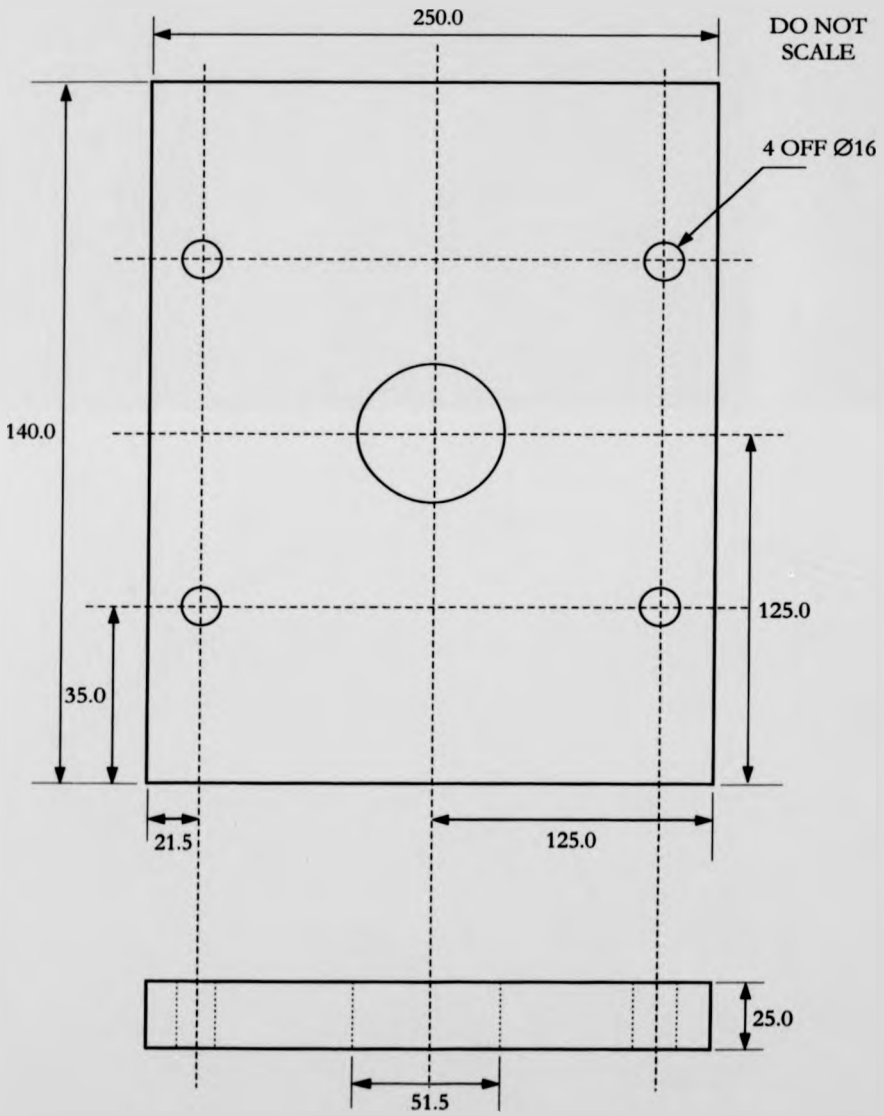

Die Base Plate - All Dimensions in Millimetres, Material: Mild Steel, 3rd Angle Projection

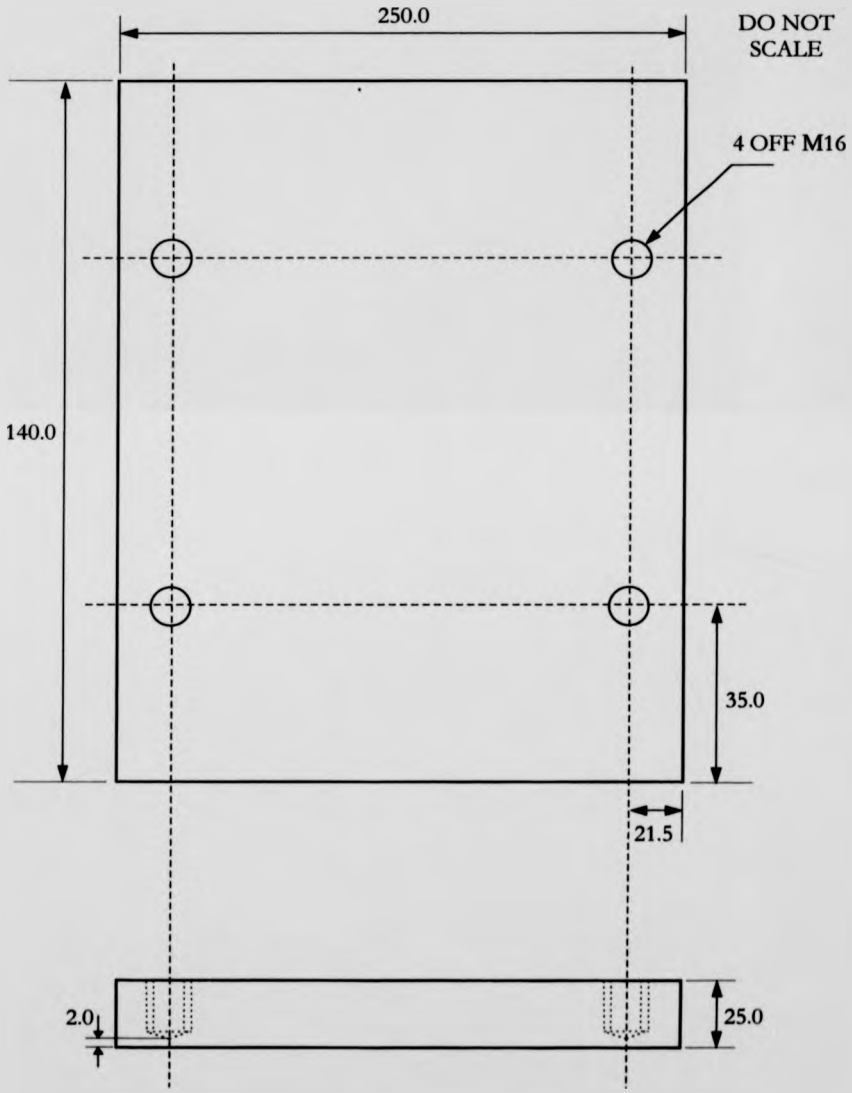

Appendix IV

Carbon Laminate Masses

10 layers of carbon and aluminium compressed simultaneously

Average force applied = 32 tonnes

Average pressing time = 60 seconds

Layer No.	Laminate Tube (A) Mass of Carbon (g)	Laminate Tube (B) Mass of Carbon (g)	Laminate Tube (C) Mass of Carbon (g)	Laminate Tube (D) Mass of Carbon (g)
1	6.225	6.224	6.221	6.224
2	6.224	6.221	6.225	6.222
3	6.222	6.222	6.229	6.228
4	6.222	6.228	6.224	6.227
5	6.222	6.226	6.224	6.225
6	6.227	6.226	6.222	6.223
7	6.222	6.222	6.220	6.229
8	6.221	6.221	6.221	6.221
9	6.220	6.220	6.223	6.223
10	6.225	6.222	6.228	6.229
11	6.227	6.226	6.223	6.225
12	6.229	6.222	6.220	6.229
13	6.223	6.222	6.221	6.226
14	6.225	6.227	6.225	6.226
15	6.221	6.222	6.228	6.224
16	6.226	6.220	6.223	6.220
17	6.222	6.224	6.221	6.222
18	6.220	6.225	6.228	6.224
19	6.220	6.228	6.224	6.225
20	6.221	6.222	6.227	6.222
21	6.222	6.222	6.221	6.220
22	6.224	6.221	6.225	6.226
23	6.220	6.222	6.224	6.226

24	6.223	6.226	6.227	6.222
25	6.227	6.221	6.223	6.227
26	6.228	6.221	6.228	6.223
27	6.222	6.227	6.222	6.225
28	6.229	6.228	6.224	6.228
29	6.229	6.226	6.229	6.221
30	6.224	6.224	6.224	6.226
31	6.225	6.225	6.225	6.221
32	6.223	6.227	6.226	6.226
33	6.228	6.221	6.224	6.222
34	6.225	6.228	6.228	6.226
35	6.221	6.228	6.222	6.223
36	6.222	6.228	6.222	6.226
37	6.221	6.224	6.224	6.221
38	6.225	6.220	6.222	6.223
39	6.224	6.224	6.223	6.221
40	6.224	6.220	6.227	6.221
41	6.223	6.220	6.227	6.227
42	6.224	6.220	6.220	6.222
43	6.221	6.226	6.224	6.225
44	6.220	6.222	6.226	6.228
45	6.224	6.222	6.224	6.222
46	6.226	6.228	6.226	6.221
47	6.227	6.224	6.226	6.221
48	6.220	6.222	6.226	6.228
49	6.222	6.227	6.224	6.222
50	6.228	6.229	6.229	6.226
51	6.226	6.228	6.224	6.223
52	6.227	6.226	6.224	6.220
53	6.223	6.226	6.227	6.220
54	6.228	6.229	6.224	6.228
55	6.222	6.228	6.222	6.221
56	6.220	6.222	6.226	6.226
57	6.222	6.220	6.225	6.229
58	6.222	6.228	6.225	6.220
59	6.222	6.225	6.222	6.224
60	6.228	6.220	6.222	6.228
61	6.222	6.226	6.223	6.224
62	6.227	6.221	6.223	6.222
63	6.225	6.222	6.227	6.220
64	6.226	6.223	6.225	6.222
65	6.226	6.220	6.220	6.229
66	6.223	6.223	6.226	6.224
67	6.225	6.225	6.227	6.226
68	6.222	6.220	6.228	6.223

69	6.224	6.228	6.226	6.221
70	6.224	6.222	6.227	6.228
71	6.222	6.226	6.226	6.229
72	6.225	6.227	6.223	6.221
73	6.220	6.222	6.226	6.229
74	6.222	6.222	6.225	6.226
75	6.225	6.228	6.228	6.220
76	6.220	6.220	6.221	6.229
77	6.224	6.226	6.226	6.227
78	6.222	6.220	6.220	6.229
79	6.221	6.224	6.220	6.223
80	6.225	6.225	6.225	6.224
81	6.220	6.222	6.224	6.224
82	6.225	6.220	6.220	6.229
83	6.227	6.223	6.225	6.220
84	6.228	6.220	6.224	6.226
85	6.222	6.224	6.222	6.224
86	6.229	6.228	6.227	6.222
87	6.222	6.226	6.224	6.226
88	6.227	6.227	6.228	6.229
89	6.224	6.229	6.225	6.228
90	6.222	6.228	6.225	6.222
91	6.225	6.226	6.225	6.228
92	6.224	6.226	6.223	6.222
93	6.222	6.222	6.229	6.222
94	6.228	6.222	6.225	6.223
95	6.226	6.226	6.221	6.227
96	6.225	6.222	6.226	6.226
97	6.221	6.221	6.225	6.226
98	6.227	6.222	6.225	6.225
99	6.222	6.220	6.228	6.225
100	6.225	6.222	6.224	6.222
101	6.222	6.228	6.222	6.224
102	6.226	6.226	6.223	6.228
103	6.224	6.228	6.227	6.229
104	6.222	6.228	6.224	6.220
105	6.227	6.226	6.226	6.223
106	6.220	6.226	6.228	6.228
107	6.224	6.225	6.222	6.229
108	6.229	6.222	6.222	6.226
109	6.228	6.227	6.229	6.229
110	6.224	6.227	6.223	6.223
111	6.222	6.224	6.227	6.226
112	6.224	6.225	6.222	6.227
113	6.224	6.225	6.225	6.226

114	6.226	6.226	6.220	6.220
115	6.228	6.226	6.228	6.226
116	6.223	6.224	6.226	6.223
117	6.227	6.224	6.229	6.229
118	6.220	6.222	6.222	6.222
119	6.221	6.228	6.223	6.220
120	6.228	6.223	6.222	6.227
121	6.225	6.221	6.220	6.224
122	6.227	6.221	6.224	6.227
123	6.227	6.224	6.228	6.220
124	6.222	6.224	6.226	6.228
125	6.224	6.229	6.226	6.224
126	6.220	6.224	6.224	6.221
127	6.227	6.225	6.224	6.228
128	6.224	6.227	6.220	6.229
129	6.220	6.220	6.224	6.226
130	6.228	6.229	6.220	6.222
131	6.221	6.222	6.220	6.220
132	6.227	6.222	6.229	6.225
133	6.220	6.222	6.220	6.224
134	6.227	6.221	6.225	6.221
135	6.225	6.227	6.220	6.223
136	6.220	6.225	6.223	6.225
137	6.224	6.224	6.221	6.223
138	6.225	6.225	6.226	6.228
139	6.223	6.221	6.226	6.225
140	6.220	6.226	6.228	6.227
141	6.224	6.226	6.222	6.223
142	6.220	6.228	6.222	6.227
143	6.229	6.226	6.225	6.223
144	6.220	6.228	6.224	6.224
145	6.220	6.226	6.222	6.220
146	6.226	6.227	6.226	6.229
147	6.220	6.220	6.222	6.228
148	6.226	6.226	6.227	6.228
149	6.227	6.229	6.226	6.220
150	6.220	6.223	6.222	6.223
151	6.228	6.227	6.225	6.220
152	6.222	6.224	6.226	6.227
153	6.225	6.229	6.221	6.220
154	6.222	6.227	6.227	6.225
155	6.226	6.224	6.225	6.223
156	6.223	6.226	6.222	6.225
157	6.226	6.220	6.226	6.227
158	6.224	6.226	6.228	6.221

159	6.227	6.223	6.221	6.228
160	6.224	6.223	6.220	6.228
161	6.226	6.228	6.220	6.222
162	6.226	6.220	6.220	6.223
163	6.225	6.220	6.222	6.223
164	6.222	6.221	6.225	6.228
165	6.225	6.222	6.224	6.220
166	6.227	6.223	6.221	6.226
167	6.225	6.225	6.228	6.221
168	6.224	6.225	6.220	6.227
169	6.222	6.225	6.226	6.228
170	6.220	6.222	6.225	6.225
171	6.226	6.226	6.222	6.224
172	6.225	6.227	6.222	6.220
173	6.223	6.226	6.224	6.224
174	6.221	6.228	6.225	6.224
175	6.222	6.224	6.221	6.225
176	6.226	6.222	6.220	6.228
177	6.221	6.220	6.225	6.221
178	6.228	6.220	6.225	6.226
179	6.224	6.220	6.221	6.224
180	6.220	6.222	6.220	6.222
181	6.226	6.224	6.221	6.222
182	6.220	6.220	6.225	6.226
183	6.224	6.222	6.222	6.228
184	6.223	6.224	6.227	6.229
185	6.224	6.228	6.224	6.226
186	6.220	6.226	6.223	6.225
187	6.223	6.221	6.227	6.224
188	6.227	6.224	6.223	6.222
189	6.225	6.224	6.223	6.224
190	6.228	6.227	6.223	6.220
191	6.221	6.222	6.223	6.227
192	6.220	6.220	6.221	6.220
193	6.226	6.226	6.227	6.229
194	6.225	6.223	6.225	6.223
195	6.222	6.222	6.229	6.224
196	6.222	6.227	6.220	6.228
197	6.222	6.223	6.225	6.228
198	6.220	6.222	6.220	6.227
199	6.224	6.225	6.222	6.228
200	6.226	6.227	6.222	6.225
201	6.224	6.225	6.224	6.227
202	6.223	6.226	6.223	6.225
203	6.222	6.221	6.225	6.223

204	6.225	6.225	6.229	6.221
205	6.220	6.223	6.223	6.223
206	6.223	6.226	6.222	6.229
207	6.220	6.224	-	6.226
208	6.220	6.220	-	6.226
209	6.223	6.222	-	6.224
210	6.228	-	-	6.227
211	6.220	-	-	6.221
212	6.223	-	-	6.227
213	6.221	-	-	6.220
214	6.221	-	-	6.222
215	6.226	-	-	6.221
216	6.226	-	-	6.220
217	6.221	-	-	6.226
218	6.224	-	-	6.224
219	6.228	-	-	6.228
220	6.221	-	-	6.226
221	6.220	-	-	6.225
222	6.227	-	-	6.225
223	6.222	-	-	6.223
224	6.228	-	-	6.226
225	6.221	-	-	6.229
226	6.220	-	-	6.222
227	6.222	-	-	6.228
228	6.224	-	-	6.223
229	6.220	-	-	6.228
230	6.220	-	-	6.228
231	6.226	-	-	6.223
232	6.228	-	-	6.224
233	6.227	-	-	6.223
234	6.220	-	-	-
235	6.222	-	-	-
236	6.223	-	-	-
237	6.224	-	-	-
238	6.221	-	-	-

Laminate tube number (A), total wet mass of carbon = **1.481 kg**

Laminate tube number (B), total wet mass of carbon = **1.301 kg**

Laminate tube number (C), total wet mass of carbon = **1.282 kg**

Laminate tube number (D), total wet mass of carbon = **1.450 kg**

Generator 1 (laminate (A) + (C)), total wet mass of carbon = **2.763 kg**

Generator 2 (laminate (B) + (D)), total wet mass of carbon = **2.751 kg**

The mass distribution within each pyrolysed dry laminate section A-D is presented below.

		Laminate (A)	Laminate (B)	Laminate (C)	Laminate (D)
Number of Layers	-	238	209	206	233
Length	(mm)	550	485	485	540
Total Dry Mass	(g)	2287.2	1985.9	1970.8	2219.8
Mass of Steel	(g)	1160.0	1022.9	1022.9	1138.9
	(% of total)	50.7	51.5	51.9	51.3
Mass of Aluminium	(g)	262.3	230.3	227.0	256.8
	(% of total)	11.5	11.6	11.5	11.6
Mass of Dry Carbon	(g)	865.0	732.7	720.9	824.2
	(% of total)	37.8	36.9	36.6	37.1
Mass of Wet Carbon	(g)	1481.3	1300.8	1282.2	1450.3
Change in Carbon Mass (including centre hole)	(%)	41.0	43.1	43.2	42.6

The mass of aluminium in each laminate section is calculated based on a measured average aluminium disc mass value of 1.102 g.

The mass of steel in each laminate section is calculated based on a measured average steel tubing mass per unit length of 2.109 g mm^{-1}.

The change in the carbon mass between the wet and the dry pyrolysed laminates is calculated assuming the 5 mm axial centre hole accounts for a 1% reduction in the wet carbon mass.

Generator 1 (laminate (A) + (C)), total dry mass of carbon = **1.586 kg**

Generator 2 (laminate (B) + (D)), total dry mass of carbon = **1.557 kg**